

Automation and Scale-Up of Human Induced Pluripotent Stem Cell Models of Cardiovascular Disease for Drug Screening

Submitted by
James Edward Brooke Crutchley, BSc. MSc.

Thesis submitted to the University of Nottingham for the degree of Doctor of Philosophy

School of Medicine

SEPTEMBER 2015

Abstract

The global cost of heart failure is USD$45 billion and set to double in the next 15 years. The only method of treatment is heart transplant but demand far exceeds supply and is projected to increase. Meanwhile, global pharmaceutical development has been hindered by poor drug development success rates. Of the drugs that make it to phase I clinical trials, only 8 % pass phase III and existing drug screens do not always accurately predict or detect adverse cardiac events. Cardiotoxicity is the underlying reason for 26 % of safety related drug withdrawals between 1990-2006. Therefore, a source of human cardiomyocytes (CMs) is required to fill the need for regenerative medicine and drug screening applications. Differentiation of human pluripotent stem cells (hPSCs) to CMs is a viable solution to this bottleneck but the number of cells required is staggering; up to 5 million novel compounds are registered annually by pharmaceutical and academic institutions, while cell replacement studies in primates suggest that 10 billion CMs will be required per patient to repair the damaged myocardium post infarction.

The objective of this thesis was to evaluate whether automated high throughput manufacture of hPSCs and CMs was possible, and to demonstrate that hPSC-CMs could be used in automated high throughput drug screening by carrying out assays in 384-well plates. This thesis started by carrying out three manual differentiation methods; an embryoid body (EB) based method and two monolayer methods. Batch variability in mouse embryonic fibroblast conditioned medium (MEF-CM) led to erratic and variable differentiation outcomes (as high as 94+/-0.3 % to as low as

25.6+/-39.7 % beating EBs per 96 well plate). Two monolayer methods, using defined media (mTeSR and E8) increased cell yields by up to 12-fold and 65-fold respectively and simplified the process technically. When these methods were automated, EB differentiation failed to generate spontaneously beating EBs, whereas both monolayer methods succeeded in generating spontaneously beating cardiomyocytes of purities >90 %. Finally, cryopreserved stocks of hiPSC-CMs produced by automation were used to evaluate whether cardiotoxicity from the anticancer drug doxorubicin could be decreased by co-treating with dexrazoxane (an existing doxorubicin cardio-protectant), carvedilol (a β-blocker), sildenafil (a vasoactive agent) and isoprenaline (a β-adrenoreceptor agonist). This was carried out in a real-time, fully automated assay setup to monitor induction of apoptosis by the marker propidium iodide using the Operetta confocal plate reader. The concentration of doxorubicin that led to 50 % hiPSC-CM death (TD_{50}) was significantly reduced by co-treatment with dexrazoxane, carvedilol and sildenafil. Carvedilol showed the highest level of cardioprotection by increasing TD_{50} of doxorubicin by 7.5-fold. In contrast, isoprenaline reduced TD_{50} of doxorubicin, suggesting that isoprenaline would be contraindicated in patients undergoing doxorubicin treatment.

Thus, this thesis demonstrated that automated differentiation of cardiomyocytes was technically feasible with capability of generating high yields (up to 39 million cells per flask) and high purity (>90 %) cardiomyocytes. Furthermore, this system was compatible with high content assays in 384-well plates for evaluating drug toxicity.

Acknowledgements

I would like to thank those who provided technical support and whose work features in some parts of this thesis. Namely, Nigel Smith for his Karyotyping help; Divya Rajamohan, Katarzyna Lis-Slimak and Gary Duncan for providing me with their immunostaining images and Gary Duncan once more for his E8 hiPSC lines.

I would also like to thank my supervisor Professor Chris Denning, for his (literally) endless patience and support which has helped me to get through this PhD and shape me as a scientist. I would also like to thank my second supervisor, Professor Lorraine Young for her caring support and enthusiasm.

Thank you to Elena Matsa, who helped me to find my feet here at Nottingham and whose early guidance and support proved invaluable and will never be forgotten. Special thanks go to Spandan who was with me from the start and who no doubt, misses the fact we no longer share a cell culture hood. Thanks to Alex Popov for his never ending support and friendship, Boots lunches won't be the same without you. My appreciation also goes out to Richard Harrison for his friendship and unique sense of humour. I also want to say thanks to Luke Flatt, Jamie Bhagwan, Gary Duncan, Lazaros Fotopoulos, and James Smith for their friendship, humour and company. A special mention also goes out to my "thesis buddy" Jamie Patient with whom I suffered in solidarity as we both wrote our theses.

Most importantly I want to thank all my family, mainly those who inspired and cared for me when I was younger but are no longer around to share this milestone with me. My parents, whose love and support has always been a bulwark from which I've garnered strength and finally, to my grandfather, George, who has been a guiding light in my life and has inspired me more than he can ever know. His maxim will always motivate me dove-tailing as it does with the profession I have chosen.

Sempre avanti.

Contents

Abstract i

Acknowledgements iii

Contents iv

List of Figures xi

List of Tables xiv

Abbreviations xv

1 Introduction 1

1.1 *In vitro* drug testing and cardiotoxicity 1

1.2 Embryonic stem cells, isolation from ICM 2

1.3 Somatic cell nuclear transfer 3

1.4 Human induced pluripotent stem cells 4

1.5 Early heart development 5

1.6 Cardiac repair and regenerative medicine 7

1.6.1 Induction of endogenous cardiac repair mechanisms 7

1.6.2 Cell delivery for cardiac repair 10

1.6.2.1 Cell delivery of hESC or hESC-derived cell types for tissue repair 10

1.6.2.2 Delivery of hiPSCs or hiPSC-derived cell types for tissue repair ... 13

1.7 hiPSCs as disease models 14

1.8 Properties of adult and foetal cardiomyocytes 15

1.9 Cardiomyocyte action potentials 16

1.10 Modelling cardiac channelopathies: long QT syndromes as disease models 17

1.10.1 Prevalence and clinical characteristics of the long QT syndromes 17

1.10.2 hiPSC models of long QT syndrome 18

1.11 Other cardiovascular disease models 19

1.12 Thesis Aims 21

2 Experimental Methods 23

2.1 Routine Cell Culture 23

2.1.1 Mouse embryonic fibroblast preparation and conditioned medium 24

2.1.2 Coating flasks in Matrigel™ 25

2.1.3 Culture of human embryonic stem cells in MEF-CM 26

2.1.4 Human pluripotent stem cell culture in mTeSR medium 26
2.1.5 Human pluripotent stem cell culture in Essential-8™ (E8) medium 27
2.1.6 Growth curves 28
2.1.7 Fixing cells for karyotype assessment 28
2.2 Cardiomyocyte differentiation protocols 29
2.2.1 EB cardiomyocyte differentiation method 29
2.2.1.1 EB purification by lactate treatment 30
2.2.2 mTeSR monolayer method differentiation to cardiomyocytes 31
2.2.3 E8 monolayer method differentiation to cardiomyocytes 31
2.3 Cardiomyocyte dissociation methods 32
2.3.1 EB cell dissociation solution method 32
2.3.2 Trypsin / Accumax methods 32
2.3.2.1 EB dissociation 32
2.3.2.2 mTeSR monolayer method dissociation 33
2.3.3 EB cold dissociation method 33
2.3.4 E8 monolayer dissociation methods 34
2.3.4.1 Sequential TrypLE method 34
2.3.4.2 Collagenase and TrypLE Express method 34
2.4 Cryopreservation of cardiomyocytes 35
2.4.1 Cryopreservation of cardiomyocytes from EB and mTeSR monolayer differentiation methods 35
2.4.2 Cryopreservation of cardiomyocytes from E8 monolayer differentiation method 36
2.5 Cardiomyocyte quantification 36
2.5.1 Immunostaining of plated cells 36
2.5.2 Immunostaining of cells for flow cytometry 37
2.6 Drug screening protocols 39
2.6.1 Quantifying cell viability using Calcein AM, Propidium iodide and Hoechst33342 39
2.6.2 Drug screening and staining with PI, CEC and Hoechst33342 39
2.6.2.1 Preparing and using Caspase 3/7 detection reagent 39
2.6.2.2 Preparation of drug compounds 40
2.6.2.3 Setting up assays in 96-well plates 40

2.7 Changing medium and setting up assays in 384-well plates 41
3 Development of hESC and hiPSC culture and differentiation methods 43
3.1 Introduction 43
3.1.1 Culturing hESCs in feeder free conditions 43
3.1.2 Defined media for culture of hESCs and hiPSCs 44
3.1.3 Embryoid Body (EB) differentiation to cardiomyocytes 45
3.1.4 Monolayer differentiation to cardiomyocytes 46
3.1.5 Chapter Aims 47
3.2 Results 47
3.2.1 Establishing technical competence in feeder-free culture of HUES7 hESCs as a prelude to EB differentiation 47
3.2.2 The EB cardiomyocyte differentiation method 50
3.2.3 Developing automated imaging based processes for assessing EB size and percent transfer using the Cellavista cell imager 52
3.2.4 Determining a suitable method for EB dissociation 54
3.2.5 Quantification of immunostained cells using the Cellavista cell imager 56
3.2.6 Culturing HUES7 hESCs in mTeSR™1 feeder free defined medium 57
3.2.7 Monitoring confluence of HUES7s in mTeSR using the Cellavista cell imager 59
3.2.8 Differentiating HUES7 and hiPSC lines using the mTeSR monolayer differentiation method 60
3.2.9 Culturing HUES7 cells in Essential 8™ feeder free defined medium 62
3.2.10 Developing cell culture in E8 with the CPVT hiPSC line 64
3.2.11 Culturing the LQT2 hiPSC line in E8 67
3.2.12 The E8 monolayer differentiation method and line-specific optimisations 68
3.2.13 Troubleshooting issues with dissociating E8 monolayer differentiations 70
3.2.14 Quantification of immunostained cardiomyocytes by Operetta confocal plate reader 73
3.2.15 Comparison of different surfaces and seeding densities of cardiomyocytes for drug screening 75

3.2.16 Optimising cardiomyocyte culture conditions to maintain cardiomyocytes for drug screening 78
3.3 Discussion 80
3.3.1 Feeder free hESC and hiPSC culture 80
3.3.2 Conditioned medium culture and EB differentiation 80
3.3.3 mTeSR medium and the mTeSR monolayer differentiation method .. 82
3.3.4 E8 medium and the E8 monolayer differentiation method 84
3.3.5 Plating and maintenance of hiPSC derived cardiomyocytes 86
4 Developing Automated Processes for Cardiomyocyte Differentiation and Drug Screening 88
4.1 Introduction 88
4.1.1 The robot and integrated hardware 88
4.1.2 Changing media on flasks using the robot 97
4.1.3 EB differentiation automation 99
4.1.4 Automation of monolayer differentiation methods 100
4.1.5 Choice of cell lines 101
4.1.6 Cell harvesting on the robot 102
4.1.6.1 Cell harvesting (stage 1) 102
4.1.6.2 Cell counting (stage 2) and dilution (stage 3) 104
4.1.6.3 Cell mixing and seeding (stage 4) 105
4.1.7 Chapter Aims 105
4.2 Results 106
4.2.1 Variables for developing and testing an automated process for EB formation 106
4.2.2 Effect of different enzymes and room temperature enzyme incubation on hESC EB formation and differentiation to cardiomyocytes 106
4.2.3 Effect of harvesting cells by contact method using accutase on hESC EB formation and differentiation to cardiomyocytes 108
4.2.4 Comparison of incubators, manual and robot cell suspension seeding and effect of penicillin/streptomycin on the formation and differentiation of EBs 110
4.2.5 Automating the process of hESC harvesting and seeding for EB formation and differentiation to cardiomyocytes 112

4.2.6 Investigation of problems with EB formation during automated cell counting and dilution steps 115
4.2.7 Testing incubation time and its effect on EB formation during the automated cell counting and dilution steps 116
4.2.8 Testing different trough formats for their effect on EB formation ... 119
4.2.9 Robot liquid handling pipette vectors and speeds for medium changes in 96 well U-bottom and V-bottom plates 120
4.2.10 Robot liquid handling pipette vectors and speeds for transferring EBs from 96 well V-bottom plates to 96-well U-bottom plates 123
4.2.11 Testing automation of the complete HUES7 EB differentiation process 125
4.2.12 Developing a centrifugation-free EB dissociation method 127
4.2.13 Testing a lactate-based method for enriching cardiomyocytes in EBs 129
4.2.14 Developing an automated process for monolayer differentiation using an in-house differentiation protocol 132
4.2.15 Generation of hESC derived cardiomyocytes by automation 133
4.2.16 Dissociation and viability of monolayer differentiations carried out manually and by automation 135
4.2.17 Automating E8 culture of CPVT and LQT2 hiPSC lines for use in monolayer differentiations 138
4.2.18 Automated differentiation of E8 cultured hiPSC lines to cardiomyocytes 139
4.2.19 Automating hiPSC derived cardiomyocyte seeding in 384-well plates for drug screening 141
4.3 Discussion 143
4.3.1 Automation of EB differentiations 143
4.3.2 Automation of monolayer differentiation methods 145
5 Developing Platforms for Drug Screening Using Cardiomyocytes 148
5.1 Introduction 148
5.1.1 CPVT hiPSC cardiomyocytes for drug screening experiments. 148
5.1.2 Assessing cell death in vitro 148
5.1.2.1 Apoptosis 148
5.1.2.2 Programmed Cell Necrosis 149

5.1.2.3 Measuring apoptosis and necrosis in vitro using Propidium Iodide 149
5.1.2.4 Caspases and Cell Event Caspase 3/7 reagent 151
5.1.2.5 Staurosporine as a positive control for caspase activation..... 152
5.1.3 Doxorubicin cardiotoxicity *in vitro* and *in vivo* 152
5.1.4 Drugs that may reduce doxorubicin cardiotoxicity *in vitro* 154
5.1.4.1 Dexrazoxane 154
5.1.4.2 Carvedilol 155
5.1.4.3 Sildenafil 155
5.1.4.4 Isoprenaline 156
5.1.5 Chapter Aims..... 157
5.1.6 Key objectives 158
5.2 Results 158
5.2.1 Designing analysis scripts for Operetta 158
5.2.2 Testing time course viability data acquisition using PI and CEC Markers 162
5.2.2.1 Evaluating toxicity of PI and CEC incubation with cardiomyocytes 162
5.2.2.2 Evaluating photo-bleaching of PI and CEC markers over 24 hours 165
5.2.3 Testing DMSO concentrations to assess vehicle toxicity..... 166
5.2.3.1 Measuring DMSO toxicity by PI staining 167
5.2.3.2 Measuring DMSO toxicity by CEC staining 169
5.2.4 Validating PI, CEC and PI-CEC co-staining quantification using staurosporine..... 172
5.2.4.1 Quantifying PI staining with or without CEC co-incubation in cardiomyocytes treated with STA 173
5.2.4.2 Quantifying CEC staining with or without PI co-incubation in cardiomyocytes treated with STA 175
5.2.4.3 Comparing TD_{50} and EC_{50} values with results from Cellular Dynamics Technical Notes 178
5.2.5 Investigating cardiotoxicity with doxorubicin..... 181
5.2.6 Identifying suitable concentrations of rescue drugs for doxorubicin-toxicity rescue..... 187

5.2.6.1 Dexrazoxane toxicity testing 187
5.2.6.2 Cavedilol toxicity testing 189
5.2.6.3 Sildenafil toxicity testing 191
5.2.6.4 Isoprenaline toxicity testing 192
5.2.7 Endpoint analysis of “rescue” drugs 193
5.2.8 Time course quantification of DOX toxicity with or without co-incubation of rescue drugs 195
5.2.9 Endpoint quantification of doxorubicin toxicity and rescue drug effects 201
5.2.10 Determining and comparing TD_{50} value for doxorubicin with and without rescue drug co-treatment 203
5.3 Discussion 206
5.3.1 Time course drug screening validation 206
5.3.2 Time course and end-point screening of DOX cardiotoxicity with or without rescue drugs 207
5.3.3 Limitations of the time course assay 208
6 Discussion 211
6.1 hPSC culture and differentiation 211
6.2 Automating differentiation and drug screening 215
6.3 DOX toxicity modelling and drug screening with hiPSC derived cardiomyocytes 216
6.4 Study limitations 219
6.5 Final remarks and future work 221
7 Bibliography 223
8 Appendix 240

List of Figures

Figure 1.1 – Formation of the cardiac tube 17-23 DPC in humans 6
Figure 2.1 – Deriving TD_{50} and EC_{50} values from dose response curves 41
Figure 3.1 – Culturing HUES7 hESCs in feeder free conditions using MEF conditioned medium. 49
Figure 3.2 – Differentiating HUES7s to cardiomyocytes using the EB differentiation method. 51
Figure 3.3 – EB Detection and size quantification using the Cellavista. 53
Figure 3.4 – Testing dissociation methods on HUES7-derived beating EBs. 55
Figure 3.5 – Quantification of immunostained cells using Cellavista. 57
Figure 3.6 – Culturing HUES7s in mTeSR. 58
Figure 3.7 – Monitoring confluence in monolayer cultures using the Cellavista. 59
Figure 3.8 – Generating cardiomyocytes with the mTeSR monolayer method. 61
Figure 3.9 – Culturing HUES7 in E8 medium. 63
Figure 3.10 – Culturing CPVT hiPSCs in E8 Medium. 66
Figure 3.11 – TrypLE passaging of LQT2 hiPSCs in E8 medium. 68
Figure 3.12 – Line-specific differentiation condition optimisations with the E8 monolayer method 69
Figure 3.13 – Testing E8 monolayer differentiation dissociation strategies to maximise cell survival post-dissociation. 72
Figure 3.14 – Quantification of immunostained AT1 hiPSC cardiomyocytes and negative control CPVT hiPSCs using the Operetta confocal plate reader. 74
Figure 3.15 – Seeding of cardiomyocytes on Matrigel, Fibronectin and Vitronectin-N to determine optimal seeding density. 77
Figure 3.16 – Testing conditions for thawing and culturing cryopreserved cardiomyocytes for seeding in drug screening assays. 79
Figure 4.1 – Hardware of the Freedom Evo 200 Robotic Platform 90
Figure 4.2 – Corning RoboFlask 91
Figure 4.3 – StoreX Incubator (STX110) 91
Figure 4.4 – Robotic Manipulator Arm (RoMa) 92
Figure 4.5 – Flask Flipper™ module 92
Figure 4.6 – Liquid Handling Arm 93
Figure 4.7 – Cedex HiRes cell counter 94
Figure 4.8 – Heated microplate carrier and 100 ml trough carriers 95
Figure 4.9 – MultiChannel Arm™ 96 96
Figure 4.10 – Illustration of the medium change protocol on the robotic platform. 98
Figure 4.11 – Cell counting, dilution, mixing and seeding on the robot 104
Figure 4.12 – Testing robot cell suspension seeding, HUES7 EB formation in the StoreX incubator and Pen/Strep incubation with EB formation. 112
Figure 4.13 – Testing automation of the different steps of day 0 HUES7 EB setup for differentiation. 114

Figure 4.14 – Testing the automated cell count and cell dilution steps to determine the cause of no HUES7 EB formation. 116
Figure 4.15 – Testing duration of incubation and format on HUES7 EB formation after 24 hours. 118
Figure 4.16 – Testing different trough formats for effect on HUES7 EB formation at 24 hr post-seeding. 120
Figure 4.17 – The vectors for medium changes carried out in 96 well U-bottom and V-bottom plates using the robot from day 8 onwards. 122
Figure 4.18 – Vectors for enabling EB transfer from V-bottom to U-bottom plate on day 4 of differentiation. 124
Figure 4.19 – Testing the full 8-day EB differentiation process using the robotic platform 126
Figure 4.20 – Developing a centrifugation-free dissociation strategy for EBs on the robot. 129
Figure 4.21 – Testing lactate enrichment of cardiomyocytes in hESC-derived beating EBs. 131
Figure 4.22 – The automated monolayer differentiation process for HUES7 cells in mTeSR 133
Figure 4.23 – Quantification of cardiomyocytes generated by manual or robot monolayer differentiation of mTeSR hESCs to cardiomyocytes. 135
Figure 4.24 – Viability of dissociated manually generated/manually harvested and robot generated/robot harvested mTeSR Hues7 monolayer differentiated cardiomyocytes. 137
Figure 4.25 – Culture of CPVT and LQT2 hiPSC lines on the robot in E8 medium. 139
Figure 4.26 – Automated differentiation of CPVT and LQTS2 hiPSCs cultured in E8 to cardiomyocytes. 141
Figure 4.27 – Matrigel coating and cell seeding in 384-well plates for high throughput and high content drug screening. 143
Figure 5.1 – Representative images of cells undergoing apoptosis or programmed necrosis. 150
Figure 5.2 – Image analysis on the Operetta confocal plate reader for toxicity assays, potential issues and identifying Hoechst toxicity. 161
Figure 5.3 – Toxic effects from incubation of hiPSC derived cardiomyocytes in Hoescht33342. 161
Figure 5.4 – Quantifying PI or CEC staining of untreated CPVT cardiomyocytes over 24 hours. 163
Figure 5.5 – Effects of incubating PI or CEC with CPVT cardiomyocytes over 24 hours. 165
Figure 5.6 – Quantifying mean object fluorescence intensity over 24 hours. 166
Figure 5.7 – Testing DMSO concentrations for toxicity in CPVT cardiomyocytes with PI staining. 169

Figure 5.8 – Testing DMSO concentrations for toxicity in CPVT cardiomyocytes with CEC staining. 170
Figure 5.9 – Comparing PI and CEC data outputs for DMSO toxicity. 172
Figure 5.10 – Time course measurements of STA toxicity in cardiomyocytes using PI. 174
Figure 5.11 – Time course measurements of STA toxicity in cardiomyocytes using CEC. 176
Figure 5.12 – Toxicity detected in cardiomyocytes treated with STA over 24 hr and stained with either PI or CEC. 177
Figure 5.13 – Comparing the rate of cell death at different concentrations of STA over the first 12 hours of the time course experiment. 178
Figure 5.14 – Determining the TD_{50} and EC_{50} of STA on cardiomyocytes after 24 hr with PI staining. 179
Figure 5.15 – Determining the TD_{50} and EC_{50} of STA on cardiomyocytes after 24 hr with PI staining. 181
Figure 5.16 – Measuring DOX toxicity over 24 hr with PI staining. 182
Figure 5.17 – Measuring DOX toxicity at 50 µM over 24 hr. 184
Figure 5.18 – Measuring DOX toxicity at 1 µM over 24 hr. 185
Figure 5.19 – DOX toxicity measured at 24 hr with Hoechst staining. 187
Figure 5.20 – Assessing toxicity of DEX over 24 hr. 189
Figure 5.21 – Assessing toxicity of CAR over 24 hr. 190
Figure 5.22 – Assessing toxicity of SIL over 24hr. 192
Figure 5.23 – Assessing toxicity of ISO over 24 hr. 193
Figure 5.24 – Quantification of DEX, CAR, SIL and ISO toxicity at 24 hr with Hoechst and PI staining. 194
Figure 5.25 – Quantification of 30 µM DOX-induced toxicity over 24 hr with or without co-treatment with rescue drugs. 197
Figure 5.26 – Quantification of 20 µM DOX-induced toxicity over 24 hr with or without co-treatment with rescue drugs. 198
Figure 5.27 – Quantification of 10 µM DOX-induced toxicity over 24 hr with or without co-treatment with rescue drugs. 199
Figure 5.28 – Quantification of 1 µM DOX-induced toxicity over 24 hr with or without co-treatment with rescue drugs. 200
Figure 5.29a – Quantification of DOX toxicity at 24 hr with Hoechst and PI staining. 202
Figure 5.29b – Quantification of DOX toxicity at 24hr with Hoechst and PI staining. 204
Figure 5.30 – Change in DOX plasma concentration in females over 24 hr. 209
Figure 5.31 – Change in CAR plasma concentration over 24 hr. 210
Figure 5.32 – Change in plasma concentration of SIL over 24 hr. 210

List of Tables

Table 2.1 – Cell lines used in this thesis. 23
Table 2.2 – Preparation of drug stocks for toxicity screening 40
Table 3.1 – Cell cluster size and frequency following harvest of CPVT hiPSCs with EDTA and TrypLE. 65
Table 3.2 – Commercial suppliers of hPSC derived cardiomyocytes and recommended seeding densities. 75
Table 4.1 – Effect of varying enzyme and temperature of incubation on EB formation and differentiation success. 108
Table 4.2 – Effect of increasing incubation time at room temperature and comparison of centrifugation and non-centrifugation prior to EB setup. 110

Abbreviations

ANOVA – Analysis of variance
AP – Arterial pole
AT1 – Adult tooth 1 hiPSC line
bFGF or FGF2 – basic fibroblast growth factor
BMP4 – Bone morphogenetic protein 4
cAP – cardiac action potential
CAR – Carvedilol
CDM3 – Chemically defined medium 3
CDS – Cell dissociation solution
CEC – CellEvent™ Caspase-3/7 Green Detection Reagent
cFBS – Cardiac differentiation-validated Foetal bovine serum
Chir – Chir99021
CPVT – Catacholaminergic polymorphic ventricular tachycardia
DAPI – 4',6-diamidino-2-phenylindole
DEX – Dexrazoxane
DM – Dorsal mesocardium
DMCT – Dunnet multiple comparison test
DMEM – Dulbecco's modified Eagle's medium
DMSO – Dimethyl sulfoxide
DOX – Doxorubicin
DPBS – Dulbecco's phosphate buffered saline
DPC – Days post coitum
E8 – Essential 8™ medium
EB – Embryoid Body
ECG – Electrocardiogram
ECM – Extracellular matrix
EDTA – Ethylenediaminetetraacetic acid
FBS – Foetal bovine serum
hERG – Human ether-a-go-go-related gene (also known as KCNH2)
hESC – Human embryonic stem cell
hiPSC – Human induced pluripotent stem cell
hPSC – Human pluripotent stem cell
Hr – Hour(s)
ICH – International Conference on the Harmonisation of Technical Requirements for the Registration of Pharmaceuticals for Human Use
ISO – Isoprenaline
ITS – Insulin Transferrin Selenium-X
LQT2 – Long QT syndrome type 2
LQTS – Long QT syndrome
LVEF – Left ventricular ejection fraction
Matrigel - Matrigel™ basement membrane matrix
MEF-CM – Mouse embryonic fibroblast conditioned medium
MEF – Mouse embryonic fibroblast
Min – Minute(s)
miPSC – mouse induced pluripotent stem cells
NCE – New chemical entities

NEAA – Non-essential amino acids
PFA – Paraformaldehyde
PI – Propidium Iodide
PVA – Poly(vinyl alcohol)
Robot – Freedom Evo 200 robotic platform
ROCKi – Y-27632 Rho associated protein kinase inhibitor
RPMI-I – Roswell Park Memorial Institute 1640 Insulin Transferring Selenium-X medium
RPMI – Roswell Park Memorial Institute 1640
RT- Room temperature
SCNT – Somatic cell nuclear transfer
SD – Standard deviation
Sec – Second(s)
SIL – Sildenafil
STA – Staurosporine
T/A – Trypsin / Accumax dissociation method
TGFβ – transforming growth factor beta 1
TMCT – Tukey multiple comparison test
USFDA – United States Food and Drug Administration
VP – Venous pole
Wnt-C59 – C59 Wnt antagonist

1 Introduction

1.1 *In vitro* drug testing and cardiotoxicity

In vitro safety testing of drugs is a core component of the drug development process and of considerable value to the pharmaceutical industry. Drug withdrawals due to toxicity undetected in the drug development process can prove costly, as drug development costs up to USD$1.5billion per drug (Rajamohan et al., 2013) with some estimates suggesting this could even be as much as USD$4billion (per drug that makes it to market) (Herper, 2012). As recently as 2010 drugs have been withdrawn from market due to cardiotoxicity which went undetected in the drug development process (such as propoxyphene and sibutramine) (Rajamohan et al., 2013). Thus, the need to develop effective screening strategies for such side effects is essential.

In vitro toxicity assessments allow pharmaceutical companies to "front-load" i.e. eliminate early in the development process, new chemical entities (NCEs) which may be unsuitable for further development due to unwanted side effects (Wakefield et al., 2002). Furthermore, the growing focus on NC3R (replace, reduce, refine) in relation to using animals in drug development, means suitable *in vitro* alternatives are needed (Lu et al., 2015). Cardiac arrhythmias are a common and potentially fatal side effect of adverse drug reactions. Drug interactions with the human *ether-á-go-go* related potassium channel (hERG) are a frequently observed side effect leading to arrhythmias in susceptible individuals (Eder et al., 2015) and

are therefore heavily tested in drug development (Lu et al., 2015) as a result of guidelines (S7B and E14) established at the International Conference on the Harmonisation of Technical Requirements for the Registration of Pharmaceuticals for Human Use (ICH) (Sager et al., 2014). This testing is frequently carried out using hERG expressing cell lines but these do not necessarily accurately model cardiomyocyte behaviour as the myocardium has compensatory mechanisms that may overcome effects detected in these lines and the effect of interplay or response from ion channels for example, are not accurately modelled in these systems (Eder et al., 2015). Additionally, the use of tissues from animals (such as canine or rabbit Purkinje fibres) also does not always accurately recapitulate the human phenotype in drug screens (Braam et al., 2010). Therefore, human heart tissue is the gold standard but limited by poor availability (Eder et al., 2015).

1.2 Embryonic stem cells, isolation from ICM

Derivation of human pluripotent stem cells (hPSCs) (Thomson et al., 1998) from the blastocyst stage (5 days post fertilisation (Gardner et al., 1998)) embryo, led to the generation of the first human embryonic stem cell lines (hESCs). These cells were capable of differentiation to constituents of all three germ layers; the ectoderm, mesoderm and endoderm (Thomson et al., 1998) and thus represented a valuable new tool for the development of regenerative medicine, drug screening applications and better understanding of developmental biology in humans (Thomson et al., 1998). Their differentiation capability, combined with the ability to proliferate indefinitely in an undifferentiated state meant that they could theoretically be used to create a near limitless supply of differentiated tissues. However, ethical concerns

regarding the use of fertilised human embryos to supply these cells and potential immunogenicity in regenerative therapy applications has slowed their translation to the clinic (Laflamme and Murry, 2011). Additionally, the lack of availability of genetic disease carrying embryos from which disease models could be derived, has limited their use in disease modelling (Tachibana et al., 2013).

1.3 Somatic cell nuclear transfer

Early experiments involving the transfer of nuclear material from *Rana pipiens* (Northern leopard frog) embryonic cells into the enucleated unfertilised egg from the same species demonstrated that normal tadpole formation could be achieved (Briggs and King, 1952). Subsequent experiments in *Xenopus laevis* demonstrated that monozygotic, sexually mature frogs could be generated by transferring nuclear material from later stage differentiating cell types and fertilised but non-enucleated eggs (Gurdon et al., 1958). Some years later, the nucleus of an adult mammalian somatic cell was transferred into an enucleated unfertilised egg of the same species (domestic sheep) which, following implantation into a surrogate sheep generated a viable offspring (Wilmut et al., 1997). This process, known as somatic cell nuclear transfer (SCNT) has been highlighted as a potential method for generating hESCs genetically matched to a donor (Chung et al., 2014, Tachibana et al., 2013); enabling generation of disease-carrying lines which could prove useful in disease modelling or for generating syngeneic hESCs for regenerative medicine applications. Despite the potential benefits of SCNT, it was not until 2013 that hESCs were successfully generated by this method (Tachibana et al., 2013) although this was only achieved using foetal and infant cells as donors. Since then, SCNT has been achieved using

dermal fibroblasts from older donors including a 35- and 75-year old (Chung et al., 2014). Exploitation of this method has been limited however due to the low survival efficiency of cloned animals (below 1-2 %) as well as phenotypic, molecular or physiological abnormalities thought to arise from incomplete genome reprogramming (Halley-Stott et al., 2013).

1.4 Human induced pluripotent stem cells

Having demonstrated that terminally differentiated cells could be driven to a pluripotent state with the correct signalling cues (Wilmut et al., 1997), subsequent studies sought to identify which cues were capable of inducing this reprogramming to a pluripotent state and were reviewed (Hochedlinger and Jaenisch, 2006). Shortly after this review, four growth factors (Oct3/4, Sox2, c-Myc and Klf4) were identified which following forced retroviral expression could cause differentiated mouse cells to reprogram to a pluripotent state similar to an embryonic stem cell with the ability indefinitely self-renew in culture and differentiate to constituents of the three germ layers (Takahashi and Yamanaka, 2006). This was subsequently achieved in humans a year later to generate the first human induced pluripotent stem cell lines (hiPSCs) by the forced expression of either *OCT4, SOX2, KLF4* and *c-MYC* (Takahashi et al., 2007) or *OCT4, SOX2, NANOG* and *LIN28* (Yu et al., 2007). These cells, sharing the same differentiation capability and indefinite proliferation capacity as hESCs have the advantage that they can be derived from donor differentiated cell types, similar to SCNT. This has enabled the possibility of generating autologous cell lines for regenerative therapy or for modelling diseases (Garbern and Lee, 2013).

Issues with retroviral and lentiviral reprogramming methods for example, which rely on the integration of reprogramming factors have driven researchers to develop non-integrating methods to avoid risks such as risk of tumourgenicity (Okita et al., 2008). Strategies including the use of minicircle DNA (Jia et al., 2010), episomal reprogramming, (Yu et al., 2011) integrating but excisable vectors (Woltjen et al., 2009, Somers et al., 2010), modified mRNA sequences (Warren et al., 2010), microRNA (Miyoshi et al., 2011), Sendai viruses (Fusaki et al., 2009) and even whole protein transduction (Kim et al., 2009) have been explored. There has also been focus on developing methods which improve the efficiency of reprogramming, as the original methods had reprogramming efficiencies of ~0.001–1 % (Takahashi et al., 2007) to ~0.1–1.1 % (Yu et al., 2007) while later methods achieved improvements of up to ~1 % with Sendai viruses (Fusaki et al., 2009) and ~1-4.4 % with modified mRNA (Warren et al., 2010).

1.5 Early heart development

Gastrulation in the developing human embryo involves the formation of the primitive streak and the specification of precursor cells into the three germ layers: mesoderm, endoderm and ectoderm (Richter et al., 2014). The primitive streak gives rise to the mesoderm from where cardiomyogenesis initiates. Brachyury and EOMES induce expression of MESP1 (Burridge et al., 2012), the master regulator of cardiac progenitor specification (Bondue and Blanpain, 2010). Downstream of MESP1, several interacting factors and genes including *Tbx5*, *Nkx2-5*, *Mef2c*, *Gata4*, *Hand2*, *Myocd*, *Isl1* and *Foxh1* all interact to promote specification to cardiogenic mesoderm (Burridge et al., 2012). From this stage, WNT and NOTCH signalling

regulate cardiac progenitor cell expansion and differentiation (Kwon et al., 2009). The cardiac mesoderm in turn develops into the first and second heart fields. Formation of cardiac tissue begins between 17-19 days post coitum (DPC) with the formation of the cardiac crescent (first heart field) adjacent to the endoderm from which agonists and antagonists of bone morphogenetic protein (BMP), fibroblast growth factor (FGF) and wingless type (WNT) growth factor families drive the cardiac differentiation process (Sylva et al., 2014). This is then followed by the formation of the cardiac tube 19-21 DPC (figure 1.1). The interior of the cardiac tube consists of endocardial cells and the exterior consists of myocardial cells (Burridge et al., 2012). The first and second heart field cells, when incorporated into the cardiac tube, respond to factors driven by Notch signalling (Grego-Bessa et al., 2007) and retinoic acid respectively and begin to proliferate (Sahara et al., 2015). The first heart field will give rise to the left ventricle and partially contribute to the atria while the secondary heart field gives rise to the right ventricle, parts of the atria and the outflow tract (Sahara et al., 2015).

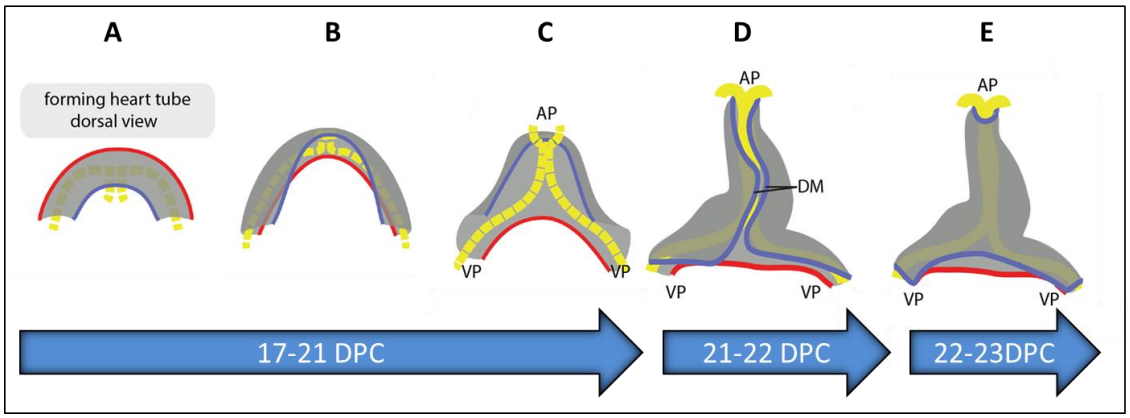


Figure 1.1 – Formation of the cardiac tube 17-23 DPC in humans
A) Flat cardiac crescent (peripheral border in red and central border in blue) transitions into a curved half-tube shape of cardiac mesoderm **(B).** This in turn expands to form an inverse T-shaped structure **(C)** with an arterial pole (AP) at the top and two venous poles (VP) at the base. **(D&E)** The central borders at the dosal

end of the developing heart (dorsal mesocardium (DM) fuse to form the cardiac tube (adapted from (Sylva et al., 2014)).

1.6 Cardiac repair and regenerative medicine

In light of the potentially life threatening effects of heart failure as well as the socioeconomic burden of heart failure worldwide, there is an ongoing effort to develop a therapeutic solution to enable repair of the damaged heart. Unfortunately, the only established method for treating heart failure is through heart transplant. This process, is limited by the lack of available organs and necessitates life-long immunosuppressive therapy and is not sufficient to meet current, let alone future demand (Garbern and Lee, 2013). The need for a more effective solution to this issue has led to the formation of two seemingly divergent approaches to addressing heart failure, generation of *de novo* cardiomyocytes *ex vivo* and transplanting these cells to the damaged heart or triggering endogenous cardiac repair mechanisms (Senyo et al., 2014).

1.6.1 Induction of endogenous cardiac repair mechanisms

In lower vertebrates such as zebrafish tissue regeneration has been observed in response injury of the spinal cord, retina and fins (Poss et al., 2002). A study investigating this process in zebrafish hearts found that when 20 % of the ventricular mass was resectioned, endogenous repair mechanisms were activated, starting with immediate localised blood clotting followed by a fibrin clotting stage between 2-4 and 7-9 days post injury. The fibrin clot was gradually replaced with *de novo* cardiomyocyte tissue from 9 to 30 days post injury until by 60 days post injury,

complete repair and restored cardiac function was observed with little or no evidence of scar formation (Poss et al., 2002). Later studies identified the source of this repair to originate from de-differentiation of existing terminally-differentiated cardiomyocytes and their subsequent proliferation following injury rather than repair by a pre-existing progenitor population (Jopling et al., 2010). Furthermore, this process was found to be mediated by the expression of *gata4*, a transcription factor gene associated with embryonic cardiac development which was absent in cardiomyocytes prior to injury (Kikuchi et al., 2010).

This finding has in turn led researchers to investigate whether adult cardiomyocytes in human hearts could be triggered to re-enter cell cycle and repair damaged cardiac tissue. Cardiomyocyte mitosis is detectable throughout life in humans but the process of cytokinesis only occurs in these cells up to 20 years of age (Mollova et al., 2013). Approaches so far have sought to influence developmental pathways that promote cardiomyocyte proliferation in the developing embryo but are then repressed later in life. An example of this is the Hippo tumour suppressor pathway which plays a role in controlling organ size and development (Zhao et al., 2011a). Hippo represses cardiomyocyte proliferation and studies of Hippo-deficient mice have shown that these mice could repair damaged myocardium post infarction (Heallen et al., 2013). Therefore, inhibition of Hippo or upregulation of Yes-associated protein (YAP), a downstream transcription coactivator inhibited by Hippo but capable of inducing cardiomyocyte proliferation (Xin et al., 2013) may provide a useful target for cardiac regeneration.

Neuregulin1 is another target that has been investigated; a growth factor and receptor tyrosine kinase agonist (primarily ErbB4) which is capable of inducing cardiomyocytes to re-enter cell cycle including cytokinesis *in vitro* with adult rat ventricular cardiomyocytes and *in vivo* in mice (Bersell et al., 2009). Furthermore, improved heart function following myocardial infarction was also demonstrated in mice following Neuregulin1 treatment (Bersell et al., 2009). This has since been followed up with two clinical studies in which improved left ventricular ejection fraction (LVEF) was observed (Gao et al., 2010, Jabbour et al., 2011) while several further studies are currently in progress or recently completed (Galindo et al., 2014).

Another approach has been to investigate the role of Micro RNAs (miRNA); short (approximately 20 nucleotides in length) sequences of RNA that regulate gene expression by binding to complementary sequences of messenger RNA (mRNA) causing post transcriptional repression (Bartel, 2009). Several reports have demonstrated that these can inhibit cardiomyocyte proliferation (ie. miR-1 and miR-133) but a more recent study identified 40 candidates that induced both DNA synthesis and cytokinesis in neonatal rat and mouse cardiomyocytes following a genome-wide miRNA library screen (Eulalio et al., 2012). Two candidates from this screen (hsa-miR-590 and has-miR-199a) were subsequently tested in a mouse model of myocardial infarction and demonstrated almost complete restoration of cardiac function (Eulalio et al., 2012).

1.6.2 Cell delivery for cardiac repair

1.6.2.1 Cell delivery of hESC or hESC-derived cell types for tissue repair

Delivery of hPSC-derived cells for tissue regeneration is another potential method by which tissue repair could be achieved. In animal models, differentiated hESCs have been used to treat spinal cord injury, diabetes milletus, Parkinson disease, liver failure and myelin diseases (de Almeida et al., 2013). Additionally, their low-level expression of major histo-compatibility complex class I and II molecules as well as expression of T cell proliferation inhibitors transforming growth factor β (TGF-B) and Serpin-6 led researchers to believe that these cells might be immuno-privileged (de Almeida et al., 2013). When the immunogenicity of hESCs was investigated in immune-competent mice, conflicting reports began to emerge either demonstrating no immune response (Li L et al., 2004), low level response (Drukker et al., 2006) or a significant immune response (Swijnenburg et al., 2008). In another series of experiments, hESCs were engrafted onto healthy or infarcted mouse myocardial tissue to assess whether endogenous factors could drive the differentiation of these cells to cardiomyocytes. In both cases, teratomas formed and there was no difference in the levels of cardiomyocyte differentiation in cardiac localised teratomas relative to control hind-limb teratomas (Nussbaum et al., 2007). Additionally, this study found that the differentiated cell types generated were immunogenic and that recipient mice required immune suppression (Nussbaum et al., 2007), an observation made by other groups as well (Drukker et al., 2006, Swijnenburg et al., 2008). Combined, the studies on immunogenicity and suitability of directly transplanted hESCs demonstrated that a more suitable approach would

require differentiating hESCs *in vitro* and transplanting these cells into recipients in conjunction with immunosuppressive therapy.

In 2010, Geron Corporation initiated the first human clinical trial investigating the use of hESC-derived progenitor cells (oligodendrocyte progenitor cells) to treat spinal cord injury (Strauss, 2010). However, due to cost considerations, the trial was abandoned before any efficacy data could be released although no safety concerns were observed (Frantz, 2012). This programme, has since been acquired by another company (BioTime Inc.) which has resumed development of this therapy (Brower, 2013). Another early clinical trial in this field carried out by Advanced Cell Technology, more recently published their first long term (up to 3 years in some patients) follow-up of a clinical trial investigating the use of hESC-derived retinal pigment epithelium cells for treating macular degeneration and Stargart's macular dystrophy. This revealed no adverse effects using these cells (no signs of unwanted proliferation, rejection (the eye is an immune-privileged tissue), ocular or other safety issues) (Schwartz et al., 2015).

A series of studies have been carried out in the last decade to demonstrate the feasibility of clinical applications of hESC derived cardiomyocytes for myocardial repair. This entailed developing scalable monolayer methods for cardiac differentiation of hESCs (Laflamme et al., 2007), establishing pre-clinical feasibility of hESC-cardiomyocyte delivery into infarcted tissues in rats (Fernandes et al., 2010, Xu et al., 2011), then in guinea pigs (Shiba et al., 2012), demonstrating coupling of engrafted cardiomyocytes to host cardiomyocytes (Shiba et al., 2012), suitability of

cryopreserved cardiomyocytes for tissue engraftment in rats (Xu et al., 2011) and finally a larger study in which $1x10^9$ cells were delivered into infarcted regions of non-human primate hearts of similar size and beat rate to human hearts (Chong et al., 2014). In this study, unlike previous studies in smaller mammals, all primates receiving hESC cardiomyocytes experienced arrhythmias in first month after administration however, these occurred without the loss of consciousness, or causing distress to the animals (Chong et al., 2014) and declined in frequency beyond several weeks post engraftment (Murry et al., 2014). Furthermore, there was no evidence of tumours, teratomas or human cells outside of the heart (Chong et al., 2014). While these studies involved intramyocardial injection of hESC-derived cardiomyocytes, others have investigated the potential of loading hESC-derived cardiomyocyte progenitor cells onto scaffolds to generate a "cardiac patch" for heart repair. hESCs were differentiated to cardiac progenitor cells and a quality control process carried out to quantify purity of cardiomyocyte progenitors (and lack of pluripotent cells), as well as microbiological and viral tests and cytogenetic studies to identify potential karyotype abnormalities. Cells that passed these criteria were delivered to immuno-compromised mice to identify any potential tumour or teratomas risk (of which there were none observed) and followed by trials where these cells were embedded in a fibrin patch and administered first in a rat myocardial infarction model and then a sheep myocardial infarction model (Menasche et al., 2015a). These studies demonstrated both the efficacy; both fibrin patch only and fibrin patch with cells improved LVEF significantly (the patch with cells gave greater improvement in function that patch-only) and safety of the procedure which in turn gained official approval for the first human trial using this

method (Menasche et al., 2015a). The subsequent human trial involved embedding $4x10^6$ hESC derived cardiomyocyte progenitor cells in a fibrin patch which was implanted into a human patient with severe heart failure post infarction (LVEF 26 %). At 3 months follow up, the patient was symptomatically improved (LVEF 36 %) with no evidence of arrhythmia or teratoma formation (Menasche et al., 2015b). It should be mentioned however that although promising, this represents a trial in one patient and for obvious ethical reasons; engraftment of cardiomyocyte progenitors to host myocardium had not been demonstrated. A subsequent study by the same group has since both confirmed in rats that the fibrin scaffold system used could itself induce a significant improvement in heart function post infarction and when loaded with hESC derived cardiomyocyte progenitors, this effect was increased further but importantly despite this, no grafted donor cells could be detected after 4 months (Bellamy et al., 2015).

1.6.2.2 Delivery of hiPSCs or hiPSC-derived cell types for tissue repair

An important limitation in the use of hESC-derived cell types for therapy (with the exception of the few tissues that are immune-privileged) is the risk of immune rejection and therefore, the requirement for immunosuppressive therapy. Current immunosuppression techniques while successful at preventing allograft rejection can, following long-term treatment be toxic to organs, increase cancer risk and susceptibility to infections (Fu, 2014). A potential benefit of hiPSCs compared to hESCs (for therapy) is that they can be derived from a patient requiring treatment and therefore act as an autologous cell source for tissue repair (Fu, 2014). Despite this, autologous mouse iPSCs (miPSCs) derived using non-integrating methods have

been shown to be immunogenic in syngeneic mouse models (Zhao et al., 2011b). Two studies subsequently demonstrated that terminally differentiated cells types derived from miPSCs and delivered to syngeneic recipient mice were not immunogenic (Araki et al., 2013, Guha et al., 2013). In a later study, these observations were also made in mice but also demonstrated that recipient mice developed tolerance to the engrafted cells (de Almeida et al., 2014). Furthermore, a comparison of miPSC-derived endothelial cells generated using either lentiviral-reprogramming (integrating) or second generation codon optimised minicircle (CoMiC)-reprogramming (non-integrating) found no difference in the level of immunogenicity from syngeneic recipients suggesting that reprogramming method may not play a role in immune response (de Almeida et al., 2014).

1.7 hiPSCs as disease models

The application of hiPSCs particularly in the field of disease modelling has seen a flurry of activity over the last 10 years (Gurdon, 2016). By deriving hiPSCs from individuals with certain genetic diseases, clinically relevant differentiated cell types have been generated to recreate disease conditions *in vitro*. This has enabled improved understanding of these diseases and facilitated drug screening in order to develop more effective methods of treatment. Disease models have been created for a range of disorders across different tissue types. Retinitis pigmentosa, a degenerative condition in the eye has been modelled with patient derived retinal cells showing internalisation of the surface marker rhodopsin and expressing markers of endoplasmic reticulum stress not seen in healthy controls (Jin et al.,

2012). Neurodegenerative conditions such as Alzheimer's, Parkinson's and Huntington's disease have also been modelled. In Alzheimers models, increased levels of amyloid β protein production and Tau protein were detected in patient derived hiPSCs relative to controls (Muratore et al., 2014) whereas in Parkinson's models, α-synuclein aggregation and formation of Lewy bodies occurred in patient hiPSC derived dopaminergic neurons (Ryan et al., 2013). In Huntington's models, increased cell toxicity was detected in neurons differentiated from hiPSC lines carrying longer CAG repeat sequences relative to controls (Consortium, 2012).

1.8 Properties of adult and foetal cardiomyocytes

Differentiation of hPSCs *in vitro* to cardiomyocytes generates cells that contract spontaneously, express ion channels needed to generate spontaneous action potentials and form sarcomeres to facilitate mechanical force generation (Yang et al., 2014). However, cardiomyocytes generated by these methods are typically considered more similar to foetal cardiomyocytes than to adult cardiomyocytes. These "immature" cardiomyocytes typically have a polygonal shape, disorganised sarcomeres, weaker contractile force, smaller action potentials compared to adult cardiomyocytes and tend to be mononuclear (Veerman et al., 2015). In regenerative therapy, these cells pose a risk of causing arrhythmias (Chong et al., 2014) therefore to mitigate this risk and to make these cells more closely resemble the adult phenotype for disease modelling and drug screening applications maturation strategies are required. Adult cardiomyocytes are rod shaped with an aspect ratio (length to width) of 5:1, have highly organised and aligned sarcomeres of greater length than immature cardiomyocytes and have a tendency to multinucleate

(approximately 30% binucleated in the adult heart) (Veerman et al., 2015). Sarcomeres in cardiomyocytes can be identified and their organisation determined by immunostaining for sarcomeric proteins including cardiac troponin T, cardiac troponin I, α-actinin and β-myosin heavy chain (Yang et al., 2014). Electrophysiologically, spontaneously beating cardiomyocytes can broadly be categorised as either ventricular, atrial or pacemaker based on their action potential profile which is typically measured by single-cell patch clamp techniques (Lin et al., 2015).

1.9 Cardiomyocyte action potentials

The cardiomyocyte action potential (cAP) is governed by the net effect of the ion channels and currents active during the cAP. The cAP can be divided into 5 different phases. Rapid influx of Na^+ ions through sodium channels (the I_{NA} current) causes the membrane to depolarise (upstroke, phase 0). Phase 1 involves brief efflux of K^+ which partially repolarises the membrane via the transient outward potassium current (I_{TO1}). Phase 2 is a plateau phase caused by the influx of Ca^{2+} through calcium channels ($I_{Ca\text{-}L}$ current). In phase 3 the K^+ delayed rectifier channels open to allow efflux of K^+ (I_{KR} and I_{KS} respectively) repolarising the cell to its resting membrane potential where it remains (phase 4) until the next depolarisation (Veerman et al., 2015).

1.10 Modelling cardiac channelopathies: long QT syndromes as disease models

1.10.1 Prevalence and clinical characteristics of the long QT syndromes

The long QT syndromes (LQTS) are a family of arrhythmogenic hereditary elecrophysiological disorders consisting of mutations identified in at least 15 different genes so far conferring an increased risk of developing arrhythmias and sudden death (Shigemizu et al., 2015). A study carried out across 18 maternity hospitals in Italy examined ~45,000 infants (51% male, 49% female) and found that approximately 1:2,000 of these were carriers of LQTS-associated mutations (Schwartz et al., 2015). Of the 15 different forms identified, the majority (approx. 75%) of identified cases fall within the first three types (30-35% LQT1, 25-30% LQT2 and 5-10% LQT3), approximately 20% have no known associated genes and 5% are covered by the remaining known LQTS types (Shigemizu et al., 2015). LQT1 is associated with mutations in *KCNQ1*, a gene encoding the α-subunit of the I_{KS} potassium rectifier channel, responsible for repolarisation in the heart (Wu et al., 2016). LQT2 is associated with mutations in *KCNH2* (hERG), a gene encoding the four α-subunits of the I_{KR} rapidly acting delayed potassium rectifier channel, also responsible for repolarisation of the heart (Smith et al., 2016). At elevated heart rates such as in response to adrenergic stimulation, individuals with LQT1 or LQT2 are at greater risk of developing arrhythmias (Malan et al., 2016). LQTS3 is associated with gain of function mutations in the *SCN5A* gene which encodes the α-subunit of the cardiac sodium channel responsible for the fast $Na_v1.5$ current, causing premature activation of the channel which at lower heart rates (in contrast to LQT1 and LQT2) increases the risk of arrhythmias (Malan et al., 2016).

LQTS typically manifest in patients as a prolongation of the QT interval on an electrocardiogram (ECG) (typically considered as >440 milliseconds in males and >460 milliseconds in females) despite having an otherwise structurally normal heart (Napolitano et al., 2012). However, the absence of a prolonged QT interval has been observed in asymptomatic carriers of the disease. Diagnosis of these cases can be achieved by monitoring patient electrocardiograms during stress tests including exercise (Hekkala et al., 2010) or pharmacological challenge using adrenaline or isoprenaline (for LQTS types 1 and 2) (Shimizu et al., 2003, Medeiros-Domingo et al., 2007). While potentially lethal, LQTS can be successfully managed with therapeutic intervention when it has been diagnosed. Treatment typically involves administering β-blockers (such as nadolol and propranolol), use of implantable cardioverter defibrillators and in the case of LQTS type 3, administration of sodium channel blockers (Medeiros-Domingo et al., 2007).

1.10.2 hiPSC models of long QT syndrome

By differentiating hiPSCs derived from individuals with LQTS associated mutations to cardiomyocytes, the disease phenotype could be recreated *in vitro.* This has been carried out for LQT1 (Moretti et al., 2010) and LQT2 (Itzhaki et al., 2011, Matsa et al., 2011). In these studies, LQT1 and LQT2 hiPSC derived cardiomyocytes had significantly longer action potential durations relative to control hiPSC derived cardiomyocytes mimicking the observed phenotypes of patients. These models were then validated by treating LQT1 or LQT2 cardiomyocytes with isoprenaline, causing early after depolarisations which were not observed in healthy hiPSC cardiomyocytes. In turn, these early after depolarisations were corrected by

administration of the β-blocker propranolol in LQT1 (Moretti et al., 2010) and either propranolol or nadolol in LQT2 cardiomyocytes (Matsa et al., 2011). LQT3 has also been modelled *in vitro* with LQT3 cardiomyocytes also showing significantly prolonged action potential durations relative to healthy hiPSC cardiomyocyte controls. In these studies, early after depolarisations were corrected by the addition of mexiletine, a sodium channel blocker (Ma et al., 2013, Malan et al., 2016).

By recreating the LQT disease phenotype *in vitro* these models could be used as predictive tools to identify potentially lethal QT prolonging side effects of novel or existing drugs or to screen for drugs that may confer a positive therapeutic effect. In LQT2 this was achieved with the potassium channel blockers E-4031 and cisapride (withdrawn from market due to its potassium channel blocking properties) which were shown to aggravate the disease phenotype by increasing the number of early after depolarisations observed (Itzhaki et al., 2011). Administration of either a calcium channel blocker (nifedipine), a potassium channel opener (pinacidil) or a late sodium channel blocker (ranolazine) were all shown to abolish early after depolarisations in an *in vitro* LQT2 model demonstrating the potential therapeutic application of these compounds in managing LQT2 (Itzhaki et al., 2011).

1.11 Other cardiovascular disease models

Furthermore, in the cardiac field, disease models have been generated for other cardiac specific diseases beyond cardiac channelopathies. Intercellular communication disorders such as arrhythmogenic right ventricular cardiomyopathy

have been studied; a disease associated with mutations in mechanical cell junction protein related genes (Caspi et al., 2013). hiPSC derived cardiomyocytes from two patients carrying these mutations showed abnormal desmosome (cell-cell junction protein) formation and decreased expression of desmosomal protein, plakoglobin as well as significant reductions in gap junction density. These cells also demonstrated decreased excitability or conduction, and greater susceptibility to apoptosis when stressed, compared to healthy controls (Caspi et al., 2013). Cardiomyocyte dysfunction diseases such as familial dilated cardiomyopathy, a condition associated with left ventricular dilation and systolic dysfunction leading to heart failure (Serio et al., 2012) has also been modelled where patient hiPSC derived cardiomyocytes carrying a mutation in the cardiac troponin T gene demonstrated altered Ca^{2+} handling and abnormal distribution of sarcomeric α-actinin, hampering contractility of these cells *in vitro.* Challenging these cells with noradrenaline led to a decrease and ultimately loss of spontaneous contractile behaviour and degeneration of cellular myofilaments, indicative of stress induced damage not seen in control cells (Sun et al., 2012). Duchenne muscular dystrophy is a disease that affects both skeletal muscle and cardiac tissue. In the heart, this can lead to dilated cardiomyopathy (Lin et al., 2015). Cardiomycoytes generated from patient derived hiPSC lines show reduced dystrophin expression levels, increased levels of mitochondrial damage and elevated cell apoptosis *in vitro* consistent with the disease phenotype in patients (Lin et al., 2015).

1.12 Thesis Aims

The hypothesis of this thesis is that automation of culture and cardiomyocyte differentiation has the potential to produce large quantities of hiPSC derived cardiomyocytes needed for regenerative medicine applications (estimated at up to 10 billion per patient) (Chong et al., 2014) or drug screening assays. Large numbers of compounds are synthesised annually (estimates suggest up to 5 million novel compounds registered annually (Lu et al., 2015)). Compounds destined to be developed as potential therapeutics would need to be tested for potential cardiotoxic side-effects necessitating large numbers of cells and high throughput analysis capability (Lu et al., 2015). The liquid handling apparatus of the Freedom Evo 200 platform (namely the 96-well head) could offer benefits in terms of speed of plating and medium change in 384-well plates over doing this manually, making it amenable to high throughput drug screening. It is also likely that automation would reduce operator variability in cell handling and experimentation (Conway et al., 2015).

The following objectives have been set for this thesis:

1) Adopt and if needed, modify an existing method and culture system that can be used to differentiate hiPSCs to cardiomyocytes. Develop processes for the dissociation, cryopreservation, resuscitation, seeding and maintenance of hiPSC derived cardiomyocytes for use in drug screening assays. [Chapter 3]

2) Develop an automated differentiation process on the Freedom Evo 200 robotic platform using the chosen method(s) from 1). Automate the process of setting up drug screening experiments including cell seeding, cell maintenance and drug compound addition to cells in 384-well plates (to enable high throughput screening). Use the Operetta confocal plate reader to scan plates (96- and 384-well) and design analysis algorithms to accurately quantify drug toxicity in drug screening experiments to enable high throughput analysis of experiments. [Chapter 4]

3) Develop a drug screening assay which is both accurate and sensitive enough to quantify drug toxicity in real time and end point experiments. Use this platform to identify whether *in vitro*, cardioprotection can be achieved using dexrazoxane, carvedilol, sildenafil or isoprenaline in co-treatment studies with doxorubicin. [Chapter 5]

2 Experimental Methods

2.1 Routine Cell Culture

All manual cell cultures were carried out in a class 2 biological safety cabinet without the use of antibiotics unless otherwise stated. Brightfield images of cell cultures were taken on a Nikon Eclipse TE2000-S inverted light microscope with Hoffman objective (Nikon microscope).

Table 2.1 – Cell lines used in this thesis.
Four human pluripotent stem cell lines were used to generate the data presented in this thesis, one being a hESC line (HUES7) and three being hiPSC lines (AT1, CPVT and LQTS2). Mouse embryonic fibroblasts were also used for the purpose of conditioning medium (see section 2.11).

Cell line	Origin	Description
HUES7	Human	Embryonic stem cell line
Mouse Embryonic Fibroblasts	Mouse	13.5-day old mouse embryos
AT1 hiPSC	Human	Human induced pluripotent stem cell line derived from a non-disease carrying patient using lentiviral vectors for *OCT4*, *SOX2*, *LIN28* and *NANOG*.
CPVT hiPSC	Human	Human induced pluripotent stem cell line derived from a patient with Catacholaminergic polymorphic ventricular tachycardia-1 using Sendai-virus based CytoTune 2.0 system
LQTS2 hiPSC	Human	Human induced pluripotent stem cell line derived from a patient with Long QT Syndrome Type 2 using Sendai-virus based CytoTune 2.0 system

2.1.1 Mouse embryonic fibroblast preparation and conditioned medium

Mouse embryonic fibroblasts (MEFs) were isolated from 13.5-day old mouse embryos. These were collected by sacrificing the pregnant female by cervical dislocation, removing the uterine horns and collecting the mouse embryos which were sacrificed by decapitation. Embryos were kept in Dulbecco's phosphate buffered saline (DPBS) (ThermoFisher Scientific, 14190-169), homogenised mechanically and by enzymatic dissociation using 0.25 % Trypsin EDTA (ThermoFisher Scientific, 10780384) and plated for expansion on 175 cm^2 T175 flasks (Nuclon Δ treated surface, ThermoFisher Scientific, 178883) with MEF culture medium. MEF culture medium was made using Dulbecco's Modified Eagle's Medium (DMEM, ThermoFisher Scientific, 10749764), 10 % (v/v) foetal bovine serum (FBS, ThermoFisher Scientific, 10664083), 1 % (v/v) L-Glutamine (ThermoFisher Scientific, 10104042) and 1 % (v/v) non-essential amino acids (NEAA, ThermoFisher Scientific, 10358342). Cultures were incubated at 37 °C and 5 % CO_2 in a humidified incubator (Heracell 150). Passaging MEFs for expansion and for cryopreservation was carried by washing with DPBS, harvesting with 0.05 % trypsin EDTA (ThermoFisher Scientific, 10462502) for 1 min, neutralising with MEF culture medium, centrifugation at 200 g for 5 min (3-16 Sigma centrifuge) and re-plating in fresh MEF medium. Cryopreserved stocks of MEFs were made at passage 1 by harvesting and then re-suspending cells after centrifugation in 10 % (v/v) DMSO (Sigma, D2650), 40 % (v/v) FBS and 50 % (v/v) MEF medium. Cell suspension was transferred to 1.8 ml cryotube™ vials (cryovials) (ThermoFisher, 377267) and stored at -80 °C for 24 hr in a Mr. Frosty™ Freezing container ((Mr. Frosty) Fisher Scientific, 5100-0001) containing isopropanol before transfer to liquid nitrogen.

For generating MEF conditioned medium (MEF-CM), MEFs were thawed from liquid nitrogen, cultured to passage 3 where they were seeded on 0.1 % Gelatin- (Sigma, G9391) coated flasks and treated with Mitomycin C (ThermoFisher Scientific, 10286710) at a concentration of 10 µg/ml in MEF medium and seeded at a density of $4.8x10^6$ cells per 75 cm^2 flask (T75, Nuclon Δ treated surface, ThermoFisher Scientific, 156472). MEF-CM was generated by incubating MEFS in hESC medium containing DMEM Ham's F12 (DMEM-F12) (Fisher Scientific, 11320-074), 15 % (v/v) KnockOut™ Serum Replacement (Fisher Scientific, 10236902) 1 % (v/v) NEAA, 1 % (v/v) Glutamax (Fisher Scientific, 10388582) 0.01 % (v/v) β-mercaptoethanol (Sigma, M7522) and 4 ng/ml human basic fibroblast growth factor (FGF, Peprotech, EC100-18) for 24 hr, after which this medium was harvested. After 7 days, MEF cultures were discarded. Multiple MEF batches were used over the course of this work. Each batch of MEFs corresponded to a different mouse from which embryos were taken.

2.1.2 Coating flasks in Matrigel™

hPSCs were routinely cultured on Matrigel™ basement membrane matrix (Matrigel) (BD Biosciences, 354234) coated flasks. Matrigel coating was achieved by diluting stock Matrigel 1:100 in cold (4 °C) DMEM, and coating 200 µl/cm^2 of surface area. Matrigel was left at room temperature (RT) for 45 min (or overnight at 4 °C) to fully polymerise. Matrigel flasks were stored at 4 °C for up to one week. Before use, medium was aspirated from Matrigel coated flasks, equal volume of PBS added and flasks were left at 37 °C to warm up prior to seeding cells.

2.1.3 Culture of human embryonic stem cells in MEF-CM

For HUES7 hESC culture and embryoid body (EB) cardiomyocyte differentiations, 25 cm^2 flasks (T25, Nunclon Δ treated surface, ThermoFisher Scientific, TKT-130-150L) were routinely used. Cultures were fed daily with MEF-CM containing 8 ng/ml FGF. Cells were passaged by washing once with 5 ml DPBS, then adding 0.5 ml of 0.05 % trypsin EDTA in a T25 (or 20 µl per cm^2 of surface area) for 1 min at 37 °C. Flasks were tapped to dislodge cells, and trypsin neutralised by adding hESC medium. Cells were centrifuged at 160 g for 4 min and cell pellets were re-suspended in fresh MEF-CM. Cell counts were carried out using a haemocytometer loaded with 20 µl cell suspension and seeded at a density of $1.25x10^6$ cells per T25 (50,000 cells per cm^2). Cultures were incubated at 37 °C and 5 % CO_2 in a humidified incubator.

2.1.4 Human pluripotent stem cell culture in mTeSR medium

hPSC lines (primarily the HUES7 hESC line and AT1 hiPSC line) were adapted for culture in mTeSR™1 (mTeSR, Stem Cell Technologies, 05850) on Matrigel coated flasks. Medium changes were carried out every 24 hr. Cells were passaged by incubation with 0.5 ml Accutase® solution (accutase) (Sigma, A6964) for 3 min at 37 °C, enzyme was neutralised with hESC medium and cells were pelleted by centrifugation at 160 g for 4 min. Cells were counted using a haemocytometer and seeded at $2x10^6$ per T25 flask (89,000 cells per cm^2). Cultures were incubated at 37 °C and 5 % CO_2 in a humidified incubator.

2.1.5 Human pluripotent stem cell culture in Essential-8™ (E8) medium

E8 culture was carried out using either HUES7 hESCs transitioned to E8 from mTeSR (which were previously transitioned to mTeSR from MEF-CM) or the CPVT and LQT2 hiPSC lines that were derived in E6 and cultured in E8 (see Chapter 3, sections 3.2.10 and 3.2.11 respectively for derivation details). Cells were cultured on Matrigel coated flasks and passaged using 0.5 mM EDTA (ThermoFisher Scientific, 15575-038) when cultures reached 70 % confluence. This involved washing cells with DPBS, adding EDTA to the cells, incubating at RT for 4-7 min depending on cell line until cells began to detach from the culture surface. After incubation, EDTA was gently aspirated to avoid disturbing cells and then the flask was tapped to dislodge cells. E8 medium containing 10 µM Y-27632 ROCK inhibitor (ROCKi) (R&D Systems, 1254/10) was then added to the flask to achieve a cell suspension. Cells were re-seeded as a ratio; either 1:4 in the first 2 passages after thaw or 1:6 to 1:8 depending on the growth rate of the cells thereafter, ensuring that confluence of cultures reached approximately 70 % after 72 hr. A medium change was carried out 24 hr after passage and at 24 hr intervals thereafter using fresh E8 without ROCKi. Later, for the purpose of carrying out growth curves, cell counts were carried out using a haemocytometer and cells were seeded at 40,000 cells per cm^2 ($1x10^6$) in T25 flasks or 32,000 cells per cm^2 ($3x10^6$ cells) in RoboFlasks. This method was then further modified to facilitate single-cell passaging using TrypLE™ Select 1x (TrypLE) (ThermoFisher Scientific, 12563029). This involved carrying out the same procedure as EDTA but TrypLE exposure was set to 4 min at RT (consistent between all lines). As with the EDTA method, cells were seeded in E8 containing 10 µM ROCKi.

2.1.6 Growth curves

In order to assess the growth kinetics of cells, growth curves were carried out with the culture conditions described in 2.1.3, 2.1.4 and 2.1.5. This involved passaging cells, carrying out a cell count to determine total cell yield and then seeding a fixed number of cells into a fresh flask. The number of cells seeded was kept the same for all passages in the growth curve and ≥5 passages were carried out for all growth curves. Cumulative population doublings and population doubling time were both calculated (Denning et al., 2006):

$$\textbf{Cumulative population doublings} = \sum \left(\frac{\textbf{Log}_{10}\ \textbf{Number of Cell Doublings}}{\textbf{Log}_{10}(2)} \right)$$

$$\textbf{Population doubling time (hr)} = \frac{\textbf{Total time in culture (hr)}}{\textbf{Cumulative population doublings}}$$

2.1.7 Fixing cells for karyotype assessment

To prepare a sample for karyotype assessment, cells in log phase of growth (to maximise the chance of getting metaphase spreads) were treated with 0.1 µg/ml Karyomax Colcemid (ThermoFisher Scientific, 15212-012) for 2 hr to halt the cells in metaphase. After this incubation, cells were harvested using the passaging methods described in 2.1.2, 2.1.3 or 2.1.4. Hypotonic solution was prepared (0.6 % sodium citrate (ThermoFisher Scientific, S/3320/53) in sterile water (Baxter, UKF7114)) and fixing solution was prepared (5:1 ratio of methanol (ThermoFisher Scientific, M/4000/17) to acetic acid (ThermoFisher Scientific, A/0400/PB17)). The pellet of cells from the cell harvest was then re-suspended in 10 ml of hypotonic solution by

adding dropwise on a vortex. Cells were incubated for 10 min to swell. Cells were centrifuged at 700 g for 4 min, supernatant was aspirated and cells were re-suspended in 10 ml fix solution by adding dropwise on a vortex. This step was repeated twice after which, cells were re-suspended in 1 ml of fix solution and stored at -20 °C. Samples were then posted to Nigel Smith of the Cytogenetics group at Nottingham City Hospital where the rest of the karyotype procedure was carried out and results collected.

2.2 Cardiomyocyte differentiation protocols

2.2.1 EB cardiomyocyte differentiation method

HUES7s cultured in MEF-CM were passaged and seeded at $2x10^6$ cells per T25 (80,000 cells per cm^2) 24 hr before (day-1) starting differentiation. On the day of differentiation (day 0), HUES7s were passaged again and seeded at 4,000 cells per well of a 96 well V-bottom plate (ThermoFisher Scientific, 249662) in 100 µl/well final volume of day 0 medium (RPMI 1640 (RPMI, ThermoFisher Scientific, 21875-034) with 4 mg/ml (w/v) Poly(Vinyl Alcohol) (PVA, Sigma, P8136), 1 % (v/v) Insulin Transferrin Selenium-X (ITS) (ThermoFisher Scientific, 51500-056), 1 % (v/v) Chemically Defined Lipid Concentrate (Lipid Concentrate, ThermoFisher Scientific, 11905-031), 400 µM 1-Thioglycerol (Sigma, S5442-2ML), 20 ng/ml Bone morphogenetic protein 4 (BMP4, R&D Systems, 314-BP-010), 6 ng/ml bFGF to form EBs. On day 2, this medium was removed and replaced with day 2 medium (RPMI, 20 % (v/v) Cardiac differentiation-validated FBS (cFBS) (PAA Laboratories, A15-101) and 400 µM 1-Thioglycerol. On day 4 this medium was replaced with RPMI-I medium (RPMI, 1 % (v/v) ITS, 1 % (v/v) Lipid Concentrate, 400 µM 1-Thioglycerol)

and EBs were transferred to 96 well U-bottom plates (Nunclon Δ treated surface) (ThermoFisher Scientific, TKT-180-050D). Images of EBs were taken using the Nikon microscope immediately after transfer to U-bottom plates to record quality of EB formation and to compare EB sizes. Later in this thesis, this process was carried out using the Cellavista to record the sizes and appearance of all the EBs in each plate. The next medium change was carried out on Day 8 using RPMI-I. Afterwards medium changes took place every 4-5 days with RMPI-I or RPMI-B27 (RPMI and 2 % (v/v) B27 supplement (ThermoFisher Scientific, 0080085-SA)). Plates were incubated at 37 °C, 5 % CO_2 throughout the differentiation. Efficiency of differentiation was determined by screening plates on Day 10 for wells containing beating cells and efficiency was calculated by:

$$\textbf{Proportion of Beating EBs} = \left(\frac{\textbf{Number of wells with beating EBs}}{\textbf{Number of wells containing EBs}}\right)\textbf{x100}$$

2.2.1.1 EB purification by lactate treatment

EB cardiomyocyte enrichment experiments were carried out using cardiomyocyte enrichment medium containing RPMI with no glucose and no pyruvate (ThermoFisher Scientific, 11879-020) supplemented with 4mM lactate (Sigma, 71717-10G) (Tohyama et al., 2013). Cardiomyocyte enrichment medium was substituted for normal RPMI-B27 medium on feed days and EBs were “recovered” by feeding for 48 hr in RPMI-B27 medium prior to harvesting.

2.2.2 mTeSR monolayer method differentiation to cardiomyocytes

HUES7 hESCs and hiPSC lines adapted to mTeSR culture conditions were passaged and seeded at a density of 80,000 cells per cm^2 in T25 format ($2x10^6$ cells) and 65,000 cells per cm^2 in T75 ($4.8x10^6$ cells) and RoboFlask® (RoboFlask) format ($6x10^6$ cells). Cells were grown to confluence of between 80 % and <100 % (measured by Cellavista in RoboFlasks, assessed by eye in T25 and T75). At this point, cells were treated with day 0 differentiation medium consisting of StemPro34 SFM (ThermoFisher Scientific, 10640-019) and 2 mM L-Glutamine, BMP4, 10 ng/ml and recombinant human activin A (activin A), 8 ng/ml (ThermoFisher Scientific, VXPHC9564) to initiate differentiation. On day 2 and day 4, medium was replaced with RPMI-B27 medium containing 10 µM of KY02111 (R&D Systems, 4731/50) and 10 µM XAV939 (R&D Systems, 3748/50) (termed day 2/4 medium). From Day 6 onwards, medium was changed every 3 days using RPMI-B27 only.

2.2.3 E8 monolayer method differentiation to cardiomyocytes

To initiate cardiomyocyte differentiation using the E8 monolayer differentiation method, cells were cultured up to between 80 % and 100 % confluence. Differentiations were carried out using chemically defined medium 3 (CDM3) consisting of RPMI, 213 µg/ml L-Ascorbic acid 2-phosphate (Sigma, A8960) and 500 µg/ml recombinant human albumin (Sigma, A0237). At the start of differentiation (day 0) CDM3 was supplemented with 4 µM Chir99021 (Chir) (Tocris Bioscience, 4424). At day 2 of differentiation this medium was replaced with CDM3 with 2 µM C59, Wnt antagonist (Wnt-C59) (Abcam, ab142216). At day 4, medium was replaced

with CDM3 only and medium exchanges were carried out every 48 hours thereafter with fresh CDM3.

2.3 Cardiomyocyte dissociation methods

2.3.1 EB cell dissociation solution method

The cell dissociation solution (CDS) method was carried out on EB differentiations as part of EB dissociation method testing and carried out in 96-well plates. CDS was prepared as a 4:4:2 ratio of RPMI, Trypsin 0.05 % and Cell Dissociation Buffer (Enzyme Free Hanks' Based) (ThermoFisher Scientific, 13150-016). EBs were washed with DPBS, then incubated in 100 µl CDS per well for 6 min at 37 °C and gently pipetted after 4 min. CDS was then neutralised by adding 150 µl FBS per well and well contents pipetted to dissociate EBs. Contents were then transferred to an Axygen 1.7 ml polypropylene microcentrifuge tube (microcentrifuge tube) (Corning, MCT-175-C). Cell suspension was then centrifuged at 300 g for 3 min (Sigma 1-14). Supernatant was removed and cell pellets re-suspended in RPMI-B27 with 10 % (v/v) cFBS and plated. After 24 to 48 hr depending on degree of cell attachment, medium was changed to RPMI-B27 only and subsequent medium changes carried out every 3 to 4 days.

2.3.2 Trypsin / Accumax methods

2.3.2.1 EB dissociation

Trypsin/Accumax (T/A) was prepared by combining trypsin 0.05 % and Accumax (Patricell, ATM105) at a 1:1 ratio. EBs were washed with DPBS, then transferred to

microcentrifuge tubes containing T/A and incubated at 37 °C for 3 min. After 3 min, EBs were agitated by gentle pipetting to encourage dissociation using a P200 pipette. If EBs were not fully dissociated, tubes were returned to 37 °C for a further 3 min. This process was repeated until EBs fully dissociated. Enzyme was then quenched by adding equal volume of RPMI with 20 % (v/v) cFBS to this suspension. Cells were then centrifuged at 300 g for 2 min, supernatant was removed and cells were re-suspended in RPMI-B27 with 10 % (v/v) cFBS and plated.

2.3.2.2 mTeSR monolayer method dissociation

Monolayer cardiomyocyte differentiations were dissociated by washing cells with DPBS, adding T/A (5 ml in T75 and 7 ml in RoboFlask) and incubating for 10 min at 37 °C. Flasks were then gently tapped to dislodge cells and RPMI-B27 with 10 % (v/v) cFBS added to quench enzyme. Cell suspension was pipetted using a 5 ml pipette to dissociate cell aggregates and centrifuged at 300 g for 3 min. Cell counts if desired, were carried out at this stage using a haemocytometer. Supernatant was then aspirated and the cell pellet re-suspended in RPMI-B27 with 10 % (v/v) cFBS and plated. Medium was changed on these cells either 24-48 hr after seeding depending on the level of cell attachment and every 3-4 days thereafter.

2.3.3 EB cold dissociation method

EBs were washed three times in DPBS, 100 µl CDS solution was added to the clusters and these were then incubated at 37 °C for 10 min. CDS was then removed without disturbing the EBs. 100 µl of RPMI-B27 was then added to the EBs which

were then incubated at 4 °C for 30 min. After incubation, cells were pipetted repeatedly to dissociate clusters. Cells were then plated in RPMI-B27 with 10 % (v/v) cFBS. After 24-48 hr depending on the attachment of cardiomyocytes, medium was then changed to RPMI-B27 without FBS and cells were maintained in this medium throughout by carrying out medium changes every 3-4 days.

2.3.4 E8 monolayer dissociation methods

2.3.4.1 Sequential TrypLE method

E8 monolayer differentiations were dissociated by washing cells with DPBS and then adding TrypLE and incubating for 10 min at 37 °C. Flasks were gently tapped to dislodge cells, enzyme and cells in suspension were collected and centrifuged at 300 g for 3 min. Meanwhile, remaining cells still attached to the flask surface were treated with fresh TrypLE for another 10 min at 37 °C. Cells harvested from this were then centrifuged at 300 g for 3 min. After spins, supernatant was aspirated and RPMI-B27 with 10 µM ROCKi added to the cells. All cells harvested from both rounds of enzyme treatment were pooled and then plated. Depending on the level of cell attachment, medium was aspirated and replaced with fresh RPMI-B27 after 24 or 48 hr and every 3 to 4 days thereafter.

2.3.4.2 Collagenase and TrypLE Express method

Due to high levels of cell death observed with the sequential TrypLE method, the process was modified to introduce a collagenase digestion step. To dissociate cardiomyocytes by this method, CDM3 was aspirated, cells were washed with HBSS

containing magnesium and calcium (HBSS) (ThermoFisher Scientific, 14025-050) and collagenase type 2 (collagenase)(ThermoFisher Scientific, 17101-015) at 500 U/ml was added for 20 min at 37 °C. Following collagenase treatment, cardiomyocyte sheets detached from the culture surface. Cells and collagenase were transferred to a 30 ml universal tube (ThermoFisher Scientific, 128C) and centrifuged at 300 g for 3 min. Supernatant was aspirated and cells were washed with 5 ml of DPBS. Cells were centrifuged again and TrypLE Express (ThermoFisher Scientific, 12604013) was added. Cells were gently agitated by periodically tapping the tube to encourage dissociation of aggregates at approximately 1 min intervals. After 10 min, cell suspension was pipetted gently (one second up, one second down) using a P1000 Gilson pipette to generate a single-cell suspension which was in turn, centrifuged at 300 g for 3 min. Cells were then re-suspended in RPMI-B27 containing ROCKi at 10 µM and plated. A medium change was carried out after 48 hr using fresh RPMI-B27 without ROCKi and subsequent medium changes were carried out at 3 to 4 day intervals thereafter.

2.4 Cryopreservation of cardiomyocytes

2.4.1 Cryopreservation of cardiomyocytes from EB and mTeSR monolayer differentiation methods

For cryopreservation of cardiomyocytes generated by the EB or mTeSR monolayer differentiation methods, cells were dissociated using the T/A dissociation methods mentioned in 2.3.2.1 (EB) or 2.3.2.2 (monolayer). Following the centrifugation step, supernatant was aspirated and the cell pellet was re-suspended in freezing mix

consisting of 90 % (v/v) cFBS and 10 % (v/v) DMSO and dispensed into cryovials. Cryovials were kept in a Mr. Frosty for 24 hr at -80 °C before transferring to liquid nitrogen.

2.4.2 Cryopreservation of cardiomyocytes from E8 monolayer differentiation method

Cardiomyocytes were cryopreserved following both the sequential TrypLE method and the Collagenase / TrypLE Express method. For both, single cell suspensions were counted, re-suspended in RPMI-B27 containing 10 % (v/v) DMSO, and seeded into cryovials at $1x10^6$ cells per vial. Cryovials were stored in a Mr. Frosty for 24 hr at -80 °C before transferring vials to liquid nitrogen. Cardiomyocytes were thawed by rapidly warming cryovials to 37 °C in a water bath for 1 min, and then gently transferring the contents of a vial into 9 ml of RPMI-B27 in a 30 ml Universal tube. The cell suspension was then centrifuged at 300 g for 3 min. Supernatant was aspirated and the cell pellet re-suspended in RPMI-B27 containing 10 µM ROCK inhibitor. The cell suspension was then plated and the first medium change carried out after 48 hr with RPMI-B27 only. Subsequent medium changes were carried out at 2-3 day intervals thereafter.

2.5 Cardiomyocyte quantification

2.5.1 Immunostaining of plated cells

Cardiomyocytes requiring immunostaining were fixed in 4 % Paraformaldehyde (4% PFA) (Sigma, P6148) for 15 min at RT. Cells were then washed 3 times in DPBS and

stored in DPBS at 4 °C for no longer than one week. On the day of staining, cells were permeabilised by incubating in 0.1 % (v/v) Triton-X100 (Sigma, T8532-100 ml) diluted in DPBS for 15 min at RT. Cells were then washed 3 times with 1 min incubations in DPBS, then incubated with 4 % goat serum (Sigma, G9023-10 ml) for 1 hr at RT. After this incubation, cells were incubated in primary antibody, either; α-actinin antibody (monoclonal IgG1 anti-α-actinin (sarcomeric) antibody produced in mouse, used at 1:800, Sigma, A7811) or cardiac troponin T (Troponin T-C monoclonal IgG_{2a} antibody raised in mouse, used at 1:500, Santa Cruz Biotechnology, sc-20025) in 4 % (v/v) goat serum overnight at 4 °C. The next day, 3 washes of 10 min were carried out using 0.1 % (v/v) Tween20 (Sigma, P9416) in DPBS. Cells were then incubated with secondary antibody (i.e. Goat anti-mouse Alexa Fluor® 488 IgG, used at 1:400, ThermoFisher Scientific, A11001) in 4 % (v/v) goat serum for 1 hr at RT protected from light. Cells were washed 3 times with 5 min washes in 0.05 % (v/v) Tween20 in DPBS. After this, cells were incubated in DAPI (1:1000, Sigma, D9542) diluted in DPBS for 10 min at RT then washed once with DPBS and imaged.

2.5.2 Immunostaining of cells for flow cytometry

Cells for immunostaining by flow cytometry were harvested by the appropriate cardiomyocyte dissociation method depending on the method by which they were differentiated. Cells were pelleted, this pellet was washed with DPBS and the pellet was then re-suspended in 4 % PFA and incubated for 15 min at RT. After incubation, the cell pellet was centrifuged at 300 g for 2 min, washed with DPBS and centrifuged again at 300 g for 2 min. Cells were then re-suspended in 20 % (v/v) FBS

in PBS and stored at 4 °C for up to 1 week. On the day of staining, cells were permeabilised by re-suspending in 0.1 % (v/v) tritonX-100 in PBS for 15 min. Cells were centrifuged at 500 g for 2 min, washed in 0.1 % (v/v) Tween-20 in PBS and centrifuged at 500 g for 2 min again. The cell pellet was then incubated in 10 % (v/v) goat serum for 30 min, centrifuged at 500 g for 2 min, incubated for 1 hr at RT in primary antibody (α-actinin 1:800 or cardiac troponin T 1:500) then centrifuged at 500 g for 2 min. Cells were washed twice with 0.1 % (v/v) Tween-20 in DPBS and incubated with secondary antibody (goat anti-mouse Alexa Fluor® 488, 1:400) for 45 min made up in in 10 % (v/v) FBS in DPBS at RT protected from light. Cells were then centrifuged at 500 g for 2 min, washed twice with 0.1 % (v/v) Tween-20 in DPBS and re-suspended in DPBS then run through a flow cytometer (FC500 Beckman Coulter).

Flow cytometry data were analysed using FlowJo analysis software (FlowJo LLC.). Marker-positive cells were determined by drawing “gates” (regions that demarcate a lower fluorescence and higher fluorescence threshold, selecting cells with fluorescence which fell within this range). The lower threshold of these selection gates where set to include between 0 and 1 % of secondary antibody-only stained control populations (a negative control) in order to be able to quantify any increase in fluorescence relative to this control population. Later, as the flow cytometry method was further optimised, pluripotent cells or fibroblasts were used as cell type controls (stained with both primary and secondary antibody but negative for the chosen marker) and gates were drawn as before using these populations to determine increases in fluorescence that marked positive cells.

2.6 Drug screening protocols

2.6.1 Quantifying cell viability using Calcein AM, Propidium iodide and Hoechst33342

Early cell viability quantification work was carried out using the ROCHE Cell Viability Imaging Kit 5x96 (Roche, 06432379001) consisting of propidium iodide (PI), Calcein AM and Hoechst33342 (Hoechst). Reagent stocks were prepared as per the kit instructions. For staining cells, staining medium was prepared consisting of DPBS, Hoechst (1:000 dilution), PI (1:200 dilution) and Calcein AM (1:1666 dilution). This reagent was added to equal volume of medium in wells, mixed 3 times and then incubated at 37 °C for 30 min then images were taken using the Cellavista. Due to high costs of this kit, PI (ThermoFisher Scientific, P3566), Calcein AM (ThermoFisher Scientific, C1430) and Hoechst33342 (ThermoFisher Scientific, H1399) were ordered in separately. Stocks of these reagents were made up per the manufacturer's instructions and used at 1:200, 1:400 and 1:400 respectively for staining experiments in either DPBS or culture medium. Medium was aspirated from wells and this mixture was added, incubated for 30 min at 37 °C and then imaged either using the Cellavista (Synentec Bio Services GmbH) or the Operetta (PerkinElmer) confocal plate reader.

2.6.2 Drug screening and staining with PI, CEC and Hoechst33342

2.6.2.1 Preparing and using Caspase 3/7 detection reagent

To assess Caspase 3/7 activity, the CellEvent™ Caspase-3/7 Green Detection Reagent (CEC) (ThermoFisher Scientific, C10423) was used. Stocks of this reagent

were prepared as per manufacturer instructions. CEC was then used at a final concentration of 1:400. CEC was prepared in RPMI-B27 and added to cells, incubated for 30 min then imaged.

2.6.2.2 Preparation of drug compounds

Table 2.2 – Preparation of drug stocks for toxicity screening
All drug compound stocks were prepared by dissolving in DMSO to the maximum soluble concentration (unless otherwise stated) and were stored at -20 °C as shown below:

Drug	Supplier	Product code	Stock Concentration
doxorubicin	Sigma	D1515	70 mM
dexrazoxane	Sigma	D1446	74.55 mM
carvedilol	Sigma	C3993	49.2 mM
sildenafil	Sigma	PZ0003	29.99 mM
isoprenaline	Sigma	15627-5G	Made up to 10 mM in H_2O, supplied by Divya Rajamohan

2.6.2.3 Setting up assays in 96-well plates

Drug concentrations for testing in 96-well plate experiments were prepared as serial dilutions from a stock concentration for use in dose response curve experiments. Drug screening assays were carried out using RPMI-B27 as a basal medium in which drugs were dissolved to their final assay concentration. All plates included untreated wells as controls as well as DMSO or H_2O vehicle controls (where needed). Due to limited space on plates however, the vehicle controls used corresponded to the two highest drug concentrations tested only. During data analysis, toxicity values were normalised to corresponding vehicle controls or, where this was not available, the untreated control values. Tests were carried after each experiment to determine whether there was a significant difference between the toxicity values detected in the lowest vehicle concentrations and the untreated

wells and if a significant difference was detected, data from that experiment was rejected. Values for TD_{50} (the concentration at which 50 % of cell death occurred) and EC_{50} (the concentration at which half the maximum observed cell death occurred) were calculated based on the dose response curves that were plotted with the data generated (see figure 2.1). As data were normalised to untreated controls, for the purpose of calculating EC_{50}, the range in percent cell death was considered to be between 0 % to cell $death_{max}$ % instead of the difference between cell $death_{max}$ % and cell $death_{min}$ %.

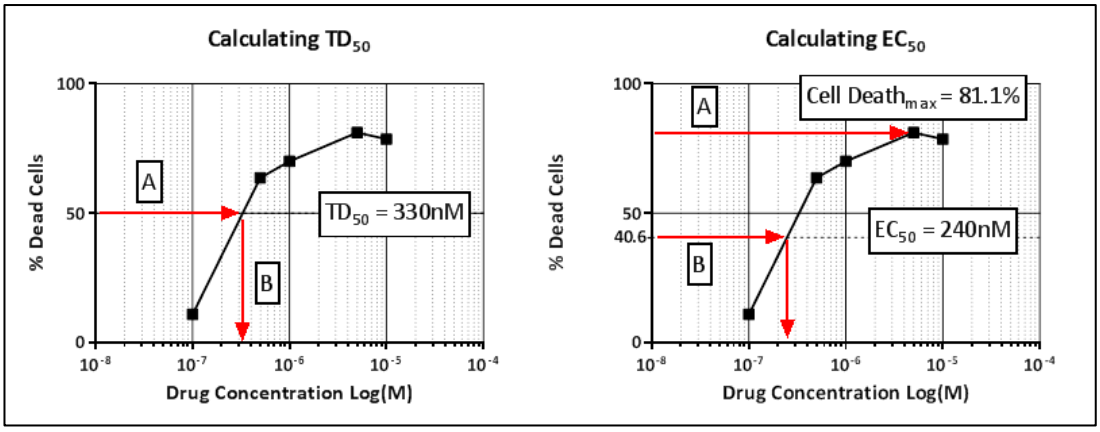


Figure 2.1 – Deriving TD_{50} and EC_{50} values from dose response curves
(Left image) TD_{50} was derived by identifying the point on the graph equating to 50 % dead cells (A). The concentration (x-axis) corresponding to this value was then determined to give the TD_{50} concentration (B). (Right image) EC_{50} was derived by identifying the maximum cell death value (A), cell $death_{max}$, or 81.1 %. Half of this value was calculated to give Cell $Death_{half}$; 40.6 %. The point on the graph equating to 40.6 % dead cells was identified (B). The corresponding concentration was determined to give EC_{50} concentration.

2.7 Changing medium and setting up assays in 384-well plates

Medium changes in 384-well plates were carried out by the robot MCA96 head (see Chapter 4, section 4.1.1 and figure 4.9). Due to issues with the plate carriers or the

MCA96 head not being level, a “dead volume” of 20 µl was required in all wells to ensure equal volumes of medium were removed from all wells across the plate. Therefore, where drug screening was carried out in 384-well plates, drugs were prepared at 150 % of the final concentration to account for the dead volume in 384 well plates (40 µl of drug solution was added to 20 µl of pre-existing medium in the well). As in 96 well plates, toxicity values were normalised to DMSO or untreated control values.

3 Development of hESC and hiPSC culture and differentiation methods

3.1 Introduction

3.1.1 Culturing hESCs in feeder free conditions

Early efforts to derive hESC lines involved culturing on inactivated mouse embryonic fibroblasts (MEFs) to promote hESC colony propagation (Thomson et al., 1998). This enabled continuous growth of these lines for up to 6 months without the appearance of karyotype abnormalities (Thomson et al., 1998). However, culturing hPSCs on feeders was laborious and not realistically amenable to automation, which is likely to be required to some degree to provide the numbers of cells required for large scale *in vitro* or *in vivo* use (Thomas et al., 2009). In drug screening for example, current estimates suggest that up to 5 million novel compounds are registered by pharmaceutical companies and academic institutions annually (Lu et al., 2015) hinting at the scale of demand for *in vitro* models for drug testing. Effects on cardiomyocyte ion channel behaviour for example, are an important test criterion, a popular candidate being hERG potassium channel block (Lu et al., 2015). For regenerative medicine, preclinical trials to test the feasibility of myocardial repair using hESC derived cardiomyocytes post-infarction in non-human primates required $1x10^9$ hESC-derived cardiomyocytes per animal to cause an improvement in heart function (Chong et al., 2014). In humans, the ventricles consist of $2\text{-}4x10^9$ cardiomyocytes (Laflamme and Murry, 2011) and following myocardial infarction approximately $1x10^9$ cardiomyocytes are lost (Murry et al., 2006) implying a need for similar if not greater numbers of hPSC-derived cardiomyocytes in cell replacement strategies.

Scaling up production of hESCs to achieve such differentiation yields required improved systems for scalable cell culture. To achieve this, processes for feeder-free culture were developed whereby hESCs could be cultured in the presence of MEF-conditioned medium (MEF-CM) on extracellular matrices (ECM) such as Matrigel™ basement membrane matrix (Matrigel)(Xu et al., 2001). Matrigel is derived from Engelbreth-Holm-Swarm mouse sarcomas, a batch variable, undefined matrix containing laminin, collagen-IV, heparin sulphate proteoglycans, entactin and growth factors (Rodin et al., 2010, Villa-Diaz et al., 2013). Later, defined substrates for hESC and (from 2007 onwards) hiPSC culture were developed such as recombinant human vitronectin (Chen et al., 2011), laminin isoforms 111, 332 and 511 (Rodin et al., 2010, Villa-Diaz et al., 2013) and the shorter laminin 511 E8 fragment (Nakagawa et al., 2014). Synthetic surfaces for hPSC culture were developed (Mei et al., 2010, Ross et al., 2012, Celiz et al., 2015) but, despite these advantages however, defined substrates were expensive, not yet developed, not yet optimised or not commercially available in the earlier part of this work. Therefore for the purpose of this thesis, Matrigel was used as it represented the best compromise between cost, reproducibility and stability of hPSC cultures.

3.1.2 Defined media for culture of hESCs and hiPSCs

Although culturing hPSCs in feeder-free conditions was less time consuming and technically challenging, for many years this approach relied on the use of MEF-CM

which was undefined and batch variable. This meant that processes such as differentiation and cell culture could not be accurately controlled (both being core processes used in this thesis). To avoid the unpredictable effect of batch variation, defined media such as TeSR1 (Ludwig et al., 2006b) and the cheaper (substituting in animal derived bovine serum albumin and zebrafish basic fibroblast growth factor) mTeSR was developed (Ludwig et al., 2006a). However, these media contained albumin of human (TeSR) or bovine (mTeSR) origin which were associated with batch variability (Chen et al., 2011). Further reductions in batch variability were achieved with the development of E8 which was a simplified medium of known composition and lacking albumin. The key essential 8 (hence E8) components were insulin, selenium, transferrin, l-ascorbic acid, basic fibroblast growth factor (bFGF), transforming growth factor beta 1 (TGFβ) in Dulbecco's modified Eagle's medium (DMEM)/ Ham's F12 (Chen et al., 2011). As these refinements in media composition became commercially available, methods for hPSC culture using these media were adopted and hPSC-cardiomyocyte differentiation processes were also developed or adopted to be compatible with these newer culture systems.

3.1.3 Embryoid Body (EB) differentiation to cardiomyocytes

Early experiments investigating the differentiation potential of hESCs demonstrated that these cells could form 3-dimensional aggregates which in turn could spontaneously differentiate to cell types representing all three germ layers *in vitro*. These EBs could also develop into spontaneously contracting EBs, demonstrating that cardiomyocytes could be produced by this method (Itskovitz-Eldor et al., 2000). Formation of EBs of uniform size by forced aggregation and directing their

differentiation with the use of growth factors demonstrated improved cardiomyocyte differentiation outcomes (up to 24 % of EBs spontaneously beating in 96-well plates) with bFGF and Activin A (Burridge et al., 2007) in the presence of supplemented defined media (Vallier et al., 2005) and polyvinyl-alcohol. This method was further improved to achieve beating EB yields of up to 95 %, while also demonstrating high differentiation efficiencies in hiPSC lines (Burridge et al., 2011). For this reason, the latest EB differentiation method was adopted as one differentiation approach for use in this thesis (termed the EB differentiation method).

3.1.4 Monolayer differentiation to cardiomyocytes

Despite being capable of achieving high yields of beating EBs, monolayer differentiation methods have also been developed using growth factors and achieving yields up to 30 % cardiomyocytes (Laflamme et al., 2007). More recently, the combination of fully defined monolayer culture conditions and the use of small molecules to initiate differentiation have meant that methods achieving up to 95 % purity and yields of 100 cells to 1 input cell have been achieved (Burridge et al., 2014). In addition to this, the ability to scale up cultures to RoboFlask® (RoboFlask) (92.6 cm^2) or higher meant that the potential for scale up was much greater with this method than it was for the EB method. For this reason, this method (termed the E8 monolayer differentiation method) was also adapted and used in this thesis.

3.1.5 Chapter Aims

- Establish competency with existing hESC and/or hiPSC culture and differentiation methods to facilitate later automation of these methods.
- Adopt or develop new culture and differentiation methods to maximise yields and improve cardiomyocyte purities where possible.
- Develop quantitative methods for carrying out quality control of differentiation processes (such as determining EB formation and size, confluency of cell cultures prior to differentiation or purities of cardiomyocytes following differentiation).
- Establish cardiomyocyte dissociation and culture methods to enable immunostaining, cryopreservation or drug screening.
- Establish suitable cardiomyocyte seeding densities for drug screening experiments.

3.2 Results

3.2.1 Establishing technical competence in feeder-free culture of HUES7 hESCs as a prelude to EB differentiation

In order to carry out EB differentiations, HUES7 hESCs (Cowan et al., 2004) were cultured in feeder free conditions on Matrigel. To demonstrate competence with culturing HUES7 cells this way and that reagents, such as the chosen MEF-CM batch were compatible with their growth, a growth curve was carried out. Later, an assessment of cell karyotype was also done. All three replicate flasks were cultured in MEF-CM from the same line of MEFs (MEF93). The population doubling time for

these cells was 43.2 +/- 0.48 hr (SD), with splits occurring at regular 3-day intervals. Rate of growth did not show a significant change (one-way ANOVA) between the 6 passages carried out over the 18 day period (figure 3.1A i,ii). A karyotype taken from HUES7 cells cultured in a later experiment under the same conditions showed these cells had a normal 46XY karyotype (30 metaphase spreads) (figure 3.1D). HUES7 cells cultured in these conditions also expressed markers of pluripotency (OCT4, SSEA4) while not staining for early differentiation marker SSEA1 (figure 3.1B). Collectively, these results indicate that in feeder free conditions, HUES7s achieved stable growth rates, showed no signs of spontaneous differentiation and maintained a normal karyotype. Therefore, this method of culture was adopted for EB differentiation experiments.

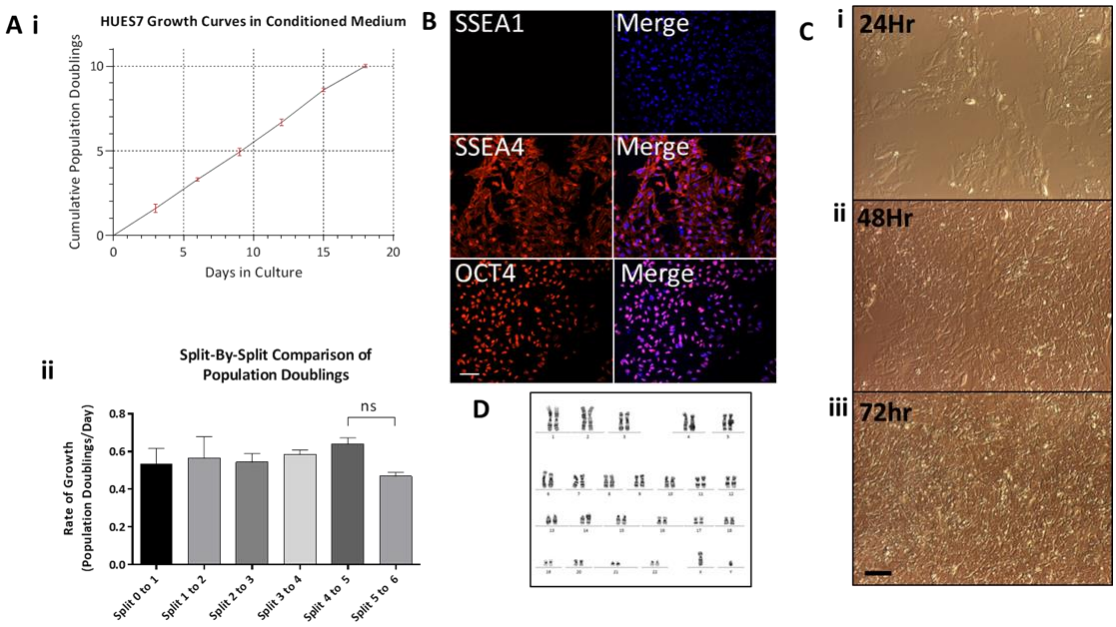


Figure 3.1 – Culturing HUES7 hESCs in feeder free conditions using MEF conditioned medium.

A i) HUES7 hESCs cultured in feeder free conditions for 6 passages over 18 days with conditioned medium provided by the same line of MEF feeders (MEF93) and seeding density of $1.25x10^6$ cells per flask (n=3, error = SD). **A ii)** Comparison of population doublings between passaging intervals demonstrating no change in proliferation rate (one-way ANOVA with TMCT, error = SD). **B)** Immunostaining of HUES7 cultured in MEF-CM for pluripotency markers SSEA4 and OCT4 (positive) and early differentiation marker SSEA1 (negative). Scale bar = 100 µm, images provided by Divya Rajamohan. **C)** Representative images of HUES7 hESCs in culture i) 24, ii) 48 and iii) 72 hr after seeding and prior to passaging. Images taken with 10x objective, scale bar = 100 µm. **D)** Karyogram from later growth curve carried out with HUES7s (cells at passage 28 in different MEF conditioned medium batch, MEF124) with normal 46XY karyotype (all karyotype results shown henceforth were provided by Nigel Smith, City Hospital Nottingham).

3.2.2 The EB cardiomyocyte differentiation method

In order to establish competency with the EB differentiation method, HUES7 cells taken from the same stocks characterised in section 3.2.1 were used. These cells were also used to evaluate whether different batches of in-house MEF-CM influenced differentiation efficiency. This involved assessing whether successful EB formation was achieved in V-bottom 96-well plates by day 2 (figure 3.2Aii - highlighted with red outline), whether these EBs in turn, transferred to U-bottom 96-well plates on day 4 (figure 3.2Aiii) and finally, by calculating the proportion of wells containing beating EBs by days 10-12 (all records of proportion of beating EBs in this thesis were made at this time point) (figure 3.2B). This showed that, while HUES7 cell cultures could differentiate to cardiomyocytes, different batches of MEF-CM had a significant effect between some batches ($p<0.01$, One-way ANOVA with TMCT) with efficiency ranging from 94+/-0.3 % (MEF93) and 82.2+/-22.8 % (MEF89) to 25.6+/-39.7 % (MEF88). Thus, efficiency was high (>90 %) with MEF-CM batch 93 (94+/-0.3 %), reduced (40-90 %) with batches 89 (88.2+/-22.8 %), 94 (75.2+/-10.1 %), 96 (41.4+/-11.5 %), 97 (66.7+/-3.5 %), and 103 (81+/-6.2 %) or low (<40 %) with batches 70 (39+/-15.6 %) and 88 (25.6+/-39.7 %). Moreover, in some cases the level of variability within the same batch of MEF-CM was high (SD>20 %). This was particularly so in batches 89 (99 % to 33 %, n=9) and 88 (79.8 % to 0 %, n=6) while greater consistency (SD<10 %) was seen with batches 93 (94.3 to 93.7 %, n=3) and 97 (69.1 to 64.2 %, n=2). These results showed the importance of selecting a batch of MEF-CM that was permissive for consistent and reproducible HUES7-cardiomyocyte differentiation.

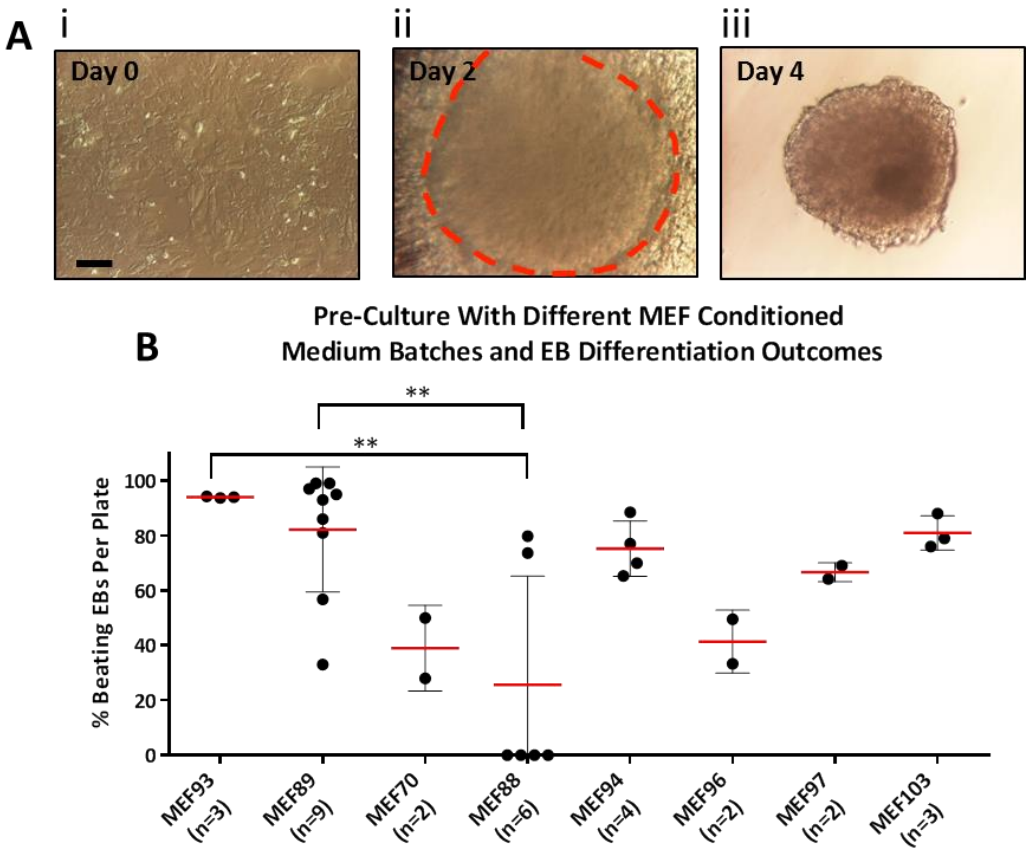


Figure 3.2 – Differentiating HUES7s to cardiomyocytes using the EB differentiation method.

A) Representative images were taken of **(i)** HUES7s cultured in MEF93 conditioned medium prior to seeding EBs, **(ii)** following EB formation at day 2 of the protocol (in v-bottom 96 well plates) and **(iii)** after EB transfer to U-bottom 96 well plates. Scale bar = 100 µm. **B)** A comparison of the outcomes of different EB differentiation experiments measured as percentage of EBs that were beating between day 10-12 of the differentiation process, carried out using HUES7s cultured in different batches of MEF conditioned medium prior to differentiation. Mean values are shown as red line with standard deviation bars in black. $p<0.01$, one-way ANOVA with TMCT.

3.2.3 Developing automated imaging based processes for assessing EB size and percent transfer using the Cellavista cell imager

Although calculating the percentage of beating EB formation gave data on differentiation efficiency, tracking EBs during the early stages of differentiation offered a route to quantify success of the process involved (Burridge et al., 2007). This included information such as number of EBs transferred from V-bottom to U-bottom plate, location of non-transferred EBs, taking photos of EBs and measuring the size of EBs. However, deriving these parameters on a well-by-well basis was a time consuming and laborious process. In addition, measuring EB dimensions was complicated due to irregular, non-spherical shapes. To simplify these processes and to enable comparison between plates or setups, scripts were written on the Cellavista cell imager (Cellavista) to enable imaging of all wells of a 96-well plate, identification of EBs and the calculation of EB sizes. In a sample plate scanned by this method (figure 3.3A), images were taken of all 96 wells and a heat map generated showing EB transfer occurred in 95 of 96 wells (99 %). A representative image of the software-generated EB image overlay (Figure 3.3 B ii – shown in white) illustrated that EB recognition was accurate and the cross sectional area of the EB could be calculated (488072 μm^2). This process was used later in chapter 4 to compare EBs generated by the robot and manually as part of the EB differentiation automation development.

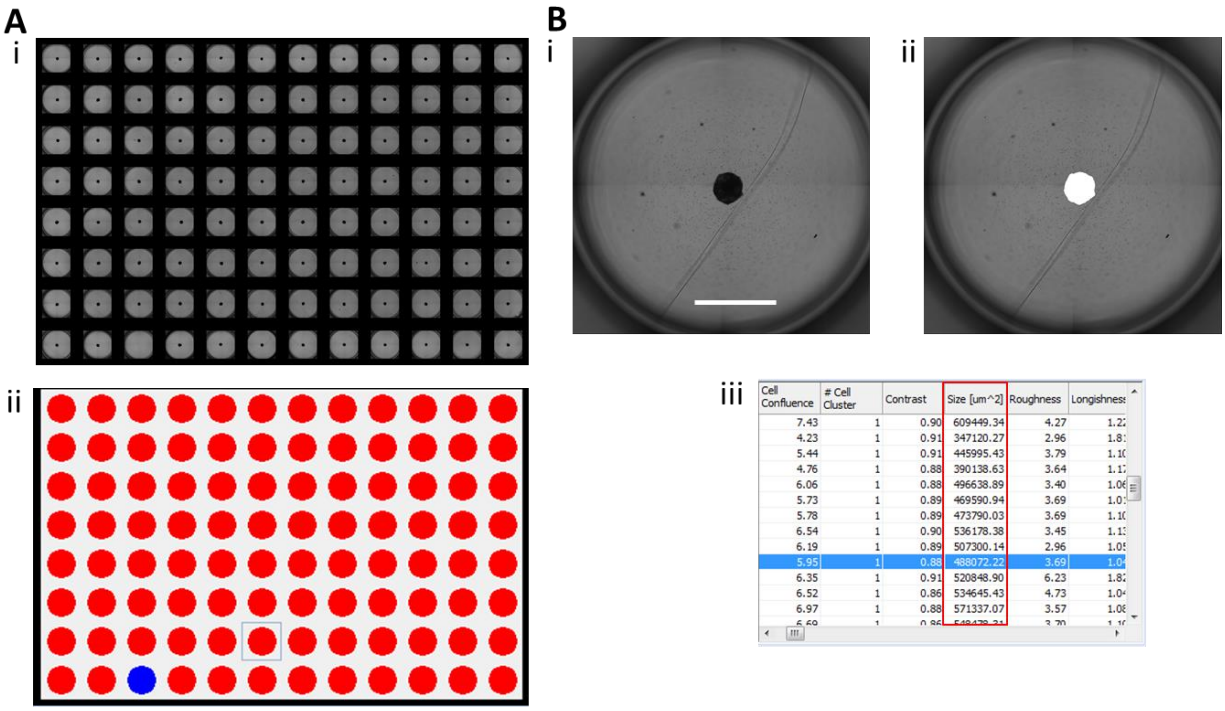


Figure 3.3 – EB Detection and size quantification using the Cellavista.
A) (i) Merged brightfield images of 96 wells from a U-bottom plate immediately following EB transfer from V-bottom plate on day 4 of EB differentiation. **(ii)** Heat map of the same plate indicated 95 EBs successfully transferred (wells in red) and one did not (in blue). **B) (i)** Representative image of EB in U-bottom well after transfer and **ii)** with a software-generated overlay (shown in white) used to determine EB cross-sectional area ("EB size") in μm^2. **(iii)** Software readout showing size of representative highlighted EBs. Scale bar = 2mm.

3.2.4 Determining a suitable method for EB dissociation

Analysing cardiomyocytes *in vitro* within EBs is challenging due to their 3D shape and so, to simplify analysis, a method was needed to dissociate EBs and re-plate the cardiomyocytes into alternative culture formats such as 96-well flat bottom plates with defined cell numbers. Three in-house methods for EB dissociation were evaluated for their suitability in achieving this by assessing the viability of dissociated cells after 24, 48 and 72 hr. (See Chapter 2 section 2.3 for methodologies). Viability of these cells was determined by quantification of cell staining using CalceinAM (a live-cell marker that generates fluorescence in response to intracellular esterase activity), PI (dead cell marker that binds to DNA in dying cells where membrane integrity is lost – see chapter 5) and Hoechst33342 (a membrane permeable marker that binds DNA – see chapter 5) using the Cellavista. After 24 hr, cell viability was significantly lower in the cell dissociation solution (CDS) method group at 75.8+/-2.3 % (SD, $p<0.05$, two-way ANOVA) compared to the trypsin/accumax (T/A) wells at 86.8+/-2.4 % (figure 3.4A). At 48 and 72 hr however, there was no significant difference between these methods nor was there any difference between T/A and the cold dissociation method at 24, 48 or 72 hr. However, the cold dissociation method did not fully dissociate EBs, (highlighted in red, figure 3.4B), making this method unsuitable for EB dissociation. The T/A method was chosen on the basis that it gave significantly higher percentage viable cells at 24 hr than CDS and higher mean values at 48 hr (80.2+/-8.2 % vs 77.6+/-2.6 %) and 72 hr (91.2+/-1.3 % vs 86.9 +/-2 %).

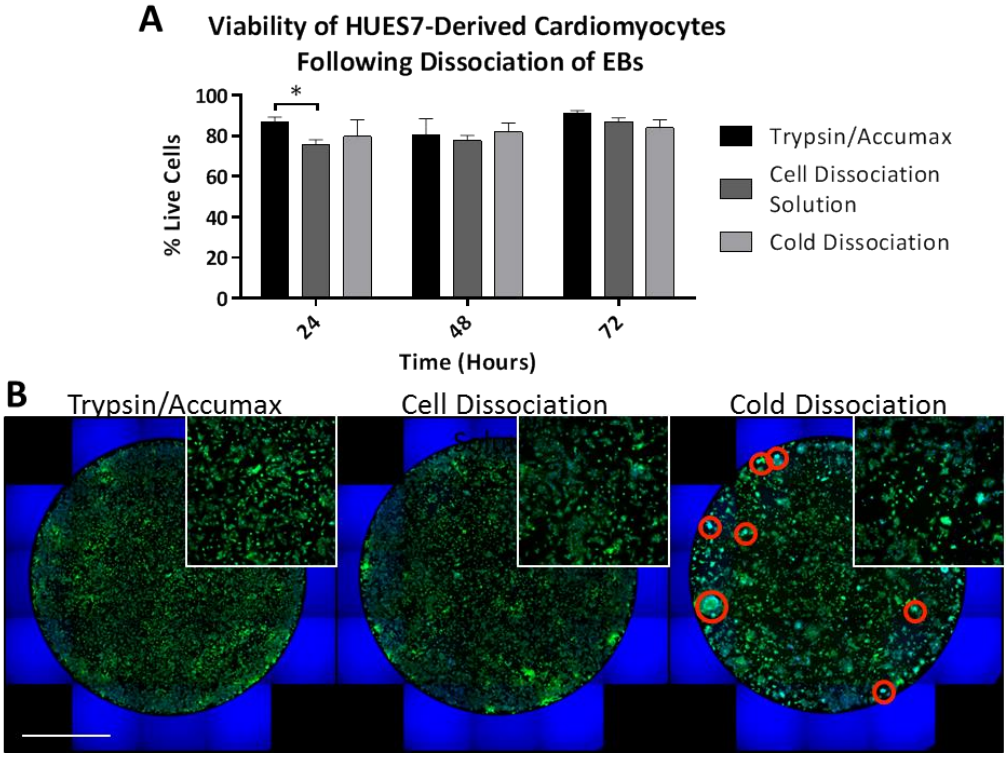
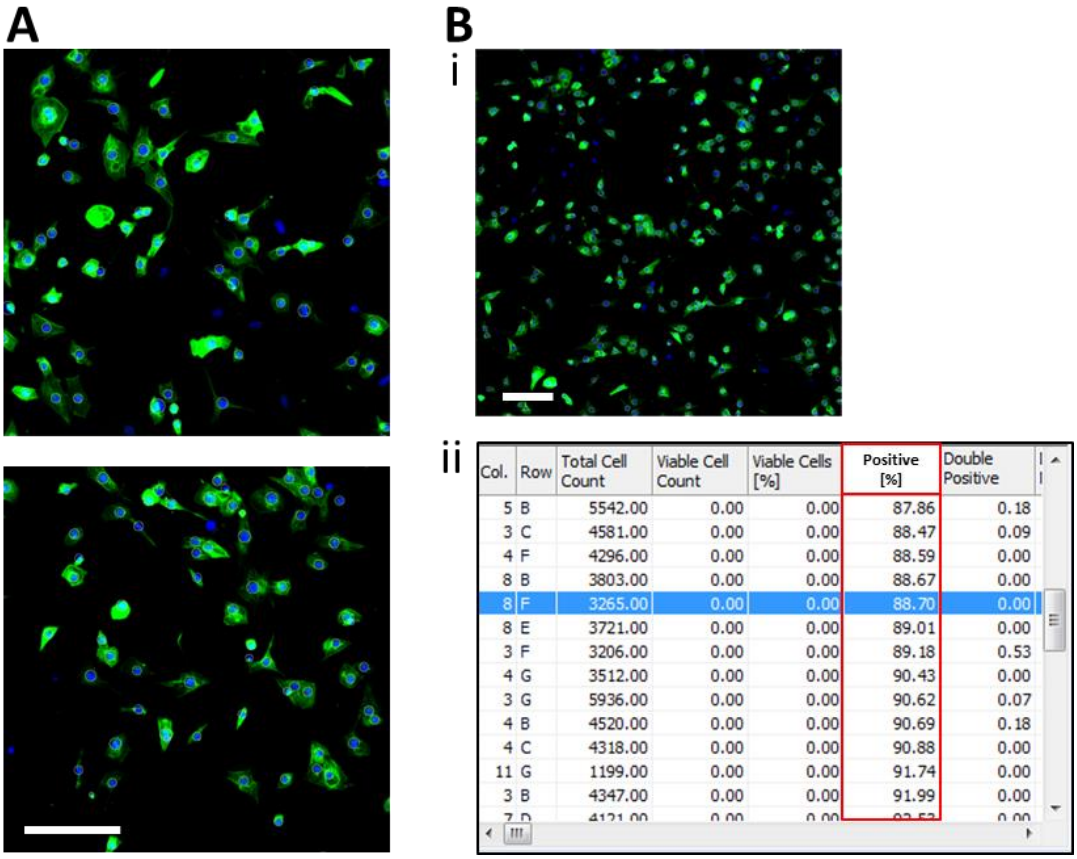


Figure 3.4 – Testing dissociation methods on HUES7-derived beating EBs. **A)** Comparison of cell viability 24, 48 and 72 hr after dissociation with either trypsin/accumax (1:1 ratio), cell dissociation solution or cold dissociation method determined by Cellavista quantification of cells stained with Hoechst33342, PI and CalceinAM. No significant difference between methods at 48 and 72 hr. A significant difference between trypsin/accumax and cell dissociation solution was observed at 24 hr ($p<0.05$, two-way ANOVA, TMCT, error bars = SD). **B)** Representative images taken from sample wells containing cells dissociated by each method. Scale bar = 2 mm.

3.2.5 Quantification of immunostained cells using the Cellavista cell imager

While calculating the proportion of beating EBs was a useful way to provisionally screen for differentiation efficiency, this may not accurately represent the proportion of cells that are cardiomyocytes at the end of differentiation. Indeed, it has been shown that differentiation methods generating 80 % spontaneously beating EBs had a cardiomyocyte purity of only 20 % (Lecina et al., 2010). Therefore, to provide a more accurate value for number and purity of cardiomyocytes generated by EB differentiations, quantification of immunostained samples was used. Since α-actinin has previously been shown to quantify cardiomyocyte purities (Lecina et al., 2010, Burridge et al., 2014), this marker was used. To enable quantification of stained cells and visual assessment of staining quality in parallel, a quantification method was developed using Cellavista. Cells were stained for α-actinin (green) with DAPI co-stain and pre-written analysis protocols for quantifying cell viability were used to quantify positively stained cardiomyocytes (figure 3.5). In a sample well, (figure 3.5 B) a heterogeneous mix of α-actinin-positive and -negative cells were quantified by the Cellavista where, of a total cell count of 3,265 (determined by DAPI staining) 88.7 % of these stained positively for α-actinin. In this example, population purity was determined with ~3,000 cells per stained well, meaning that only 36,000 cells of a sample population would be needed for purity to be determined (including appropriate controls).



Col.	Row	Total Cell Count	Viable Cell Count	Viable Cells [%]	Positive [%]	Double Positive
5	B	5542.00	0.00	0.00	87.86	0.18
3	C	4581.00	0.00	0.00	88.47	0.09
4	F	4296.00	0.00	0.00	88.59	0.00
8	B	3803.00	0.00	0.00	88.67	0.00
8	F	3265.00	0.00	0.00	88.70	0.00
8	E	3721.00	0.00	0.00	89.01	0.00
3	F	3206.00	0.00	0.00	89.18	0.53
4	G	3512.00	0.00	0.00	90.43	0.00
3	G	5936.00	0.00	0.00	90.62	0.07
4	B	4520.00	0.00	0.00	90.69	0.18
4	C	4318.00	0.00	0.00	90.88	0.00
11	G	1199.00	0.00	0.00	91.74	0.00
3	B	4347.00	0.00	0.00	91.99	0.00

Figure 3.5 – Quantification of immunostained cells using Cellavista.
A) Two representative images showing HUES7-EB derived cardiomyocytes immunostained for α-actinin. Detected positively stained cells were highlighted (shown as white circles around the nuclear region). **B) (i)** Representative image showing heterogeneous population of cardiomyocytes and non-cardiomyocytes. **(ii)** Quantification of positively stained cells relative to total cell number (measured as number of DAPI stained nuclei) indicated that the population was 88.7 % pure for cardiomyocytes. Scale bars = 200 µm

3.2.6 Culturing HUES7 hESCs in mTeSR™1 feeder free defined medium

To overcome the variability in EB differentiation outcomes observed in section 3.2.2 resulting from culture of HUES7 cells in undefined and batch variable MEF-CM, a new culture system was adopted using mTeSR™1 (mTeSR), a fully defined feeder free cell maintenance medium. To demonstrate competency and that HUES7s could be cultured in these conditions, growth curves were carried out over 5 passages,

lasting up to 19 days (figure 3.6A) with a population doubling time of 69.9 +/-7.7 hr and no significant change in growth rate between passage intervals (figure 3.6B). HUES7s cultured in this system had a 46XY karyotype after 5 passages (30 spreads). These data confirmed that HUES7s could be cultured in fully defined feeder free conditions without developing karyotype abnormalities.

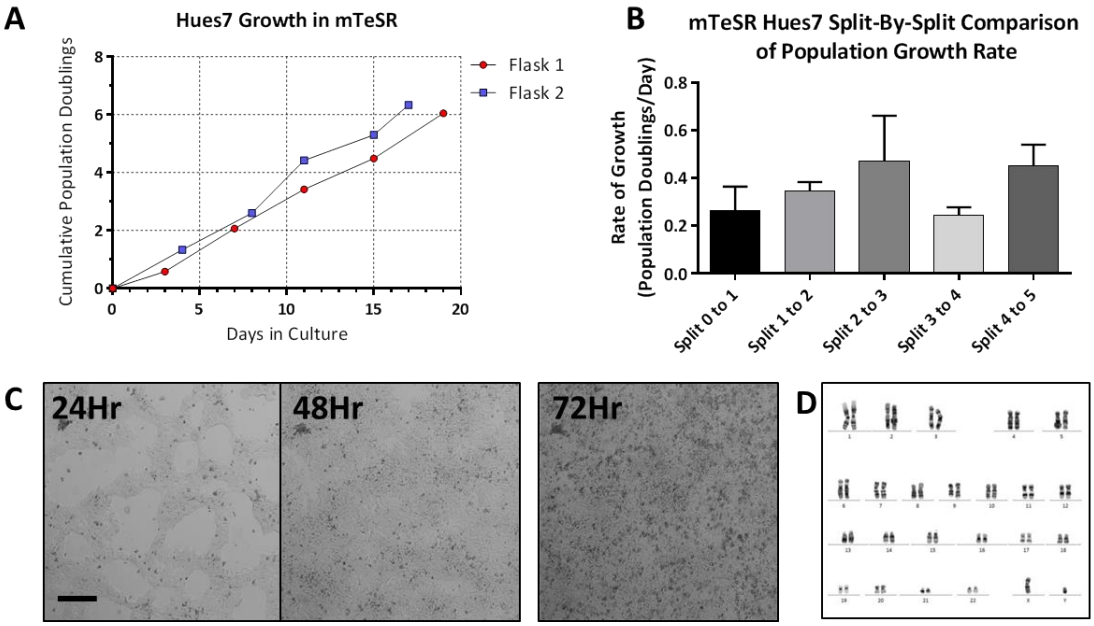


Figure 3.6 – Culturing HUES7s in mTeSR.
A) Growth curve of two flasks cultured in parallel with HUES7s. **B)** Comparison of population doubling rate per day between passaging intervals demonstrated no significant difference (one-way ANOVA with TMCT, error = SD). **C)** (from left to right) Representative images showing HUES7 cells in culture 24, 48 and 72 hr after seeding, morphology at 48 hr is representative of the latest stage at which cells would be passaged while image at 72 hr shows cells at full confluence needed to initiate monolayer differentiation, all images taken using the Cellavista, scale = 100 µm. **D)** Representative karyogram of HUES7s following growth curve in mTeSR depicting normal 46XY karyotype.

3.2.7 Monitoring confluence of HUES7s in mTeSR using the Cellavista cell imager

A novel in-house monolayer differentiation method was developed (by Vinoj George) using cells cultured in mTeSR. This method required initiating differentiation when cultures were between 80-90 % confluence. In order to measure this accurately, a script was developed on the Cellavista for assessing confluence of cells grown in mTeSR. Images of cell colonies identified by the Cellavista software were overlaid (shown in white – figure 3.7 A, B, C) and the area of the overlay was quantified (by the software) relative to the area of the well (figure 3.7 C i) to determine confluence.

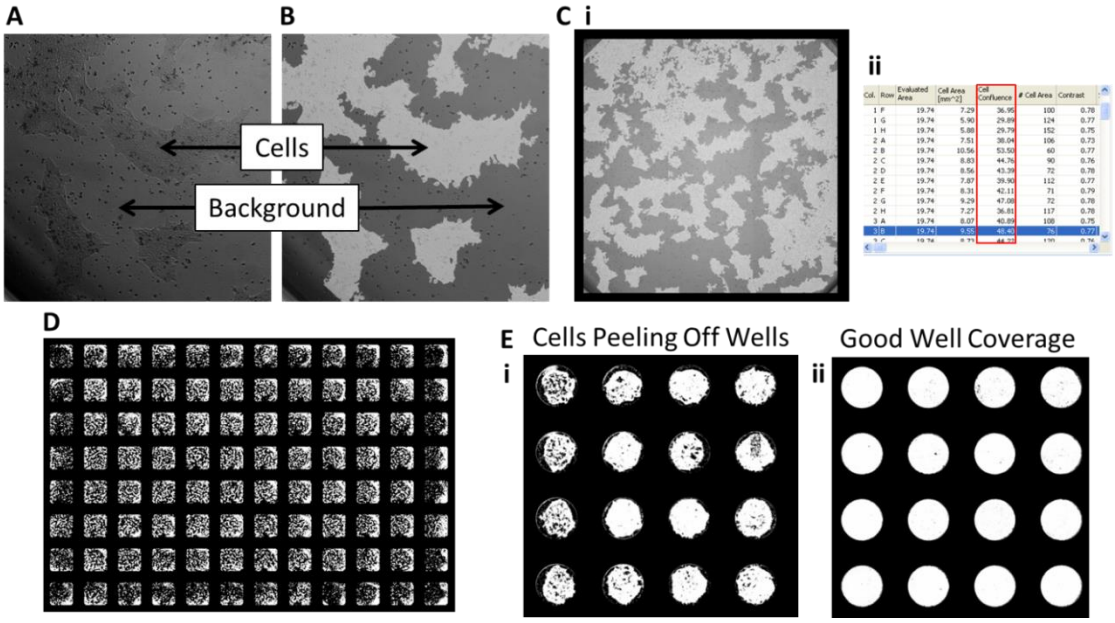


Figure 3.7 – Monitoring confluence in monolayer cultures using the Cellavista.
A) HUES7s in culture on a Matrigel coated 96-well flat bottom plate. **B)** Software recognition accurately identified adherent cell colonies and highlighted the "cell region" in white overlay, non-adherent floating cells were ignored. **C) (i)** Representative image of confluence detection across an entire well of 96 well plate, **(ii)** confluence readout shows well in (i) with cell confluence of 48.4 %. **D)** A plate mosaic was generated for all 96 seeded wells and the confluence overlays shown (white). **E)** Images showing examples of wells where AT1 Cardiomyocytes were beginning to peel off the edges of the wells (left) and example wells where this was not occurring (right) indicating that this analysis script could also be used for quality control of cardiomyocyte cultures.

3.2.8 Differentiating HUES7 and hiPSC lines using the mTeSR monolayer differentiation method

To generate banks of cardiomyocytes for use in drug screening experiments and to translate this method onto the robotic platform, manual differentiations were first attempted using both HUES7s and a healthy human iPSC line (AT1). The AT1 line was derived from a healthy female dental pulp sample reprogrammed using lentiviral vectors carrying *OCT4*, *SOX2, NANOG* and *LIN2.* Reprogrammed cells were grown in colonies on MEF feeders then pooled together to create a polyclonal line which was subsequently cultured in feeder free conditions with MEF-CM (the AT1 hiPSC line derived by Divya Rajamohan). Both HUES7 and AT1 lines were transitioned from MEF-CM culture to mTeSR culture and differentiated in RoboFlasks to generate cardiomyocytes for cryopreservation to establish cell banks. Due to cost and time considerations, multiple banks were not made. These banks were characterised for cardiomyocyte purity by flow cytometry (n=1 for each bank, figure 3.8). Cardiomyocyte markers α-actinin and cardiac troponin T (another marker used to determine cardiomyocyte purity (Burridge et al., 2014) were used. With HUES7, cells were 98.7 % positive for α-actinin and 97.4 % positive for cardiac troponin T. For AT1, cells were 99.5 % positive for α-actinin and 90.9 % positive for cardiac troponin T. These results indicate that the mTeSR monolayer method was capable of generating >90 % cardiomyocytes although reproducibility of this method (in terms of cardiomyocyte purity) was not tested. Comparison of total cell yield between mTeSR monolayer differentiations carried out in T75 flasks and RoboFlasks relative to EB differentiations revealed significant differences in cell yields from these methods relative to EB differentiations (measured as total cell

number harvested per 96-well plate) of 4.3x10^6 more cells with T75s (n=2, 4.9+/-1.4x10^6 cells) and 6.7x10^6 more cells from RoboFlasks (n=2, 7.3+/-1.2x10^6 cells) relative to 0.6+/-0.3x10^6 cells per 96 well EB plate (n=9) ($p<0.0001$, One-Way ANOVA, TMCT). Additionally, as expected, increasing surface area yielded significantly higher numbers of cells in RoboFlask relative to T75s ($p<0.001$) indicating that the mTeSR monolayer method could achieve higher cell yields with increasing surface area.

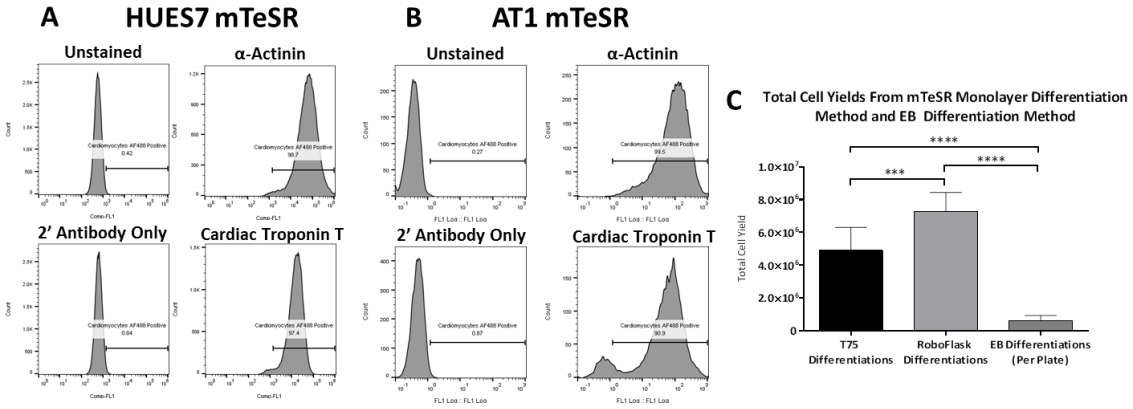


Figure 3.8 – Generating cardiomyocytes with the mTeSR monolayer method.
HUES7 and AT1 hiPSC lines were differentiated using the mTeSR monolayer method. **A)** Quantification of HUES7 cardiomyocytes by flow cytometry for cardiomyocyte markers α-actinin and cardiac troponin T (50,000 cells per sample) **B)** Quantification of AT1 cardiomyocytes by flow cytometry using the same markers as in A) (20,000 cells per sample, 10,000 cells for unstained). **C)** Comparison of total cell yields from mTeSR monolayer differentiations carried out in T75 and RoboFlask format compared to yields from entire 96-well plate demonstrating significant increase using monolayer method compared to EB method and also demonstrating significant increase in cell yield with increasing surface area. n=2 T75 flasks, n=2 RoboFlasks, n=17 EB plates. One-way ANOVA, TMCT.

3.2.9 Culturing HUES7 cells in Essential 8™ feeder free defined medium

During the course of this work, Essential 8™ (E8) medium became commercially available and was marketed as a reliable, stable product for hPSC culture. Therefore, growth rate of HUES7 cells cultured in this medium was compared to those in MEF-CM or mTeSR. These studies showed the proliferation rates varied significantly between MEF-CM and mTeSR ($p<0.01$, t-test). HUES7 population doubling time was 43.2+/-0.4 hr (n=3) for MEF-CM and 69.9+/-7.7 hr (n=2) with mTeSR, while HUES7 in E8 (n=1) was lower than both at 30.1 hr. It is worth noting however, that seeding densities differed between methods. $1.25x10^6$ cells per T25 were routinely used for MEF-CM cultures however, mTeSR cultures could not be maintained at this seeding density due to high levels of cell death after seeding and required a minimum of $2x10^6$ cells. In E8 cultures, $1x10^6$ cells were seeded in T25s but in the presence of ROCK inhibitor (Y27632, herein referred to as ROCKi) which was not used in the previous two methods. While karyotypes of HUES7s cultured in MEF-CM and mTeSR were normal after growth curves (figures 3.1 and 3.6 respectively) at the end of the E8 growth curve a trisomy of chromosome 12 was observed in 2 of 30 spreads analysed (figure 3.9Dii) that was not present at the start of the growth curve (figure 3.9Di). Immunostaining of HUES7 cells cultured in E8 showed that they expressed pluripotency markers (figure 3.9E) suggesting that no detectable spontaneous differentiation was occurring when HUES7s were cultured in this medium.

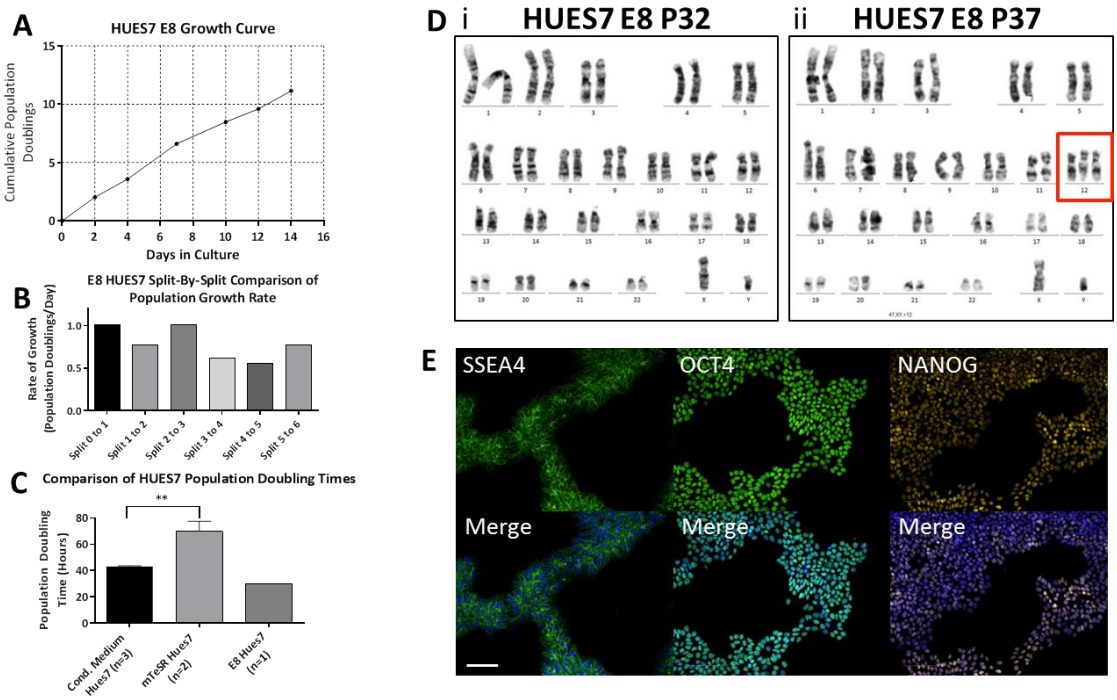


Figure 3.9 – Culturing HUES7 in E8 medium.
HUES7 cells were transitioned to E8 medium from mTeSR. **A)** A growth curve was carried out over 6 passages for 14 days. **B)** Rate of population doubling was determined between each passage interval during the growth curve. **C)** A comparison of HUES7 growth rates in conditioned medium, mTeSR and E8, showing HUES7s in mTeSR having a significantly lower rate of population doubling than in MEF-CM ($p<0.01$, t-test, error bars = SD). **D)** Representative karyograms of HUES7s before and after growth curve with normal 46XY at the start but trisomy of chromosome 12 (highlighted in red) in 2 of 30 spreads at the end of the growth curve. **E)** Pluripotency marker staining of HUES7 cells cultured in E8 medium showing expression of SSEA4, OCT4 and NANOG. Scale bar = 100 µm, images provided by Katarzyna Lis-Slimak.

3.2.10 Developing cell culture in E8 with the CPVT hiPSC line

Although HUES7 cells developed karyotypic abnormalities, this was inconsistent with other data in the literature for hESC lines in E8 (Chen et al., 2011), and in our lab, which usually showed genetic stability in this medium. This was true of the hiPSC line CPVT which was derived by reprogramming fibroblasts from a patient harbouring CPVT. This entailed the use of the Sendai-virus based CytoTune 2.0 system (Life Technologies) wherein colonies were derived in E6 medium and subsequently expanded in E8 medium with EDTA harvesting, ratio splitting and use of ROCKi (see chapter 2 section 2.1.5). In order to confirm whether these cells could grow at a constant rate and maintain a stable karyotype, a 7-passage growth curve was carried out over 14 days with cell harvests occurring at regular 48 hr intervals (figure 3.10A). The population doubling time for CPVT hiPSCs harvested with EDTA was 21.3 hr (n=1) and a representative karyogram generated at the end showed that these cells had a normal 46XY karyotype (from 30 spreads). Immunostaining of CPVT cells in E8 and cultured with EDTA passaging revealed expression of pluripotency markers SSEA4, OCT4 and NANOG.

In order to carry out a growth curve of cells using EDTA passaging, cell counts of cell suspensions were necessary. EDTA harvesting generated cell clusters (rather than single cell suspensions) some of which could not be counted accurately (example highlighted in figure 3.10Ci). This was not enough to render the cell counts inaccurate when carried out manually (as indicated by the even growth rate in figure 3.10A), however, there was a risk that clumps of these sizes would cause inaccuracies in cell counts using the automated Cedex hiRes cell counter (referred

to hereafter as "Cedex"; for automation work on the robot, Chapter 4). To address this, an enzymatic harvesting approach was tested using TrypLE™ Select (1x) (TrypLE) to see if single cell suspensions could be achieved. This was not achieved however, no cell clusters greater than 4 cells in size were observed, indicating an improvement in the dissociation process (see example representative image figure 3.10 Ci bottom image, see also comparison of cluster size and frequency, table 3.1 below) and this was deemed to be acceptable for cell counting on the Cedex.

Table 3.1 – Cell cluster size and frequency following harvest of CPVT hiPSCs with EDTA and TrypLE.
CPVT hiPSCs were harvested using either TrypLE or EDTA (0.5 mM). Cells were seeded on a haemocytometer, a random field of the haemocytometer was chosen and cluster size and frequency were quantified.

Cluster Size (# cells)	1	2	3	4	5-9	10+	Sum
Frequency (EDTA)	16	12	2	2	1 (6 cells)	1	70(+)*
% of total cell number	23 %	34.3 %	8.6 %	11.4 %	8.6 %	14(+) %	99.9 %
Frequency (TrypLE)	22	6	4	1	0	0	50
% of total cell number	44 %	24 %	24 %	8 %	0 %	0 %	100 %

*Cell total includes "10+" column as clump size could not be accurately determined, it was assigned a value of 10 (see Figure 3.10 Ci top image).

In order to identify whether TrypLE passaging was capable of giving a steady growth rate, a growth curve was carried out giving a population doubling time of 21.7 hr (n=1) (compared to 21.3 hr for EDTA) indicating that cells harvested by both methods still retained a similar rate of growth. As these experiments were carried out in RoboFlasks (in parallel to work carried out on the robot and covered in Chapter 4) and due to cost considerations, replicates were not carried out. A

comparison of the growth rates between passaging intervals under both conditions indicated a more consistent rate was achieved using TrypLE passaging (range = 0.27 population doublings/day (pd/d)) compared to EDTA (range = 0.61 pd/d)(figure 3.10Bi and ii). Representative karyograms showed that TrypLE passaging also gave a normal 46XY karyotype after the growth curve (from 30 spreads). As it did not elicit a negative effect on karyotype but did improve dissociation of cells, TrypLE was adopted for subsequent cell culture work in E8 along with continued use of ROCKi.

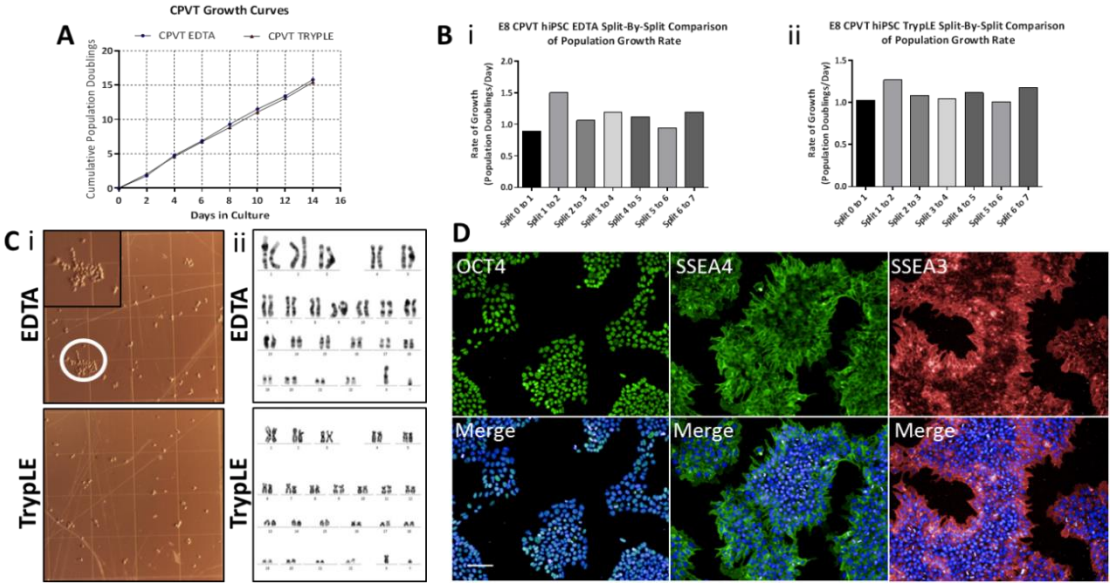


Figure 3.10 – Culturing CPVT hiPSCs in E8 Medium.
CPVT hiPSCs were cultured in E8 medium by passaging with either EDTA solution (0.5 mM) or TrypLE. **A)** Growth curve of CPVT hiPSCs showing population doubling time of 21.3 hr (EDTA) and 21.7 hr (TrypLE) over 7 passages and 14 days in culture when harvested with either EDTA or TrypLE (n=1). **B) (i)** Growth rate of CPVT hiPSCs between passage intervals with EDTA and **(ii)** TrypLE passaging. **C) (i)** Representative images of cell suspensions generated by passaging with EDTA or TrypLE illustrating that with EDTA passaging, cell clumps of >10 cells were generated (highlighted in white circle) which was not the case with TrypLE passaging (clumps do not exceed 4 cells in size). **C (ii)** Representative karyograms generated from cells at the end of growth curve had regular 46 XY karyotype when passaged with EDTA or TrypLE. **D)** CPVT hiPSCs supplied for this work were pluripotent as demonstrated by staining for pluripotency markers OCT4, SSEA4 and SSEA3, scale bar = 100 µm, images supplied by Gary Duncan).

3.2.11 Culturing the LQT2 hiPSC line in E8

In order to expand the repertoire of hiPSC lines going into the differentiation process and to generate cardiomyocyte banks across different lines, the Long QT Syndrome Type 2 (LQT2) hiPSC line was also adapted to TrypLE culture in E8. As with the CPVT hiPSC line, LQT2 hiPSCs were derived by reprogramming skin fibroblasts from a patient with a *G1681A* mutation in the *KCNH2* potassium channel manifesting clinically as long QT syndrome type 2 (hence LQT2) (Matsa et al., 2011). As before, the Sendai-virus based CytoTune 2.0 system was used, colonies were derived in E6 medium and expanded in E8 medium with EDTA harvesting and ratio splitting. A growth curve of these cells was carried out using TrypLE harvesting over 7 passages giving population doubling time of 30.9 hr over 17 days (n=1, figure 3.11A) after which, these cells exhibited a normal 46XX karyotype (figure 3.11 C ii). A comparison of the rate of growth between passage intervals suggested a higher variability in growth rates than observed with CPVT hiPSCs harvested with TrypLE in 3.2.10, with a range of 0.65pd/d (lowest rate, 0.45pd/d, highest, 1.1pd/d). Pluripotency marker staining for these cells cultured in EDTA revealed expression of SSEA4, SSEA3, OCT4 and NANOG.

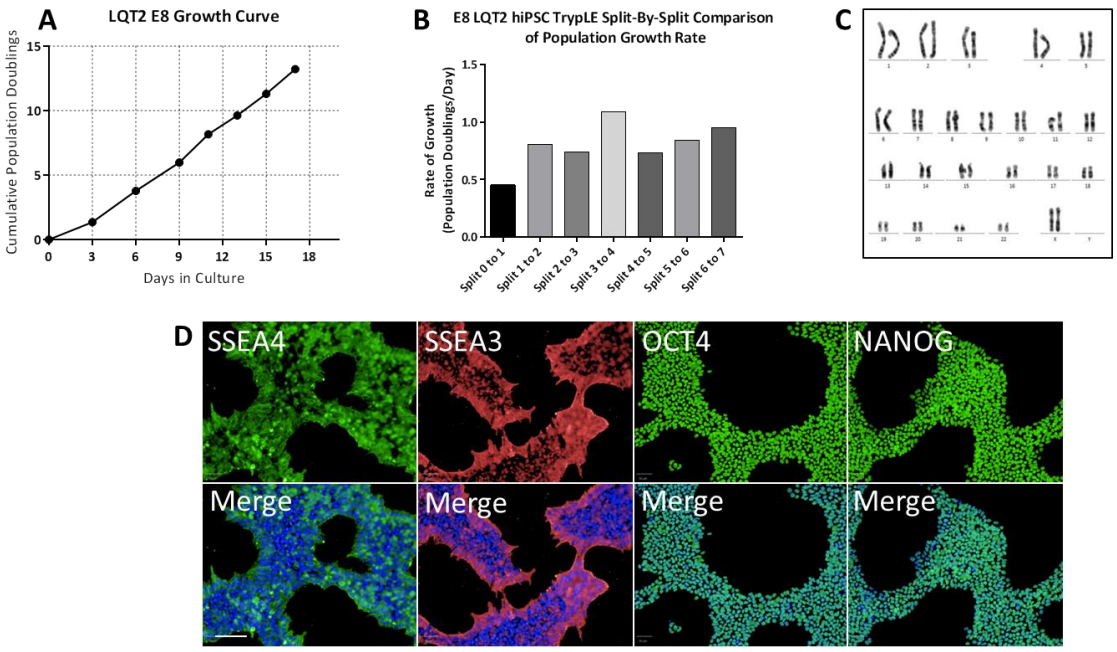


Figure 3.11 – TrypLE passaging of LQT2 hiPSCs in E8 medium.
A) Growth curve of LQT2 hiPSCs in E8 passaged with TrypLE Select over 7 passages with population doubling time of 30.9 hr over 17 days of culture. **B)** Rates of cell growth between cell passage intervals. **C)** Representative karyogram showing normal 46XX karyotype. **D)** Immunostaining for pluripotency markers shows cells expressing SSEA4, SSEA3, OCT4 and NANOG. Scale bar = 100 µm.

3.2.12 The E8 monolayer differentiation method and line-specific optimisations

To identify the optimal concentrations of Chir99021 (Chir) and C59-Wnt antagonist (Wnt-C59) needed to differentiate the LQT2 hiPSC line, a range of concentrations (2, 4, 6 and 8 µM Chir and 1, 2, 4 and 6 µM Wnt-C59) were tested for their ability to generate spontaneously beating sheets of cardiomyocytes by day 10 of differentiation (figure 3.12). Video recordings were made of cells for all conditions tested (see supplementary files: Videos 1 to 16). Cells were then harvested from the wells to determine cardiomyocyte purity under each condition. By day 10 of the differentiation, all wells treated with either 4 µM or 6 µM Chir regardless of Wnt-C59 concentration achieved the highest beating score (= score of 3) with the entire

wells beating (see supplementary videos 5-12). At 2 and 8 µM Chir, beating was observed in <50 % of the well surface (see supplementary videos 1-4 for 2 µM Chir and 13-16 for 8 µM Chir). When 4 µM Chir and 2 µM Wnt-C59 were used to differentiate CPVT hiPSCs, these differentiations also achieved the highest beating score (=3) suggesting consistency of response to differentiation induction between both lines. Dissociation of these cells was attempted using the T/A method which had been used previously with EB and mTeSR monolayer method-differentiated cardiomyocytes. However, in this case and in subsequent tests, this led to complete cell death following dissociation, preventing assessment of cardiomyocyte purity.

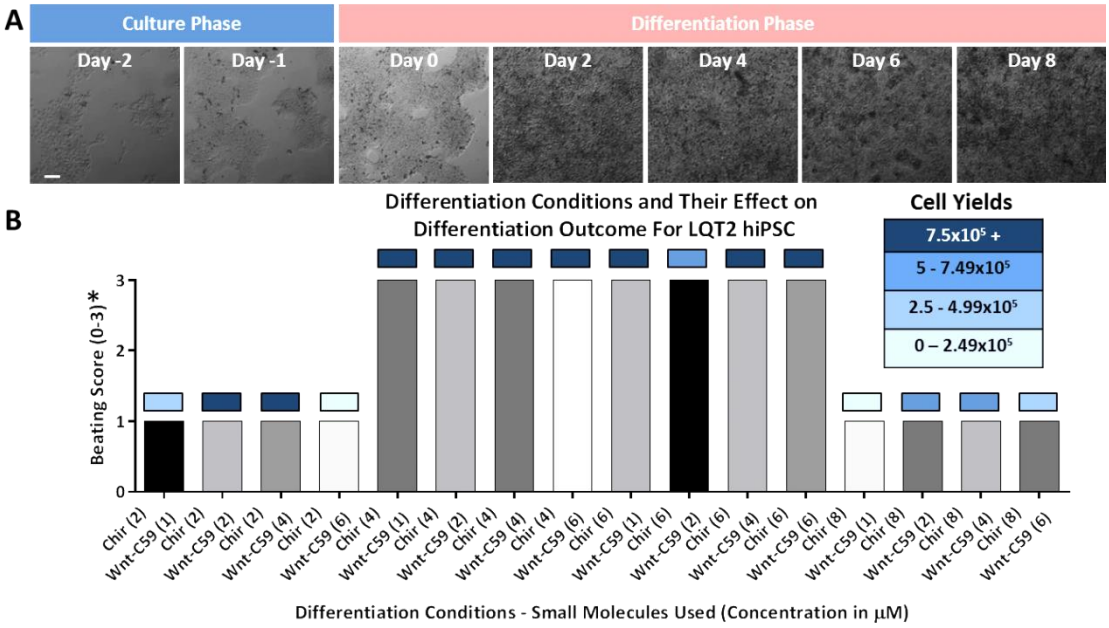


Figure 3.12 – Line-specific differentiation condition optimisations with the E8 monolayer method

(A) Representative images from the same field of view showing time course of the E8 differentiation method following seeding of cells to the point when cells were beating (CPVT hiPSCs differentiated with 4 µM Chir99021 on day 0 and 2 µM Wnt-C59 on day 2), scale bar = 100 µm. **(B)** Testing LQT2 hiPSC differentiation with different concentrations of Chir99021 and Wnt-C59 (displayed in brackets, in µM, below x-axis) for their effect on beating quality on day 10 and total cell yield following dissociation in a 24 well plate. Coloured boxes represent heat map score of cell yields to differentiate between high yields ($7.5x10^5$ to $1x10^6$) and low yields ($<2.49x10^5$). Videos for each well condition can be found in the supplementary videos folder, from left to right, video 1 to video 16. * Score of 0 = no beating observed, 1= less than 50 % of surface area beating, 2= greater than 50 % of surface area beating but less than 100 %, 3 = entire surface beating.

3.2.13 Troubleshooting issues with dissociating E8 monolayer differentiations

In order to seed well plates for drug screening, a method of cardiomyocyte dissociation was needed that did not adversely affect viability of the cells. A repeat test of the T/A dissociation method gave complete cell death on re-seeding (figure 3.13 Ai), seeding TrypLE Express dissociated cardiomyocytes gave some cell survival (with ROCKi) (figure 3.13 Aii) but also high levels of cell death, this was tested as TrypLE Express was used to dissociate cardiomyocytes in the publication from which this differentiation method was derived (Burridge et al., 2014). Dissociation with collagenase for 20 min before TrypLE Express treatment for 5 min gave good survival and low amounts of cell death (figure 3.13 Aiii). Dissociation attempts with TrypLE Express enabled partial dissociation from the culture surface but also revealed cells that were attached to a basement membrane (figure 3.13 B). In order to develop a method for dissociating cells and this matrix on which they were attached, methods for dissociating heart tissue were investigated. An early study that compared dissociation of rat heart tissue using trypsin or collagenase showed that trypsin was damaging to heart cells while collagenase appeared to be minimally invasive (Mason-Pivet et al., 1976). Later studies developed methods for dissociating cardiac tissue isolated from children (Powell et al., 1981) and adult hearts (Bustamante et al., 1982) both relying on the use of collagenase. A comparison of collagenases available from Life Technologies (https://tools.thermofisher.com/content/sfs/manuals/Collagenase_man.pdf) highlighted collagenase type II (herein referred to as collagenase) specifically for heart cells (Life technologies product information sheet, 2014). When collagenase

was used, beating sheets detached from the culture surface and continued to beat in suspension but remained as intact sheets. These sheets were then dissociated by exposure to TrypLE Express for 5 min. Increasing collagenase exposure time from 5 to 20 min made dissociation of these intact sheets easier using TrypLE Express without seeing a change in the amount of beating occurring in suspension. Cells dissociated this way and re-seeded into culture-ware re-formed confluent spontaneously beating monolayers up to 5 days following seeding and were used for subsequent drug screening experiments.

Method	A	B	C	Total Score (column A x column B x column C)
	Complete Dissociation from Culture Surface? (0-3)*	Ease of Dissociation of Clumps in Suspension (0-3)+	Survival of Cells After Re-seeding (0-3)¤	
Trypsin/Accumax (1:1)	2	1	0	0
TrypLE Express	2	2	1	4
TrypLE Express + ROCK inhibitor pre-treatment	2	2	2	8
Collagenase (5 min) TrypLE Express (5min)	3	2	2	12
Collagenase (20 min) TrypLE Express (5min)	3	3	3	27

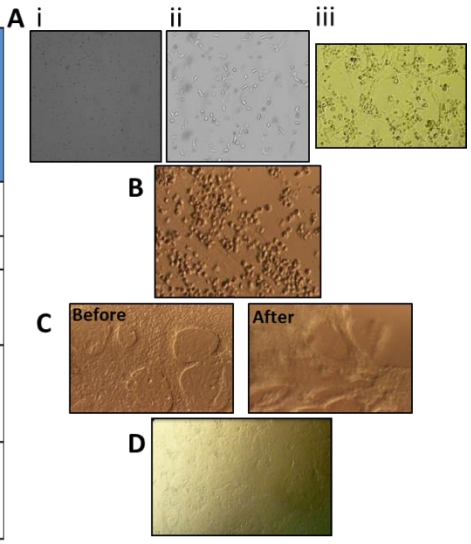
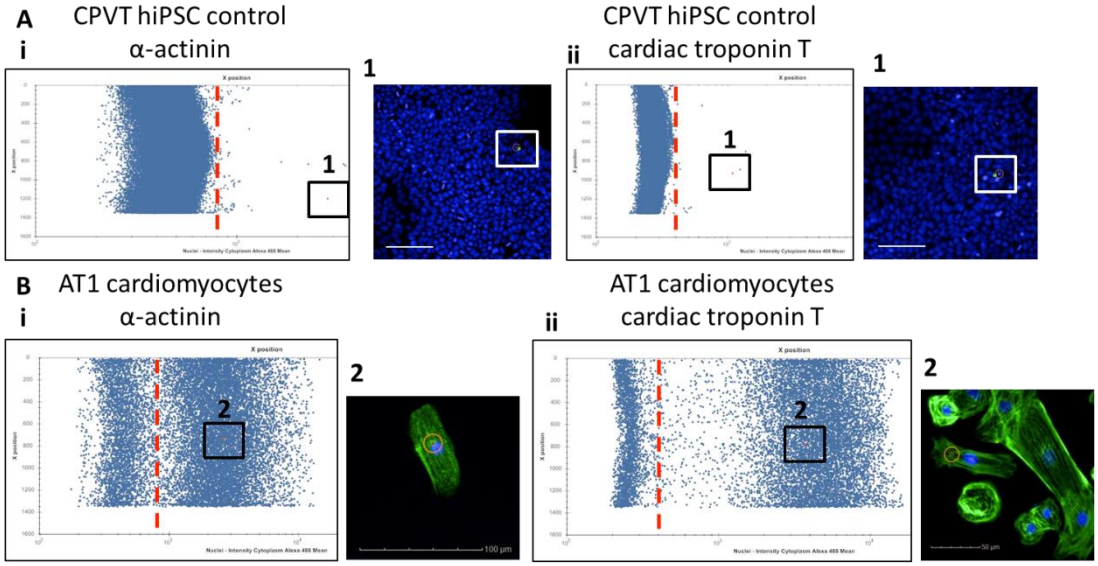


Figure 3.13 – Testing E8 monolayer differentiation dissociation strategies to maximise cell survival post-dissociation.

Five different dissociation methods were attempted to find one that would give improved cell survival following dissociation. Scoring systems were created to assess the quality of each method in three categories: 1) Ability to fully harvest cells from culture surface, 2) ease of dissociating clumps in suspension after removal from culture surface, 3) viability of cells 24 hr after seeding on fresh culture surface. * - 0 = no dissociation from culture surface, 1 = less than half of the culture harvested, 2 = majority of culture harvested but incomplete harvest, 3 = complete cell harvest. + - 0 = No dissociation of clumps achieved, 1 = large clumps which are not dissociated with repeated vigorous pipetting, 2 = most clumps dissociated but with repeated and vigorous pipetting required, 3 = complete dissociation of clumps with minimal pipetting required. ¤ - 0 = No cell survival on reseeding, 1 = poor cell survival (small colonies of cells) before first medium change after reseeding, 2 = improved survival, but with high levels of cell death also observed prior to first medium change after cell re-seeding, 3 = low levels of cell death observed prior to first medium change following re-seeding. **(A) (i)** Representative images showing complete cell death with T/A method, **(ii)** partial cell survival with TrypLE Express + ROCKi method and **(iii)** high cell survival with collagenase 20 min / TrypLE 5 min method. **(B)** Cells attached to extracellular-matrix-like basement membrane following successive rounds of enzyme treatment, indicating incomplete dissociation of cells from culture surface. **(C)** Beating monolayer of hiPSC cardiomyocytes before addition of collagenase and after 20 min incubation in collagenase, entire cell layer detached from culture surface and beating in suspension. **(D)** Cells dissociated with collagenase (20 min) and TrypLE Express (5 min) 5 days after seeding on fresh surface, spontaneously beating and at full confluence.

3.2.14 Quantification of immunostained cardiomyocytes by Operetta confocal plate reader

While immunostaining quantification was achieved using the Cellavista cell imager, its functionality was limited. The protocol used for this was limited to simultaneous quantification of one whole-cell marker and two nuclear markers. The Operetta plate reader was later purchased and had increased functionality allowing any combination of whole cell and nuclear markers. To enable cardiomyocyte quantification and potentially, downstream multiplexing with other markers or morphology properties, a protocol was written for the quantification of cardiomyocytes by immunostaining. Like the process in 3.2.5, this had the advantage of using far fewer cells than flow cytometry. Wells containing a negative control (in this case CPVT hiPSCs) were stained for either α-actinin or cardiac troponin T with Alexa Fluor® 488 secondary antibody. A scatter plot was generated with log fluorescence on the x-axis allowing logical thresholding to be carried out based on negative samples (figure 3.14 A). This threshold could then be set to select and quantify positively stained cells while outliers could be selected in the software and identified (figure 3.14i-1 and ii-1).



AT1 cardiomyocytes stained with α-actinin	AT1 cardiomyocytes stained with cardiac troponin T
74% +/- 2.9% SD (n=4 wells)	71% +/- 1.6% SD (n=4 wells)

Figure 3.14 – Quantification of immunostained AT1 hiPSC cardiomyocytes and negative control CPVT hiPSCs using the Operetta confocal plate reader.
A) (i) CPVT hiPSCs stained with α–actinin as a negative control to determine negative-selection fluorescence threshold, set at 800 fluorescence units (shown with dotted red line). (Inlay marked with 1) An outlier was detected and could be shown by clicking on it in the graph. **(ii)** CPVT hiPSCs stained for, cardiac troponin T, as before an outlier was detected and is shown, and threshold was set at 400 fluorescence units (dotted red line). **B)** A population of cardiomyocytes generated by differentiating AT1 hiPSCs was quantified for **(i)** alpha-actinin staining and **(ii)** cardiac troponin T staining using the thresholds identified in **A (i)** and **(ii)** respectively.

3.2.15 Comparison of different surfaces and seeding densities of cardiomyocytes for drug screening

Table 3.2 – Commercial suppliers of hPSC derived cardiomyocytes and recommended seeding densities.
Different seeding densities were identified according to product information sheets or specialised application notes.

Supplier	Cell Line	Application	Recommended Seeding Density
Axiogenesis	Cor.4U	Mitochondrial Toxicity Assays	100-120,000 /cm^2
Cellular Dynamics	iCell Cardiomyocytes^2	Recommended seeding density for confluent beating sheets	156,000 /cm^2
GE Healthcare	Cytiva Cardiomyocytes 1E6	High-Content Multiplexed Cytotoxicity Assay	120,000 /cm^2
Pluriomics	Pluricyte Cardiomyocytes	Recommended seeding density	75-120,000 /cm^2

According to user protocols supplied by commercial suppliers (table 3.2), a confluent sheet of hPSC cardiomyocytes was preferable so that a synchronised beating sheet could be formed prior to drug screening experiments. The values from table 3.2 also took into account percentage cell loss in the thawing and cell seeding process. In order to identify a suitable final cell concentration needed to achieve confluence in wells, cardiomyocytes were seeded at a range of densities starting at 60,000 cells per well (180,000 cells per cm^2) down to 20,000 cells per well (60,000 cells per cm^2). Wells were stained with Calcein AM, PI and Hoechst33342 at either 72 hr, 96 hr or 120 hr after seeding. Representative images showing cells at final densities of 30,000, 20,000 and 10,000 cells per well were chosen to illustrate how this translated into well confluence. At 30,000 cells per

well, nearly complete confluence was achieved (equivalent to 90,000 cells/cm^2). For this reason, this was the target final cell density used for drug screening experiments. Additionally, cardiomyocyte attachment on Matrigel, Fibronectin and Vitronectin-N was carried out. On all surfaces, cardiomyocyte attachment was achieved and spontaneous contraction of sheets observed suggesting that all three surfaces were compatible with cardiomyocyte seeding. Matrigel was chosen for drug screening work as this had been used extensively in our labs already for cardiomyocyte differentiations and re-seeding. However, a comparison of cost between Vitronectin-N and Matrigel revealed that (after discount) Vitronectin-N was marginally cheaper than Matrigel (£0.03 compared to £0.04 per cm^2 respectively) and was fully defined unlike Matrigel but due to time limitations, Vitronectin-N use could not be optimised in time for later drug screening experiments (Chapter 5).

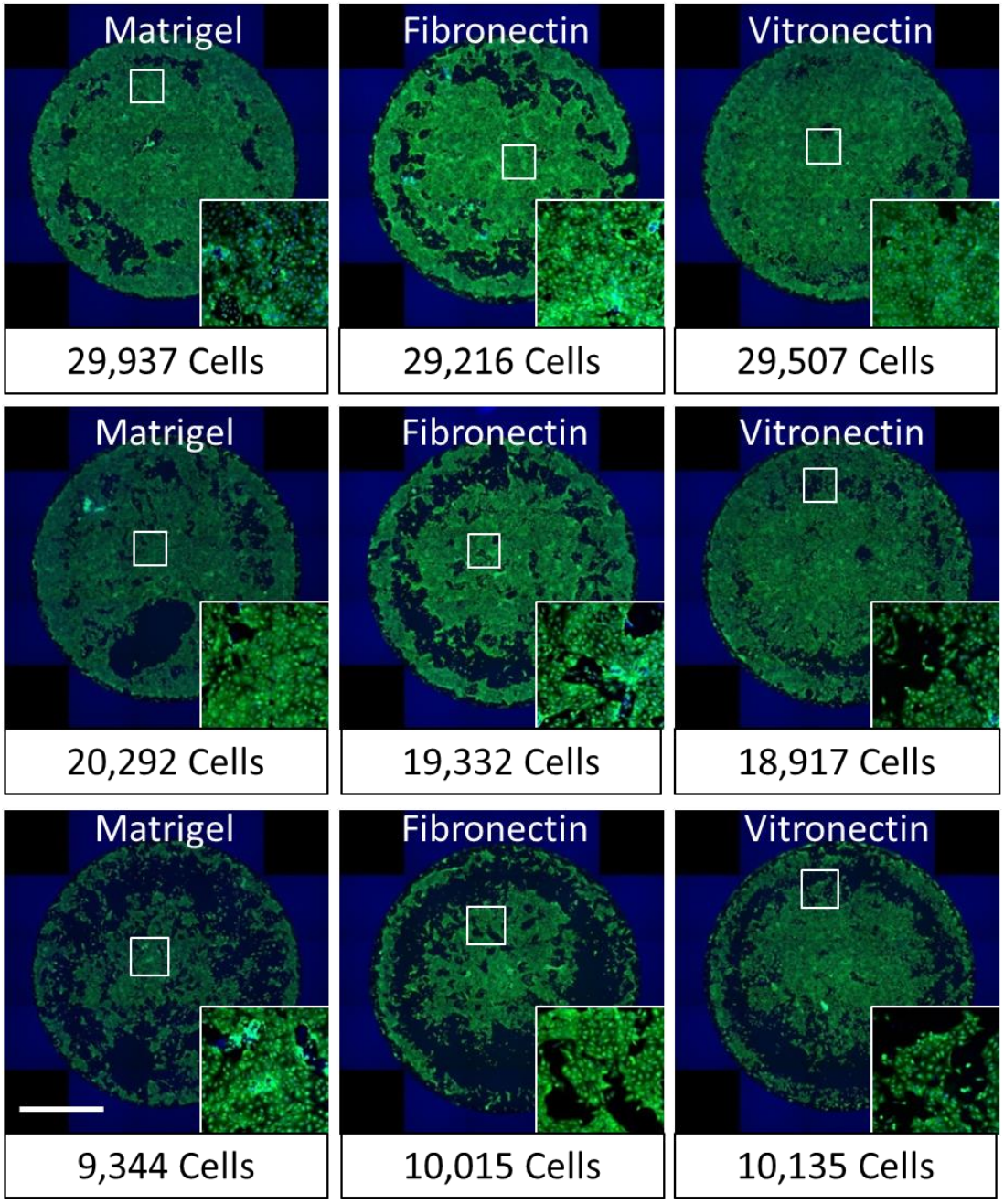


Figure 3.15 – Seeding of cardiomyocytes on Matrigel, Fibronectin and Vitronectin-N to determine optimal seeding density.
CPVT hiPSC derived cardiomyocytes were thawed and seeded in 96-well flat bottom plates coated with Matrigel, Fibronectin, or Vitronectin-N to determine suitability of surfaces and seeding densities for drug screening. Images were taken 96hr (4 days) after seeding when cardiomyocytes began to contract spontaneously after thawing. **(Top row)** Wells containing approximately 30,000 cells (exact numbers shown below). **(Middle row)** Wells containing approximately 20,000 cells. **(Bottom row)** Wells containing approximately 10,000 cells. Scale bar = 2 mm.

3.2.16 Optimising cardiomyocyte culture conditions to maintain cardiomyocytes for drug screening

While cardiomyocytes dissociated by the new collagenase / TrypLE method showed improved survival after dissociation, cell death was observed from day 5 onwards in these cells when cultured in CDM3 medium. Images taken from three different wells (figure 3.16 B) on day 6 after seeding from the same plate showed different levels of spontaneous cell death. While differentiations could be carried out in CDM3 medium, it appeared that maintenance of cardiomyocytes after dissociation using this medium was not suitable for more than 5 days. To test this more thoroughly, CPVT cardiomyocytes from the same bank were thawed and seeded at identical seeding densities in either RPMI-B27 or CDM3 medium, with or without ROCK inhibitor for 48 hours, and maintained in culture without ROCK inhibitor up to 12 days (post seeding) before scanning with the Cellavista to determine well confluence. Cells thawed without ROCK inhibitor had significantly lower cell survival in both media types, 54.8+/-8.5 % vs 95.2+/-1.6 % in RPMI-B27 and 21.8+/-8 % vs 58.6+/-6.2 % for CDM3 ($p<0.0001$) (figure 3.16 A). Additionally, at 95.2+/-1.6 %, RPMI-B27 with ROCK inhibitor thaw was significantly higher than all other conditions (at nearly full confluence) ($p<0.0001$). For this reason, thawing or seeding of cardiomyocytes was done in RPMI-B27 with ROCK inhibitor and subsequent maintenance of cardiomyocytes was also carried out in RPMI-B27 to maximise cell viability for drug screening experiments.

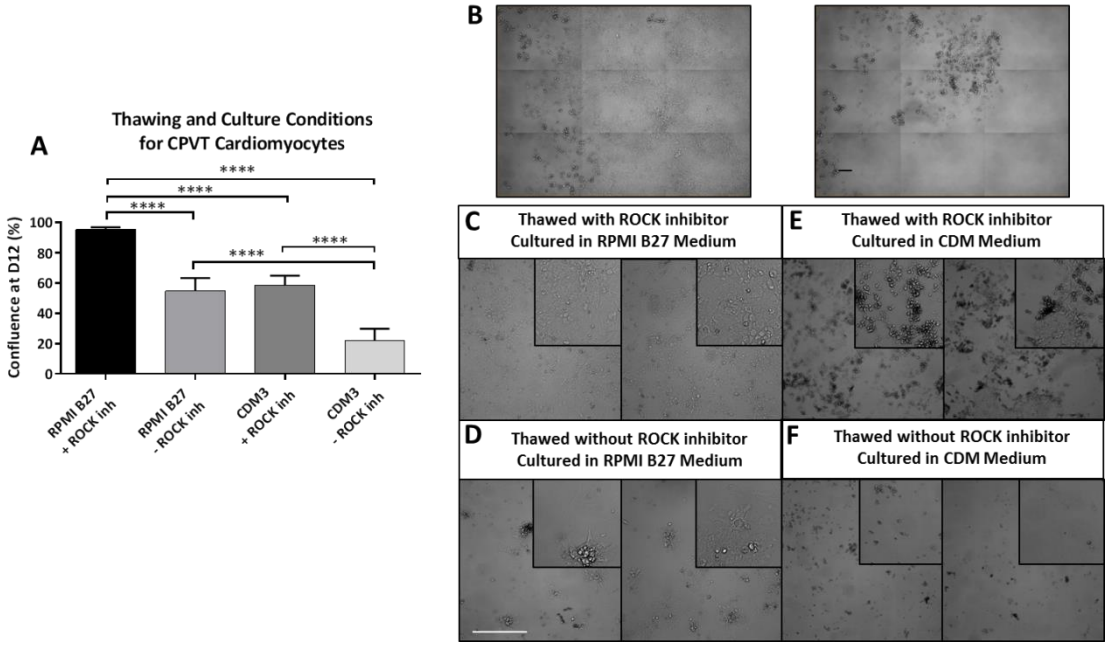


Figure 3.16 – Testing conditions for thawing and culturing cryopreserved cardiomyocytes for seeding in drug screening assays.
A) Comparison of well confluence reflecting loss of cells by day 12 of culture with cardiomyocytes thawed into RPMI-B27 +/- ROCKi or CDM3 +/- ROCKi on Matrigel coated wells (one-way ANOVA, TMCT). **B)** Composite images from two different wells of a 96 well plate at day 6 post seeding containing AT1 cardiomyocytes in CDM3 medium, showing spontaneous cell death in both wells, scale bar = 100 µm. **C)** Cardiomyocytes thawed in RPMI-B27 medium containing ROCKi (48 hr exposure) followed by a further 10 days culture in RPMI-B27 medium without ROCKi with good survival. **D)** Cardiomyocytes thawed without ROCKi but in the presence of RPMI-B27 showed poor survival post thaw but surviving cells continued to survive in culture. **E)** Cardiomyocytes thawed in CDM3 medium with ROCKi showing large proportion of dead/dying cells with some cells still attached to the culture surface. **F)** Cardiomyocytes thawed in CDM3 medium without ROCKi showing almost complete cell death.

3.3 Discussion

3.3.1 Feeder free hESC and hiPSC culture

In this chapter, culture of the HUES7 hESC line was achieved across three different systems, the feeder-free conditioned medium method, mTeSR feeder free system and Essential 8 feeder free system. The decision to adopt different culture methods rather than selecting one and using it throughout was determined primarily by weighing up the disadvantages observed in one method with the potential benefits of newer culture systems. For reasons described in greater detail below, advantages associated with mTeSR culture meant that this culture system was adopted over conditioned medium and subsequently mTeSR culture was superseded by the E8 culture system.

3.3.2 Conditioned medium culture and EB differentiation

Feeder free culture of hPSC lines in MEF-CM on Matrigel coated surfaces at the start of this work was well established in our labs (Matsa et al., 2011, Denning et al., 2006). For this work, the HUES7 hESC line was cultured in these conditions with a stable growth rate over 6 passages, no change in karyotype and no signs of spontaneous differentiation of cultures. HUES7 cultures maintained in MEF-CM were capable of differentiation to cardiomyocytes by EB differentiation using the most recently published version of the EB differentiation method at the time (Burridge et al., 2011), an observation that was also demonstrated by others in the group (Pascut et al., 2013, Matsa et al., 2014). High yields (measured as percentage of spontaneously beating EBs per plate) were achieved using HUES7 hESCs of up to

93+/-0.3 %, however, variability in differentiation outcome was observed between differentiations using different batches of conditioned medium (yields as high as 100 % in MEF89 and as low as 0 % in MEF88). MEFs secrete growth factors such as activin A which play an important role in maintaining pluripotency in hPSCS (Jozefczuk et al., 2012). Variations in levels of activin A secretion have also been observed between feeders of different sources, with mouse feeders being preferred due to their high levels of activin A secretion (Jozefczuk et al., 2012). Therefore, variations in differentiation outcome arising between batches of MEFs may have been a result of batch to batch variations in levels of growth factor secretion. Even using the same batches of MEFs, variability was observed in the yields of differentiations, ranging from 99 % to 33 % (MEF89, n=9) and 79.8 % to 0 % (MEF88, n=6). This may have resulted from user variability if a MEF batch was prepared by multiple users during processing prior to banking, or user variability in handling of these cells after thawing.

Protocols for preparing MEF feeder cells required that they be grown to passage 3 before they were mitotically arrested through the use of Mitomycin C (see chapter 2 section 2.1.1) in order to allow medium conditioning to take place. Therefore, these cells were a finite resource and as stocks became depleted, fresh batches were used for continued routine culture. While other groups have demonstrated that these lines could be immortalised (Choo et al., 2006), this was not attempted in our labs.

While capable of generating large numbers of spontaneously beating EBs, harvesting cardiomyocytes of sufficient numbers to produce cell banks or to carry out drug screening in multiple 96- or 384- well plates proved challenging. While attempts were later made to simplify and speed up the process using automation (chapter 4), the manual process of harvesting was both time consuming and low-throughput using either the T/A or CDS methods. These were limited to a maximum of 8 EBs dissociated at a time, yielding between 30-60,000 cells in a process lasting approximately 20 minutes to 40 minutes depending on the age of the EBs (EBs older than a month become considerably more difficult to dissociate). To place this in context, approximately 30,000 cells were needed in one well of 96-well plate (or 10,000 per well of a 384-well plate) for drug screening. Harvesting entire plates of EBs gave 0.6+/-0.3x10^6 cells per plate (n=9) indicating that 5 plates worth of EBs would be needed to seed one 96-well plate or 6.5 plates for one 384-well plate for drug screening.

3.3.3 mTeSR medium and the mTeSR monolayer differentiation method

The mTeSR monolayer method used fully defined maintenance media for both the culture of cells and the differentiation process (albeit still on Matrigel, which was undefined). This had the benefit of avoiding batch variations associated with using MEFs. When growth curves were carried out, a steady rate of growth was achieved and no karyotype abnormalities arose after 5 passages in this system over 17-19 days in culture. A comparison of HUES7 population doubling times between

conditioned medium and mTeSR revealed a significant increase in the population doubling time of these cells in mTeSR (69.9+/-7.7 hr vs 43.2+/-0.4 hr in conditioned medium, $p<0.01$, t-test). However, the cost of using mTeSR (estimates include manufacturer discounts where applicable) was much higher at £0.34/ml compared to approximately £0.11/ml for MEF-CM (MEF-CM costs calculated by Maria Barbadillo-Munoz). Finally, high cell seeding densities were required to prevent crashing of cultures after splitting (80,000 cells/cm^2 compared to 50,000 cells/cm^2 for conditioned medium) representing the equivalent of 1:2 to 1:3 splits and limiting the rate of scale-up achievable with these cultures.

Despite its limitations, several benefits arose from changing to the mTeSR monolayer differentiation method. Firstly, by carrying out the differentiations on flat surfaces, cell confluence could be monitored and timing of differentiation standardised/controlled with the aid of the Cellavista (when carried out in well plates or RoboFlask formats), furthermore, the process of differentiation involved changing media in flasks, a process that was more simple and less time consuming than changing medium in 96-well plates using multi-channel pipettes. This also had the benefit of simplifying the automation of this process (discussed in chapter 4). Finally, dissociation of cardiomyocytes at the end of the differentiation process was made considerably easier, using the existing cell passaging method but with T/A enzyme mixture for 7 min and neutralising with foetal bovine serum containing medium. The added benefit of carrying this process out in RoboFlask format was that cell yields of 7.3+/-1.2 million cells could be achieved per flask, allowing cell

banks of high purity (≥90 % by α-actinin and cardiac troponin T staining) to be created and providing sufficient numbers of cells to seed 96-well ($2.9x10^6$ cells needed) and 384-well ($3.8x10^6$ cells needed) plates for drug screening.

3.3.4 E8 medium and the E8 monolayer differentiation method

More recently, a monolayer differentiation method was published achieving comparable cardiomyocyte purities of up to 95 % but with much higher yields of 100 cells to 1 input cell (Burridge et al., 2014), compared to yields of approximately 1:1 achieved with the mTeSR monolayer method. Additionally, there was the added benefit that E8 medium was cheaper than mTeSR (after discount, £0.20/ml compared to £0.34/ml for mTeSR) while removing batch variability due to the complete removal of bovine serum albumin from the formulation (Chen et al., 2011). A growth curve of HUES7 hESCs in E8 carried out over 6 passages gave a population doubling time of 30.14 hr (the lowest of the three media conditions) however, a trisomy of chromosome 12 was, suggesting the appearance of a karyotypically abnormal clonal population. Acquisition of chromosome 12 has been observed by others in both hESCs and hiPSCs (Robinton and Daley, 2012) and may result from a selective advantage due to NANOG and growth/differentiation factor 3 over-expression (Ben-David and Benvenisty, 2011). That said karyotype abnormalities did not arise in CPVT and LQT2 hiPSCs which were also cultured in E8 and had normal karyotypes after 7-passage growth curves. CPVT-hiPSCs derived and cultured in E6/E8 had population doubling times even lower than that of HUES7 at 21.3 hr (EDTA) and 21.7 hr (TrypLE) while LQT2 hiPSCs were 39.2 hr (TrypLE).

Compared to mTeSR, E8 cultures showed improved scalability with seeding as low as 32,000 cells per cm^2 representing the equivalent of 1:6 split ratios. This was likely aided by the routine use of ROCKi which promotes cell survival by selectively inhibiting p160-Rho-associated coiled-coil kinase (Watanabe et al., 2007) and may aid in preventing clonal selection mechanisms (such as cell death following passage) that favour proliferation or improved survival of karyotypically abnormal populations (Barbaric et al., 2014). However, ROCK inhibitor was not used in mTeSR cultures and a fairer comparison of these media could have been achieved had this been done. Furthermore, replicates of growth curves in E8 are needed before accurate comparison could be made between E8 and other media as all E8 growth curves were n=1.

In addition to benefits of using E8 in culture, improvements were also achieved with the differentiation of the CPVT and LQT2 hiPSC lines in E8. Cell yields of up to 40 million (CPVT-hiPSC) were achieved when carried out in RoboFlasks (an automated differentiation but dissociated manually), 5.5-fold higher than what was achieved using HUES7s in the mTeSR differentiation method (7.3+/-1.2 million). This represented an output of approximately 13 cells per 1 input cell (3 million cells seeded), much lower than reported (Burridge et al., 2014) but representing a considerable improvement over the mTeSR method (1.2 cells per 1 input cell, 6 million seeded). Furthermore, purity of these cells was comparably high at >90 % (by α-actinin and cardiac troponin T staining) with both the published E8 monolayer

method (Burridge et al., 2014) and the purities achieved with the mTeSR differentiation method.

3.3.5 Plating and maintenance of hiPSC derived cardiomyocytes

Despite the considerable improvement in cardiomyocyte output with the E8 monolayer method, a key challenge arose when complete cell death occurred following dissociation using the T/A method which had not been seen when dissociating using mTeSR-method or EB-method cardiomyocytes. Using TrypLE Express (Burridge et al., 2014) improved harvesting and cell survival but did not remove all cells from the flask surface and cell death after dissociation was still high. Images showing cells attached to a "basement membrane" appeared to suggest the formation of an extracellular matrix during the differentiation process on which a large proportion of cells remained firmly attached (figure 3.13B) during the dissociation process. T/A and TrypLE Express appeared to be ineffective at dissociating this matrix. Therefore, by using collagenase to digest these anchoring proteins, improved cell survival and full dissociation from the flask surface was achieved. However, this solution was not developed until after the experiments carried out in 3.12 and therefore, purity of cardiomyocyte differentiations using different small molecule concentrations could not be generated. Additionally, these experiments could not be repeated later due to time limitations.

RPMI-B27 medium was used to maintain EB and mTeSR monolayer-derived cardiomyocytes in culture and has been used for successful cardiomyocyte culture

and differentiation by other groups (Laflamme et al., 2007, Burridge et al., 2014). However, as E8 differentiation was carried out in CDM3, and because CDM3 was cheaper than RPMI-B27 (£0.03 and £0.13 per ml respectively), this medium was used for cardiomyocyte cultures. While CDM3 was capable of supporting differentiation and maintenance of cardiomyocytes *in situ* following differentiation, following dissociation, this medium proved unable to maintain cardiomyocytes with varying levels of cell death observed from 5 days onwards (measured by confluence of wells) (figure 3.16B) following cell seeding. For this reason, RPMI-B27 was used and a comparison of the two media and the effect of thawing and seeding these cells with or without ROCKi showed RPMI-B27 with ROCKi (92+/-1.6 % confluence) to be significantly better ($p<0.0001$, one-way ANOVA, TMCT) at maintaining cardiomyocytes for up to 12 days in culture than CDM3 with (58.6+/-6.3 %) or without ROCKi (21.8+/-7.9 %) or RPMI-B27 without ROCKi (54.8+/-8.5 %).

4 Developing Automated Processes for Cardiomyocyte Differentiation and Drug Screening

4.1 Introduction

The purpose of this chapter was to develop processes on the Tecan Freedom Evo 200 robotic platform (henceforth referred to as the robot or robotic platform) to produce cardiomyocytes from either HUES7 or hiPSC lines that could then be used for drug screening. Secondary to this aim, was to maximise the total yield and cardiomyocyte purity from differentiations carried out on the robot. When new differentiation methods such as the mTeSR monolayer method and the E8 monolayer differentiation method (Burridge et al., 2014) became available that generated improved yields or purity, these were translated onto the robot.

4.1.1 The robot and integrated hardware

The robotic platform that was used for this work consisted of several core hardware components (see figure 4.1 for an overview and figures 4.3 to 4.9 for more detailed descriptions). Cell cultures were stored in a heated StoreX incubator (figure 4.3) at 37 °C, with 5 % CO_2 and a humidified environment. Additionally, there was a cold StoreX incubator which was maintained at 4 °C for storage of media. Both StoreX incubators were connected to the robot with access gates and flask transfer stations that allowed for the transport of RoboFlasks, plates or media troughs between the incubators and the robot work surface. Plasticware brought out by either of the StoreX incubators was collected by the robotic manipulator arm

(RoMa) by clasping plasticware between two eccentric gripper fingers (figure 4.4) and transporting them to the desired position on the robotic work surface. RoboFlasks were placed on the FlaskFlipper module (FlaskFlipper) in order to carry out medium changes or cell harvests (figure 4.5) the FlaskFlipper was capable of rotating clockwise and anticlockwise to create a rocking motion to enable mixing of liquids in flasks as well as tapping flasks to dislodge cells. To facilitate removal or addition of media, enzymes or DPBS in flasks, the FlaskFlipper could rotate anti-clockwise 90° in order to present the septum of the flask cap (figure 4.2) to enable the liquid handling arm (LiHa) to enter the flask and aspirate or dispense medium accordingly. Pipetting of liquids with the LiHa was controlled by a series of syringes and valves which precisely controlled the volume of internal system liquid (sterile distilled water) in the tubing that in turn controlled the volumes of liquids aspirated or dispensed by the LiHa tips (figure 4.6). Reagents such as fresh media or cell suspension were stored either on a warm carrier to heat them or keep them warm or they could be stored at RT in 100 ml troughs. Cell suspensions also were kept in these troughs during cell harvests to allow cell counting and mixing of cell suspension with the LiHa (figure 4.8). The LiHa tips dispensed unwanted media into a waste station and tips were regularly cleaned during processes by rinsing with system liquid (figure 4.10 second row far left image). During cell harvests, cell suspensions were collected using the LiHa and dispensed (300 µl) into a collection cup (figure 4.7Bii) to allow cell counts to be performed using an integrated Cedex HiRes cell counter. The cell counter quantified viable cell number based on Trypan Blue exclusion in live cells and uptake in dead cells. Cell counts were then used by the robot to calculate dilutions of cell suspensions for re-plating. For seeding cells or

changing media in 96- or 384-well plates, a MultiChannel Arm™ 96 (MCA96) was used which could simultaneously aspirate or dispense from 96 channels when fitted with disposable tips (figure 4.9). Medium or cell suspension was placed either in 96-well source plates or a 300 ml baffled trough (figure 4.8C) to enable access for the MCA96.

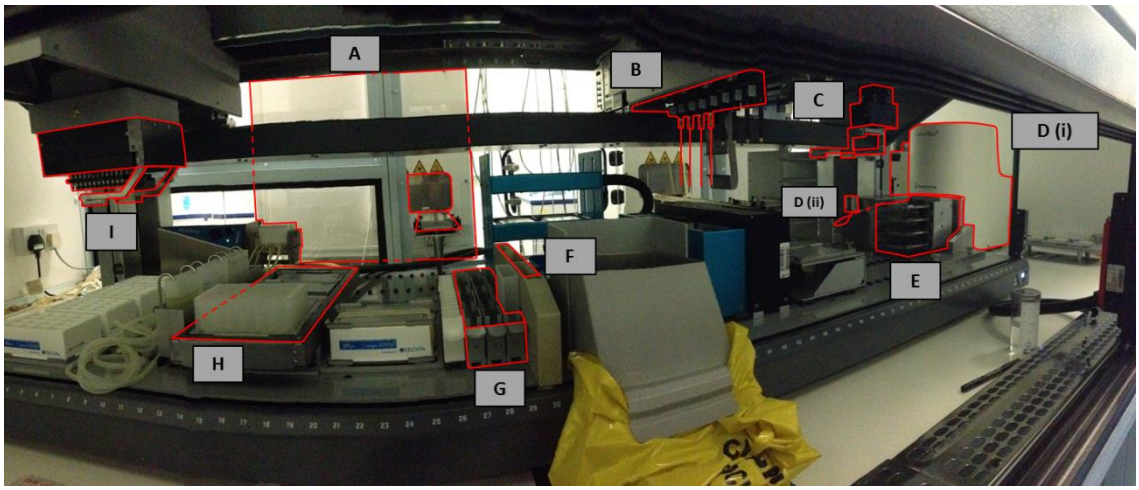


Figure 4.1 – Hardware of the Freedom Evo 200 Robotic Platform
Panoramic image of the Freedom Evo 200 robotic platform contained within a BigNeat LAC class-II type enclosure (robot enclosure) with key hardware components highlighted in red. **A)** Warm StoreX incubator for storing cell cultures at 37 °C with 5 % CO_2 with humidified atmosphere and attached cell transfer station (see figure 4.3). **B)** LiHa liquid handling arm for addition and removal of medium (see figure 4.6). **C)** RoMa robotic manipulator arm for carrying and moving plates, troughs and flasks across the robot workspace (see figure 4.4). **D) (i)** Integrated Cedex HiRes cell analyser for cell counting and **D) (ii)** collection cup for collecting cell suspension for cell counting (see figure 4.7). **E)** FlaskFlipper module for holding plates, flasks or troughs and allowing LiHa access for addition and removal of reagents to/from RoboFlasks (see figure 4.5). **F)** LiHa wash/waste station for discarding reagents from the LiHa tips and washing tips to remove waste reagent and cells from tips. **G)** Trough storage station for 100 ml troughs which are used to store cell suspension after cell harvesting (see figure 4.8). **H)** Warm carrier heated to 37 °C for placing troughs or plates containing medium to maintain temperature at 37 °C (see figure 4.8). **I)** MCA96 multichannel arm for pipetting 96 channels simultaneously (see figure 4.9).

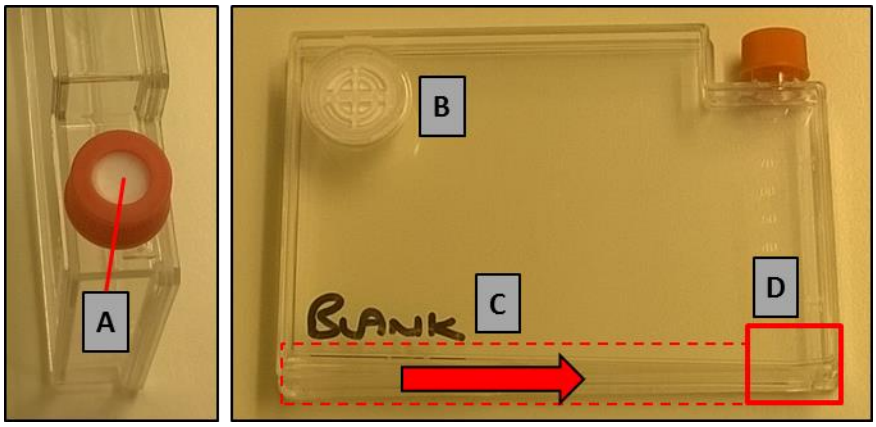


Figure 4.2 – Corning RoboFlask

The Corning® RoboFlask® (RoboFlask) has a culture surface of 92.6 cm^2, is stackable and comes with a pierceable and re-sealing septum (A) in the cap to allow access of liquid handling tips such as the LiHa (see figure 4.4). As the cap is removable, manual culture can also be carried out using these flasks. A gas permeable membrane (B) is situated on the top to allow gas exchange and the base of the flask (when positioned as shown in the left image) (C) is sloping (highlighted in dotted red region) to allow residual liquid to collect (see arrow) towards the cap-side (D, red box) to aid complete aspiration of media.

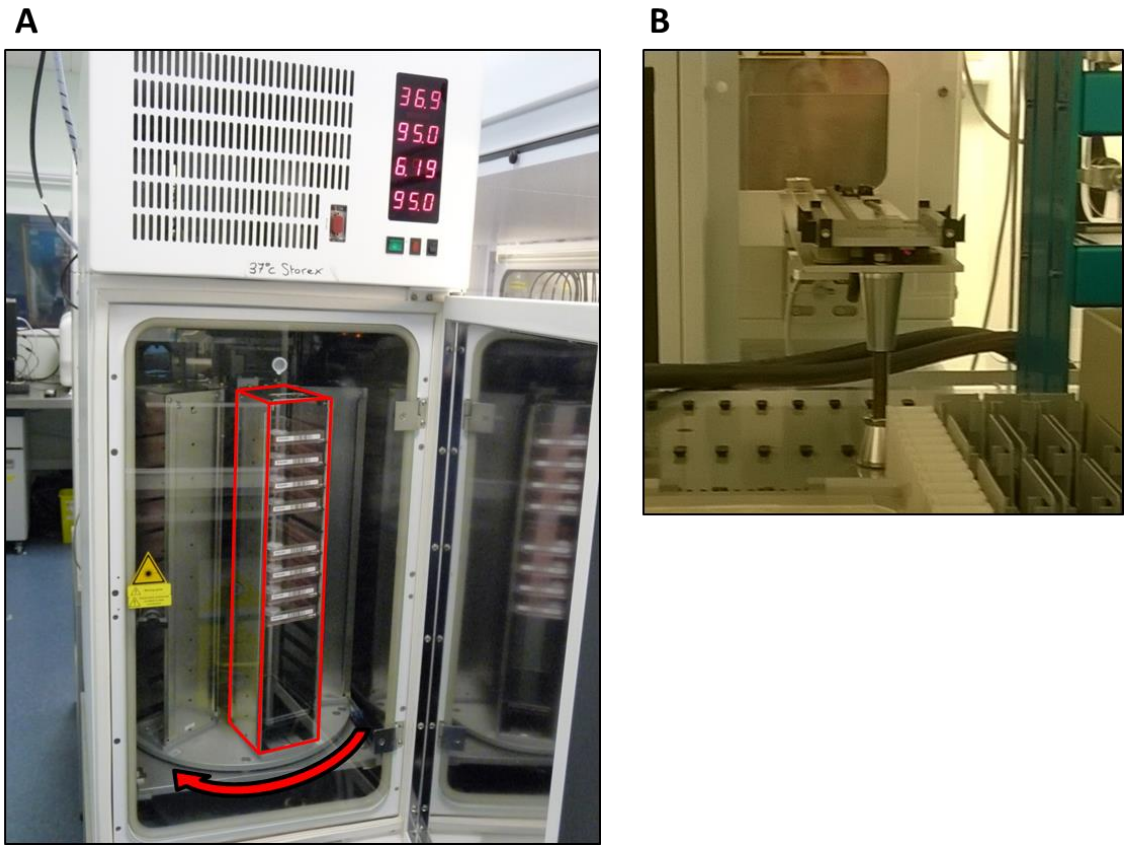


Figure 4.3 – StoreX Incubator (STX110)

A) Liconic Instruments automated STX110 incubator (StoreX) containing a clockwise-rotating carousel with towers (highlighted in red) for holding plates and RoboFlasks with a maximum capacity of 110 RoboFlasks or plates. The StoreX is heated to 37 °C, maintains atmospheric CO_2 at 5 % and is humidified. **B)** Features a robotic access gate to allow automated transfer of flasks or plates to and from the robot.

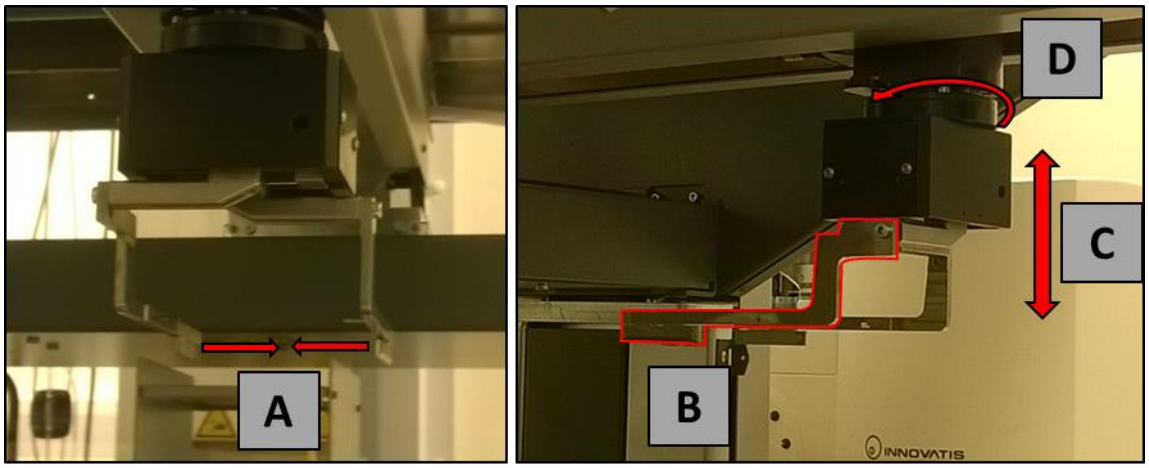


Figure 4.4 – Robotic Manipulator Arm (RoMa)
RoMa arm for carrying and transferring plates or flasks throughout the robot. Plasticware is clasped (**A)** between two eccentric gripper fingers **(B)**. The RoMa arm is capable of vertical movement **(C)** and rotating 380° **(D)**.

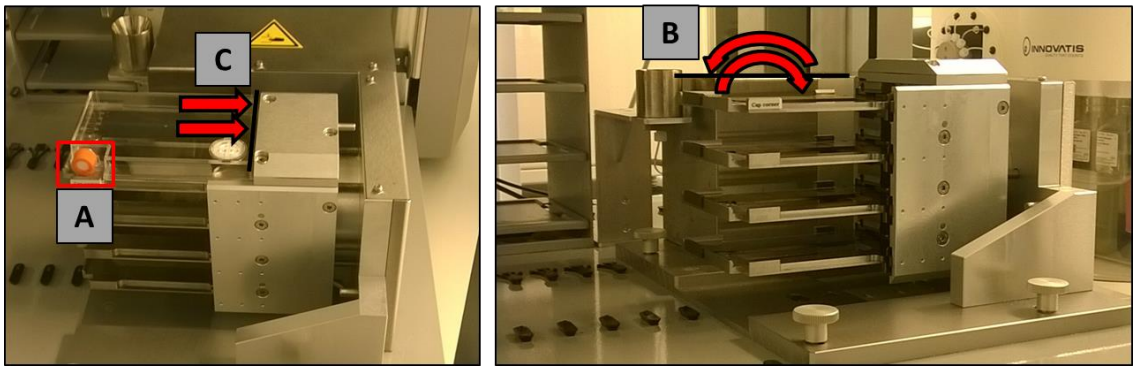


Figure 4.5 – Flask Flipper™ module
The Flask Flipper™ module (FlaskFlipper) can hold up to 4 RoboFlasks simultaneously. In the resting position, the FlaskFlipper is horizontal (left and right images) but can be rotated 90° anticlockwise to expose the septum of a RoboFlask **(A)** to enable LiHa access. An inbuilt holding mechanism prevents flasks from moving while the FlaskFlipper is not in the horizontal position. RoboFlasks can be rocked **(B)** to enable mixing of reagents by sequential clockwise and anticlockwise rotation or tapped **(C)** to dislodge cells from the culture surface.

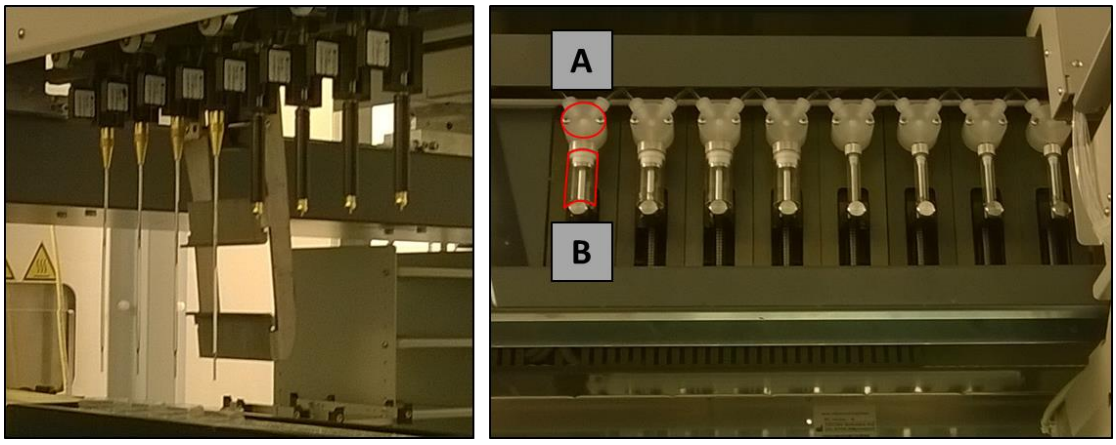


Figure 4.6 – Liquid Handling Arm

The liquid handling arm (LiHa) equipped with four stainless steel 5 ml capacity fixed tips (left image). Each LiHa tip is capable of up moving in a vertical direction. The LiHa arm can move from left to right across the robot but is not capable of rotation. Pipetting is achieved using a microfluidics system controlled by valves (right image, A) and syringes (right image, B) which control the quantity and flow of system liquid through tubing connected to the LiHa which in turn, determines the quantity of liquid collected or dispensed by the LiHa tips. The LiHa was used in all protocols where medium changes occurred in RoboFlasks (including passaging of cells). The LiHa also mixes cell suspensions and transfers cell suspensions to the collection cup for the Cedex HiRes to carry out cell counts (figure 4.7).

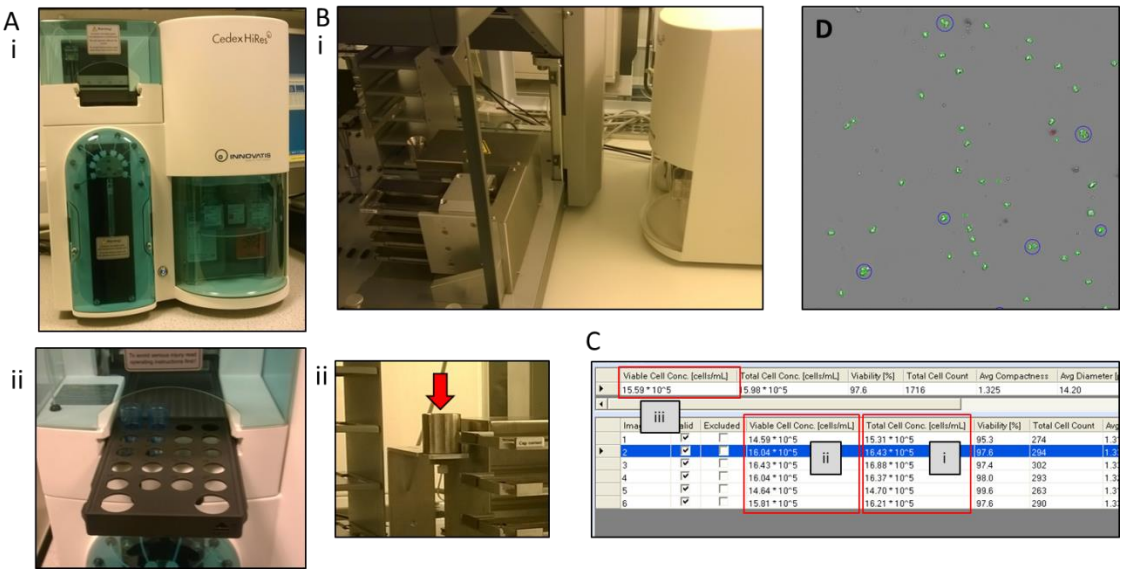


Figure 4.7 – Cedex HiRes cell counter

The Cedex HiRes is a fully automated high resolution image scanning system for quantifying cell number, cell viability (by Trypan Blue exclusion) and cell morphology based on properties such as cell size and compaction. **A) (i)** Benchtop Cedex HiRes Analyser used for manual cell counting **(ii)** Cell suspensions are loaded into collection cups which are placed on a carrier (shown in black). **B) (i)** Cedex HiRes Analyser integrated with the robot and used for automated cell counting. **(ii)** A collection cup inside the robot for collecting cell suspension for automated cell counts. **C)** Six images are taken of the cell suspension, these images are analysed using algorithms to detect cells which are in turn, quantified and displayed to give total cell number **(i)**. Dead or dying cells stain with Trypan Blue and are also detected. This value is then used by the software to determine the proportion of viable cells in the population **(ii)**. A final mean value of viable cell number is then calculated from the six counts performed **(iii)**. **D)** Sample image of the cell suspension being counted in **(C)**. Identified cells are either highlighted with green circles (viable cells) or red circles (dead cells stained with Trypan Blue). Blue circles highlight clusters of >1 cell.

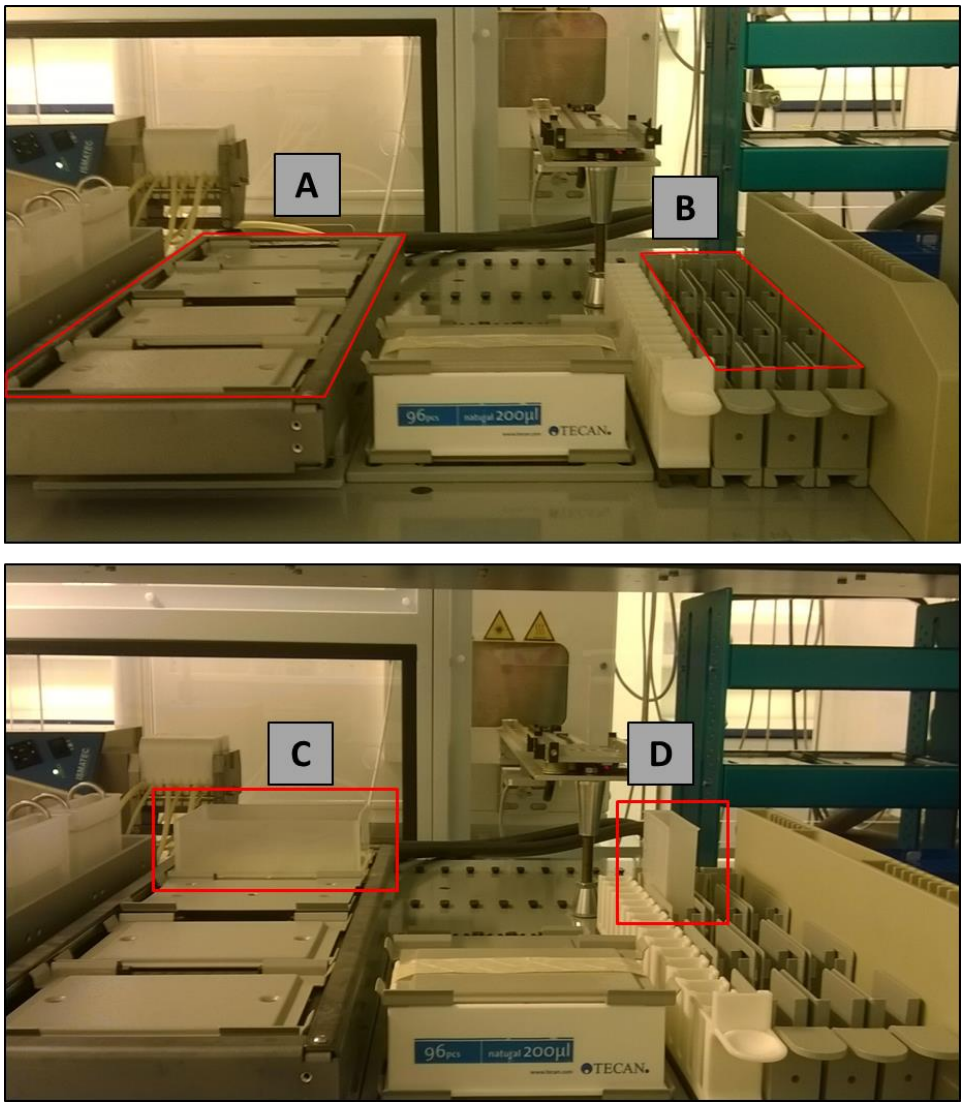


Figure 4.8 – Heated microplate carrier and 100 ml trough carriers
(A) A heated carrier to keep medium, enzyme or other reagents at 37 °C for use during processes such as medium changes or cell harvests. **(B)** 100 ml trough carriers to store reagents at room temperature. These troughs **(D)** are used to hold cell suspension during counting and dilution steps during the passaging procedure (see section 4.1.4). Cell suspensions for seeding 96- or 384- well plates are diluted in troughs on the heated carrier (**C**, a baffled trough) to enable MCA96-seeding.

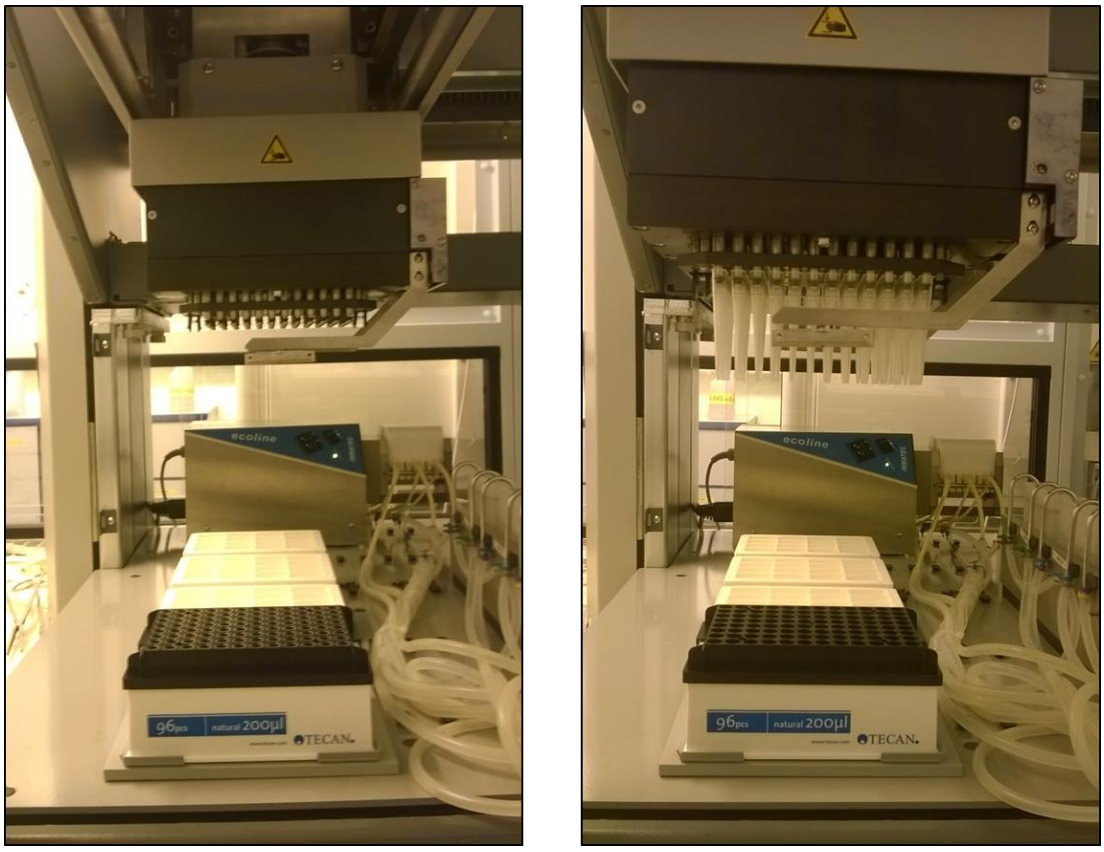


Figure 4.9 – MultiChannel Arm™ 96

The MultiChannel Arm™ 96 (MCA96) is a 96-channel head that can simultaneously aspirate or dispense from 96 channels. Disposable tips are positioned below the MCA96 which then loads these tips (left and right images represent before and after tip loading respectively) by lowering itself into the tips. The MCA96 was used for seeding cells, changing medium and dissociation of EBs in 96-well plates and also used to seed cells and change medium in 384-well plates.

4.1.2 Changing media on flasks using the robot

The medium change process for cultures in RoboFlasks on the robot was used to maintain routine automated cell cultures and in the automated mTeSR and E8 monolayer cardiomyocyte differentiations carried out in RoboFlasks. Automated processes such as medium changes consisted of a sequential list of instructions to the robot (or other integrated hardware) to carry out tasks. These instructions (scripts) were written and carried out using an integrated PC and EVOware® software. Scripts allowed the user to command hardware components to carry out functions such as moving to a particular location and aspirating or dispensing a chosen medium. These processes in turn could be further optimised to control the volume of medium pipetted or the speed of pipetting etc. For illustrative purposes, the medium change script is described here (see also figure 4.10). Firstly, the warm StoreX incubator removes a chosen RoboFlask from a tower and transfers it to the robot work surface via the transfer station. The RoMa arm then moves to the flask clasps it and transports it to the FlaskFlipper. The FlaskFlipper rotates 90° anticlockwise so that the cap of the RoboFlask is facing upwards. The LiHa tips sterilise themselves in IMS, dip a droplet of IMS on the outside of the RoboFlask septum and waits (1 min) for it to evaporate to ensure sterility. Afterwards, the LiHa enters the flask, removes the medium from the flask and dispenses this in the waste station. Meanwhile the FlaskFlipper returns to its original position. The LiHa tips then rinse themselves in the cleaning station. The LiHa tips then move to the trough containing fresh medium, collect a suitable volume, the FlaskFlipper rotates again 90° anticlockwise and LiHa tips enter and dispense fresh medium into the flask.

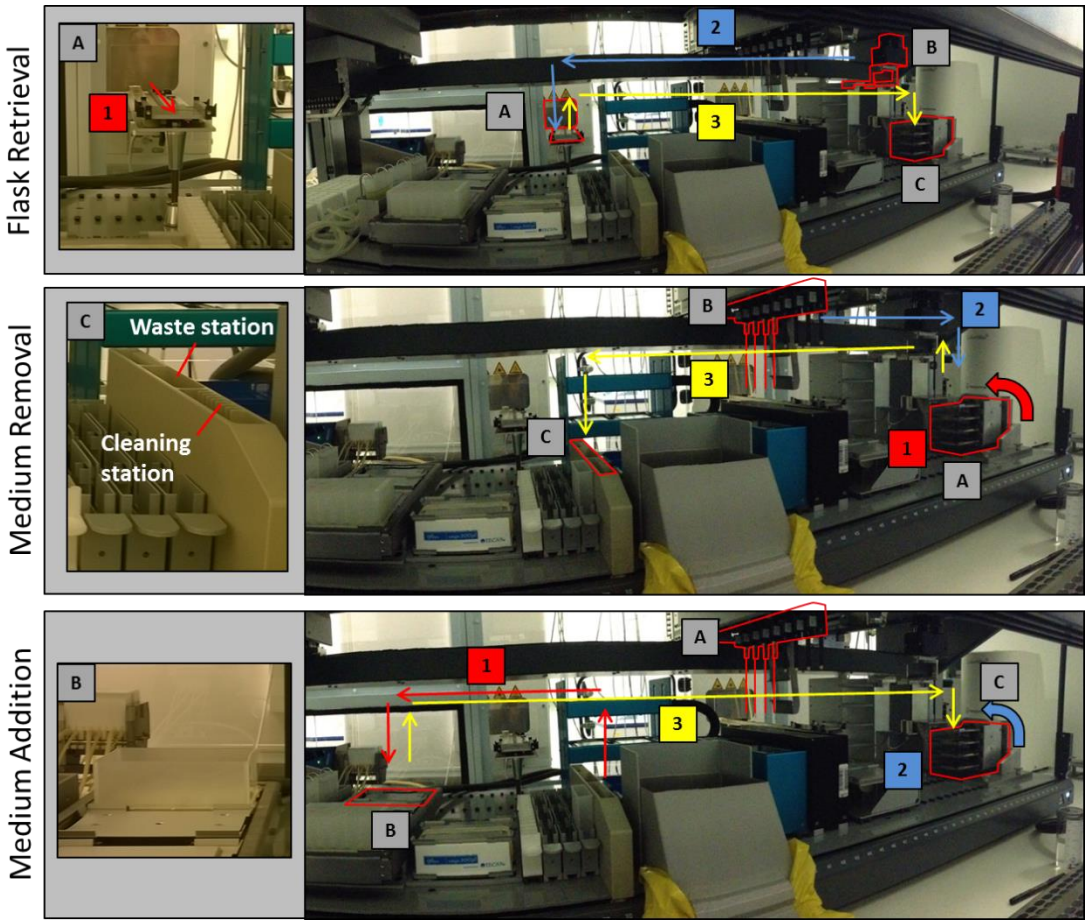


Figure 4.10 – Illustration of the medium change protocol on the robotic platform. Hardware (highlighted in red outlines) and processes (highlighted in chronological order) with red (first), blue (second) and yellow (third) that occur during a medium change protocol. **(Top row images)** A RoboFlask is retrieved from the warm StoreX. **(A)** The RoboFlask is brought out by the flask transfer station. **(B)** (see blue arrows marked 2) RoMa arm moves to flask transfer station, retrieves the RoboFlask and transfers to the FlaskFlipper module **(C)** (highlighted with yellow arrows marked 3). **(Second row images)** Unwanted medium is removed from the RoboFlask. **(A)** FlaskFlipper module (with flask locked in place) rotates 90° anticlockwise (highlighted with red arrow marked 1) so that the RoboFlask septum is pointing upwards allowing the LiHa arm **(B)** to enter the flask to aspirate medium (highlighted with blue arrows marked 2). After collecting unwanted medium, the LiHa arm moves to waste station **(C)** (see yellow arrows highlighted 3), the FlaskFlipper returns to its original position and the LiHa arm dispenses unwanted medium into the waste station then moves to the cleaning station (see far left image) and rinses tips in cleaning solution. **(Bottom row images)** Fresh medium is added to the RoboFlask. **(A)** The LiHa arm navigates from the cleaning station to the heated carrier **(B)**(highlighted with red arrows marked 1) and collects fresh medium from a trough (example in far left image). **(C)** The FlaskFlipper module rotates 90° anticlockwise again (see blue arrow marked 2) and the LiHa arm moves to the flask (highlighted with yellow arrows marked 3) and dispenses fresh medium into the flask. The LiHa returns to its original position, the FlaskFlipper returns to its original position and the RoMa arm then collects the RoboFlask and returns it to the flask transfer station and the flask is returned to the warm StoreX for incubation.

4.1.3 EB differentiation automation

The EB cardiomyocyte differentiation method (Burridge et al., 2011) was the first method chosen for automation as it was widely used in our lab at the time (Matsa et al., 2014, Pascut et al., 2013). This method was reported to differentiate both hESCs and hiPSCs to spontaneously beating cardiomyocytes (yields of 94.7+/-2.4 % beating EBs per plate) with cardiomyocyte purities between 64 % to 89 % (Burridge et al., 2011). A core objective of this work was to generate cardiomyocytes from hESCs and hiPSCs for drug screening; therefore at the start, this represented an ideal differentiation method for achieving this (although the EB development work was carried out using HUES7 only). The limitation of carrying out EB differentiations manually was that using 8-channel pipettes to change medium on EBs or to transfer EBs between V- and U-bottom 96-well plates was low throughput and time consuming especially where multiple plates were involved. Furthermore, these differentiations yielded 0.6+/-0.3x10^5 cells per plate and a 96 well plate for drug screening required 2.9x10^6 cells and 384-well plate required 3.8x10^6 cells meaning between 5 and 7 plates of EBs were needed to be able to seed a plate of either format respectively. As a result, there was a need to increase the throughput of the differentiations. The MCA96 (figure 4.9) could remove or add medium in 96-wells simultaneously in a matter of seconds potentially increasing the speed of medium changes and EB transfers from V- to U-bottom plates. It also had potential for speeding up the process of dissociating EBs as manually this was also a time consuming and low throughput process. Additionally, scaling up cell production to RoboFlask format meant that existing robot cell harvesting processes could be used. In RoboFlask format, if cell numbers were scaled accordingly (in T25s, 2x10^6 cells

per were used for EB seeding per flask, or 80,000 cells per cm^2), $7.4x10^6$ cells could be harvested per RoboFlask for EB seeding, which would be sufficient number to make 18.5 x 96-well plates (at 4,000 cells per well) with a potential differentiation output of approximately $11x10^6$ cells.

4.1.4 Automation of monolayer differentiation methods

While the EB method appeared to be scalable with a potential yield of $11x10^6$ cells from 18.5 x 96-well plates, attempts to automate the method (discussed later in this chapter) proved unsuccessful at the EB-setup stage. The mTeSR monolayer method which became available later in the timescale of this work, was successfully carried out manually in RoboFlasks with yields of $7.3+/-1.2x10^6$ cells per RoboFlask (>12-fold higher than in EB plates). This method also appeared to be less technically challenging to automate as it could be carried out by passaging cells and carrying out medium changes in RoboFlask format, both processes which had already been established on the robotic platform by others in our group. Furthermore, up to 4 RoboFlasks could be seeded or fed at a time (the FlaskFlipper could hold 4 flasks simultaneously, and 4 LiHa tips were fitted, enabling access to all 4 flasks simultaneously) meaning the process could be scaled with existing protocols already in place on the robot to produce up to nearly 30 million cells at a time. The secondary objectives of this work were to achieve cardiomyocyte differentiations with high purities as well as high yields. In addition to achieving increased yields relative to the EB method (on a flask vs plate basis), cardiomyocyte purity from the monolayer method was also very high when differentiations were carried out manually (98.7 % positive for α-actinin and 97.4 % positive for cardiac troponin T).

Therefore, the decision was made to abandon EB development work on the robot to develop the mTeSR monolayer method instead.

At a later stage in the work, a newer monolayer cardiomyocyte differentiation method was published (Burridge et al., 2014) which relied on E8 for routine cell culture, a medium which was cheaper than mTeSR (after discount, £0.20/ml compared to £0.34/ml respectively) and less susceptible to batch variation as it did not contain albumin (Chen et al., 2011). It was also claimed that purities of >95 % hPSC-cardiomyocytes could be achieved and yields of 100 cardiomyocytes to each input hPSC using this differentiation method (Burridge et al., 2014) suggesting that this method was even more scalable than the mTeSR monolayer method (yields were approximately 1:1 for input and output of cells respectively). To investigate whether this method would be capable of generating improved cardiomyocyte yields, it was also tested on the robot. As with the mTeSR monolayer method, automating this method only required the passaging and medium change scripts on the robot which meant that minimal process development would be required to automate this method.

4.1.5 Choice of cell lines

The HUES7 hESC line was used for the automation of the EB differentiation method and the mTeSR monolayer method development. This line was chosen because it was the most commonly used cell line in our labs at the time, was used for EB differentiation (Matsa et al., 2014, Pascut et al., 2013) and had also been used in

the development of the mTeSR monolayer method before this method was used for this work. It was also intended over the course of this work, that once a suitable method had been automated, to carry out the process using hiPSC lines to make patient specific cardiomyocyte banks so that drug screening could be carried out using these cells. Efforts were made by others in the group (Gary Duncan) to generate a library of integration-free hiPSC lines derived in E6/E8. The first two lines to become available from this work were the LQT2 and CPVT hiPSC lines (also used in Chapter 3). It was for this reason that these two lines were used in the testing of E8 culture on the robot and for differentiations on the robot.

4.1.6 Cell harvesting on the robot

Routine passaging of hPSCs on the robot was carried out by a process that could be split into four stages, cell harvesting, cell counting, cell dilution and cell suspension mixing/seeding. These processes were used for setting up both monolayer and EB differentiations on the robot. To illustrate the context in which manual processes were adapted for automation, an explanation of these four stages is warranted.

4.1.6.1 Cell harvesting (stage 1)

The script for cell harvesting on the robot was previously developed and optimised by other in the group. This process was not modified for the work carried out in this thesis. Cell harvesting began with a RoboFlask being brought out of the warm StoreX, placed onto the FlaskFlipper and medium was removed and disposed of in the waste station by the LiHa tips. DPBS was added, the flasks were then rocked by

the FlaskFlipper to remove/dilute residual medium and DPBS was then discarded. Enzyme (accutase) was added to the RoboFlask, which was then rocked to ensure complete coverage of the cell surface. The accutase was then aspirated to leave a thin film of residual enzyme and the FlaskFlipper set to the horizontal position. Cells were incubated for 10 min, after which the FlaskFlipper tapped the flask to dislodge cells. Plating medium was then collected by the LiHa tips and added to the flask, the flask was rocked to ensure cells entered suspension and cell suspension was then transferred to a 100 ml trough (Figure 4.11 top right image, A). A further wash with plating medium was carried out to maximise the number of cells harvested and the old flask was discarded.

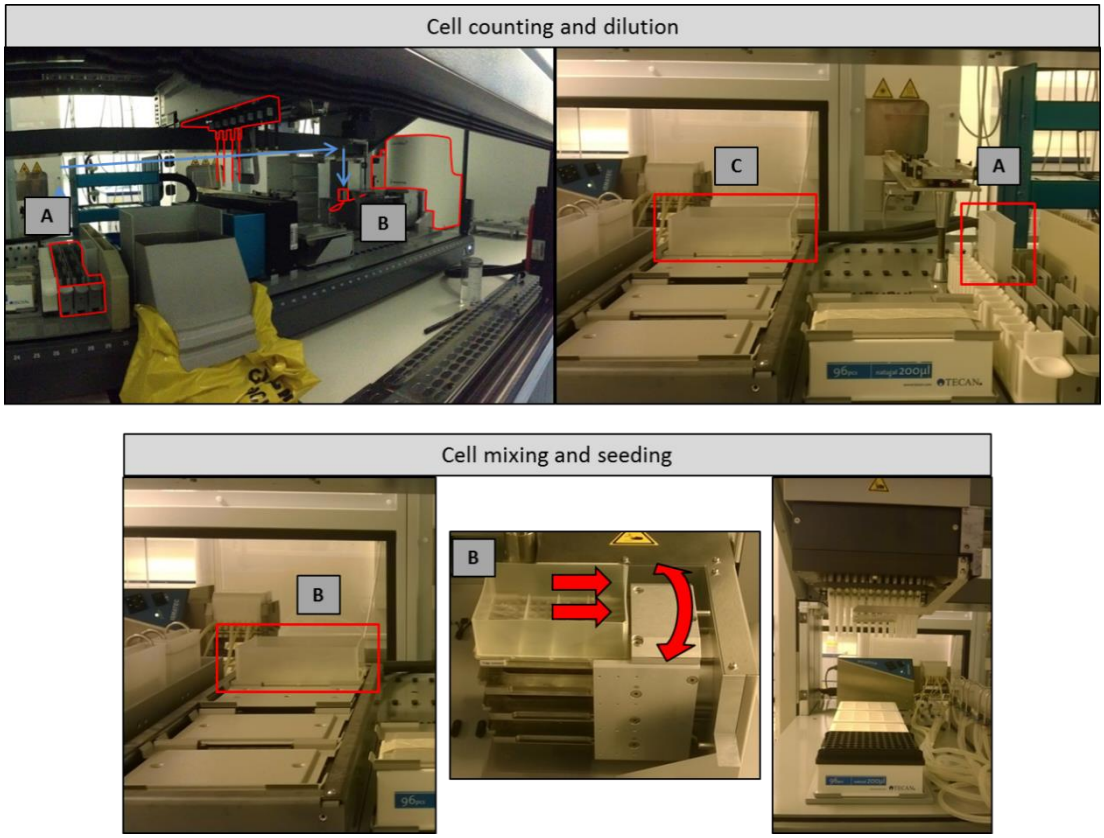


Figure 4.11 – Cell counting, dilution, mixing and seeding on the robot
(Top images) Cell suspension is transferred to a 100 ml trough after harvesting from a RoboFlask **(A)**. A cell count is performed by collecting 300 µl cell suspension with a LiHa tip and dispensing it into a collection cup **(B)** connected to the Cedex HiRes. After the cell count is performed a dilution of the cell suspension is made by transferring an appropriate quantity of medium from **(C)** into **(A)** and mixing with the LiHa tips then transferring appropriate cell number into RoboFlask(s). For seeding EB differentiations, cell suspension is taken from **(A)** and transferred to **(C)** instead. **(Bottom images)** To mix and seed cell suspension for EB differentiations, the trough containing cells **(B)** is picked up by the RoMa arm, placed on the FlaskFlipper and rocked then tapped. The trough is then returned to the warm carrier and cell suspension is collected by the MCA96 and seeded into a 96-well plate.

4.1.6.2 Cell counting (stage 2) and dilution (stage 3)

The cell suspension in the 100 ml trough was mixed by the LiHa and a 300 µl sample was taken and dispensed into a collection cup connected to the integrated Cedex HiRes cell counter for cell counting. When a cell count was generated, this was used to calculate a suitable cell dilution to seed fresh flasks (these calculations were done manually for routine seeding but could be carried out by the robot if needed). To seed RoboFlasks for routine passaging, diluent medium was taken from a 300 ml baffled trough (figure 4.11 bottom images B) to generate a cell suspension at correct cell concentration for plating. To seed EBs, the process was modified whereby; cell suspension was taken from the 100 ml trough (figure 4.11 top right image A) and added to the diluent medium in the baffled trough. Stages 2 and 3 required 8 min to complete for the EB setup process.

4.1.6.3 Cell mixing and seeding (stage 4)

The cell suspension prepared in stages 2 and 3 required mixing to ensure an evenly distributed cell suspension so that even cell seeding could occur in the recipient plates. To achieve this, the baffled trough containing cell suspension was transported to the FlaskFlipper, rocked and tapped to mix the suspension. The trough was then returned to the heated carrier, the MCA96 carried out a final mix by pipetting up and down 3 times and then collected cell suspension which was then seeded in recipient 96-well V-bottom plates for EB formation.

4.1.7 Chapter Aims

- Develop an automated method(s) for differentiating hESCs and hiPSCs to cardiomyocytes. With the aim of maximising cell yield, throughput and purity of output cardiomyocytes.
- Where necessary, develop processes for culturing hPSCs in new culture conditions on the robot if they have not already been tested or developed (ie. E8 culture).
- Develop and test automated methods for dissociation of differentiated EBs or monolayers.
- Develop automated processes for Matrigel coating 384-well plates for cell seeding, for even cell seeding in 384-well plates and for carrying out medium changes.

4.2 Results

4.2.1 Variables for developing and testing an automated process for EB formation

The first objective of this chapter was to automate HUES7 harvesting and plating for EB formation, which constituted the start of the EB differentiation process. To achieve this, a comparison was made between the cell harvesting process used by the robot and the manual process. Several variables arose from this comparison, including: 1) different enzymes (trypsin 0.05 % manually and accutase on the robot); 2) manual passaging was carried out with enzyme incubation at 37 °C while robot enzyme treatment was at RT; 3) harvested cell suspensions were centrifuged when passaging manually and not centrifuged in robot passaging; and 4) duration of enzyme exposure in manual passaging was 1 min and on the robot; 10 min. A series of experiments were carried out to test these variables for their suitability in forming EBs and whether these EBs would spontaneously beat between day 10 and 12 of differentiation.

4.2.2 Effect of different enzymes and room temperature enzyme incubation on hESC EB formation and differentiation to cardiomyocytes

Routine hPSC passaging on the robot involved incubating cells treated with accutase at RT, a process that was well established on the robot. However, routine manual passaging and passaging to set up EB differentiations using HUES7 cells involved carrying out this incubation step using 0.05 % trypsin at 37 °C (Matsa et al., 2014, Pascut et al., 2013). Furthermore, the method from which our EB differentiation protocol was derived used TrypLE in routine culture and during EB setup (Burridge

et al., 2011). To determine whether RT cell harvesting was compatible with EB formation and differentiation, the manual process was carried out using trypsin, accutase and TrypLE at RT and at 37 °C. Following 37 °C incubation cell harvesting was achieved by tapping the flask to dislodge cells and re-suspending cells in hESC medium containing KnockOut serum replacement to neutralise enzyme. Cells were centrifuged and then re-suspended in day 0 EB differentiation medium and plated in 96-well V-bottom plates for EB formation. To harvest cells at RT, enzyme was added and the flask was rocked periodically to assess when cells had fully dissociated from the culture surface, when this was achieved, the time was recorded and as before, cells were re-suspended, centrifuged, then plated for EB formation. With 37 °C enzyme incubation, EB transfer was achieved in >95 % of wells (95.5+/-0.7 % for trypsin, 99+/-0 % for accutase and 96+/-1.4 % for TrypLE) (table 4.1). With RT enzyme harvest, EB transfer was >97 % (99+/-1.4 % for trypsin, 98.5+/-0.7 % for accutase and 97.5+/-0.7 % for TrypLE, (all SD, all n=2 plates per condition)) and there was no significant difference between any of these conditions (one-way ANOVA with TMCT). When differentiation outcome was assessed by quantifying the proportion of wells with beating EBs (for 37 °C enzyme setups), accutase achieved the highest proportion with 92.5+/-7.8 % followed by trypsin at 73.5+/-5 % and TrypLE achieved the lowest with 67+/-14.1 %. With all three enzymes, proportion of beating EBs declined with RT enzyme incubation relative to 37 °C enzyme incubation however, for trypsin and TrypLE, this change was only significant between trypsin at 37 °C (73.5+/-5 %) or TrypLE at 37 °C (67+/-14.1 %) and TrypLE at RT (3.5+/-0.7 %) ($p<0.001$ and 0.01 respectively, one-way ANOVA with TMCT). For accutase, the difference was significant between accutase at 37 °C

(92.5+/-7.8 %) and all EB setups with RT enzyme harvest (trypsin, 48.5+/-5 % p<0.01, accutase, 58+/-7.1 % p<0.05, TrypLE, 3.5+/-0.7 % p<0.001). As accutase gave the highest proportion of beating EBs from 37 °C and RT harvest and because it was already being used on the robot, it was used for all further EB automation work.

Table 4.1 – Effect of varying enzyme and temperature of incubation on EB formation and differentiation success.
HUES7 cells were harvested using trypsin, accutase or TrypLE at either room temperature (21 °C) or 37 °C. Duration at room temperature was determined by the time taken for cells to fully detach by rocking (n=1 flask per condition), for 37 °C incubations, duration of enzyme exposure was determined by existing lab protocols. Two replicate 96 well plates were set up for each differentiation (values +/- SD).

Enzyme	Temperature	Duration (min)	Spin?	% EB transfer	% Beating EBs
Trypsin	37 °C	1	+ spin	95.5+/-0.7 %	73.5+/-5 %
Accutase	37 °C	3	+ spin	99+/-0 %	92.5+/-7.8 %
TrypLE	37 °C	3	+ spin	96+/-1.4 %	67+/-14.1 %
Trypsin	RT	2:13	+ spin	99+/-1.4 %	48.5+/-5 %
Accutase	RT	2:35	+ spin	98.5+/-0.7 %	58+/-7.1 %
TrypLE	RT	3:30	+ spin	97.5+/-0.7 %	3.5+/-0.7 %

4.2.3 Effect of harvesting cells by contact method using accutase on hESC EB formation and differentiation to cardiomyocytes

There were several other variables (than temperature of enzyme treatment) in the automated cell harvesting process compared to manual cell harvest. In the automated process, 0.03 ml/cm^2 (3 ml) of enzyme was added the flask to coat the cells in enzyme before most of this (excluding some residual volume) was aspirated

to leave a thin film of enzyme. It required 10 min of incubation before cells were then dissociated by gentle repeated tapping using the flask handling device. Fresh medium was then added to the cells which were then harvested from the flask and deposited into a collection trough without a centrifugation step (there was no capacity for centrifugation on the robot). By contrast, the manual method involved adding 0.1 ml/cm^2 enzyme, incubating for 1 min at 37 °C, tapping the flask and then adding hESC medium containing KnockOut serum replacement to the enzyme and cells. This suspension was then centrifuged and cells were re-suspended in plating medium. Therefore, two variables were tested (all carried out manually) to further assess the compatibility of the robot method with EB formation and differentiation of HUES7 hESCs. Firstly, enzyme incubation time was extended to 5 min and 10 min and secondly, the process of aspirating enzyme to leave a thin film, with RT incubation, followed by harvesting cells using gentle tapping of the flask and re-suspension of cells directly in "plating media" was tested (i.e. in the absence of centrifugation, referred to as "–spin" in table 4.2, "+spin" refers to cells being harvested using the manual method with centrifugation). Where cells were harvested with 10 min incubation and "–spin", EB transfer was 99+/-0 % and proportion of beating EBs was 81.5+/-3.5 % (table 4.2). With the same conditions and 5 min incubation, EB transfer and proportion of beating EBs were both lower at 94+/-5.6 % and 68+/-18.4 % (both n=2 plates). These data suggested that 10 min enzyme treatment was better than 5 min (using accutase) and that the conditions used by the robot (10 min incubation at RT, gentle tapping and resuspension directly in plating medium) were compatible with the EB differentiation method and even gave good differentiation outcomes for both EB transfer and proportion of

beating EBs. For this reason, the robot cell harvesting method was tested without any modifications.

Table 4.2 – Effect of increasing incubation time at room temperature and comparison of centrifugation and non-centrifugation prior to EB setup.
Accutase dissociation at 37 °C for 3 min with centrifugation was used as a control to test that the starting HUES7 cell population and reagents were able to give successful differentiations as this condition was shown to work previously (table 4.1). Incubation time in accutase was increased to 5 min and 10 min at RT to determine whether these durations were compatible with EB differentiation (10 min is needed by the robot to carry out cell harvesting). Cell harvest without centrifugation involved adding enzyme, aspirating to leave a thin film of enzyme, tapping flasks to dislodge cells at the end of the incubation period and re-suspending in desired media for plating. Two replicate plates were set up for each condition unless otherwise stated (values+/- SD).

Enzyme	Temp	Duration (min)	Spin?	% EB transfer	% Beating EBs
Accutase	37 °C	3	+ spin	96 %	72 % (n=1)
Accutase	RT	5	+ spin	97.5 +/- 0.7 %	88 +/-7.1 %
Accutase	RT	5	- spin	94 +/- 5.6 %	68 +/- 18.4 %
Accutase	RT	10	- spin	99 +/- 0 %	81.5 +/- 3.5 %

4.2.4 Comparison of incubators, manual and robot cell suspension seeding and effect of penicillin/streptomycin on the formation and differentiation of EBs

Before the robot could seed a 96-well plate, the harvested cell suspension in the collection trough was mixed with plating medium in a larger, 300 ml baffled trough. From this trough, the MCA96 could then collect cell suspension to seed a 96-well plate. At this stage, three further variables required testing. Firstly, whether HUES7-EBs could form and differentiate after the robot MCA96 seeded the cell suspension into a 96-well plate. Secondly, whether HUES7 cells seeded by the robot could be

stored in the StoreX warm incubator and still form EBs and differentiate. The StoreX incubators consist of 5 towers for holding culture flasks and plates resting on a rotating plate. This plate rotated whenever the incubator door was opened or when the robot needed to retrieve a flask or plate from the incubator. This test was needed to confirm that the rotation did not have an adverse effect on the formation of EBs. Thirdly, whether the addition of 0.5 % penicillin/streptomycin (pen/strep) to EB differentiation medium would impact EB formation or differentiation. Standard practice for all cultures on the robot was to add pen/strep to avoid contaminations as the process of decontamination was both costly and time consuming while the standard practice in the manual labs was to not use pen/strep in cultures. When a 96-well plate was seeded by the robot using a manually-prepared, counted and mixed cell suspension in a baffled trough, stored in the StoreX and differentiated with medium containing pen/strep, the proportion of EBs transferred was high at 98 % and proportion of beating EBs was 100 % (figure 4.12). Manually seeded EBs with the same conditions also gave 100 % beating EBs but with fewer EBs transferred (88 %) (n=1 for each). These results indicated that cell suspensions seeded by the robot could successfully differentiate, that EB formation and differentiation was not negatively affected by pen/strep or incubation in the StoreX incubator.

A

Conditions	% EB transfer	% Wells with Beating EBs
Manually Seeded Stored in Manual Lab	98	100
Robot Seeded Stored in Manual Lab + Pen/Strep	96	100
Robot Seeded Stored in Storex +Pen/Strep	98	100
Manually Seeded Stored in Manual Lab + Pen/Strep	96	100
Manually Seeded Stored in Storex +Pen/Strep	88	100

B

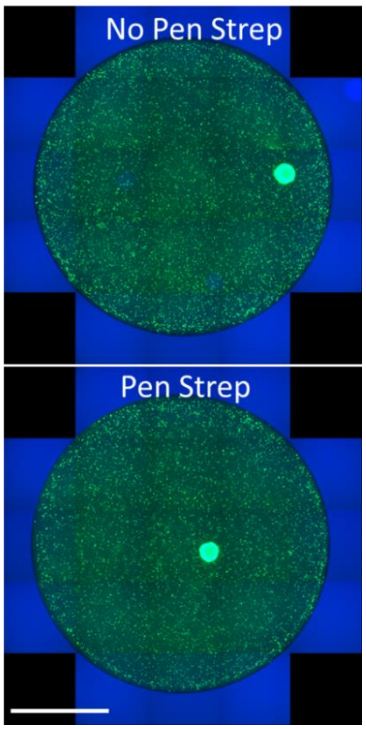


Figure 4.12 – Testing robot cell suspension seeding, HUES7 EB formation in the StoreX incubator and Pen/Strep incubation with EB formation.
Manually harvested and counted cell suspensions were either plated manually or by the robot where shown. **A)** Table comparing storage of EBs in either robot StoreX incubator or manual incubator and comparing EB formation from robot seeded cell suspension with manually seeded. One 96 well plate seeded per condition tested. **B)** Images show EB formation after 24 hr in the presence or absence of pen/strep in the day 0 differentiation medium. Scale bar = 2 mm.

4.2.5 Automating the process of hESC harvesting and seeding for EB formation and differentiation to cardiomyocytes

In the previous section, a manually prepared suspension was dispensed by the robot MCA96 into 96-well plates and gave good EB transfer and differentiation outcome. However, to fully automate the process, the robot was required to perform a cell harvest, count and dilution prior to seeding 96-well plates. Several initial attempts to do this in one continuous process were unsuccessful with no EB formation and therefore no successful differentiation. Therefore, to identify the cause of the issues, the process was broken up into 4 separate stages: 1) cell

harvest; 2) cell count; 3) cell dilution and 4) cell suspension mix and seed (figure 4.13). These stages were carried out by the robot or manually or a combination of the two. For each condition, 10,000 cells were seeded per well and EB formation was tested after 24 hr by staining cells with Calcein AM, Hoechst33342 and PI to determine cell viability. When all four stages were carried out by the robot, 0 % EB formation occurred but 10,621+/-1054 cells transferred (92.7+/-0.7 % PI positive and therefore dead), indicating that the robot process led to the death of most cells (figure 4.13C). When the process was carried out manually (mimicking the robot harvesting method), 8078 cells transferred, (57.5 % PI positive) but EB formation had occurred indicating the process had worked and that the input cells and reagents were permissive to cell survival and EB formation.

Since EB formation was successful when all four stages were carried out manually (mimicking the robot process for harvesting; counting; diluting; mixing and seeding) each step was systematically carried out manually in isolation and the remaining steps carried out by the robot to identify where the failure in the process was occurring (figure 4.13A). Therefore, when the cell harvest was carried out manually (stage 1) but the remaining stages (counting; dilution; mix and seeding) were carried out by the robot, most cells died (9436+/-317.3 cells transferred, 93.9+/-1.1 % PI positive) and no EBs formed. Similarly, when the robot carried out the first three stages, no EB formation occurred and most cells died (7638+/-1730 cells transferred, 87.6+/-3.3 % PI positive). Finally, when stages 1 and 4 (harvesting and cell suspension mix and seeding) were carried out manually and stages 2 and 3

carried out by the robot (cell counting and cell dilution) again, no EB formation occurred and most cells died (11046+/-1249 cells transferred, 96.7+/-0.6 % PI positive). This suggested that the issue was with either stage 2 or 3 (or both) in the process.

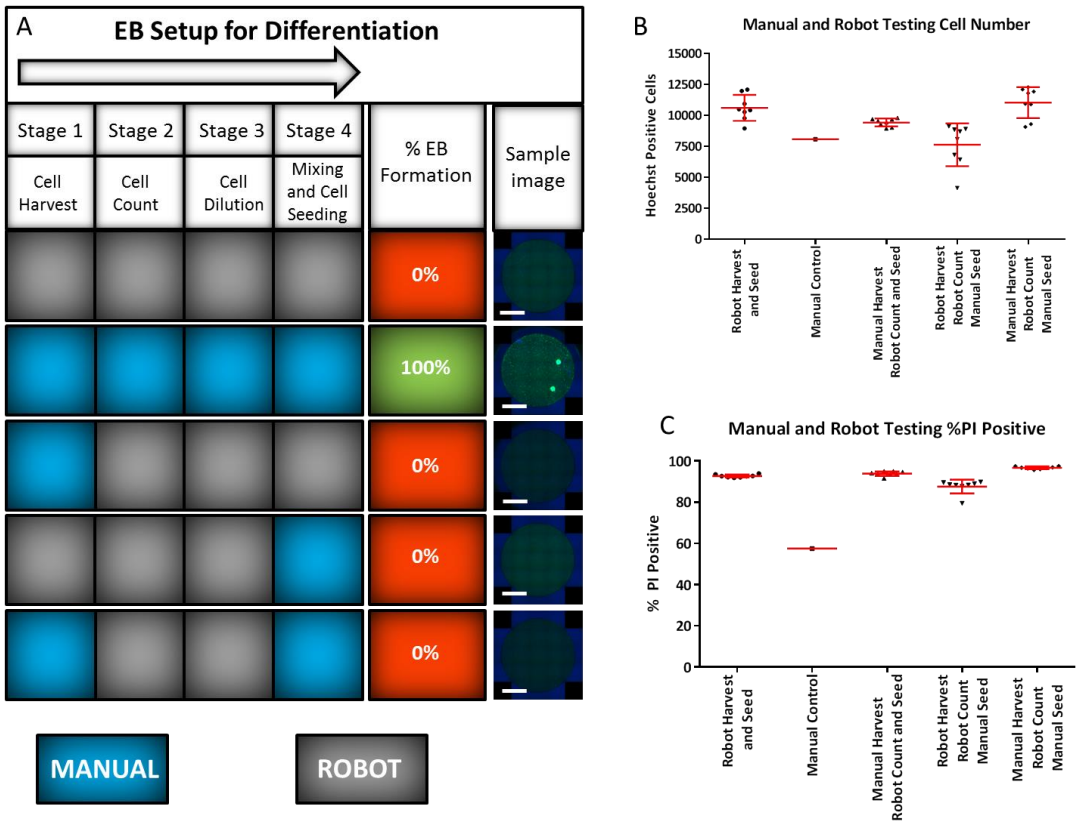


Figure 4.13 – Testing automation of the different steps of day 0 HUES7 EB setup for differentiation.

A) The EB setup process was split into four steps: cell harvest, cell count, cell dilution and mixing/seeding of cell suspension. Boxes in grey denote processes carried out by the robot, boxes in blue denote processes carried out manually. After 24 hr, EB formation was tested by transferring the entire contents of randomly selected wells or columns in V-bottom plates to flat bottom plates for staining with Calcein AM, Hoechst33342 and PI for imaging. Second row, contents of two wells were pooled into one flat-bottom well for analysis (represents n=2 wells). All other conditions were n=8 wells. **B)** Quantification of cell number transferred from v-bottom to flat-bottom wells for each condition. **C)** Percentage of cells staining positively for PI per condition. Scale bars = 2 mm

4.2.6 Investigation of problems with EB formation during automated cell counting and dilution steps

To identify whether the problems with EB formation were originating from stage 2, stage 3, or both stages in the differentiation process, another experiment was carried out to isolate each process (figure 4.14). Where stages 2 and 3 were tested by the robot, cell suspension was kept in a collection trough to enable counting, while diluent medium was kept in a 300 ml baffled trough. When all four stages were carried out manually, EB formation was achieved (and 7433+/-801.3 cells transferred) confirming there were no issues with the cells or reagents. However, where only stage 2 (cell count only, 5209+/-598.1 cells transferred, 95.6+/-2 % PI positive) or stage 3 and 4 (cell dilution and cell seeding, 8617+/-622.2 cells transferred, 95.9+/-0.8 % PI positive) was carried out by the robot, EB formation did not occur suggesting that the issue was either with both processes or something occurring in the background.

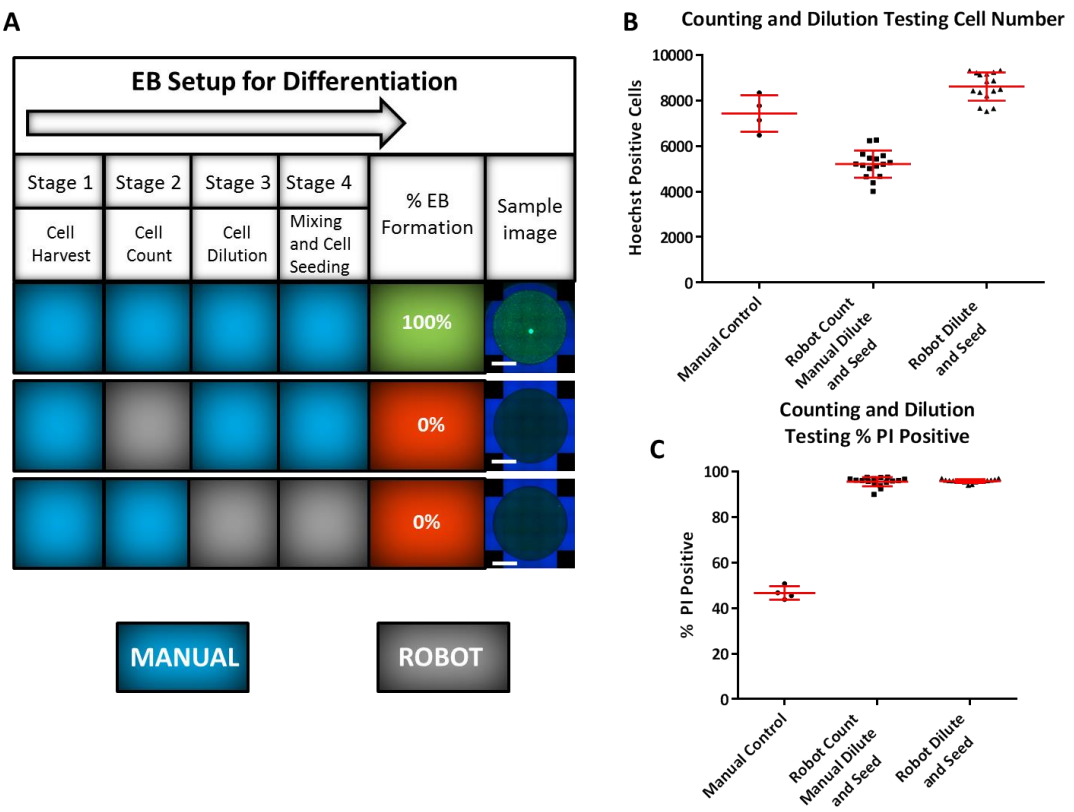


Figure 4.14 – Testing the automated cell count and cell dilution steps to determine the cause of no HUES7 EB formation.
A) EB setup for differentiation was carried out with either automated cell counting process only or automated cell dilution process only (blue boxes – processes carried out manually, grey boxes – processes carried out by the robot). Cells were kept at room temperature in an autoclaved 300 ml baffled trough while each process was carried out by the robot. Cell harvest and mix/cell seeding were carried out manually from these troughs. After 24 hr, EB formation was tested by transferring the entire contents of randomly selected wells or columns in V-bottom plates to flat bottom plates for staining with Calcein AM, Hoechst33342 and PI for imaging. **B)** Quantification of cell number transferred from v-bottom to flat-bottom wells for each condition. **C)** Percentage of cells staining positively for PI per condition. Scale bars = 2 mm. Top row n=4 wells second and third row n= 16 wells.

4.2.7 Testing incubation time and its effect on EB formation during the automated cell counting and dilution steps

In order to test whether EB formation problems were a result of background issues instead of the process of cell counting or dilution by the robot, an experiment was set up to replicate the environmental conditions the cells underwent during the cell

count and dilution stages without physically carrying out a count or dilution using the robot. To ensure no issues were occurring with reagents or cells, the process was carried out manually and EB formation was achieved with 6724+/-411.9 cells transferred (figure 4.15B). Carrying out stages 3 and 4 with the robot led to no EB formation as seen in figure 4.14A with 10990+/-435.7 cells transferred and most cells died (94.1+/-3.4 % cells positive for PI). Cells harvested manually were then counted, diluted and the cell suspension was plated by the robot, this led to EB formation (8525+/-238.1 cells transferred). The length of time taken for the robot to carry out a cell count and cell dilution was 8 min. To test whether following harvest, incubating cells at RT for this length of time may be the reason for lack of EB formation, cells were incubated in a 30 ml universal tube (routinely used during manual EB setups) for 8 min, afterwards, the cell suspension was transferred to a baffled trough and seeded by the robot. This led to successful EB formation, suggesting that this added incubation time was not the problem (cell transfer was 6766+/-789.7). When the same process was carried out but cells were incubated in an autoclaved 300 ml baffled trough, this led to no EB formation and most cells died (cell transfer was 10663+/-481.3 and 98.1+/-0.5 % PI positive cells) suggesting that the issue lay with the choice of plasticware used during this incubation step.

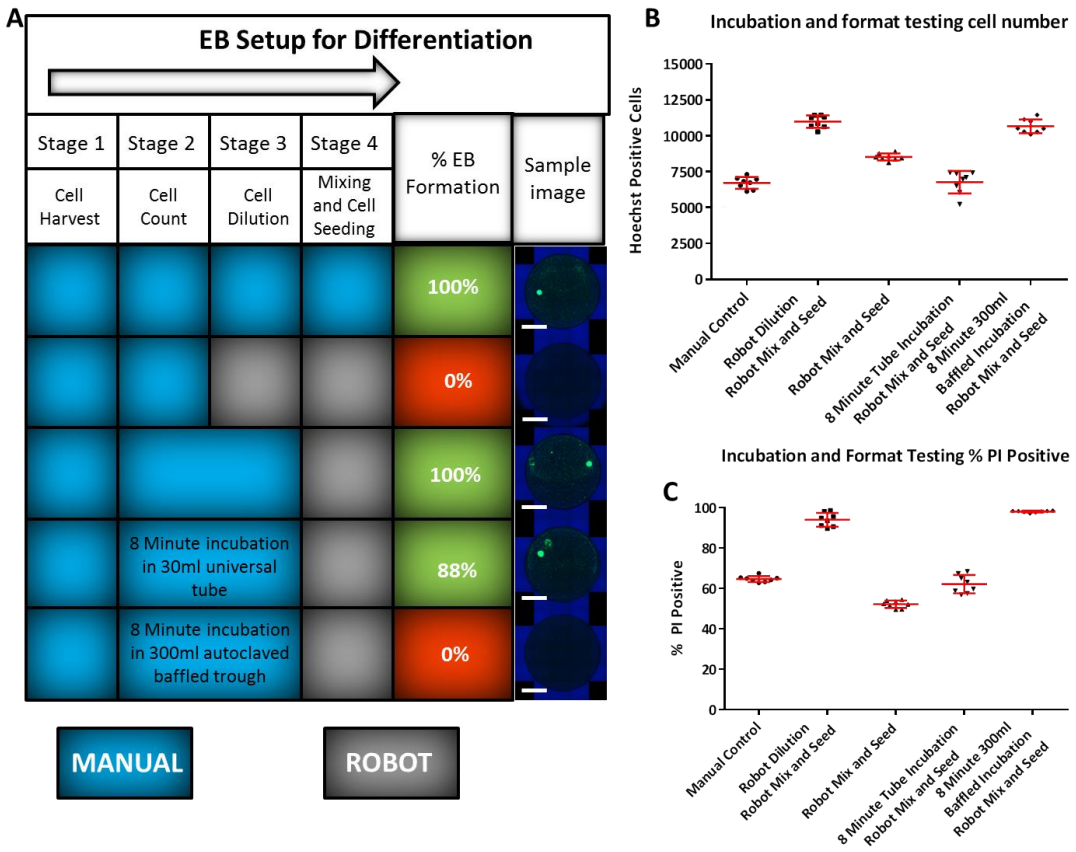


Figure 4.15 – Testing duration of incubation and format on HUES7 EB formation after 24 hours.

(A) (Top row) hESCs were seeded for EB differentiation manually, (far right) a representative image of an EB formed after 24 hr. **(Second row)** hESCs were incubated in a baffled trough while the robot carried out a cell dilution from a manual cell count and then seeded the cells for EB formation, a representative image shows no EB formation after 24 hr (far right). **(Third row)** hESCs were harvested, counted and diluted manually in a 30 ml universal tube prior to adding the cell suspension to a baffled trough for the robot to seed for EB formation, a representative image shows EB formation occurred after 24 hr. **(Fourth row)** Cells harvested manually were incubated for 8 min (the time taken for the robot to carry out a count and cell dilution) in a 30 ml universal tube prior to adding cell suspension to a baffled trough for the robot to seed hESCs for EB formation, a representative image shows EB formation after 24 hr (far right). **(Bottom row)** manually harvested hESCs were incubated for 8 min in an autoclaved 300 ml baffled trough from which cells were seeded by the robot for EB formation. A representative image shows no EB formation after 24 hr (far right). EB formation was tested by transferring the entire contents of randomly selected columns in V-bottom plates to flat bottom plates for staining with Calcein AM, Hoechst33342 and PI for imaging. **(B)** Quantification of cell number transferred from v-bottom to flat-bottom wells for each condition. **(C)** Percentage of cells staining positively for PI per condition. Scale bars = 2 mm, all n=8 wells.

4.2.8 Testing different trough formats for their effect on EB formation

In the next set of experiments surface area and type of plasticware were tested to see whether either of these factors was the cause of EB formation issues. Different types of trough of different sizes were tested to identify whether there was a relationship between exposed surface area and the effect on EB formation (figure 4.16A). When HUES7 cells were incubated for 8 min in a 30 ml universal tube as in figure 4.15, EB formation was achieved, with 6849+/-646.5 cells transferred. When this incubation was carried out in one well of a fresh 24 or 4 well trough in both cases EB formation was achieved (8950+/-658.2 and 5377+/-1339 cells transferred respectively). When carried out in a fresh 300 ml baffled trough, EB formation was achieved (8208+/-1288 cells transferred), but when carried out in an autoclaved baffled trough, EB formation did not occur, cell transfer was 10102+/-4585 and most cells died (92.3+/-3.7 % cells positive for PI). This identified the issue as being a result of using autoclaved plasticware. As a result, autoclaved plasticware was not used in any further EB setups on the robot.

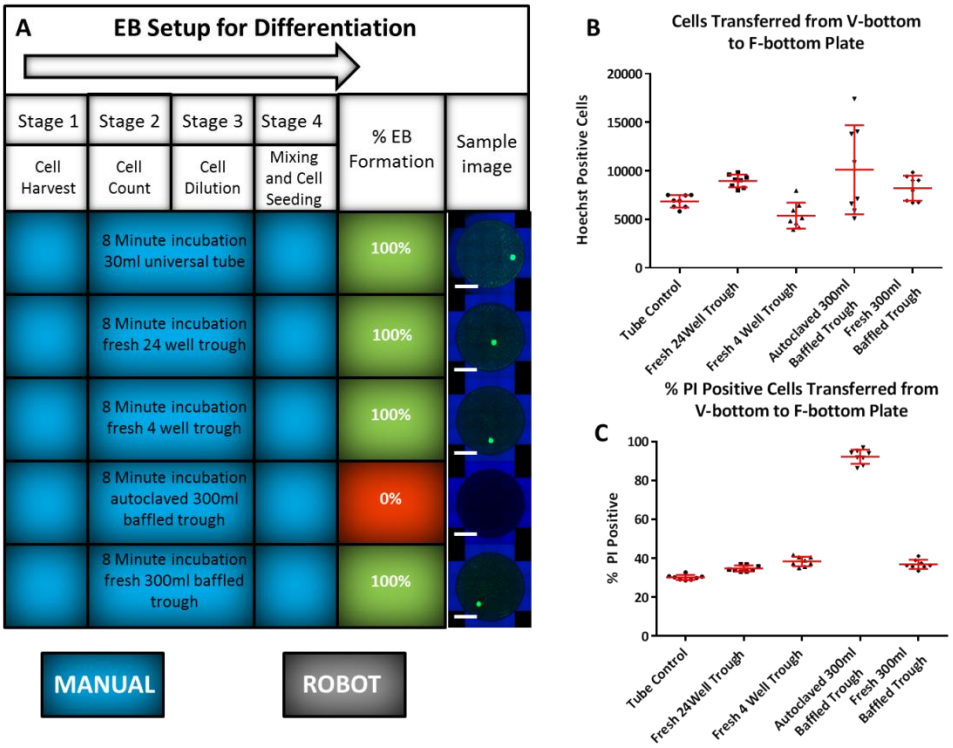


Figure 4.16 – Testing different trough formats for effect on HUES7 EB formation at 24 hr post-seeding.
(A) Cells were harvested, counted, diluted and seeded manually. During the cell count and dilution step, cells were incubated for 8 min in either a 30 ml universal tube, one well of a fresh 24-well trough, one well of a fresh 4-well trough, in an autoclaved 300 ml baffled trough and a non-autoclaved (fresh) 300 ml baffled trough. After 24 hr, EB formation was tested by transferring the entire contents of randomly selected wells or columns in V-bottom plates to flat bottom plates for staining with Calcein AM, Hoechst33342 and PI for imaging. **(B)** Quantification of cell number transferred from v-bottom to flat-bottom wells for each condition. **(C)** Percentage of cells staining positively for PI per condition. Scale bars = 2 mm. All n=8 wells.

4.2.9 Robot liquid handling pipette vectors and speeds for medium changes in 96 well U-bottom and V-bottom plates

In order to carry out medium changes in 96-well plates containing EBs, experiments to test and identify appropriate vectors and dispense speeds were performed. To avoid issues such as tip collisions with wells (which would cause the robot to enter an “error” state and prematurely interrupt any process being carried out), inappropriate aspiration of EBs or damage to EBs, three variables required optimising for medium changes in 96 well plates (figure 4.17). These were: 1) tip

positioning vectors (the “Z” (or vertical) vector, “X” vector (from left to right when facing the robot) and “Y” vector (from closer to further away when facing the robot)); 2) aspiration rate for collecting spent medium from the well and 3) fresh medium dispense rate within the well. The “Z” vector was set at 158 mm (termed Z-maximum) below the starting location of the MCA head which was sufficiently above the well bottom to avoid collision. Below this point there was also a risk that the EB would be aspirated with the medium, damaged by the tip or by the dispensing of medium. This vector was also optimised to ensure the maximum amount of medium was removed from the well during medium changes, which is particularly important on day 2 of EB-differentiation to ensure maximum removal/dilution of insulin from the medium which can prevent successful differentiation (Burridge et al., 2011). This vector was found to be suitable for both U-bottom and V-bottom 96-well plates. In order to avoid directly dispensing medium on to the EB which could damage it or increase the risk of it being aspirated, an offset was needed in either the Y- or X-axis. The Y-axis was left unchanged and an offset in the X-axis of 2.5 mm to the left of the centre of the well (0.75 mm from the well edge) was set for routine medium change scripts. To further minimise risk of EB aspiration or damage, the rate of medium aspiration or dispensing was also adjusted (normally 100 µl/sec). This was reduced to 10 µl/sec for aspirations and 20 µl/sec for dispensing. At this rate, dispensed medium had the effect of dislodging and lifting the EB in the wells but this was not enough to cause damage to EBs (which remained intact even following feeds on day 2 when EBs were relatively newly formed).

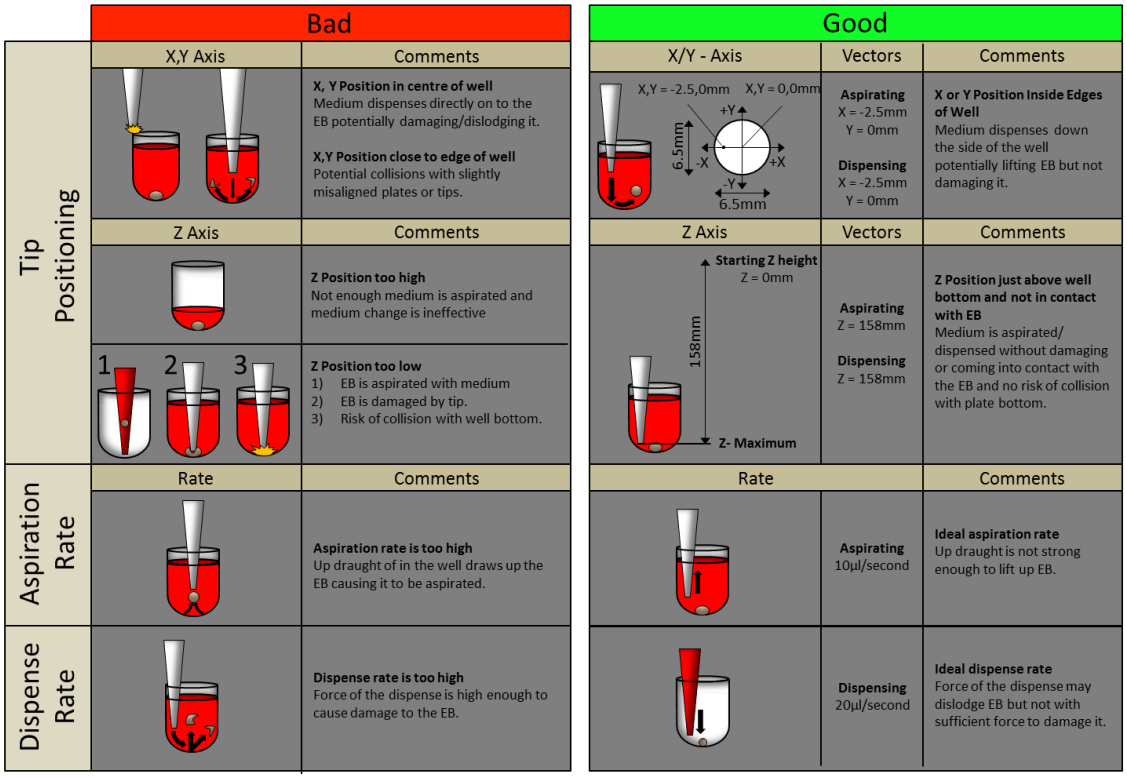


Figure 4.17 – The vectors for medium changes carried out in 96 well U-bottom and V-bottom plates using the robot from day 8 onwards.
(Left two columns) illustrated examples of potential issues encountered when non-optimal tip positioning vectors, aspiration rates or dispense rates are chosen for medium changes with explanations associated with each potential issue. (Right three columns) illustrated examples of ideal vectors for optimal medium changes with vectors chosen through testing with EBs in 96 well U-bottom and V-bottom plates and relevant comments.

4.2.10 Robot liquid handling pipette vectors and speeds for transferring EBs from 96 well V-bottom plates to 96-well U-bottom plates

As in 4.2.9, it was also necessary to identify suitable vectors and aspirate/dispense speeds for transferring EBs from V-bottom plates to U-bottom plates. In order to achieve this, tests were carried out to identify the correct vectors and pipetting speeds needed to dislodge the EBs suitably so that they could then be taken up by aspiration and then dispensed into fresh U-bottom wells without damaging them (figure 4.18). To ensure this, EB-collection was achieved by dispensing medium at 20 µl/sec with the offset used in 4.2.9 (2.5 mm to the left of well centre in the X-axis) to cause the EB to be dislodged. The MCA tips were then moved to the centre of the well (X,Y = 0,0) and Z-height was raised by 2 mm above Z-maximum to allow improved clearance in the well. Aspiration speed was increased to 40 µl/sec and this was sufficient to enable EB capture in the tip and a suitable volume of media transfer to the U-bottom plate (EBs required 4 days without a medium change so maximum transfer of medium was desirable). EBs were dispensed using the 2.5 mm X-axis offset and at 3 mm above Z-maximum giving suitable clearance to avoid dispensing / impaling the EBs directly against the bottom of the well.

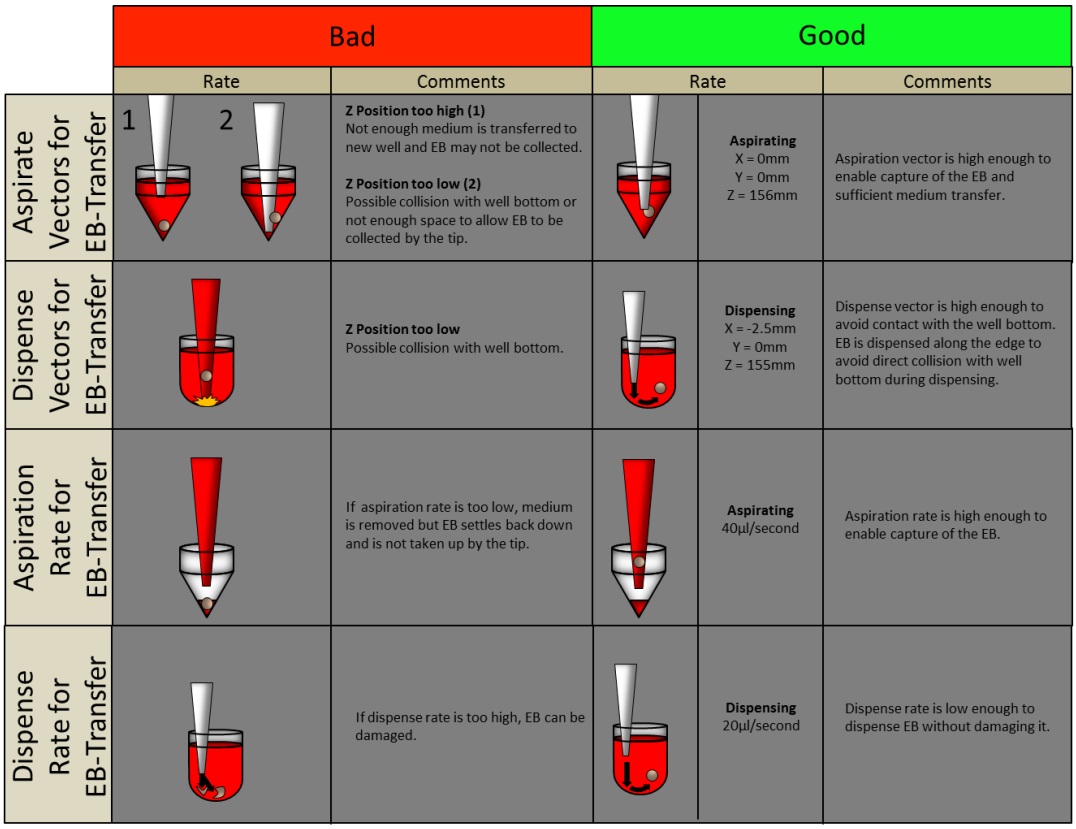


Figure 4.18 – Vectors for enabling EB transfer from V-bottom to U-bottom plate on day 4 of differentiation.
(Left two columns) illustrated examples of potential issues encountered when non-optimal aspiration rates or dispense rates are chosen for EB transfer with explanations associated with each potential issue. **(Right three columns)** illustrated examples of ideal aspiration and dispense rates for successful transfer of EBs from V-bottom to U-bottom plates chosen through testing and relevant comments.

4.2.11 Testing automation of the complete HUES7 EB differentiation process

In section 4.2.9 the appropriate vectors and liquid aspiration and dispense rates were established for the medium changes on day 2, 4 and 8 of differentiation while in section 4.2.10, these were established for the EB transfer process from V-bottom to U-bottom plates. Having also identified the issues preventing correct EB formation in 4.2.7, the next step was to test whether all the different steps in the EB differentiation process could now be carried out and give good differentiation efficiencies (proportion of beating EBs). To this end, different combinations of processes were carried out either manually or by the robot (figure 4.19A), these included the day 0 EB setup, day 2 medium change, day 4 medium change with transfer to U-bottom plates and the day 8 medium change. When the robot carried out the EB setup step, EB formation occurred (figure 4.19B images 1-4) indicating that the EB formation problem had been solved by replacing autoclaved plasticware with fresh plasticware. EB transfer was ≥98 % across all plates seeded by the robot. Mean size of EB measured after transfer on day 4 ranged from 222.7+/-32.2 to 262.8+/-61.3x10^3 μm^2. However, although the EBs formed successfully, none of the EBs generated by the robot were beating at day 10. However, in all cases where EBs were set up manually, differentiations succeeded with proportion of beating EBs ranging from 85.4 % to 96.8 % on day 10. EB formation and transfer on day 4 was ≥99 % in all cases and mean EB sizes ranged from 468.5+/-55.3 to 550.4+/-54.2x10^3 μm^2 representing an approximately 2-fold increase over the size of EBs seeded by the robot. EB maintenance by the robot from day 2 onwards gave 95.8 % beating EBs indicating that all processes except for day 0 setup were amenable to successful differentiations. Although problems remained with the process of EB setup on day

0, overall, the rest of the processes were capable of generating good differentiation outcomes of (in all but one case where the outcome was 85.4 %) >90 % beating EBs. The presence of fully formed/intact EBs from day 2 of robot handling onwards demonstrated that the vectors and liquid transfer speeds from 4.2.9 and 4.2.10 were adequate in avoiding damage to EBs across all stages and that medium transfers were sufficient to allow EBs to survive and differentiate successfully.

A

Day 0	Day 2	Day 4		Day 8	Day 10
Cell Seeding	EB Medium Change	% EBs Transferred	Mean EB size x10³ µm²	EB Medium Change	Success?
		100%	229.1+/-33.6 [1]		0%
		98%	255.3+/-40.8 [2]		0%
		99%	222.7+/-32.2 [3]		0%
		100%	262.8+/-61.3 [4]		0%
		100%	501.9+/-68 [5]		95.8%
		99%	497.1+/-71.9 [6]		95.7%
		99%	550.4+/-54.2 [7]	*Lid came off on D6 – discarded	
		99%	498.8+/-64.7 [8]		93.7%
		99%	534.9+/-66.4 [9]		96.8%
		100%	537.7+/-61.9 [10]		94.8%
		100%	468.5+/-55.3 [11]		85.4%

B

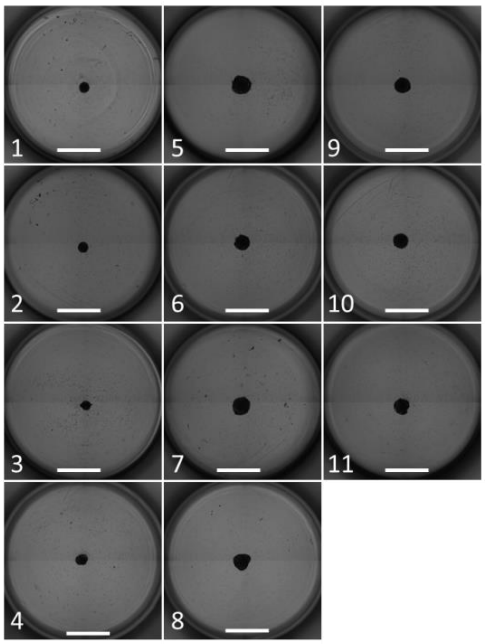


Figure 4.19 – Testing the full 8-day EB differentiation process using the robotic platform.

Day 0 cell harvest and EB setup, day 2 media change, day 4 media change and EB transfer and day 8 media change were all tested with automated scripts or manually for ability to generate beating EBs by day 10 of differentiation, measured as percentage of total EBs beating by day 10 **(A)**. Percentage EB formation and EB size were also determined on day 4 by imaging using the Cellavista plate reader. **(B)** Representative images of EBs taken from each plate shown in A). Row 7, highlighted with * was discarded on day 6 due to loss of the plate lid. Scale bars = 2 mm, values +/- SD. One 96 well plate set up per condition with all 96 wells seeded per plate.

4.2.12 Developing a centrifugation-free EB dissociation method

As mentioned in chapter 3, manual dissociation of EBs was low throughput with only 8 EBs being dissociated at a time. To increase the rate at which EBs could be dissociated to generate cardiomyocyte cell suspensions, an automated dissociation method was developed to take advantage of the MCA96's capability to add, remove or mix medium in 96 wells simultaneously. Manual testing of different dissociation conditions revealed that while the existing T/A method was effective at dissociating EBs (figure 4.20 ii, far left image), addition of RPMI-PVA to the enzyme mix had the effect of increasing the rate at which cells deposited on the bottom of the well following 10 min incubation. In the absence of PVA, (figure 4.20A ii – far left image) cells still remained in suspension however, where T/A and RPMI-PVA were combined in a 3:1 ratio, good dissociation was achieved and full deposition of cells was achieved after 10 min incubation (figure 4.20Aii - far right image). This deposition property offered a potential alternative to plate centrifugation which was not possible on the robot. T/A:RPMI-PVA (3:1) dissociation was tested with a range of pipetting speeds and incubation (37 °C, warm StoreX) times on the robot until EBs were sufficiently dissociated (figure 4.20B i). The maximum "safe" (for the equipment) pipetting speed for the MCA96 was 300 µl/sec and this was chosen as the highest speed used decreasing with graduations of 50 µl/sec down to 150 µl/sec . At higher pipetting speeds less enzyme incubation time was required to achieve full dissociation (see images - figure 4.20 B ii)). When cells were transferred to flat bottom plates and incubated for 24 hr, cell viability was 74.9+/-0.5 and 75.6+/-1 % for 300 µl/sec and 250 µl/sec respectively decreasing ($p<0.0001$) to 53+/-1.1 and 52.8+/-2.5 % at 200 µl/sec and 150 µl/sec suggesting that further rounds of enzyme

treatment and pipetting had the effect of decreasing cell viability. For this reason, Accumax/RPMI-PVA (3:1), with 2 rounds of 4 min incubation and pipetting at 300 µl/sec was chosen as the desired EB dissociation method on the robot.

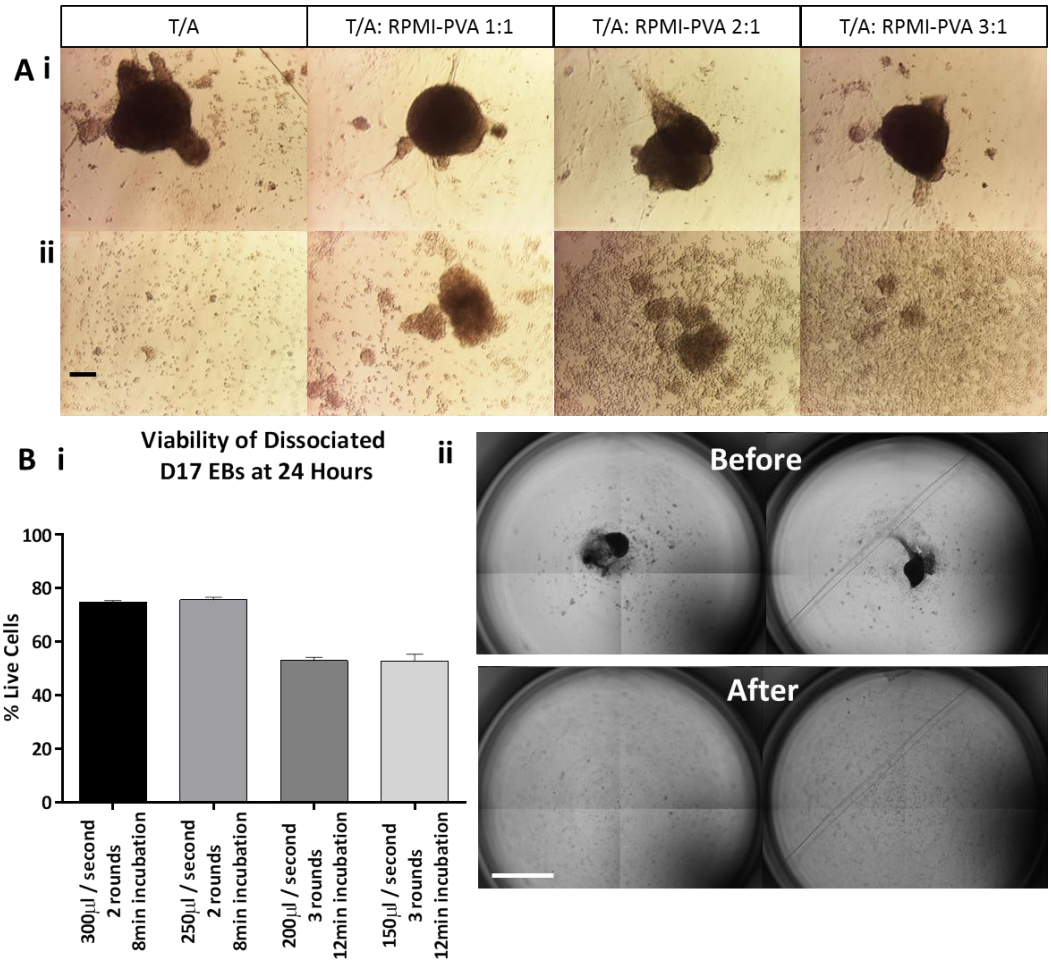


Figure 4.20 – Developing a centrifugation-free dissociation strategy for EBs on the robot.
(A) hESC derived beating EBs were manually dissociated using the trypsin/Accumax method or Accumax combined with RPMI-PVA at a 1:1, 2:1 or 3:1 ratio. **(i)** EBs prior to dissociation. **(ii)** After 20 min of incubation in the presence of enzyme, the solution was neutralised with either RPMI-PVA containing 20 % FBS **(right three columns)** or regular RPMI with 20 % FBS **(left column)** and cells were incubated for 10 minutes to allow sedimentation. Cells in PVA containing media had deposited on the bottom of the well **(right three columns)** while cells not in the presence of PVA were still in suspension **(left column)**. **(B) (i)** This method was tested on the robot with pipetting speeds of 300, 250, 200 and 150 µl/sec (20 up/down pipetting actions per round) to break up day-17 hESC EBs following 4-min rounds of incubation in enzyme prior to pipetting. Cells were then transferred to flat-bottomed 96 well plates and viability was measured by combined Hoescht33342, PI and CalceinAM staining after 24 hr (error bars = SD) (from left to right, n=6, 7, 8 and 8 wells). No difference between 300 µl and 250 µl/sec but 200 µl and 150 µl were significantly lower than 300 ($p<0.0001$, One-way ANOVA) **(B) (ii)** Representative images of 20 day old EBs before and after dissociation by this method. Scale bars in **(A)** = 100 µm, scale bar in **(B) (ii)** = 2 mm.

4.2.13 Testing a lactate-based method for enriching cardiomyocytes in EBs

While the EB differentiation method was capable of achieving yields of up to 100 % beating EBs per 96-well plate (figure 4.12), this did not reflect the cardiomyocyte purities in HUES7-derived EBs which were found to be as low as 32.6+/-0.5 % (figure 4.21 A). In order to test whether a combined process of automated purification and harvesting of cardiomyocytes could be used to generate high purity cardiomyocyte cell suspensions from EB differentiations, cardiomyocyte enrichment and dissociation was testing on the robot (figure 4.21) using a lactate-based enrichment method (Tohyama et al., 2013). EBs manually treated with glucose-free lactate containing medium for 4 days and dissociated manually were enriched 2.8-fold up to 90.1+/-2.1 % cardiomyocytes compared to untreated controls with purities of 32.6+/-1.1 %. When enrichment and dissociation was carried out by the robot the

value was marginally lower at 89.5+/-6.6 %. That this difference in purity was likely a result of lactate purification was supported by 3.2-fold and 6.5-fold decreases in total cell number per well compared to untreated manual dissociated controls, in manual treated/manual dissociated (from 16036+/-1002 cells to 5033+/-347 ($p<0.0001$, all one-way ANOVA with Dunnet's multiple comparison test (DMCT)) and robot treated/robot dissociated wells (from 16036+/-1002 cells to 2473+/-1734 ($p<0.0001$). EBs enriched and dissociated by the robot (total cell number of 2473+/-1743 and cardiomyocyte yield of 2239+/-1658) gave lower cell and cardiomyocyte yields compared to EBs treated by the robot but dissociated manually (4691+/-792 and 4414+/-707.4 ($p<0.0001$ for both) and EBs treated manually and dissociated manually (5033+/-347 and 4534+/-317.9 ($p<0.05$ for both) suggesting that the combination and purification and dissociation by the robot may have been causing additional cell death and reducing potential cardiomyocyte yields.

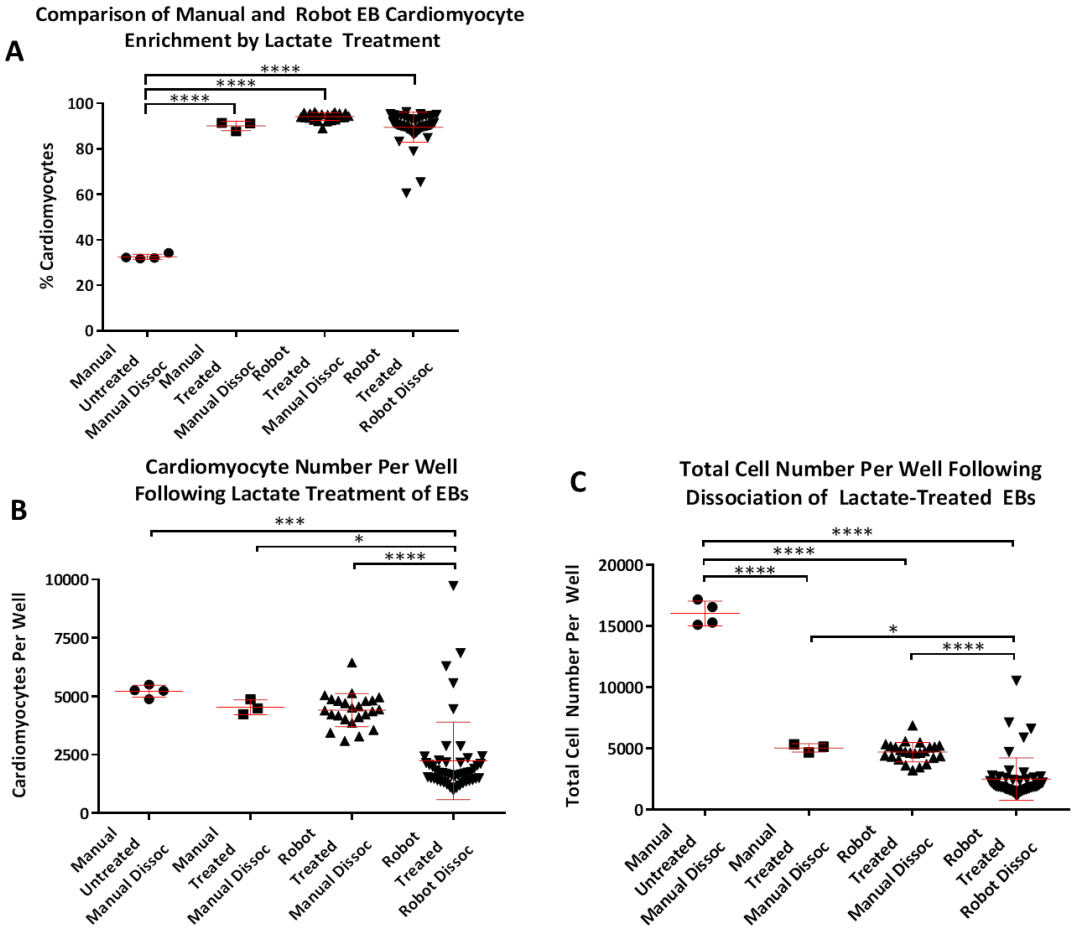


Figure 4.21 – Testing lactate enrichment of cardiomyocytes in hESC-derived beating EBs.

Day 13 hESC EBs from the same plate were treated with RPMI (no glucose) supplemented with lactate for 4 days to enable cardiomyocyte enrichment either by manual or robot addition of medium to the EBs. After treatment, EBs were given RPMI-B27 for 24 hr to recover prior to dissociation either manually or by the robot using the 300 µl/sec 4 min enzyme incubation protocol. **(A)** Cells harvested and seeded in flat bottom-96 well plates were stained for α-actinin and DAPI and quantified by the Cellavista to give % cardiomyocytes for each method. **(B)** Total cardiomyocyte cell number per well for each condition. **(C)** Total cell number per well from EB differentiations set up with 10,000 cells per well. (Manual/untreated/manually dissociated n=4 wells, manual/treated/manually dissociated n= 3 wells, robot treated/manual dissociated n=24 wells, robot treated/robot dissociated n=30 wells).

4.2.14 Developing an automated process for monolayer differentiation using an in-house differentiation protocol

Limitations of the EB differentiation method included low cell yields (0.6+/-0.3x10^6 cells per plate) and reliability issues due to batch variations resulting from the undefined nature of MEF-CM used to culture hESCs prior to differentiation. An in-house, fully defined, monolayer differentiation method using mTeSR was developed to overcome these issues (developed by Vinoj George, covered in section 3.2.8). In order to improve differentiation reproducibility and increase cardiomyocyte yields in the automated cardiomyocyte differentiation process, this method was chosen to replace EB differentiation. The existence of robust processes for changing medium and harvesting cells from robot flasks meant that this method was amenable to automation on the robotic platform and required a minimal amount of testing in order to be achieved.

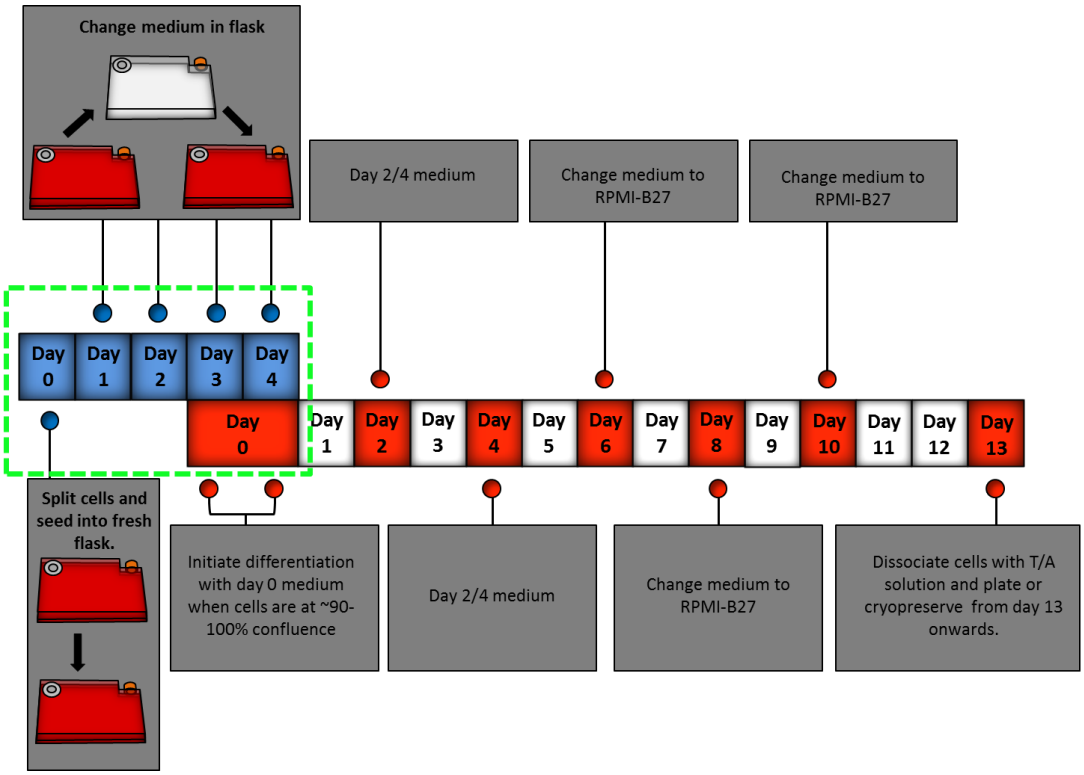


Figure 4.22 – The automated monolayer differentiation process for HUES7 cells in mTeSR.
(Chronologically from left to right) HUES7s are harvested and seeded into a RoboFlask at 6x10^6 cells per flask (65,000 cells per cm^2) and a medium change is performed every 24 hr. When cells reach between 80 % and <100 % confluence, medium is changed to day 0 medium (see Chapter 2 section 2.2.2 for recipes). After 48 hr this medium is replaced with day 2/4 medium. After a further 48 hr, medium is replaced again with fresh day 2/4 medium. From day 6 onwards, medium changes are carried out with RPMI-B27. Dissociation is carried out using T/A (see Chapter 2 section 2.3.2.2) using the existing cell harvesting scripts on the robot and is carried out after day 13.

4.2.15 Generation of hESC derived cardiomyocytes by automation

In order to confirm whether the mTeSR monolayer differentiation method could successfully generate cardiomyocytes using HUES7 hESCs, the process outlined in figure 4.22 was carried out. mTeSR cultured cells were dissociated by the robot in RoboFlasks, seeded in mTeSR and maintained by the robot with daily medium changes of mTeSR until suitable confluence was reached (as determined by scanning with Cellavista)(achieved by 72 hr). Differentiation was initiated and

carried by the robot over the required 10-day period after which cells appeared as spontaneously beating sheets in both robot-maintained RoboFlasks and parallel manual control RoboFlasks. These beating sheets were dissociated by the robot using existing passaging protocols but exchanging accutase with T/A). Cells were seeded in flat bottom 96-well plates for immunostaining quantification (by Cellavista) with α-Actinin or fixed in suspension for quantification by flow cytometry for both α-actinin and cardiac troponin T. Manually differentiated and dissociated cells were 97.4 % and 98.7 % positive for α-actinin and cardiac troponin T respectively by flow cytometry and 96.9 +/- 1.2 % positive for α-actinin by immunostaining quantification while robot differentiated cells were 96.9 % and 98.5 % positive for both α-actinin and cardiac troponin T respectively and 92.8+/-1 % positive by immunostaining (figure 4.23). Immunostained cells also showed evidence of stained sarcomeres confirming specificity of antibody staining (figure 4.24A left and right pairs of images). These results demonstrated that cardiomyocytes of high purity could be generated using the robot although total cell yields were lower in the robot differentiation compared to the manual differentiation ($4.5x10^6$ and $6.5x10^6$ cells respectively). Nevertheless, the robot differentiation outcome represented a 7.5-fold increase compared to the mean total cell yield from EB differentiations (per plate, $0.6+/-0.3x10^6$ cells).

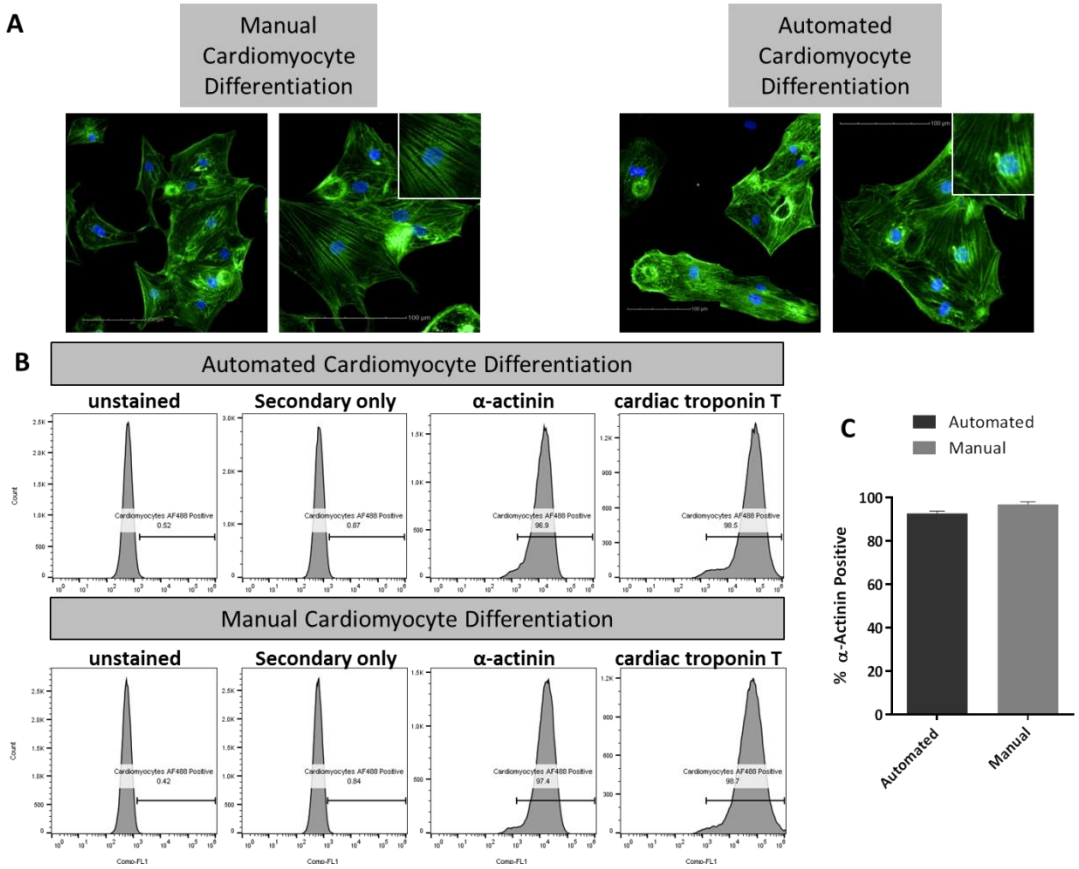


Figure 4.23 – Quantification of cardiomyocytes generated by manual or robot monolayer differentiation of mTeSR hESCs to cardiomyocytes.
(A) Representative images of cardiomyocytes stained for DAPI and α-Actinin from manual differentiations (left) and from robot differentiations (right). **(B)** Flow cytometry histograms showing quantification of cells stained for cardiac troponin t and α-actinin from robot differentiation (top row) and manual differentiation (bottom row). **(C)** Cellavista quantification of cardiomyocytes stained for α-actinin from robot differentiation and manual differentiation difference between manual and automated significant ($p<0.0001$, t-test) n=7 wells.

4.2.16 Dissociation and viability of monolayer differentiations carried out manually and by automation

In order to use these cells for drug screening or other applications, successful dissociation and cell survival were necessary. To assess the viability of cardiomyocytes generated by the robot and dissociated by the robot using the T/A method, viability after dissociation was measured at 24, 48 and 72 hr by staining

with Hoechst33342, PI and CalceinAM in 96-well flat bottom plates (figure 4.24). Cell viability from dissociations was 87.3+/-0.9 %, 86.9+/-0.8 % and 88.7+/-0.2 % at 24, 48 and 72 hr respectively, showing no significant change over time but being significantly higher ($p<0.0001$ for all timepoints) than cells dissociated manually at 81.1+/-1 %, 79.4+/-1.3 % and 81.8 +/-0.4 % for 24, 48 and 72 hr respectively. The difference between manually dissociated cells at 48 and 72 hr was also significant ($p<0.05$). Representative images of stained cells (Figure 4.24B) also showed that cells dissociated by this method were seeded as a near-single-cell suspension as demonstrated by the absence of cell clusters at 24 hr indicating that the method did not have a sizeable negative effect on cell viability, that viability remained stable for 72 hr and that single-cell suspensions of cardiomyocytes could be generated using the T/A method to dissociate monolayers.

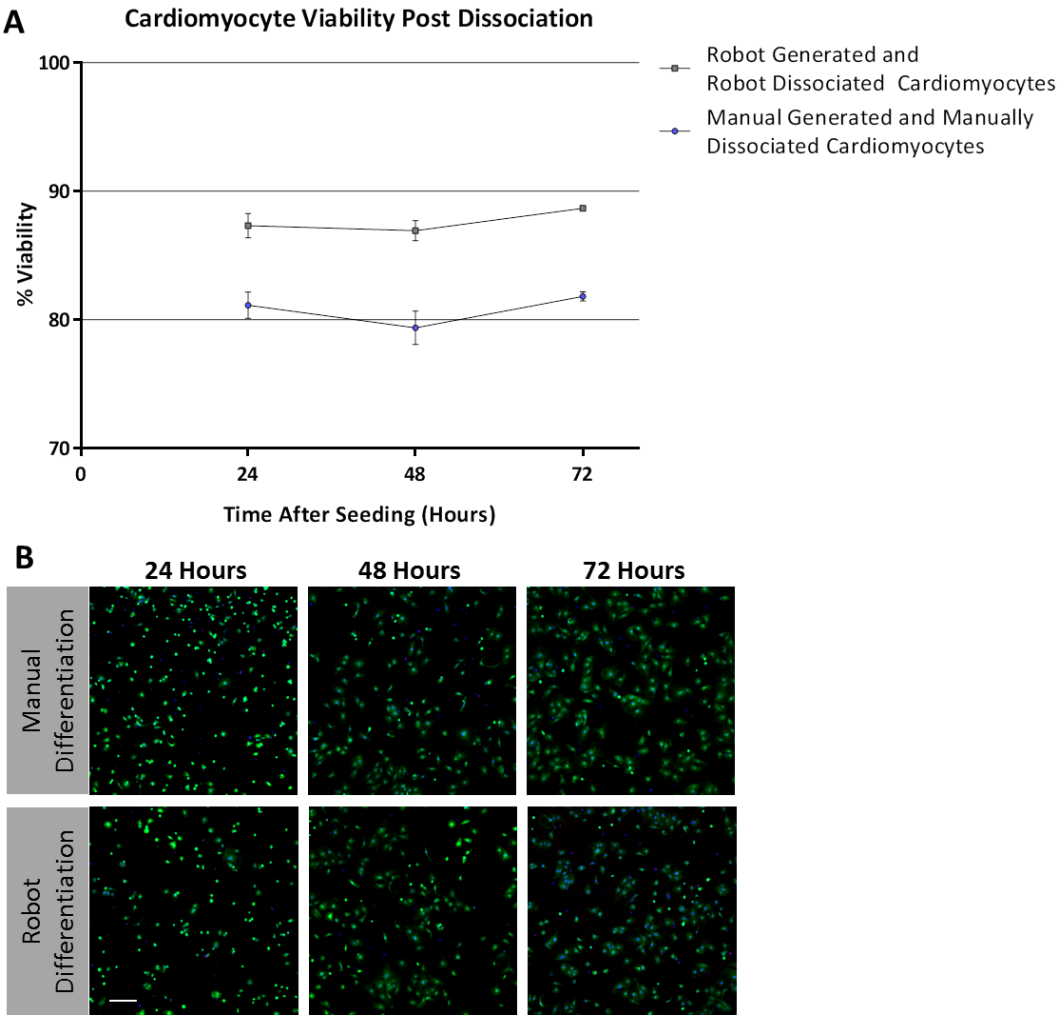


Figure 4.24 – Viability of dissociated manually generated/manually harvested and robot generated/robot harvested mTeSR Hues7 monolayer differentiated cardiomyocytes.

Cardiomyocytes were dissociated using the T/A method either manually or by the robot and neutralised with RPMI-B27 with 10 % (v/v) FBS. **(A)** Manually generated cells were dissociated manually (blue) and robot generated cells were dissociate using the robot (grey). **(B)** Viability of cardiomyocytes was measured with Hoescht33342, PI and Calcein AM at 24, 48 and 72 hr after seeding. Scale bar = 200 µm, n=3 wells for each condition.

4.2.17 Automating E8 culture of CPVT and LQT2 hiPSC lines for use in monolayer differentiations

While successful in increasing the scale of hESC-derived cardiomyocyte production up to 7.3+/-1.2 million cells per RoboFlask, the mTeSR method required the use of expensive defined media such as mTeSR (£0.34/ml) and StemPro34 (£0.30/ml), whereas MEF-CM cost was £0.11/ml (excluding staff costs). Additionally, while HUES7 differentiations were successful, this was not the case across several hiPSC lines tested (with the exception of the AT1 hiPSC line). When the CPVT and LQT2 E8-derived lines were derived, these were successfully differentiated with the E8 monolayer differentiation method manually (chapter 3, section 3.2.12). In order to replicate this success on the robot, E8 culture of these lines was attempted. These lines were cultured over 5 (CPVT) or 7 (LQT2) passages on the robot in parallel with manual cultures in order to generate growth curves (figure 4.25A and B). The population doubling time for CPVT hiPSC cultured manually was 21.8 hr compared to 24.7 hr on the robot while, LQT2 hiPSCs had a longer population doubling time of 30.9 hr in manual culture and 29.3 hr on the robot. In both cases however, growth rate was stable and karyotype assessment of both lines showed they all had normal karyotype (46XY for CPVT and 46XX for LQT2 for manual and robot growth curves, figure 4.25C and D). Therefore, these results indicated that culture of hiPSCs in E8 medium with TrypLE passaging was compatible with our robotic platform.

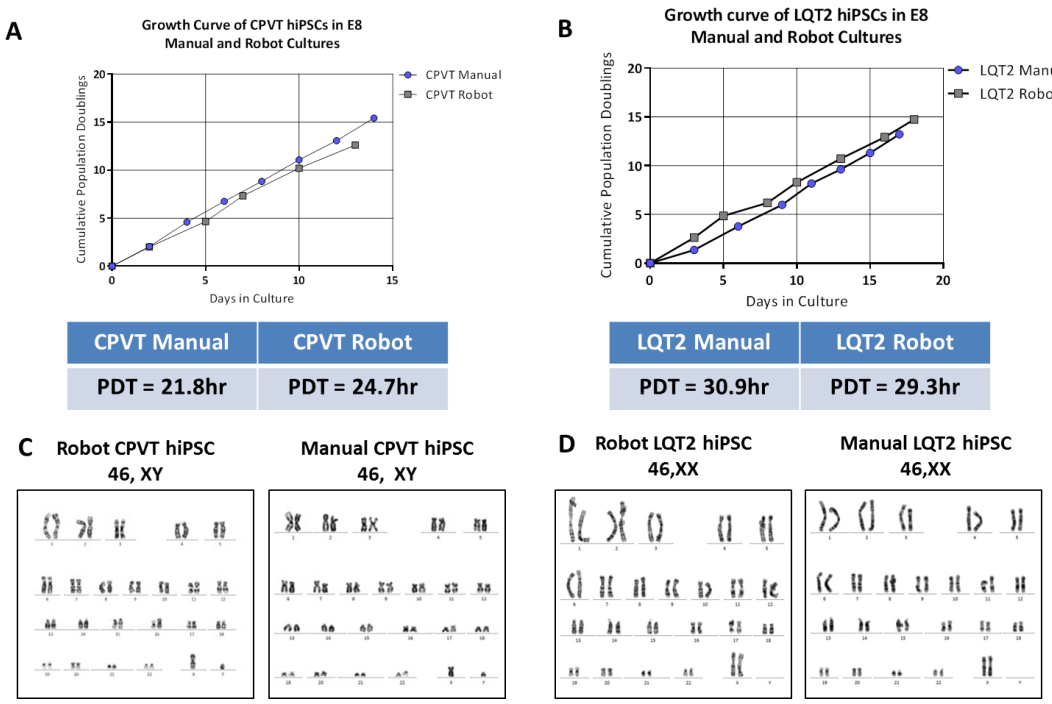


Figure 4.25 – Culture of CPVT and LQT2 hiPSC lines on the robot in E8 medium. **(A)** CPVT and **(B)** LQT2 hiPSCs in E8 were cultured manually and by the robot using TrypLE for harvesting for 5 or more passages. **(C)** and **(D)** representative karyograms of CPVT and LQT2 hiPSCs cultured for 5 or more passages either manually or by the robot.

4.2.18 Automated differentiation of E8 cultured hiPSC lines to cardiomyocytes

In order to demonstrate that the E8 monolayer differentiation method could also be automated, CPVT hiPSCs were seeded at approximately 30,000 cells per cm^2 in a RoboFlask and the differentiation process carried out using the same process as the mTeSR monolayer method (figure 4.22) but using reagents specific to the E8 monolayer method (CDM3 medium with 4 µM Chir on day 0 and 2 µM Wnt-C59 on day 2 (same as chapter 3, section 3.2.12). This differentiation was successful and generated monolayers that beat as uniform waves (video still figure 4.26D, see video file, video 17, appendix). These cells were harvested by sequential treatments using TrypLE (TrypLE Select) to harvest cells on day 14 of differentiation. TrypLE was used as the collagenase method had not yet been developed. $39.3x10^6$ cells were

harvested from one RoboFlask and cryopreserved to create a stock of cells for drug screening experiments. Differentiated CPVT cells thawed and immunostained for cardiac markers α-actinin and cardiac troponin T, were 91.4+/-2.1 % and 96.85+/-0.9 % pure for both respectively (figure 4.26A) indicating that this differentiation method when carried out on the robot generated cardiomyocytes with high purity and a yield of $4.24x10^5$ cells per cm^2. A subsequent differentiation carried out manually to supply additional CPVT cardiomyocytes for drug screening also gave high purity when immunostained with α-actinin (97.1+/-3.4 % positive). These two banks were sufficient to supply all the cardiomyocytes needed for the drug screening optimisations and experiments carried out in chapter 5.

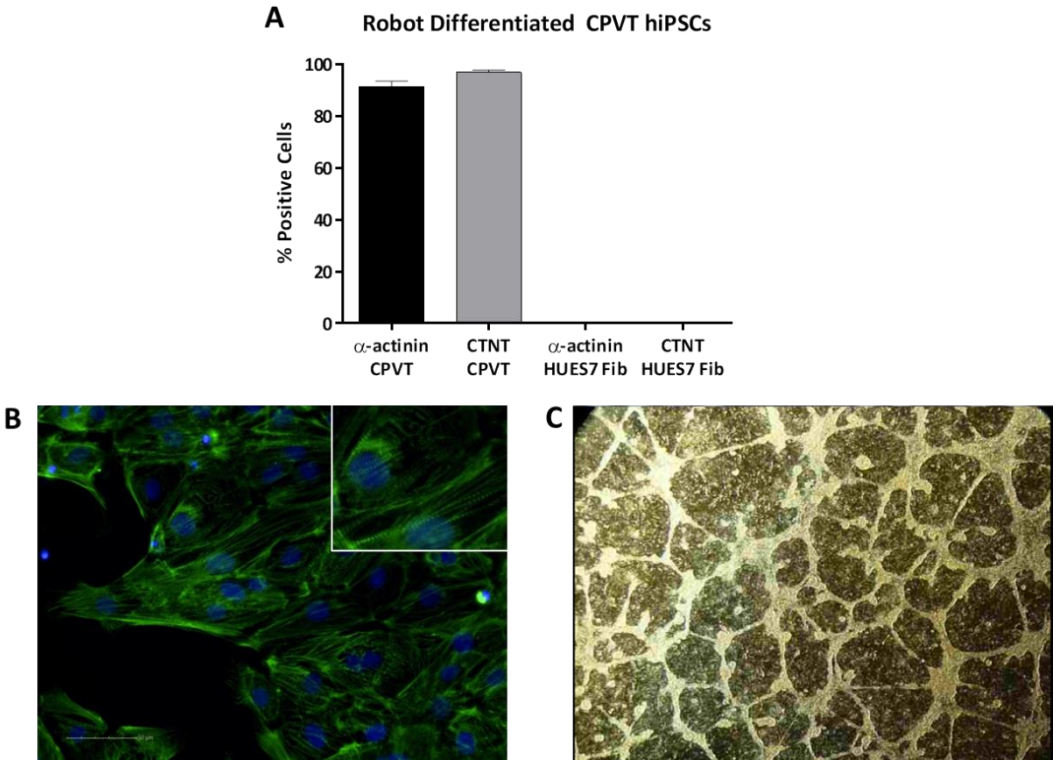


Figure 4.26 – Automated differentiation of CPVT and LQTS2 hiPSCs cultured in E8 to cardiomyocytes.
Cardiomyocytes generated using the CPVT line were differentiated by the robot, dissociated manually using the sequential TrypLE method and cryopreserved to make a cardiomyocyte bank for drug screening. **(A)** Cells were thawed and seeded in a 96-well plate and immunostained to quantify purity of the bank for α-actinin and cardiac troponin T with HUES7 fibroblasts used as a negative control. (n=4 wells) **(B)** A representative immunostaining image of cardiomyocytes stained with α-actinin showing cells with characteristic actin banding (see inlay). **(C)** Still image taken from a video recording showing cells spontaneously beating as a wave (see video 17, supplementary folder).

4.2.19 Automating hiPSC derived cardiomyocyte seeding in 384-well plates for drug screening

Although considerable work had been carried out using 96-well plates on the robot, no work had been attempted with 384-well plates. However, by scaling out to 384-well plates, 96 variables could be tested in quadruplicate compared to 24 in a 96 well plate (or 32 variables in triplicate). This required seeding 1 million more cells per plate than in 96-well plates (3.84 million compared to 2.88 million). However, when a comparison was made for the number of cells needed to test a variable in quadruplicate in each plate format, the number of cells needed was $4x10^4$ cells per condition in 384-well plates compared to $1.2x10^5$ cells in 96-well plates (ie. 3-fold higher number of cells required in 96-well plates). Therefore, it was decided that processes for cell seeding and drug screening in 384-well plates should be developed. To achieve this, appropriate vectors were identified to carry out cell seeding and medium changes without disrupting cells. For aspiration of medium from 384-well plates, these vectors were set at X=0, Y=0 (ie. the centre of the well) and Z-maximum was set at 1699 mm, to ensure most medium could be aspirated

without tips coming into contact with cells or dispensing directly onto cells potentially dislodging them (figure 4.27Ai and ii). Additionally, issues with the plate holder (or MCA96) not being level meant medium was not removed uniformly across the plate. To ensure equal volume of medium removal across the plate, processes were developed to ensure a residual volume of 20 µl was left in the wells at all times.

To test cell seeding in 384-well plates, and well-to-well variation, a manually dissociated, pre-counted cardiomyocyte cell suspension was supplied to the robot for seeding at 10,000 cells per well. This suspension was seeded into two robot-Matrigel-coated 384-well plates. After 24 hr, cells were stained with Hoechst33342 to quantify the number of cells seeded per well using the Operetta confocal plate reader. A comparison of the two plates gave 4634+/-471.6 cells and 3904+/-550.8 cells per well (only 1/3 of each well was screened to avoid excessively long scans, figure 4.27B ii, scanned areas shown in dark grey). The second plate had a significantly lower mean seeding density than the first ($p<0.0001$, unpaired t-test) suggesting that there was plate-to-plate variation with cell seeding. In the first plate, the coefficient of variation (CV) was 10.2 % (10 was considered the limit of what was acceptable) and the second plate was 14.1 % (outside the acceptable range). These results suggested that there was scope to improve the uniformity of seeding density in 384-well plates. However, as there was limited time available to attempt such optimisations and to conserve cardiomyocyte stocks for drug screening experiments, no changes to the 384-well seeding process were made.

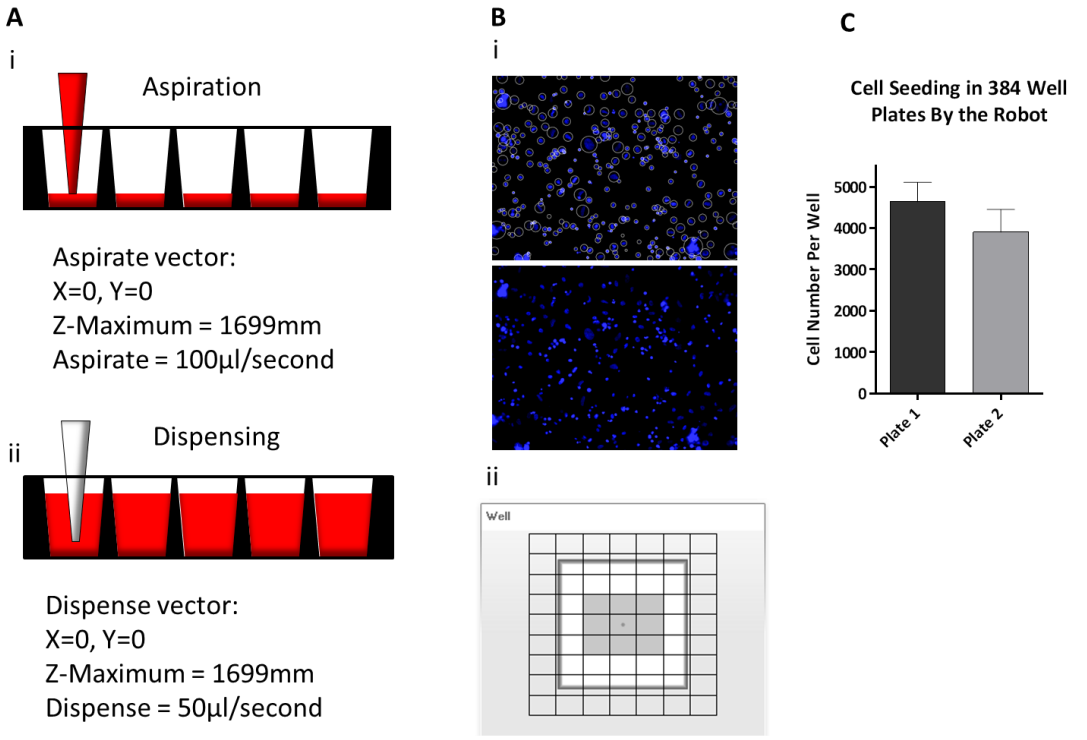


Figure 4.27 – Matrigel coating and cell seeding in 384-well plates for high throughput and high content drug screening.
(A) Illustration showing cross-section of wells from a 384-well plate with representation of the position of tips in 384-well medium change scripts indicating that some residual volume is left be behind (by design) in order to achieve equal amounts of medium across the plate (see section 4.2.20 for more detail). **(B)** LQT2 hiPSC cardiomyocytes were seeded at 10,000 cells per well and after 24 hr, stained with Hoescht3334 **(i)** the chosen fields of view for imaging occupied approximately 30 % of the well **(ii)**. **(C)** Quantification of cell numbers per well for two 384-well plates seeded by the robot back-to-back showing significant difference between plate 1 and 2 ($p<0.0001$) n=384 wells per plate.

4.3 Discussion

4.3.1 Automation of EB differentiations

In order to develop a method for automated and scalable generation of EB-derived cardiomyocytes, the manual EB setup and maintenance methods were translated into processes that could be carried out on the robot. Testing robot EB transfer on day 4 gave ≥99 % EB transfer; while robot medium changes on the EBs at days 2, 4

and 8 along with EB transfer on day 4 gave 100 % EB transfer and 95.8 % beating EBs. This demonstrated that robot medium changes and EB transfers were compatible with generating high proportions of beating EBs. However, where EBs were set up by the robot, differentiations failed completely (no plates >0 % beating EBs). Although the issue with autoclaved plasticware was identified and corrected, additional unknown variables appeared to also be negatively affecting both EB formation (a near two-fold decrease in the size of EBs at day 4 compared to manual EBs) and differentiation at the cell harvesting/counting/dilution stages. Seeding cell suspensions on day 0 and maintenance of EBs onwards gave 100 % beating EBs (figure 4.12) indicating that this issue was not likely to originate in the interim period between day 0 and 2 of differentiation either. Experiments that tested the duration of time of cell harvest with manual setup (table 4.2) did not reveal any negative effects of prolonged incubation time (up to 10 min) on ability of EBs to differentiate (81.5+/-3.5 % EBs beating when 10 min setup was carried out at room temperature) suggesting that time of incubation throughout the setup process was not likely to be the cause, however a test of both enzyme incubation periods and the time taken to carry out the cell count and dilution steps was not carried out. Under-seeding of wells was also an unlikely cause. When the number of cells seeded by the robot was quantified after 24 hr (figure 4.13) 10621+/-1054 cells were counted (when all steps had been carried out by the robot) and when the cells were manually harvested but counted by the robot and seeded by the robot, this gave 9436+/-317.3 cells after 24 hr.

Further investigations may have revealed the cause of the failure of the robot plated EBs to differentiate, in fact, others have demonstrated the formation and differentiation of EBs is possible in automated systems. This was achieved by spontaneous differentiation of EBs and identifying expression of early-stage differentiation markers including βIII-tubulin, α-fetoprotein and brachyury in mouse ESCs (mESCs) (Hussain et al., 2013) but also using directed differentiation of mESC-EBs (although cardiomyocyte purities were relatively low at 43 %)(Kowalski et al., 2012). However, as the mTeSR monolayer differentiation method was less technically challenging to automate, was scalable and generated >7.5-fold increases in cell yields with high cardiomyocyte purities (>90 %), this meant that the EB method development was abandoned in order to use time and resources more efficiently.

4.3.2 Automation of monolayer differentiation methods

To provide cardiomyocytes for use in drug screening at sufficient scale to seed 384-well plates (3.84 million cells per 384-well plate plus further 4 million cells to provide adequate dead-volume in a baffled trough for the robot to seed accurately), significant scale up of differentiation capabilities was needed. The EB method generated 0.6+/-0.3x10^6 cells per plate meaning approximately thirteen 96-well plates of EBs would be needed to supply sufficient cells for one 384-well plate. In some cases, the proportion of cells that were cardiomyocytes was as low as 30 % of the total per well (figure 4.21). Using these cells in drug screening for example, would make it difficult to determine whether any response observed was due to cardiomyocytes or the other 70 % of cells of different cell type. While purification of

EBs using lactate treatment could improve the purities of cardiomyocytes (Tohyama et al., 2013, Burridge et al., 2014), this caused a reduction in cell number, meaning that >13 plates of EBs would be needed to set up drug screening in a 384-well plate.

In contrast to this, the manual mTeSR monolayer differentiations in RoboFlasks gave up to 6.5 million cells (purity >90 %) and 4.5 million cells when fully automated (purity >90 %) which represented approximately 10- to 7.5-fold improvement in absolute cell yields over the EB method. A further improvement in yields was made when differentiations with CPVT hiPSCs in E8 using the E8 monolayer method on the robot generated 39 million cells of purity >91 % in a RoboFlask meaning up to 9x384-well plates could be seeded from one differentiation (this equates to 864 different drug concentrations in quadruplicate, for example) and raising the possibility of making large-scale, high-purity cardiomyocyte banks. In a trial investigating post infarct myocardial repair with non-human primates, $1x10^9$ cardiomyocytes were manually generated using a monolayer differentiation method that gave 73 % purity and demonstrated improved cardiac function (Chong et al., 2014) as such, achieving such scales of production are desirable to enable high throughput screening or therapeutic application of hiPSC derived cardiomyocytes.

While automated culture of hESCs (Thomas et al., 2009), mouse ESCs (Kowalski et al., 2012) and hiPSCs (Valamehr et al., 2011), (Conway et al., 2015) in both 2D systems and in 3D suspension systems (Soares et al., 2014, Wang et al., 2014) has

been demonstrated including derivation and differentiation of hiPSCs (Paull et al., 2015), few groups have demonstrated automated differentiation of hiPSCs or hESCs to cardiomyocytes. Cardiomyocyte differentiations have been carried out in automated suspension culture yielding up to 40 million cells (up to 59 % or approximately 23.6 million of which were positive for α-actinin) per 100 ml of medium (Kempf et al., 2014) while the automated E8 monolayer differentiation method generated up to 39 million cells with 20 ml medium (5-fold less) and achieved a 34 % higher yield of cardiomyocytes (35.5 million compared to 23.6 million). Additionally, achieving nearly complete automation with minimal human intervention is challenging. This was largely achieved for the production of cardiomyocytes (see supplementary video 17 of cardiomyocytes generated using a completely automated process from routine cell passaging to beating cardiomyocytes) certain elements were performed manually (provision of enzyme, flasks for seeding cells and media) and a prediction of differentiation timing needed to be made in advance of the experiment commencing. Systems exist for imaging-based feed-back for automated user-free passage decision making (Ker et al., 2011) which could also be used to aid differentiation decision making. With this in mind, other systems for monitoring biomarkers *in situ* and non-invasively such as impedance, extracellular pH and oxygen consumption (Weiss et al., 2013) could also be employed to aid in automated feed-back controlled culture process decision making.

5 Developing Platforms for Drug Screening Using Cardiomyocytes

5.1 Introduction

5.1.1 CPVT hiPSC cardiomyocytes for drug screening experiments.

In order to maximise consistency between optimisation experiments and drug testing experiments, the decision was made to use one method of differentiation to produce stocks of hiPSC cardiomyocytes. To this end, CPVT cardiomyocytes generated using the E8 monolayer method carried out by the robot were used in these experiments. This line was chosen because, at the time, it was the only one from which suitably-sized cardiomyocyte banks had been generated for use in this work. Unless otherwise stated, all data shown in this chapter was generated using CPVT-hiPSC cardiomyocytes (from here on referred to as “hiPSC cardiomyocytes” or “cells”).

5.1.2 Assessing cell death in vitro

5.1.2.1 Apoptosis

Apoptosis is a controlled process of cell death first identified in 1972 (Kerr et al., 1972). During this highly regulated process, intracellular components such as cytoskeleton proteins and protein complexes are broken down leading to endonuclease release, cell shrinkage, plasma membrane blebbing, cell detachment from culture surfaces, nuclear condensation, DNA fragmentation and formation of apoptotic bodies (Krammer et al., 2007, Brauchle et al., 2014). *In vivo*, these

processes culminate in the cells expressing markers such as phosphatidyl serine on the cell surface marking them for clearance by phagocytosis (Krammer et al., 2007, Czabotar et al., 2014).

5.1.2.2 Programmed Cell Necrosis

Cell necrosis is another regulated process of cell death mediated by alternative pathways to apoptosis. Traditionally necrosis was thought to be exclusively a result of sudden unregulated/uncontrolled response to physiochemical triggers but more recent studies using inhibitors of necrosis have revealed it to also be highly regulated (Vanden Berghe et al., 2014). A number of processes have been described including, necroptosis, parthanatos, oxytosis, ferroptosis, ETosis, NETosis, pyronecrosis and pyroptosis all falling under the umbrella of regulated necrosis (Vanden Berghe et al., 2014). In contrast to apoptotic cells, cells undergoing programmed necrosis do not fragment but remain intact with a “balloon-like” appearance, intact nucleus/nuclear swelling and organelle swelling. Like apoptosis however, cell membrane does lose its integrity (Vandenabeele et al., 2010, Pietkiewicz et al., 2015).

5.1.2.3 Measuring apoptosis and necrosis in vitro using Propidium Iodide

Propidium Iodide (PI) is an irreversible DNA-binding, membrane impermeable dye that is excitable at 488 nm and is detected between 520-570 nm (Chen et al., 2012). The use of PI in measuring apoptosis was first developed as a flow cytometric method for quantifying percentage of cells undergoing apoptosis (Nicoletti et al.,

1991). As PI is not membrane permeable, in live cells, it is not capable entering the cell to bind to the DNA. At later stages of apoptosis or early stages of necrosis, membrane integrity is lost and PI is able to enter the cell and bind to the DNA (Pietkiewicz et al., 2015) (figure 5.1). As a result, both apoptotic and necrotic cell death can be identified by PI staining. Studies investigating the effect of co-incubating human cancer lines with PI for up to 72 hr have found no evidence of toxicity (Wlodkowic et al., 2009) making this dye suitable to real-time monitoring of cell death *in vitro* as well.

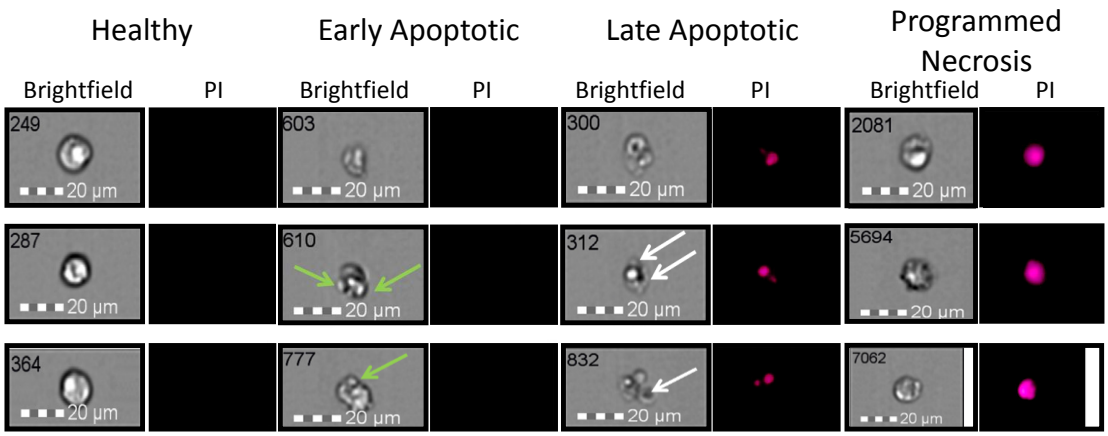


Figure 5.1 – Representative images of cells undergoing apoptosis or programmed necrosis.
Healthy, early- late- apoptotic and programmed necrotic cells as seen through an imaging flow cytometer. Left, healthy cells have a uniform spherical shape and do not stain for PI. Left of centre, early apoptotic cells adopt an uneven spherical shape as a result of irregular protrusions (blebbing) from the plasma membrane (marked with green arrows) but still do not stain positively for PI. Right of centre, in late apoptosis, cells become more irregular in shape, in some cases (marked with white arrows) dividing up into smaller apoptotic bodies and staining positively for PI. DNA fragmentation from apoptosis means the PI stained area is small and may be broken up into more than one spot per cell. Right, in programmed necrosis, cells maintain a uniform spherical shape with no signs of blebbing but stain positively for PI with a high nuclear to cytoplasm ratio. Figure taken and adapted from (Pietkiewicz et al., 2015).

5.1.2.4 Caspases and Cell Event Caspase 3/7 reagent

Caspases are a group of cysteine-dependent aspartic-acid-directed proteases unique to the process of apoptosis which are found in cells in an inactive form and when activated function to trigger effectors or directly carry out cell breakdown (McStay and Green, 2014). There are two types of caspases, initiators (caspases 2, 8, 9 and 10) and executioners (also referred to as effectors) (3, 6 and 7). Initiator caspases are activated by death ligands or mitochondrial outer membrane permeabilisation and in turn, directly or indirectly trigger the cleavage and activation of executioner caspases (McStay and Green, 2014). Executioner caspases are responsible for cleaving cellular substrates such as organelles, leading to the formation of apoptotic bodies (Czabotar et al., 2014). Therefore, activation of caspases marks an irreversible commitment to cell death and as such, caspase activity can be used to identify cells that are undergoing apoptosis. CellEvent Caspase 3/7 reagent (CEC) is a commercially available substrate can be used to detect active caspases 3 and 7 in cells. This substrate (DEVD) is a 4-amino acid sequence (Asp-Glu-Val-Asp) which is selectively cleaved by activated caspases 3 and 7 (Walsh et al., 2008) and is conjugated to a nucleic acid binding dye. When the DEVD substrate is cleaved, the dye is released, binds to DNA and fluoresces, (excitation at 502 nm and emission at 530 nm – FITC/green channel) (Life Technologies CellEvent Caspase 3/7 reagent product manual, 2015).

5.1.2.5 Staurosporine as a positive control for caspase activation

Staurosporine (STA) is a protein kinase C inhibitor first identified in bacterial extracts from *Streptomyces* sp (Omura et al., 1977) from which chemical analogues were synthesised as potential anti-cancer drugs (Gescher, 2000). STA has been shown to induce apoptosis/caspase activity and in cases where caspase activity is compromised, has also been shown to induce programmed cell necrosis (Dunai et al., 2012). STA induced caspase-mediated apoptosis has been demonstrated in a range of cell lines including in human cancer cell lines such as HeLa and U-2OS (Life-Technologies, 2011), rat neonatal cardiomyocytes (Yue et al., 1998), rat adult ventricular cardiomyocytes (Henaff et al., 2000) and hiPSC derived cardiomyocytes (Cellular Dynamics International, 2015a, Cellular Dynamics International, 2015b).

5.1.3 Doxorubicin cardiotoxicity *in vitro* and *in vivo*

Doxorubicin (DOX) is a member of the anthracycline antibiotic family of compounds and has been used for over 30 years in the treatment of a range of cancers including haematological malignancies, soft tissue sarcomas and solid tumours (Holmgren et al., 2015). The anti-cancer properties of DOX originate from its ability to target Topoisomerase 2 and induce DNA breaks, its primary mode of action in killing proliferating cancer cells and reducing tumour growth. Clinical trials of DOX identified a dose dependent cardiotoxic effect of the drug in patients (3 %, 7 % and 18 % of patients experiencing heart failure resulting from cumulative doses of 400, 550 and 700 mg/m^2) and therefore, to minimise adverse effects, maximum cumulative DOX dosage was set at ≤550 mg/m^2 (Lefrak et al., 1973). Improved cardiac functional assessment techniques increased the detection of heart failure

post DOX treatment with cumulative percentage estimates of 5 %, 16 %, 26 % and 48 % from cumulative dosages of 400, 500, 550 and 700 mg/m^2 respectively (Swain et al., 2003) leading to a further reduction in recommended cumulative dosage to 400-450 mg/m^2 (Vejpongsa and Yeh, 2014). In a follow-up study of 2625 patients who received anthracycline therapy, 226 (9 %) experienced cardiotoxicity (determined by reduction in left ventricular ejection fraction) following mean cumulative dose of 359+/-172 mg/m^2 with 98 % of these cases occurring within a year of treatment (Cardinale et al., 2015). Other estimates have suggested that >50 % of individuals treated with some form of anthracycline experience cardiac dysfunction in the 20 years post treatment with 5 % developing heart failure (Lipshultz et al., 2014). Combined, these studies suggest a high prevalence of adverse effects from DOX/anthracycline therapy.

Cardiomyocytes are rich in mitochondria, metabolically active and have relatively low antioxidant producing enzymes (Roca-Alonso et al., 2015) making them a uniquely susceptible cell type to DOX-induced oxidative stress and production of reactive oxygen species in the mitochondria (the site of DOX metabolism). Another proposed method of toxicity is via Topoisomerase 2 which comes in two forms, 2α and 2β. DOX forms a DNA cleavage complex with Topoisomerase 2 and DNA in proliferating cells where Top2α is normally present. Top2α is not found in mammalian cardiomyocytes but Top2β is (Capranico et al., 1992). DOX induced cardiotoxicity has been proposed via DNA breaks induced by DOX complex formation with Top2β in cardiomyocytes (Zhang et al., 2012b). Additionally, secondary alcohol metabolites from DOX metabolism have been implicated in

disrupting regulation in redox balance and energy metabolism and have been shown to be retained in mitochondria even after DOX treatment has ended due to poor clearance mechanisms suggesting that these too may play a role in DOX-cardiotoxicity (Minotti et al., 2010).

5.1.4 Drugs that may reduce doxorubicin cardiotoxicity *in vitro*

Identifying compounds with the potential to reduce DOX/anthracycline induced cardiotoxicity without negatively affecting its therapeutic effect would provide considerable clinical benefit. Several groups have assessed the use of compounds to reduce DOX cardiotoxicity such as dexrazoxane (DEX) (Lipshultz et al., 2004)(the only US Food and Drug Administration (USFDA)-approved drug for use as an anthracycline cardioprotectant (Salvatorelli et al., 2015)), carvedilol (CAR) in a 50-patient clinical study (Kalay et al., 2006) and sildenafil (SIL) using *in vivo* mouse models and isolated mouse ventricular cardiomyocytes *in vitro* (Fisher et al., 2005). However, the efficacy of these compounds has never been compared to one another in models of DOX/anthracycline cardiotoxicity.

5.1.4.1 Dexrazoxane

DEX is a free radical scavenger which has also been shown to block DOX binding to topoisomerase 2β (Lyu et al., 2007) protecting cardiomyocytes from DOX damage. DEX has been approved by the USFDA for use as a cardioprotectant with anthracycline treatment (including DOX) (Salvatorelli et al., 2015) and combined data from 10 studies with a total of 1600 patients found that DEX reduced heart

failure risk relative to placebo controls. Despite this, there exist concerns that DEX may reduce anthracycline efficacy, allow secondary malignancies to occur and elicit a myelosuppressant effect (Colombo et al., 2013). The American Society of Clinical Oncology only recommends its use for patients with metastatic breast cancer (Colombo et al., 2013) while in 2011, the European Medicines Agency determined that DEX was contraindicated in children (Lipshultz et al., 2014) which has limited its use in the clinic as a DOX cardioprotectant and necessitating further studies and/or alternative strategies to be developed.

5.1.4.2 Carvedilol

CAR is a β1, β2 and α1-adrenergic receptor blocker that also functions as an antioxidant, anti-inflammatory and anti-apoptotic agent (Dulin and Abraham, 2004). A small number of patients treated with either DOX or epirubicin and given prophylactic CAR treatment had reduced left ventricular dysfunction in a 50 patient (25 treated, 25 placebo) trial (Kalay et al., 2006) although, since then, no other randomised/placebo-controlled trials have been attempted (Colombo et al., 2013). Therefore, there is need for further studies to identify whether CAR could be used as a DOX-cardioprotectant.

5.1.4.3 Sildenafil

SIL is a phosphodiesterase-5 inhibitor that causes the opening of mitochondrial K_{ATP} channels (Fisher et al., 2005) which have been shown to confer cardiac protection following reperfusion-mediated reactive oxygen species insult (Ertracht et al., 2014,

Zhao et al., 2015). Additionally, sensitivity of cancer cell lines to DOX treatment was not affected by co-treatment with SIL (Di et al., 2010) suggesting that it may be a promising candidate for testing in a clinical setting. Despite this, no clinical trials have been attempted to assess the efficacy of SIL in preventing DOX or anthracycline toxicity.

5.1.4.4 Isoprenaline

Isoprenaline (ISO) is a β1, β2 and β3 adrenergic receptor agonist (Shin et al., 2014). In the healthy human heart the estimated ratio of β1 to β2 is 70 %:30 %, however, in instances of heart failure, reductions in β1 receptor and mRNA of up to 50 % have been observed (Lohse et al., 2003). β1 and β2 receptors have been shown to elicit different responses on stimulation, with β1 being primarily associated with apoptosis via cyclic AMP signalling pathways while β2 stimulation is associated with survival signals via G_i-coupled signalling and downstream increases in Bcl-2 expression (Shin et al., 2014). Electrophysiological analysis of hiPSC derived cardiomyocytes has shown that these cells express β adrenergic receptors as demonstrated by their response to ISO-mediated β-adrenergic stimulation up to 1 µM (Khan et al., 2013) and subsequent β-adrenergic block using β-blockers in healthy and disease models such as LQT2 (Matsa et al., 2011). In a previous model of STA-induced cardiotoxicity using adult rat ventricular myocytes, ISO was shown to reduce toxicity at 1 µM (Henaff et al., 2000), while more recently, another study in adult rat ventricular cardiomyocytes found that ISO treatment alongside H_2O_2 or ionomycin insult gave no significant change in cell death at ISO concentrations of 1 or 10 µM but at 10 nM there was a significant decrease (both $p<0.05$, t-test)(Shin et

al., 2014). This cardioprotective effect was associated with increased Bcl-2 expression at 10 nM ISO (Shin et al., 2014). ISO was therefore chosen in order to investigate this process in a human model to identify whether a cardioprotective or cardiotoxic effect would be observed.

5.1.5 Chapter Aims

High throughput *in vitro* models of anthracycline cardiotoxicity using hiPSC derived cardiomyocytes could be used to both confirm the ability of existing drugs and to identify novel compounds that can reduce toxicity. Furthermore, different individuals show varying levels of susceptibility to anthracycline induced cardiotoxicity. hiPSC derived cardiomyocytes may be useful in modelling this variability to provide a tool for predicting susceptibility or increased tolerance to anthracyclines and in turn, allowing tailored patient treatment. In order to demonstrate that both drug-induced cardiotoxicity and cardioprotective effects could be modelled *in vitro*, using hiPSC derived cardiomyocytes, a drug screening platform was created and validated to enable quantification of DOX cardiotoxicity over 24 hr and to test the cardioprotective effects of DEX, CAR and SIL *in vitro*. Furthermore, this chapter sought to demonstrate that this process was amenable to high-throughput by scaling it out to 384-well plates which were seeded and treated using the Freedom Evo 200 robotic platform and screened in time course experiments over 24 hrs using the Operetta confocal plate reader to monitor drug toxicity.

5.1.6 Key objectives

- Develop end-point and time course data acquisition and analysis methods using the Operetta confocal plate reader for the purpose of visualising and quantifying key markers such as PI, CEC and Hoechst33342.
- Develop the capability to monitor multiple markers simultaneously (PI and CEC) in 96- and 384- well format.
- Test the developed processes by evaluating cardiotoxicity from known cardio-toxic compounds such as DOX and STA.
- Carry out a drug screen testing compounds for their ability to reduce DOX cardiotoxicity.

5.2 Results

5.2.1 Designing analysis scripts for Operetta

To manually count stained cells accurately for high content assays is technically challenging, time consuming and highly subjective/error prone in nature. These limitations were overcome with the use of the Operetta High Content Imaging System (Operetta). For drug screening experiments, analysis protocols were designed to allow accurate quantification of fluorescent signals generated either in time course experiments or as end point assays. A pipeline was designed for the quantification of PI positive cells in time course experiments (figure 5.2). Identification of PI stained nuclei was achieved (figure 5.2A) with each nucleus being recorded as a separate “object” the edges of which were marked by green borders.

In this example, the region of interest was segregated three ways: background (400 fluorescence units (FU)), low fluorescence/auto-fluorescent objects (<2000 FU, figure 5.2A v – blue circles) where 277 objects were detected with mean fluorescence was 924+/-504 FU (all +/- values SD unless otherwise stated) and PI positive objects (≥2000 FU) where 128 objects were detected with a mean of 4634+/-2329 FU. Low fluorescence/auto-fluorescent cells were excluded using two building blocks. In the first, the mean fluorescence intensity (the mean intensity of all pixels falling within the green borders of each object) was calculated for all objects in the field of view (figure 5.2 B). In the second, a threshold defined by the operator was set to "select" any objects with mean fluorescence intensity above a chosen value (ie. 2000 FU) (see example in figure 5.2C). In time course experiments this method was used to quantify dead cells.

To calculate a value for percentage cell death, a total cell number was needed. This was achieved by adding Hoechst33342 dye (Hoechst) to the wells at 24 hr and then counting cell number by nuclear staining. This way, percentage cell death could be calculated using the following equation:

$$\text{Percentage Cell Death} = \left[\frac{\text{Number of Objects Positive for Hoescht and Dead Cell Marker}}{\text{Number of Objects Positive for Hoescht}} \right] \text{x } 100$$

For time course assays, co-staining with Hoechst during the assay was not possible. Hoechst is a membrane permeable nuclear dye that is toxic to cardiomyocytes over

prolonged incubation periods (i.e. 24 hr, figure 5.3) and so could only be used as part of end point analyses. In the absence of a non-toxic pan nuclear stain, the number of objects positive for dead cell marker(s) was converted to a percentage cell death value by using the mean number of Hoechst-positive objects in the untreated wells stained at the end of the assay to give percentage "death marker" positive cells relative to 24 hr untreated controls and was calculated as follows:

$$\text{Percentage Cell Death} = \left[\frac{\text{Number of Objects Positive for Dead Cell Marker}}{\text{Mean Number of Objects Positive for Hoescht at 24 Hr in Untreated Wells}}\right] \text{x } 100$$

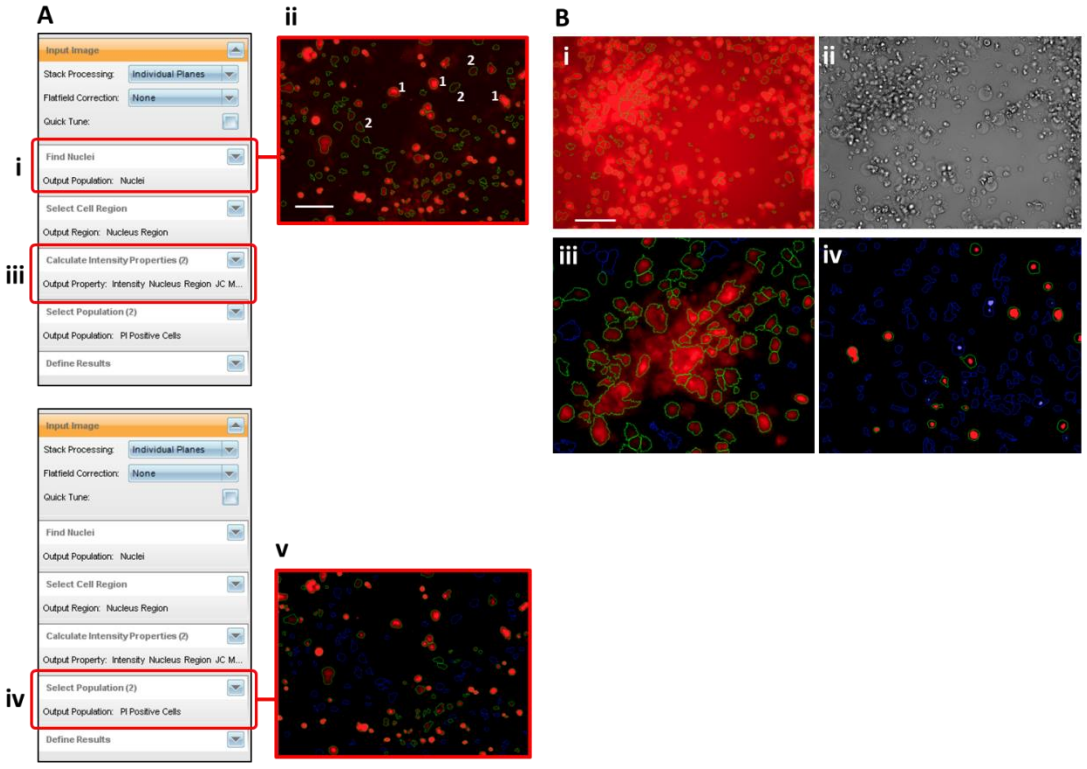


Figure 5.2 – Image analysis on the Operetta confocal plate reader for toxicity assays, potential issues and identifying Hoechst toxicity.
(A) Representative analysis "pipeline" used in the Harmony software associated with the Operetta platform. Analysis pipelines were laid out as sequential chains of image analysis algorithms termed "building blocks" (running from top to bottom). **(i)** Cells or nuclei were identified as "objects" (shown with green borders) for further analysis irrespective of fluorescence intensity. **(ii)** PI positive cells (examples marked with a 1) were identified with high fluorescence (>2000 FU, mean 4634+/-2329 FU (SD)) while auto-fluorescent/low fluorescence cells (marked with a 2) were lower (<2000 FU, mean 924 +/- 405 FU SD). Background fluorescence was (≤400 FU). Exclusion of unwanted cells was achieved using building blocks in iii and iv. **(iii)** Objects from i) were analysed to calculate mean fluorescence intensity. **(iv)** Objects were selected using an intensity threshold determined by the user. **(v)** Representative image showing objects that met that criteria (green borders) and those that didn't and were excluded (blue borders). **(B)(i)** At high concentrations of doxorubicin (≥50 µM) fluorescence background was high (>3000 FU) and dead cell aggregation resulted **(ii)**. **(iii)** These aggregates made object recognition inaccurate (cells appeared merged as large objects or not identified at all). **(iv)** Accurate object recognition was achieved at lower (1 µM) doxorubicin concentrations. Scale bars = 100 µm.

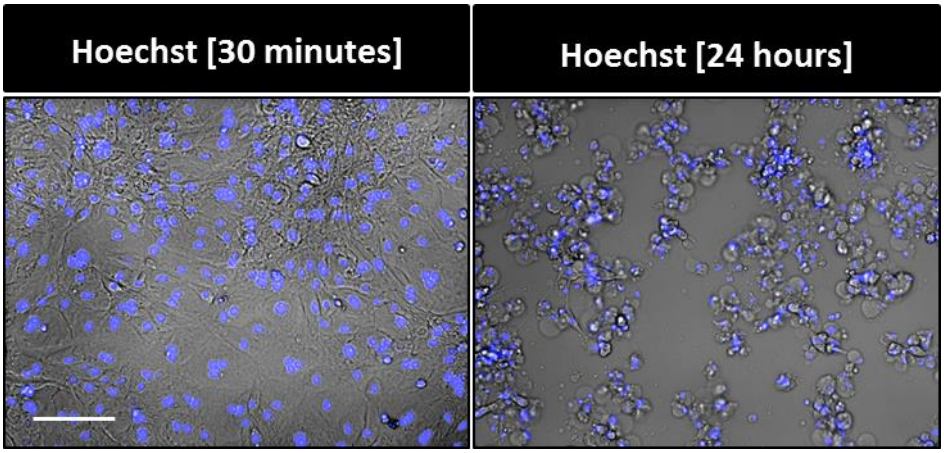


Figure 5.3 – Toxic effects from incubation of hiPSC derived cardiomyocytes in Hoescht33342.
CPVT hiPSC cardiomyocytes were incubated with Hoechst33342 in RPMI-B27 and images taken after 30 min and 24 hr of incubation on the Operetta confocal plate reader using the Hoechst and brightfield channels. When incubated in Hoechst33342 for 30 min cells appear healthy (left image). The same cells after 24 hr showed features of cell death including blebbing and detachment from the cell surface (right image). Scale bar = 100 µm.

5.2.2 Testing time course viability data acquisition using PI and CEC Markers

In this section, tests were carried out to identify whether PI and CEC were suitable for use in time course experiments where these markers would be incubated with cells over a 24 hr period and the fluorescent signals they generated would be quantified periodically.

5.2.2.1 Evaluating toxicity of PI and CEC incubation with cardiomyocytes

If reagents used to detect cytotoxicity are themselves cytotoxic in prolonged incubation (i.e. 24 hr) then the accuracy of any time course measurement would be compromised. In order to test whether this was the case when using PI or CEC, (figure 5.4) cardiomyocytes were incubated in the presence of PI or CEC reagent for 24 hr and positively stained cells quantified. At the beginning of the assay (0 hr), 7.5+/-2.5 % cells stained positively for PI. Over the subsequent 24 hr the number of PI positive cells ranged from 7.3+/-2.3 % (25 min) to 8.5+/-2.3 % (22 hr 30 min) but this did not represent a significant increase relative to 0 hr (one-way analysis of variance (ANOVA), Tukey multiple comparison test (TMCT) figure 5.4B and 5.5A). This confirmed that PI did not induce toxicity in cardiomyocytes with 24 hr incubation.

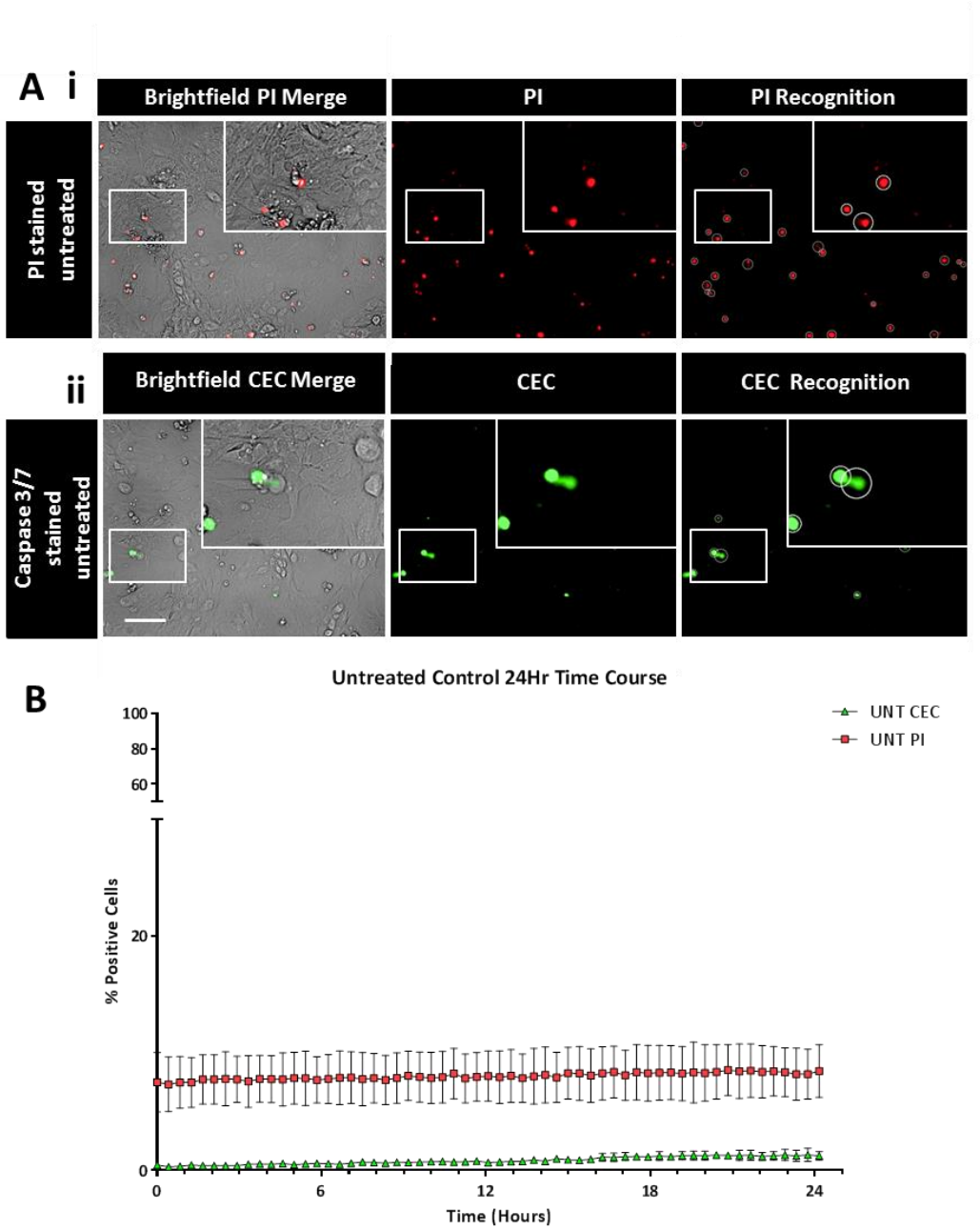


Figure 5.4 – Quantifying PI or CEC staining of untreated CPVT cardiomyocytes over 24 hours.

CPVT hiPSC cardiomyocytes that were not treated with any drug were incubated in the presence of either CEC or PI over a period of 24 hr in a 96-well plate in fresh RPMI-B27 maintenance medium and images were taken at 25 min intervals for 24 hr. **(A) (i)** Representative images showing CPVT cardiomyocytes after 24 hr in PI-containing medium with a small proportion of cells staining positively (left and centre images). (Right image) Object identification (white circles) following analysis. **(ii)** As in **(i)** but in separate wells where CEC was substituted for PI. **(B)** Quantification of detected objects over a 24 hr period. Experiment was carried out uninterrupted at 37 °C in a contained 5 % CO_2 but non-humidified environment. (n=3 wells for PI and for CEC, error bars = SD, scale bars = 100 µm).

A parallel experiment was carried out to evaluate potential toxicity of CEC. Cell death detected at 0 hr for CEC was significantly lower (0.5+/-0.1 %) than for PI (7.5+/-2.5 %, $p< 0.05$, t-test) (figure 5.4B). This was also true at the 24 hr time point (8.5+/-2.3 % for PI compared to 1.2+/-0.4 % for CEC, $p<0.05$, t-test). At 0 hr, the percentage of CEC positive cells were 0.5+/-0.1 % (0 hr) increasing significantly to 1.2+/-0.3 % (17 hr 5 min $p<0.05$) and remaining significantly higher until 24 hr (1.2+/-0.4 % $p<0.05$) (at three time points, $p<0.01$ at 20.4 hr (1.3+/-0.3 %), 22.9 hr (1.3+/-0.5 %) and 23.7 hr (1.3+/-0.6 %) (one-way ANOVA) (figure 5.4B). When identical time points were compared between PI and CEC at different points over 24 hr (figure 5.5A, B) a significant increase can be seen for CEC ($p<0.01$ 0.5+/-0.1 % at T=1 hr 15 min, increasing to 1.2+/-0.2 % at T=17 hr 55 min and 1.2+/-0.4 % at T=24 hr 10 min) whereas no significant increase was observed with PI (one-way ANOVA). When the net change in number of positively stained cells was calculated for PI and CEC wells at 24 hr (figure 5.5C) the increase in cell death was low, 26.7+/-21.8 cells for PI and 21.7+/-9.2 cells for CEC relative to the mean cell number of those wells of 2703.7+/-245.9 (n=6 wells) and there was no significant difference between the two groups (two-way ANOVA, TMCT). In conclusion, a low level of cell death occurred over 24 hr in both in PI and CEC wells over 24 hr but this was not considered large enough to warrant abandoning time course experiments with these markers.

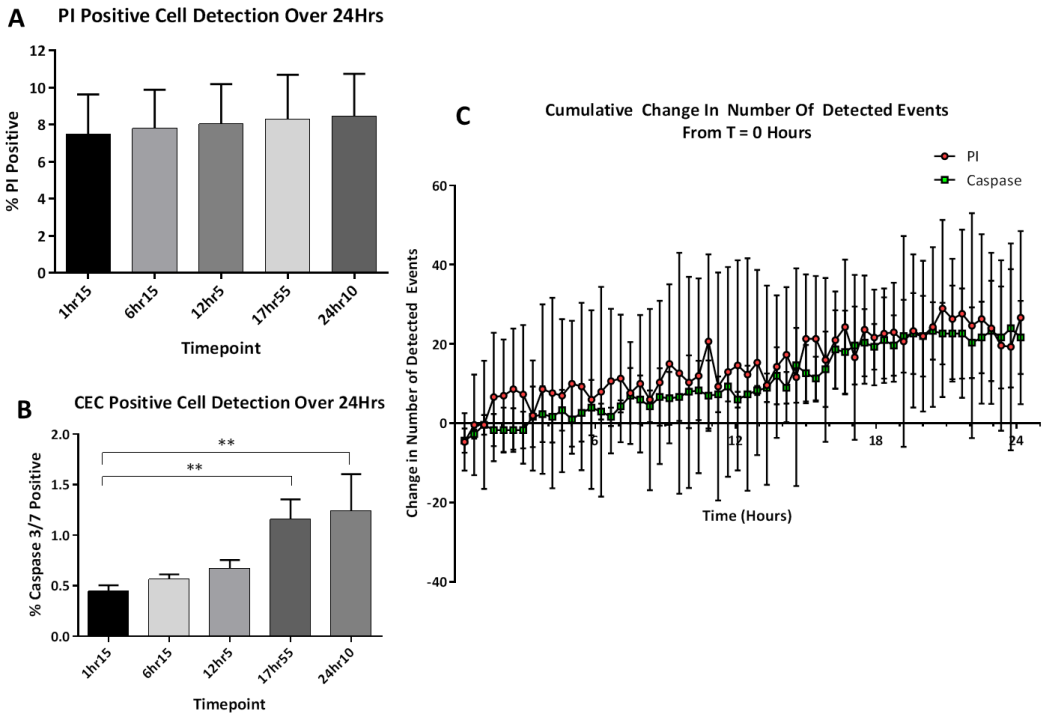


Figure 5.5 – Effects of incubating PI or CEC with CPVT cardiomyocytes over 24 hours.

(A) A comparison of percent PI objects at selected time points over 24 hr revealed no significant increase (one-way ANOVA). **(B)** Comparison of percent CEC positive objects at selected time points over 24 hr indicated a significant increase in CEC positive objects (one-way ANOVA, $p<0.05$). **(C)** Comparison of change in number of detected PI and CEC objects over 24 hr shows a marginal increase in number of objects but no significant difference (two-way ANOVA) between conditions. Experiment was carried out uninterrupted at 37 °C in a contained, 5 % CO_2 but non-humidified environment. (n=3 wells for each condition, error bars = SD).

5.2.2.2 Evaluating photo-bleaching of PI and CEC markers over 24 hours

Over 24 hr, positively stained cells in time course experiments underwent repeated photo-excitation. To assess whether photo-bleaching of these markers was taking place, mean object fluorescence intensity was measured over the 24 hr assay period (figure 5.6). For CEC, there was a significant increase in signal intensity between 0 and 5 hr (1167.7+/-119.3 FU to 1664.9+/-339.3 FU respectively, $p<0.05$), but from 5 hr onwards there was no significant change (both one-way ANOVA with Dunnet

multiple comparison test (DMCT). For PI, there was no significant change in intensity over 24 hr (one-way ANOVA, DMCT). Additionally, in unstained wells there was no fluorescent signal for PI and one auto-fluorescent debris-like object that was detected at 2 hr and disappeared at 5 hr (figure 5.6 A iii, B iii) and was ignored. In summary, PI and CEC reagent did not show any evidence of photo-bleaching over 24 hr despite repeated photo-excitation at 25 min intervals throughout.

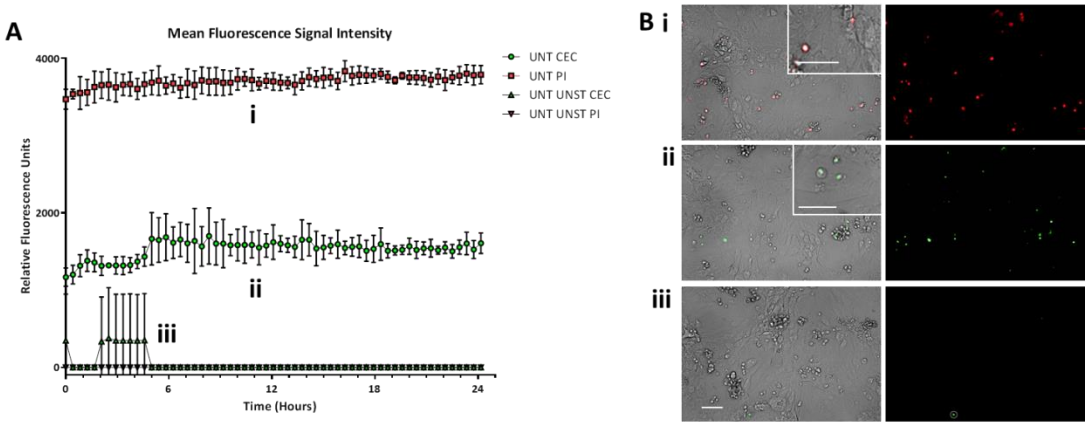


Figure 5.6 – Quantifying mean object fluorescence intensity over 24 hours.
An assessment of fluorescence intensity was carried out to determine if photo-bleaching occurred over 24 hr. **(A) (i)** Mean fluorescence intensity of PI-positive objects (no significant change over 24 hr, one-way ANOVA), **(ii)** CEC-positive objects (significant change between 0-5 hr $p<0.05$, no significance from 5 hr onwards, one-way ANOVA) and **(iii)** unstained controls. **(B)** Representative images showing brightfield and fluorescence images corresponding to **(A) (i)**, **(ii)** or **(iii)**. Experiment was carried out uninterrupted at 37 °C in a contained, 5 % CO_2 but non-humidified environment. For all conditions, n=3 wells. Scale bar = 100 µm.

5.2.3 Testing DMSO concentrations to assess vehicle toxicity

Having demonstrated that PI and CEC had no cytotoxic effect over 24 hr on cardiomyocytes, the next question was whether this platform could be used to accurately detect and quantify cell toxicity. To do this staurosporine was needed as

a positive control for caspase-dependent apoptosis. However, staurosporine and most of the compounds tested in later sections were dissolved in DMSO, which can induce toxicity in cells (Rowley and Anderson, 1993). Therefore before this test could be performed, an assessment of DMSO toxicity was needed in order to determine a suitable concentration range that could be used.

5.2.3.1 Measuring DMSO toxicity by PI staining

In two recent technical notes, Cellular Dynamics tested the effect of staurosporine on cardiomyocytes with a final DMSO concentration of 1 % implying that no toxicity would be observed at this concentration (Cellular Dynamics International, 2015a, Cellular Dynamics International, 2015b). Other groups have also suggested that 1 % DMSO can be tolerated by cells such as human pluripotent stem cells (Chetty et al., 2013). To confirm whether this was the case with hiPSC cardiomyocytes, a range of concentrations were chosen for testing above and below 1 % DMSO. To this end, 5 % was chosen to see whether a toxic response would be observed while 1 %, 0.5 %, 0.1 %, 0.05 % and 0.01 % were also tested.

Time course measurements (figure 5.7 B) were taken at 25 min intervals over 24 hr. At 0.5 % DMSO and lower, the fold change in percentage PI positive cells between 0 and 24 hr was <1.1, implying that these concentrations were not toxic. For 1 % DMSO, there was no toxic response between 0 and 18 hr (fold change was <1) however, between 18 and 24 hr there was a 2.2-fold increase (from 1.04 % at 0 hr or 0.94 % at 18 hr to 2.07 % at 24 hr) suggesting a low level toxic response was occurring. At 5 % DMSO, the starting toxicity was 0.93 % at 0 hr. This increased to

2.81 % (3-fold), 9.9 % (10-fold) and 24.7 % (26.6-fold) at 6, 12 and 24 hr, showing that at this concentration DMSO was causing overt toxicity on the cells. Brightfield-PI overlay images (figure 5.7 A - top and bottom panel) confirmed that PI was selectively staining dead cells as they displayed features of programmed cell necrosis (high PI-stained nucleus to cytoplasm ratio, detachment from culture surface and absence of blebbing) (see figure 5.1 and figure 5.7 C).

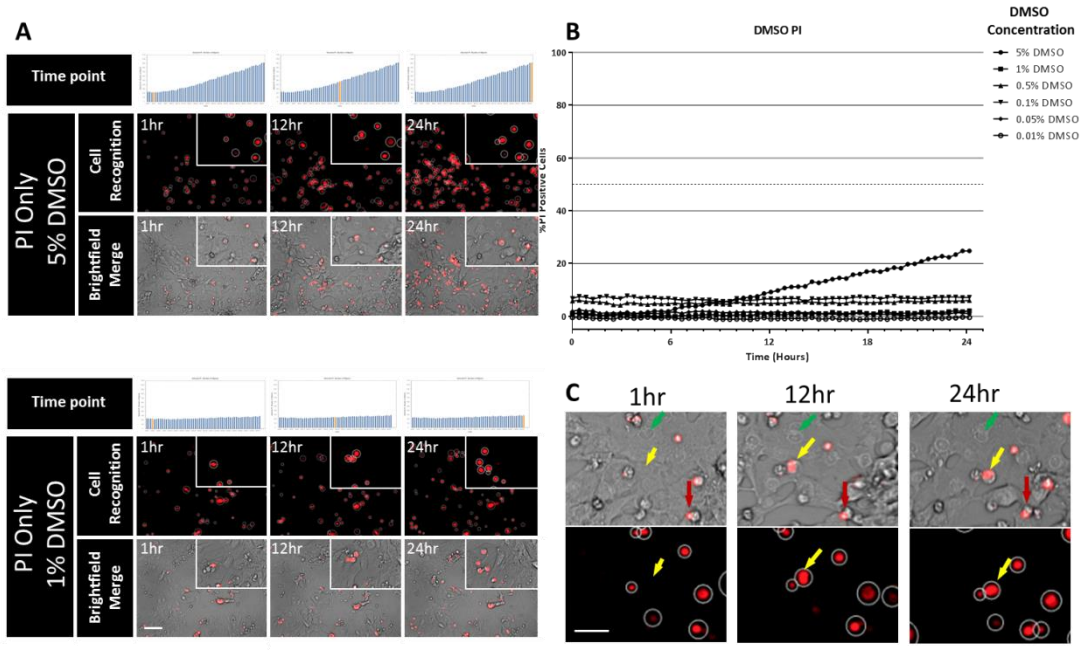


Figure 5.7 – Testing DMSO concentrations for toxicity in CPVT cardiomyocytes with PI staining.
(A) (top panel) Object quantification (graphs top of panel) over 24 hr, (middle row of images) representative images of object identification at 1,12 and 24 hr and (bottom row of images) representative brightfield/PI overlay images of PI positive cells incubated with 5 % DMSO over 24 hr. **(Bottom panel)** as with top panel but with DMSO at 1 %. **(B)** Quantification of PI positive objects detected at 25 min intervals over 24 hr for DMSO concentrations (shown in key-top right). **(C) (top row)** Brightfield/PI merged images of one field of view at 1, 12 and 24 hr (corresponding to 5 % DMSO) with associated PI object recognition images **(bottom row)**, show PI staining typical of programmed necrosis (an example is marked with red arrows) (see figure 5.1). Cells maintain a "regular" spherical shape throughout the time course instead of forming blebs and apoptotic bodies typical of apoptosis. Adherent, unstained, live cells were also present in the culture (marked with green arrows). The absence of PI staining in these cells confirmed PI staining showed specificity towards dead/dying cells. An example of an initially live cell undergoing cell death (yellow arrow) indicated it to be unstained and adherent at 1 hr (left image), stained with PI at 12 hr (centre image) with a spherical morphology and detaching from the cell surface. At 24 hr the same cell had a spherical morphology no longer attached to the cell surface (green arrow-marked cell for comparison) with a high PI to cell size ratio consistent with programmed necrosis. Scale bars = 100 μm. N=1 for each condition.

5.2.3.2 Measuring DMSO toxicity by CEC staining

As in 5.2.3.1, DMSO toxicity was assessed with the same experimental conditions but cells were instead stained with CEC. At all DMSO concentrations investigated, an increase in %CEC positive cells was detected between 0 hr and 24 hr, 423-fold for 5 % DMSO (0.08 to 33.8 %), 91-fold for 1 % (0.12 to 10.9 %), 7.2-fold for 0.5 % (1.97 to 14.09 %), 2.5-fold for 0.1 % (4 to 9.95 %), 4.7-fold for 0.05 % (0.7 to 3.29 %) and 8-fold for 0.01 % (0.99 to 7.96 %) (figure 5.8 B, D). For concentrations between 1 % and 0.01 % the amount of cell death detected did not show a concentration-dependent change in response at either 12 or 24 hr suggesting a lack of specificity of CEC (figure 5.8 D). At 24 hr, 5 % DMSO toxicity (33.8 %) was higher than other concentrations: 3-fold greater than 1 % DMSO (11 %) and 2.4-fold greater than 0.5 % DMSO (14.1 %). Brightfield / fluorescent merge images showed positively stained

cells with signs of apoptosis in brightfield images (blebbing and irregular spherical shape, see figure 5.1 and figure 5.8 C – highlighted with red arrows).

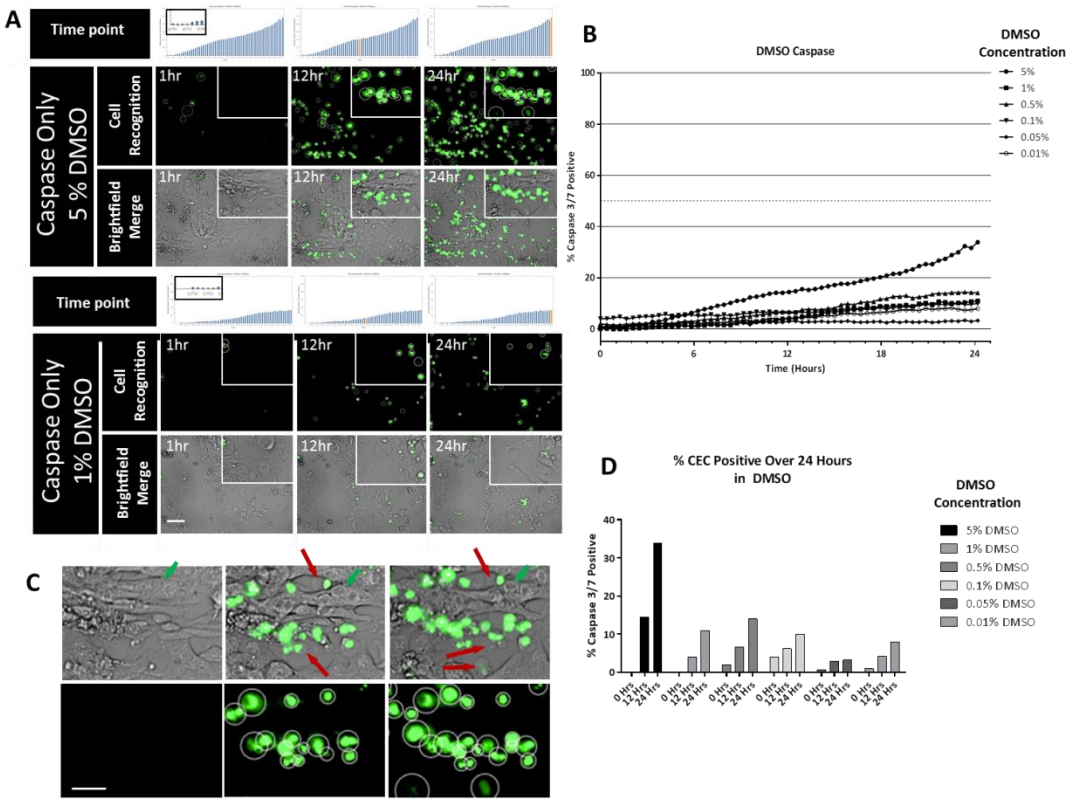


Figure 5.8 – Testing DMSO concentrations for toxicity in CPVT cardiomyocytes with CEC staining.
(A) (top panel) Object quantification (graphs top of panel) over 24 hr, **(middle row of images)** representative images of object identification at 1,12 and 24 hr and **(bottom row of images)** representative brightfield/CEC overlay images of CEC positive cells incubated with 5 % DMSO over 24 hr. **(Bottom panel)** as with top panel but with DMSO at 1 %. **(B)** Quantification of CEC positive objects detected at 25 min intervals over 24 hr for DMSO concentrations (shown in key-top right). **(C) (top row)** Brightfield/CEC merged images of one field of view at 1, 12 and 24 hr (corresponding to 5 % DMSO) with corresponding CEC object recognition images **(bottom row)**, brightfield/fluorescent merge images showed cells with signs of apoptosis, including blebbing and irregular spherical shape – red arrows. The presence of unstained and adherent cells suggests that CEC was staining cells with specificity. **(D)** Change in percent CEC positive cells for all DMSO concentrations at 0, 12 and 24 hr. Scale bars = 100 µm. N=1 for each condition.

In untreated wells, the change in the number of dead cells detected between 0 and 24 hr using either PI or CEC was the same, in this experiment; this was not the case (figure 5.9 A). At all DMSO concentrations tested, the change in number of dead cells detected over 24 hr in CEC wells was higher than in PI wells. In 1 % DMSO, this change was 5.8-fold greater in the CEC well than PI (55 objects in PI compared to 320 in CEC) or 2 % of the cells in the PI well and 11.6 % in CEC. For 0.5 % DMSO, there was an 11-fold difference (32 objects in PI, 356 objects in CEC, or 1.1 % and 13 % respectively). At 24 hr the EC_{50} for DMSO with PI was 2.1 % which was 35.5 % higher than the EC_{50} for CEC at 1.55 % (figure 5.9 B) reflecting the difference in toxicity levels detected. The results from the CEC and the PI wells both suggest that between 1 and 5 % DMSO there was a toxic response with some evidence of late stage toxicity in 1 % DMSO. It was decided that in future experiments DMSO concentration would not exceed 1 % (1 % being considered the highest “safe” concentration to be used) and where possible, would be used at or below 0.5 %.

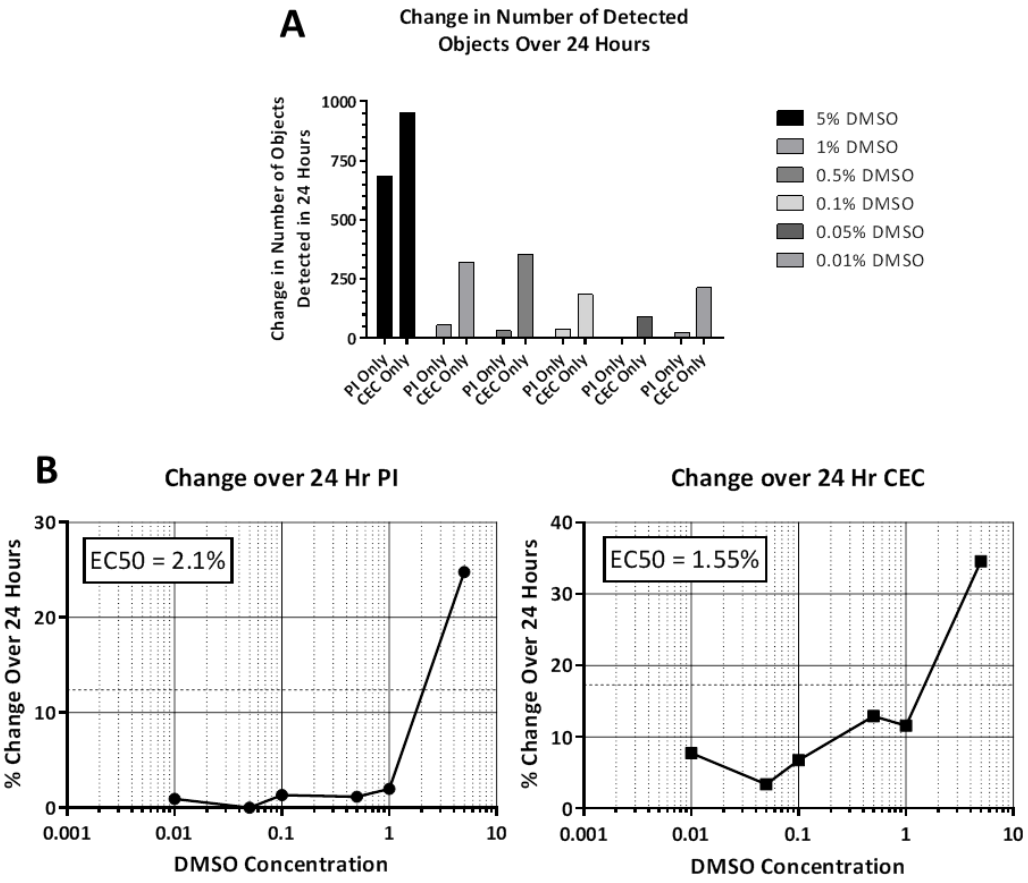


Figure 5.9 – Comparing PI and CEC data outputs for DMSO toxicity.
(A) A comparison of the change in number of objects detected at 24 hr between PI treated wells and CEC treated wells for DMSO concentrations tested (shown top right). **(B)** Toxicity curves showing the effect of DMSO on CPVT hiPSC cardiomyocytes at 24 hr. Values plotted as percent of well population positive for either PI or CEC.

5.2.4 Validating PI, CEC and PI-CEC co-staining quantification using staurosporine

As a positive control for caspase-mediated cell death (Yue et al., 1998), staurosporine (STA) was used to induce toxicity in cardiomyocytes to assess the accuracy of CEC. To achieve this, a pilot study (n=1 for each condition, due to limited space on 96-well plates and to conserve cells) was carried out where wells were treated with STA at 10, 5, 1, 0.5 or 0.1 µM (10 µM having been shown to induce toxicity in rat ventricular cardiomyocytes (Henaff et al., 2000) and 1-0.25 µM

in rat neonatal cardiomyocytes (Yue et al., 1998)) and co-incubated with PI, CEC or PI and CEC combined for 24 hr and images taken at 25 min intervals.

5.2.4.1 Quantifying PI staining with or without CEC co-incubation in cardiomyocytes treated with STA

In order to validate PI staining in models of cell toxicity and to determine whether PI and CEC could be used simultaneously in drug screening assays, cardiomyocyte toxicity was quantified over 24 hr using these markers. When the percentage cell death detected with PI was plotted, (figure 5.10 C) a concentration-dependent change in the rate of toxicity (change in percentage PI positive cells per hour) was observed. In the first 12 hr, for 10 µM and 5 µM STA, rate of cell death was 6.7 % and 6.1 % per hour, lowering to less than 0.5 % from 12 hr to 24 hr indicating maximal cell death had been achieved in the first 12 hr. Representative images taken from the wells (figure 5.10 A i) indicate complete cell death at 12 hr due to all cells staining positively with PI at 10 µM STA and cells undergoing apoptosis as indicated by membrane blebbing (brightfield/fluorescence merge images). When PI and CEC were co-incubated (PI-CEC), this did not have an effect on the detection of cell death by PI staining with the time course graphs (figure 5.10 C) showing similar rates of cell death in the first 12 hr (6 % for PI-CEC vs 6.7 % for PI-only) for 10 µM, 6.3 % vs 6.1 % for 5 µM, 3.7 % vs 3.5 % for 1 µM, for 1.6 % vs 2.4 % for 0.5 µM and 0.4 % vs 0.4 % for 1 µM). When percentage PI positive cells at 24 hr were compared between PI only and PI from PI-CEC staining at 24hr, the difference never exceeded 6 %, with the exception of 1 µM staurosporine at 13 % (figure 5.10 D). Therefore, these preliminary data suggest that CEC does not have an effect on the

quantification of PI staining when the two markers are incubated together over 24 hr.

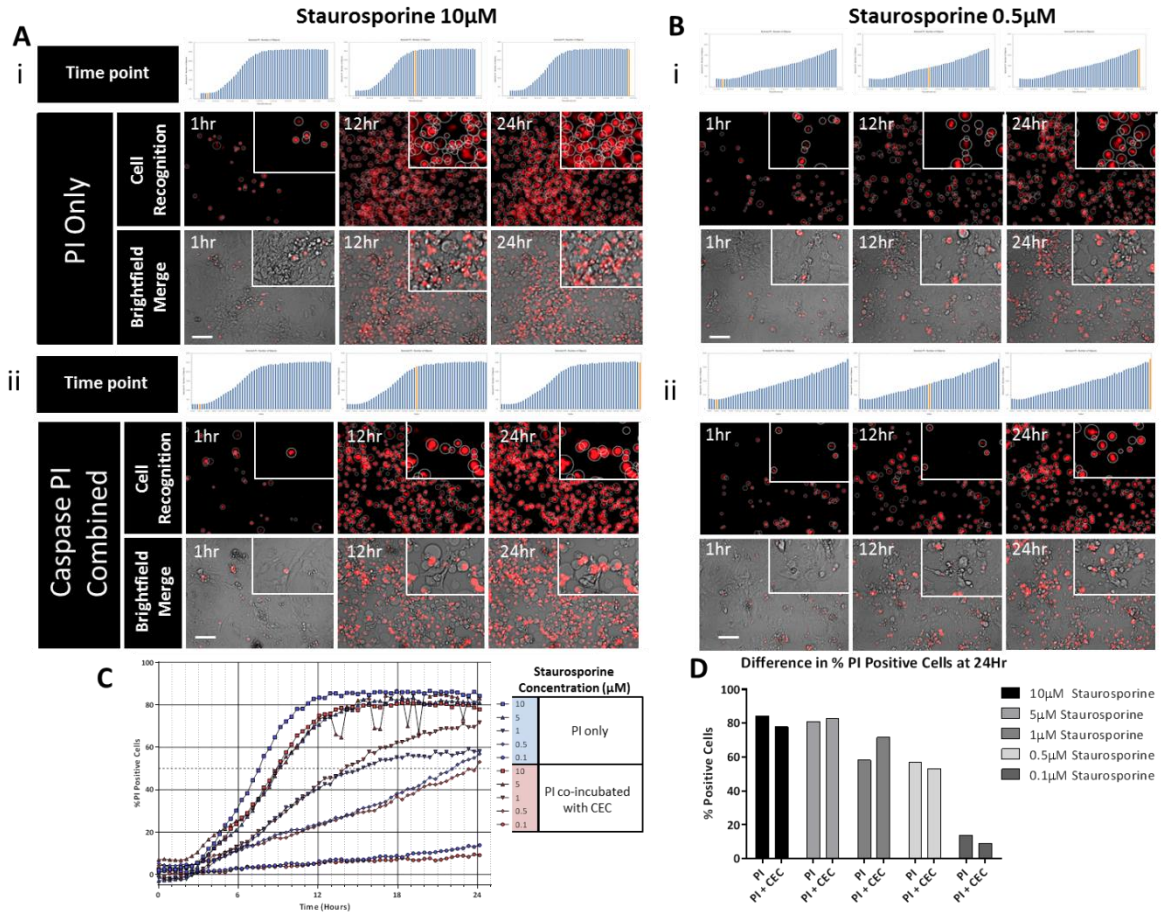


Figure 5.10 – Time course measurements of STA toxicity in cardiomyocytes using PI. Cardiomyocytes were incubated with STA at 10, 5, 1, 0.5 and 0.1 µM in wells (n=1 for each concentration) either treated with PI (shown here) or CEC (shown in figure 5.11). PI-CEC co-treatment (but only displaying PI fluorescence is shown in **(A) (ii)** (n=1 for each condition). **(A)** Toxicity of STA at 10 µM over 24 hr. **(i) (top row)** Quantification of number of PI-positive objects detected at selected time points (highlighted as orange bars) of 1, 12 and 24 hr (from left to right). **(Middle row)** PI positive objects detected at 1, 12 and 24 hr (shown with white circles). **(Bottom row)** Brightfield and PI merge images at 1, 12 and 24 hr. **(ii)** As with **(i)** but with PI and CEC reagent co-incubation, with only PI objects quantified. **(B)** As with **(A)**, but with STA at 0.5 µM. **(C)** Time course plot of STA toxicity. Wells incubated in the presence of PI only are plotted in blue, wells incubated with PI and CEC combined (but displaying PI-positive objects only) plotted in red. **(D)** Comparison of number of PI positive objects detected in wells treated with STA and co-incubated with either PI or PI-CEC to assess the effect of CEC co-incubation on detection of PI-positive objects.

5.2.4.2 Quantifying CEC staining with or without PI co-incubation in cardiomyocytes treated with STA

To demonstrate that CEC could be used to detect toxicity on its own or when also incubated with PI, wells were treated with STA and staining quantified. When incubated with CEC only, the rate of cell death in the first 12 hr was 6.3 % vs 6.7 % per hr for PI at 10 µM (6.2 % for CEC vs 6.1 % for PI at 5 µM, 4.2 % vs 3.5 % for 1 µM, 2.4 % vs 2.4 % for 0.5 µM and 0.4 % vs 0.4 % for 1 µM). These results indicated that CEC staining and PI staining gave very similar values for toxicity quantification. This was confirmed when the data from both were plotted together (figure 5.12 A).

In the PI-CEC co-incubation wells intensity of CEC staining was lower than in CEC-only wells (figure 5.11 A ii brightfield/fluorescence merged images) affecting the detection of CEC-stained objects and causing some apoptotic (blebbing visible in brightfield images) cells to appear negative for CEC. When percentage CEC positive objects and percentage CEC (from CEC-PI wells) were plotted together, CEC-PI gave lower toxicity values (figure 5.11 C). The rate of cell death in CEC-PI wells measured by CEC staining was >2-fold lower per hour for all concentrations tested (at 0.1 µM staurosporine this represented a 22-fold decrease) (figure 5.13). At 24 hr (figure 5.11 D) the difference between percentage CEC positive cells detected in CEC only and CEC-PI was 33.9 % at 10 µM STA (78.9 % for CEC-only and 45 % for CEC from CEC-PI), 60 % at 5 µM (80.3 % vs 21 %), 42 % at 1 µM (66.4 % vs 23.8 %), 45 % at 0.5 µM (64.8 % vs 19.9 %) and 8.9 % at 0.1 µM (10.3 % vs 1.4 %). Additionally, when plotted together, the cell death detected by PI and by CEC incubated in the same

wells differed from one another (figure 5.12C) demonstrating clearly that different levels of toxicity detection were taking place when the markers were co-incubated.

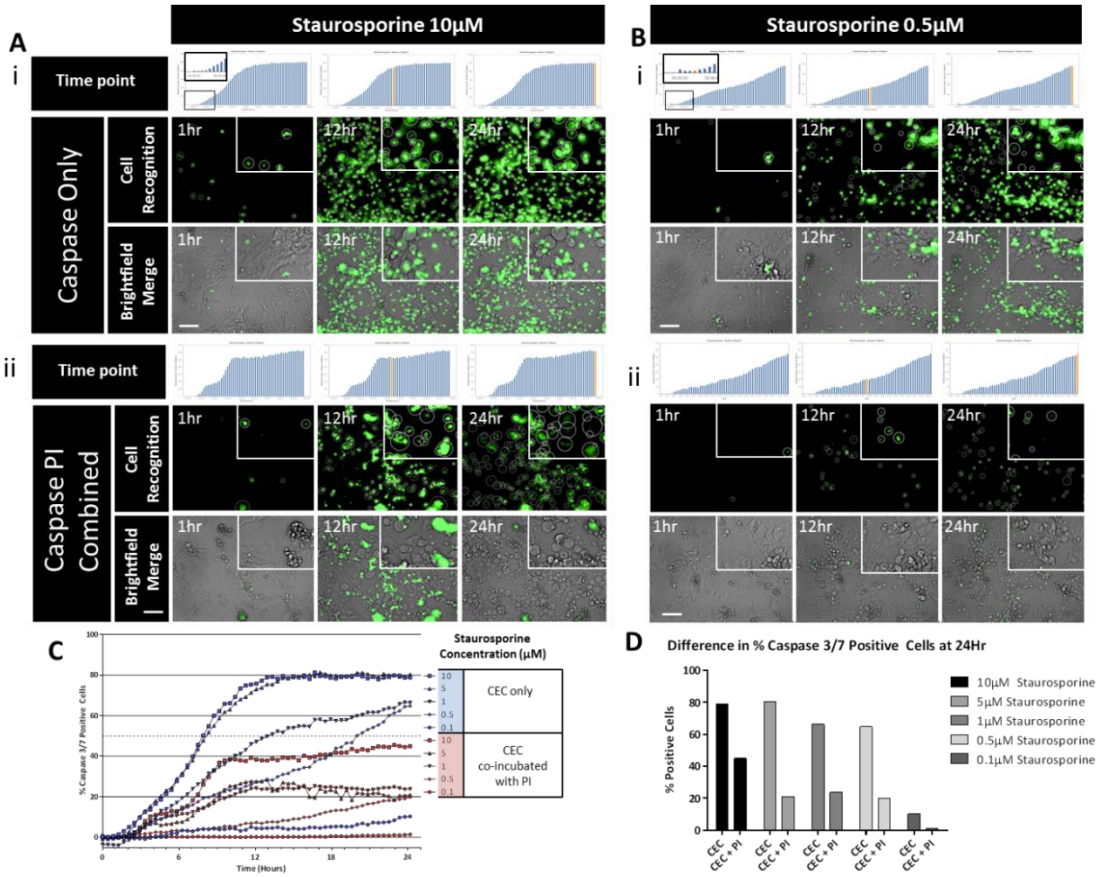


Figure 5.11 – Time course measurements of STA toxicity in cardiomyocytes using CEC.

(A) Toxicity of STA at 10 µM over 24 hr. **(i) (top row)** Quantification of number of CEC-positive objects detected at selected time points (highlighted as orange bars) of 1, 12 and 24 hr (from left to right). **(Middle row)** CEC positive objects detected at 1, 12 and 24 hr (shown with white circles). **(Bottom row)** Brightfield and CEC merge images at 1, 12 and 24 hr. **(ii)** As with **(i)** but with CEC and PI co-incubation, with only CEC objects quantified. **(B)** As with A, but with STA at 0.5µM. **(C)** Time course plot of STA toxicity. Wells incubated in the presence of CEC only are plotted in blue, wells incubated with CEC and PI combined plotted in red. **(D)** Comparison of detected CEC objects at 24 hr between wells stained only with CEC and wells stained with CEC and PI. N=1 for each drug concentration.

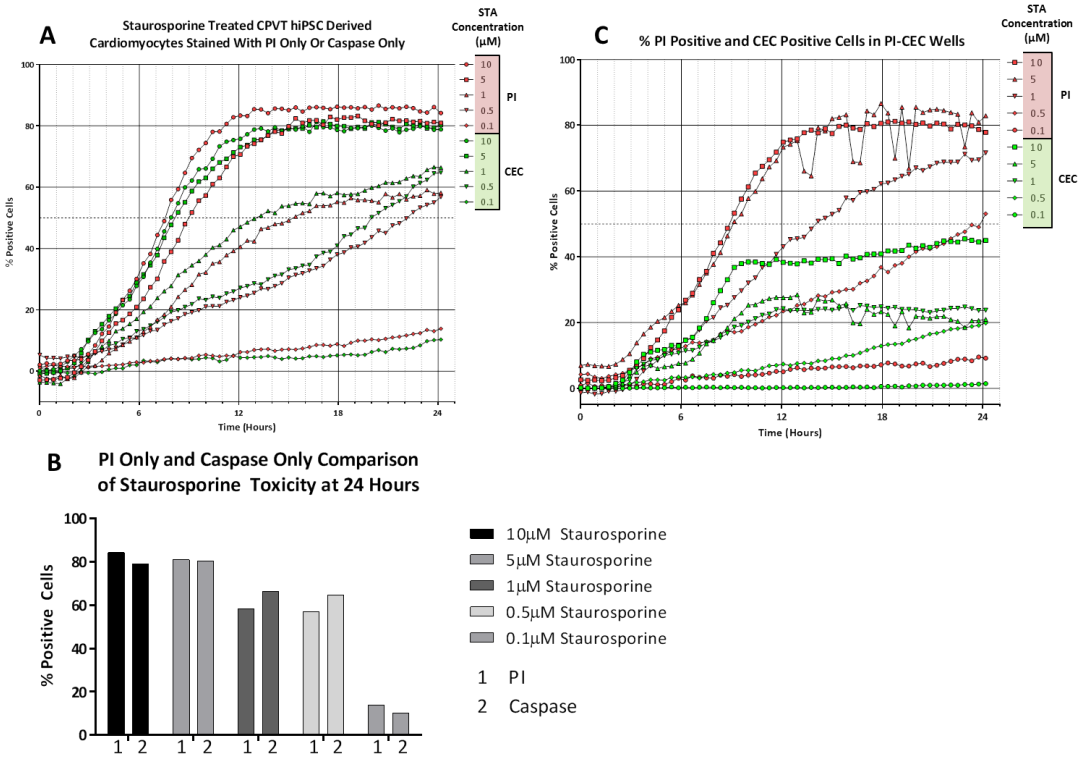


Figure 5.12 – Toxicity detected in cardiomyocytes treated with STA over 24 hr and stained with either PI or CEC.
(A) Time course measurement of toxicity in cardiomyocytes treated with STA for 24 hr and incubated either with PI or CEC reagent plotted together to enable comparison of the two markers over 24 hr. **(B)** Side-by-side comparison of STA-treated cardiomyocyte toxicity at the 24 hr time point of the time course experiment in **(A)**. **(C)** Quantification of CEC staining and PI staining when both markers were incubated together along with STA. N=1 for each drug concentration.

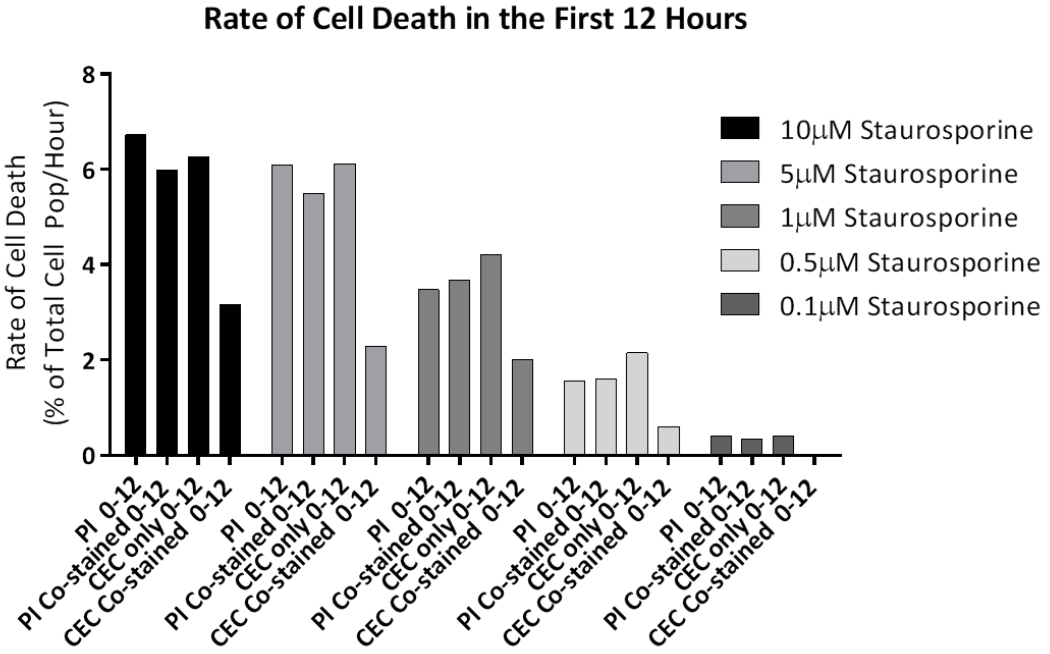


Figure 5.13 – Comparing the rate of cell death at different concentrations of STA over the first 12 hours of the time course experiment.
Rate of cell death was calculated as change in cell death between 0 hr and 12 hr divided by time. 12 hr was chosen as after this point; 10 μM and 5 μM wells showed a "levelling" off of cell death (maximal effect achieved). Bars displayed (from left to right) correspond to PI positive only, PI positive objects detected when co-treated with CEC, CEC positive objects and CEC positive objects detected when co-treated with PI for each concentration of STA investigated.

5.2.4.3 Comparing TD_{50} and EC_{50} values with results from Cellular Dynamics Technical Notes

In order to gauge whether the results of the STA testing were accurate, a comparison was made with data published by Cellular Dynamics in two technical notes which tested STA caspase induction and cardiotoxicity respectively in hiPSC derived cardiomyocytes (Cellular Dynamics International, 2015a, Cellular Dynamics International, 2015b). STA toxicity measured by PI staining at 24 hr (figure 5.14 B and C) gave a TD_{50} of 470 nM for PI-only and 510 nM for PI when co-incubated with CEC, or combined, 490 +/- 28.3 nM, 123 nM less than the EC_{50} result from CDI (613

nM – figure 5.14 A). Given the similarity of these values, the PI staining results were considered accurate.

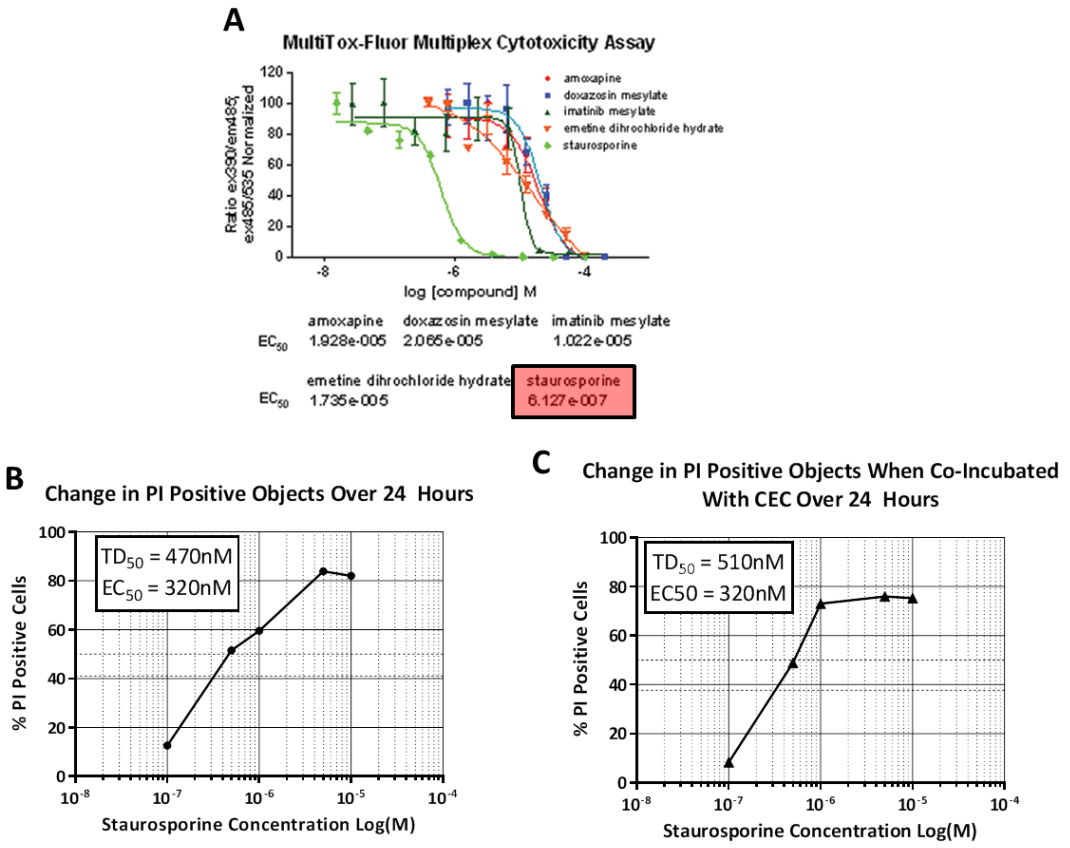


Figure 5.14 – Determining the TD_{50} and EC_{50} of STA on cardiomyocytes after 24 hr with PI staining.
(A) Cytotoxicity measured at 24 hr using the MultiTox-Fluor Multiplex Cytotoxicity assay and a fluorescent plate reader. Graph taken from Cellular Dynamics International application note entitled "Assaying Cytotoxicity"(Cellular Dynamics International, 2015b). **(B)** Change in percent cardiomyocytes staining positively for PI between 0-24 hr at different concentrations of STA with TD_{50} and EC_{50} values shown. **(C)** As in **(B)** but data taken from wells co-stained with CEC.

The tests carried out by Cellular Dynamics to quantify caspase activity were done after 6 hr incubation in STA. For comparison, CEC values measured at 6 hr were plotted (figure 5.15 A ii and iii) for CEC only and CEC-PI wells. In both cases, TD_{50} values could not be calculated as toxicity had not occurred in 50 % of cells.

Therefore, EC_{50} was calculated and the values generated were >2-fold lower at either 650 nM (CEC only) or 700 nM (CEC-PI) compared to 1.49 µM for CDI. A TD_{50} of 1.5 µM wasn't achieved until 11 hr 15 min in the CEC only well. Toxicity curves for CEC only wells gave a TD_{50} of 330 nM, which was 140 nM lower than the PI-only wells (470 nM). At 24 hr, the CEC toxicity curve from the CEC-PI wells could not be used to derive a TD_{50} value while EC_{50} was calculated as 780 nM (>3-fold higher than in the CEC-only well).

The discrepancies observed in CEC staining from CEC-PI wells indicated that CEC was not suitable for multiplexing with PI. This meant that simultaneous quantification of apoptosis and programmed cell necrosis could not be achieved. Additionally, the erratic staining profile observed at concentrations of DMSO <0.5 % in section 5.2.3.2 also highlighted some concerns with CEC staining accuracy. Furthermore, continued use of CEC in screening assays would have required staining separate wells in turn, reducing the number of variables that could be tested per plate. For these reasons, the use of CEC was abandoned in future work.

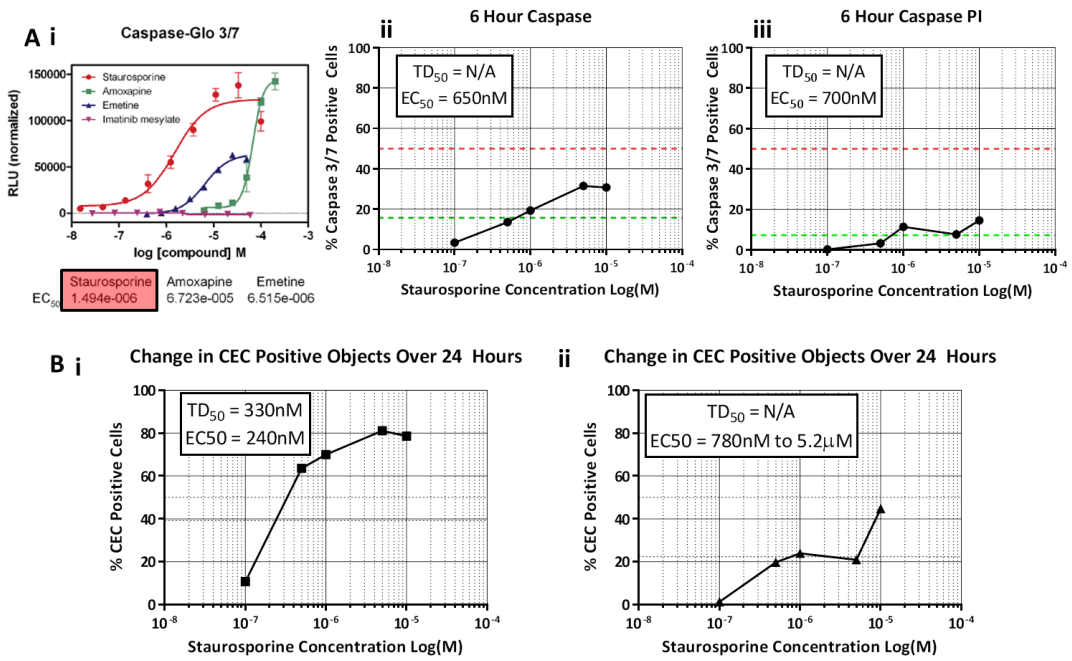


Figure 5.15 – Determining the TD_{50} and EC_{50} of STA on cardiomyocytes after 24 hr with PI staining.
(A) (i) Caspase activity quantification at 6 hr using Promega Caspase Glo 3/7 reagent and a fluorescent plate reader. Graph taken from Cellular Dynamics International application note entitled "Assaying Caspase Activity and Apoptosis". **(ii)** Change in percent of cardiomyocytes staining positively for CEC between 0-6 hr and **(iii)** when co-stained with PI at different concentrations of STA with TD_{50} and EC_{50} values shown for comparison with data shown in **(A) (i)**. **(B)** As in **(A) (ii) and (iii)** but data collected at 24 hr.

5.2.5 Investigating cardiotoxicity with doxorubicin

DOX is an auto-fluorescent compound that fluoresces in the same channel as PI (excitable at 488 nm and emission is detectable between 520-570 nm (Chen et al., 2012)). In order to investigate whether PI was compatible with testing DOX cardiotoxicity, a pilot study time course and end point experiment was carried out over a 24 hr period. If successful, the toxicity curve generated could be used to estimate the TD_{50} of DOX which would aid in choosing DOX concentrations for future toxicity testing experiments. DOX was incubated with cardiomyocytes at 100

µM, 50 µM, 10 µM, 5 µM, 1 µM and 0.5 µM mimicking concentrations previously tested with hESC derived cardiomyocytes (100 µM to 1 µM (Andersson et al., 2010)). The highest concentration of DMSO vehicle used was 0.12 % (100 µM DOX).

At 50 µM DOX in the first 6 hr, a spike in percentage PI-positive objects was detected, starting at 4.1+/-1.5 % at 0 hr, increasing to 61.4+/-1.9 % at 4 hr (figure 5.16) decreasing to 20.7+/-0.8 % at 5 hr 30 min and then increasing to 56.4+/-1.2 % by 12 hr. This pattern was also observed at 100 µM but crossed above 100 % PI-positive in the first 6 hr before declining to 60 %, so this data was excluded from the time course graph. This pattern was not observed at 10 µM DOX or lower.

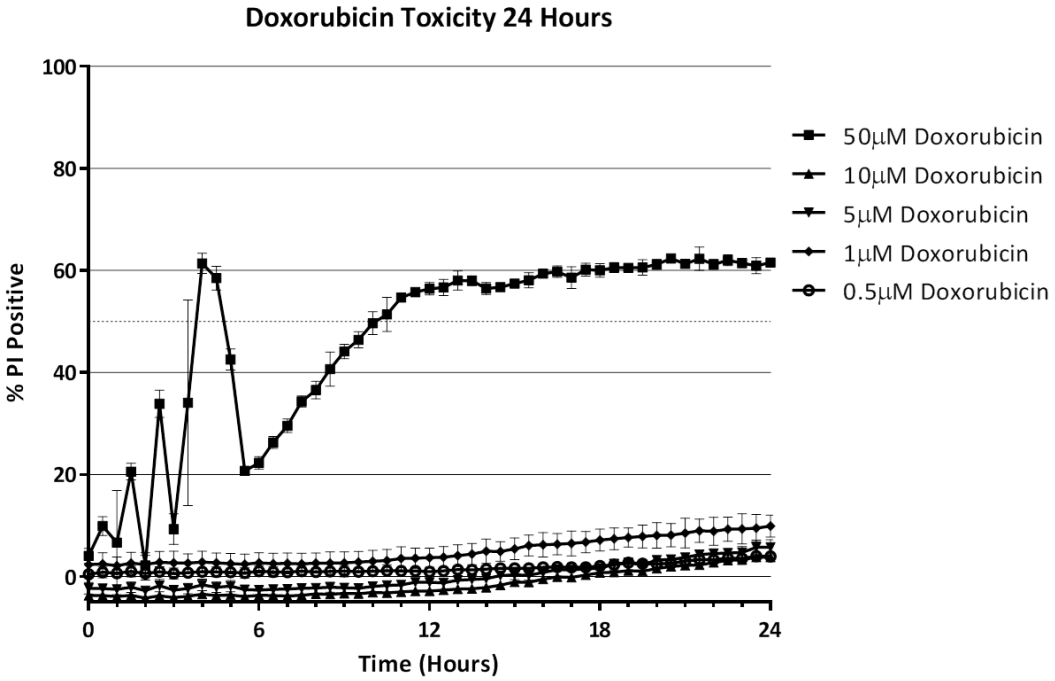


Figure 5.16 – Measuring DOX toxicity over 24 hr with PI staining.
Cardiomyocytes were treated with DOX at 50, 10, 5, 1 and 0.5 µM with each concentration co-incubated with PI. Images were taken over a 24 hr period at 30 min intervals (n=3 wells for each DOX concentration).

As PI binds irreversibly to DNA, the increase and subsequent decrease ("spike") in number of detected objects observed at 50 µM DOX was unexpected. To investigate this further, representative images from 50 µM DOX at 2 hr (pre-spike) 4 hr 30 min (at the peak of the spike), 6 hr 30 min (post-spike) and 22 hr 30 min (near the end of the assay) (figure 5.17) were taken to visualise this effect. The increase and decrease in signal detected was not localised to the nuclei of cells (figure 5.17 image rows 1-3, see inlays with green arrows). Furthermore, cells staining at this stage did not show signs of cell death by either apoptosis (blebbing, formation of apoptotic bodies, and detachment from culture surface) or programmed necrosis (high nucleus to cytoplasm ratio with PI staining and detachment from culture surface). This suggested that the signal detected was not PI. By 22 hr 30min, there was complete cell death in these wells (figure 5.17 - bottom row images) with blebbing cells detected (yellow arrows) and presence of apoptotic bodies (green arrows) indicative of apoptosis. Due to the tight clustering of apoptotic bodies accurate cell recognition was not possible (see figure 5.17 bottom row – far right image for object recognition). At 1 µM, DOX had higher levels of cell death than at 10 µM and 5 µM and the highest level of toxicity after 50 µM so, for comparison, images were taken (figure 5.18). At this concentration, no fluorescence spike was visible between 2 and 6 hr. Furthermore, quantification of PI-objects was accurate as no clustering of dead cells or apoptotic bodies was observed indicating that this was an issue primarily found with more toxic drug concentrations.

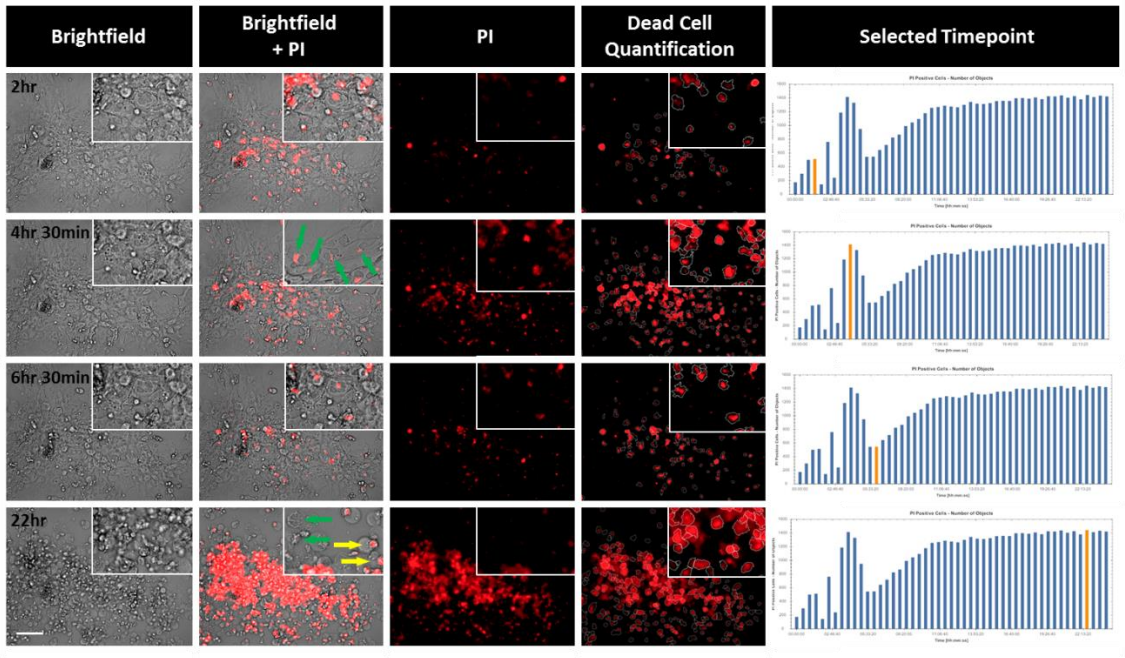


Figure 5.17 – Measuring DOX toxicity at 50 µM over 24 hr.
Representative images were taken from the same field of view at four different time points to illustrate the toxic response observed over 24 hr. Between 4 to 6 hr a spike in fluorescence was detected in the red channel which decreased in intensity only to increase again afterwards. Images taken to illustrate this spike were taken before (at 2 hr - top row) during (4 hr 30 min - second row), immediately afterwards (6 hr 30 min - third row) and at 22 hr (bottom row). (From left to right) Representative images taken from the same field of view at each time point showing, brightfield, fluorescence and object quantification. Scale bar = 100 µm.

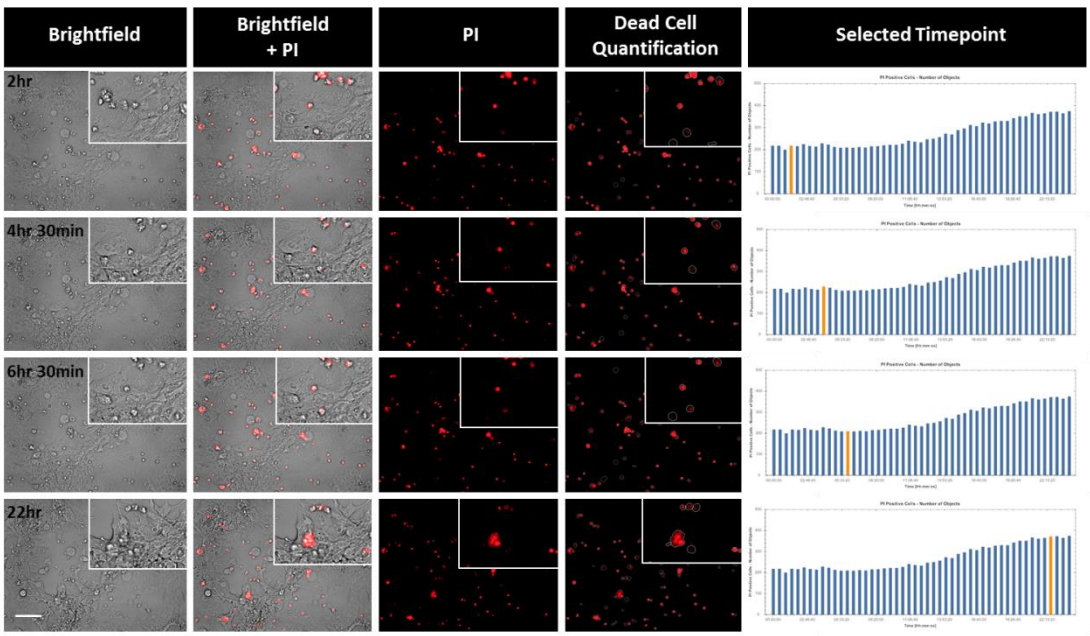


Figure 5.18 – Measuring DOX toxicity at 1 µM over 24 hr.
Representative images were taken from the same field of view at four different time points to illustrate the toxic response observed over 24 hr. At this concentration, no spike in fluorescence was detected between 4 and 6 hr. To provide comparison, images were taken at the same time points as in figure 5.17. Time points were 2 hr, 4 hr 30 min, 6 hr 30 min and 22 hr. (From left to right) Representative images taken from the same field of view at each time point showing, brightfield, fluorescence and object quantification. Scale bar = 100 µm.

After 24 hr, an endpoint scan was performed on the plate and a dose response curve plotted from the data (figure 5.19). The TD_{50} for DOX was 16 µM, while the results taken from the time course experiment at 24 hr gave a TD_{50} of 37 µM. A comparison of toxicities detected at 50 µM gave 61.5+/-0.7 % (time course) vs 96.4+/-0 % (end point) (identical triplicate values, as all were 100 % prior to normalising with controls), 10 µM gave 3.8+/-0.7 % vs 31.4+/-1.4 %, 5 µM gave 5.8+/-1.5 % vs 18.9+/-2.7 %, 1 µM gave 9.9+/-2.2 % vs 9.3+/-0.9 % and 0.5 µM gave 4+/-0.4 % vs 7.9+/-0.7 %. All concentrations except for 1 µM, were significantly different between both sets of data ($p<0.0001$ for 50 µM, 10 µM, 5 µM and $p<0.05$ for 0.1 µM). Due to the different results from both approaches, it was decided that a concentration range of between 50 µM and 1 µM DOX would be used in future experiments to ensure both TD_{50} values fell within the range being tested.

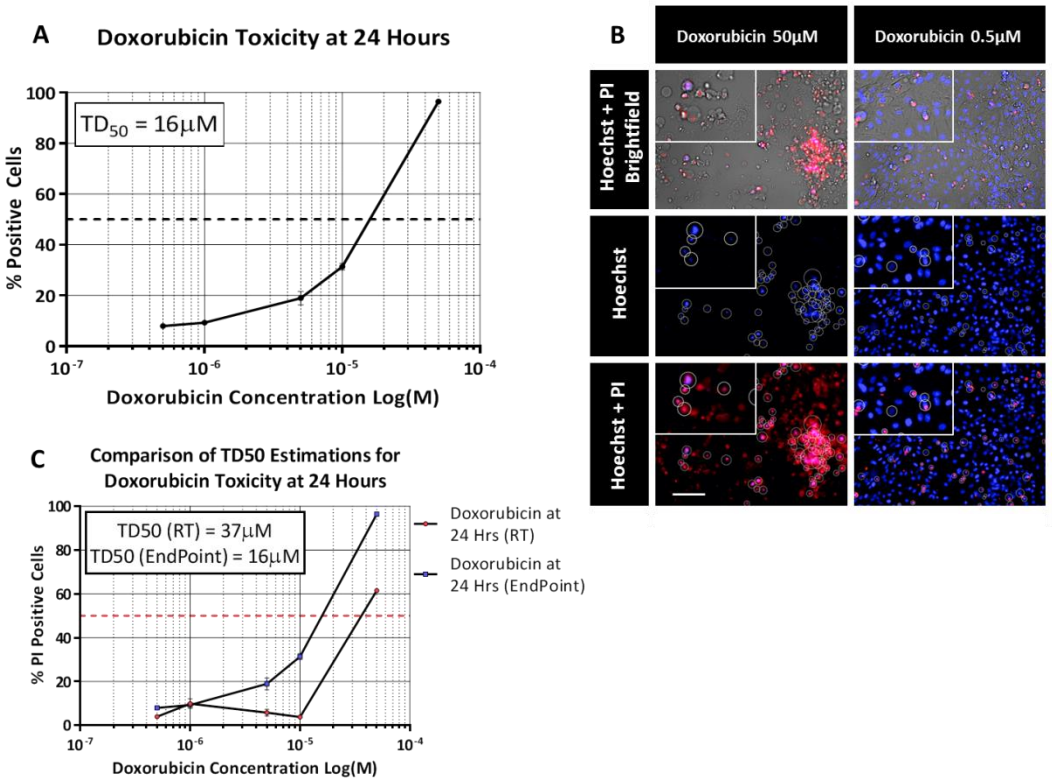


Figure 5.19 – DOX toxicity measured at 24 hr with Hoechst staining.
At 24 hr, wells treated with DOX at 50, 10, 5, 1 and 0.5 µM were stained with Hoechst and percent cell death determined as proportion of Hoechst positive cells co-staining positively for PI. **(A)** Dose response toxicity curve for DOX treated cardiomyocytes at 24 hr when co-stained with Hoechst. **(B)** Representative images at 50 µM (highest) and 0.5 µM (lowest) DOX showing merged fluorescence with brightfield as well as quantification of PI-positive cells. **(C)** Toxicity curve corresponding to doxorubicin toxicity at 24 hr from the time course scan and immediately following Hoechst staining and re-scanning to compare outputs of both methods.

5.2.6 Identifying suitable concentrations of rescue drugs for doxorubicin-toxicity rescue

Four drug compounds were highlighted for their potential to reduce DOX cardiotoxicity: DEX, CAR, SIL and ISO (combined, referred to as “rescue drugs”). In order to test these drugs *in vitro*, it was necessary to identify concentrations of these compounds that could be used that would maximise the dose given while not inducing toxicity in cardiomyocytes.

5.2.6.1 Dexrazoxane toxicity testing

In order to identify the highest non-toxic concentration of DEX that could be used, it was prepared to its maximum soluble concentration in DMSO and then diluted to give a final DMSO concentration of 1 % (the highest safe DMSO concentration – see section 5.2.3). This gave a concentration of 745.5 µM. A further three concentrations (74.55 µM, 7.45 µM and 0.75 µM) were tested each 10-fold lower than the former.

At 745.5 µM DEX, between 1 hr and 12 hr, there was a significant increase in toxicity from 0.9+/-0.8 % to 1.6+/-0.8 % ($p<0.05$). This increased further to 12.1+/-0.9 % at 24 hr (from 13 hr onwards, $p<0.0001$ compared to 1 hr) (figure 5.20 B). For DEX at 74.5 µM, there was a significant increase in the toxicity starting at 18 hr (3.9 +/-2.1 % compared to 2.9+/-1.5 % at 1 hr) ($p<0.05$, $p<0.01$ at 24 hr). At 7.45 µM and 0.745 µM there was no significant change in toxicity. Only two concentrations for each rescue drug could be taken forward due to limitations in the number of variables that could be tested. At 745.5 µM, DEX proved too toxic to justify its use in future experiments, therefore the next two highest concentrations were used instead (74.55 µM and 7.45 µM) corresponding to DMSO vehicle concentrations of 0.1 % and 0.01 %.

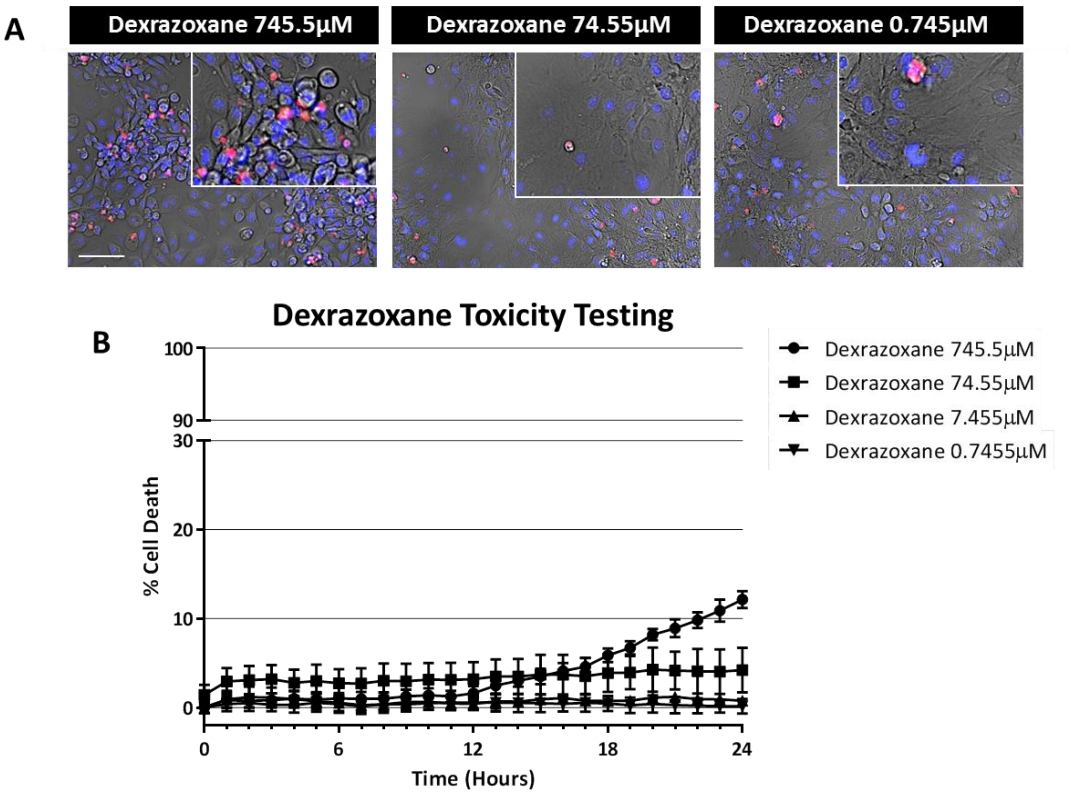


Figure 5.20 – Assessing toxicity of DEX over 24 hr.
Cardiomyocytes were treated with DEX at 745.5 µM (1 % vehicle), 74.55 µM, 7.455 µM or 0.7455 µM for 24 hr. Images were taken at 1 hr intervals. **(A)** Representative images of fluorescent signal and brightfield taken at 24 hr following DEX treatment of cardiomyocytes at 745.5 µM, 74.55 µM and 0.7455 µM. **(B)** Quantification of PI staining measured at 1 hr intervals over 24 hr. N=3 for each concentration.

5.2.6.2 Cavedilol toxicity testing

In order to test the toxicity profile of CAR, as with DEX, the drug was dissolved in DMSO to its highest soluble concentration and diluted to 1 % DMSO with serial 10-fold dilutions thereafter starting at 492 µM then 49.2 µM, 4.92 µM and 0.492 µM. When 490 µM was prepared, CAR formed precipitates in the culture medium (figure 5.21 A bottom row of images) which also auto-fluoresced in the Hoechst and PI detection channels when imaged, making the data from this concentration unsuitable and was excluded. At 49.2 µM and lower, no precipitates were formed in the media. At this concentration, CAR was toxic to cardiomyocytes (see figure 5.21 A top left image). The initial rate of cell death was 1 % per hour accelerating from 5 hr onwards to 11 % per hour up to 12 hr before decelerating and eventually reaching 100 % cell death at 20 hr (figure 5.21 B). This toxic response was significant from 6 hr (17.3+/-3 %) onwards compared to 1 hour (3.4+/-0.6 %) ($p<0.0001$). For CAR at 4.92 µM there was a low level, but significant increase from 16 hr onwards (see graph inlay) from 0.12 +/- 0.9 % at 1 hr to 1 +/-1.4 % ($p<0.05$ reaching $p<0.01$ from 20 hr onwards) reaching 1.5+/-1.9 % at 24 hr. At 0.492 µM there was no change in cell death observed over 24 hr. As the two highest concentrations tested either formed precipitates or proved toxic over 24 hr, the lower two concentrations

were taken forward (4.92 µM and 0.492 µM) corresponding to DMSO vehicle concentrations of 0.01 % and 0.001 %.

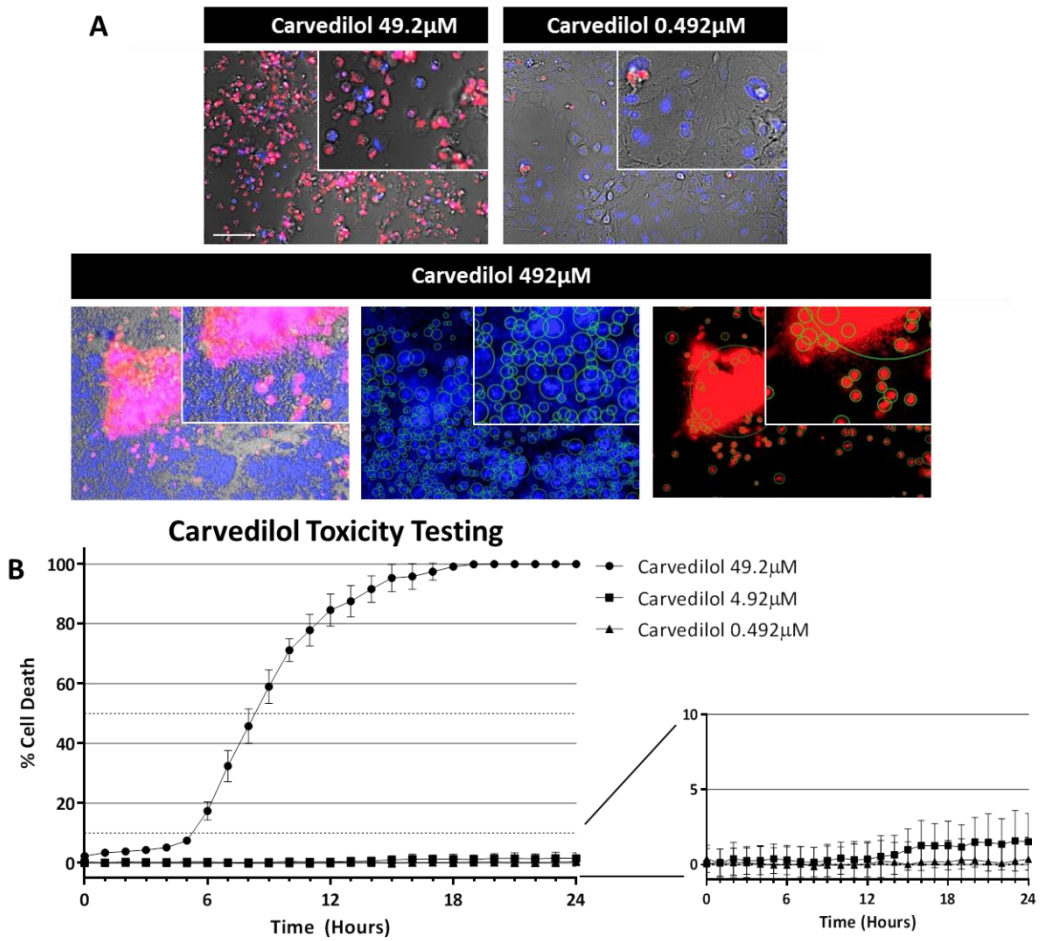


Figure 5.21 – Assessing toxicity of CAR over 24 hr.
Cardiomyocytes were treated with CAR at 492 µM (1 % vehicle), 49.2 µM, 4.92 µM or 0.492 µM for 24 hr. Images were taken at 1 hr intervals. **(A)** Representative images of fluorescent signal and brightfield taken at 24 hr following CAR treatment of cardiomyocytes at 492 µM, 49.2 µM and 0.492 µM. **(B)** Quantification of PI staining measured at 1 hr intervals over 24 hr. Due to precipitate formation at 492 µM, accurate quantification of cell death could not be achieved so data was not plotted. N=3 for each concentration.

5.2.6.3 Sildenafil toxicity testing

SIL was prepared in DMSO to the highest soluble concentration with 1 % DMSO vehicle corresponding to 299.9 µM with subsequent concentrations of 29.99 µM, 2.99 µM and 0.29 µM. When 299.9 µM SIL was added to media it formed precipitates but unlike with CAR, these precipitates did not affect object recognition (figure 5.22 A left image) meanwhile, 29.9 µM and lower did not form precipitates in the media. At 299.9 µM SIL, a toxic response was observed which, when compared to 1 hr (2.8+/-0.8 %) was statistically significant from 12 hr onwards (5.4+/-0.7 %, $p<0.05$, $p<0.01$ at 14 hr, $p<0.0001$ 19 hr onwards) reaching 9.2+/-2.8 % at 24 hr (figure 5.22 B). At 29.99 µM a significant increase in toxicity was observed (relative to 1 hr, 1.1+/-0.7 %) from 18 hr (2.5+/-1.7 %, $p<0.05$, $p<0.01$ from 20 hr onwards) reaching 2.9+/-1.7 % at 24 hr. For 2.99 µM and 0.299 µM SIL there was no significant change in toxicity. As toxicity was observed with 299.9 µM SIL, 29.99 µM and 2.99 µM were taken forward for future testing corresponding to vehicle concentrations of 0.1 % and 0.01 % DMSO respectively.

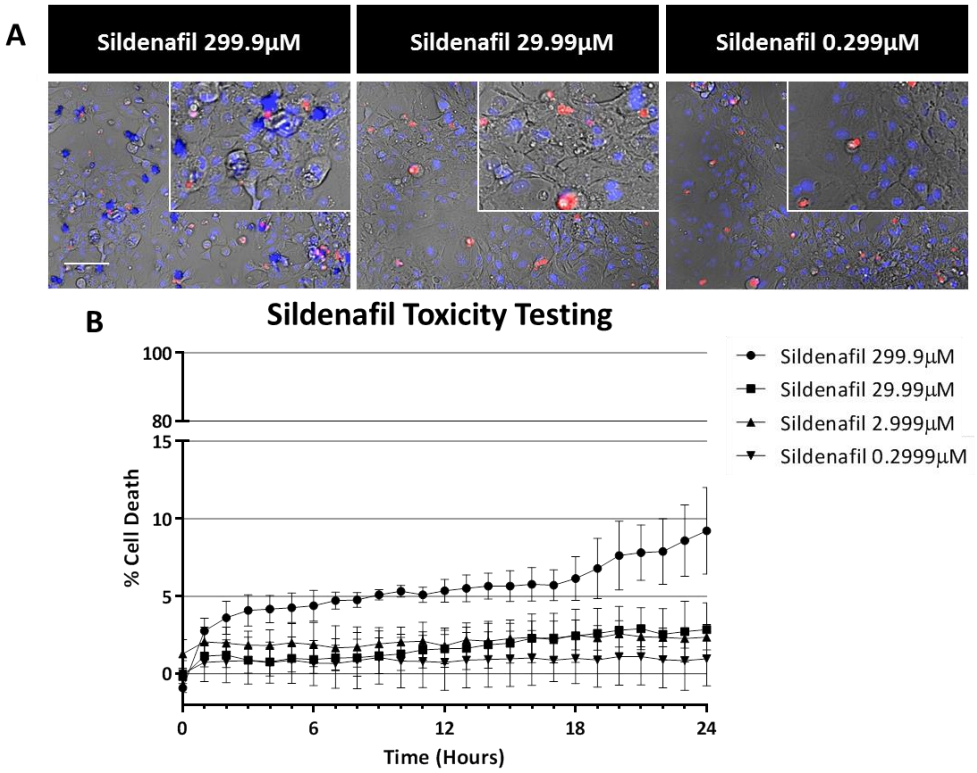


Figure 5.22 – Assessing toxicity of SIL over 24hr.
Cardiomyocytes were treated with SIL at 299.9 µM (1 % vehicle), 29.99 µM, 2.999 µM or 0.2999 µM for 24 hr. Images were taken at 1 hr intervals. **(A)** Representative images of fluorescent signal and brightfield taken at 24 hr following SIL treatment of cardiomyocytes at 299.9 µM, 29.99 µM and 0.2999 µM. Precipitate formation was observed at 299.9 µM but did not affect toxicity quantification. **(B)** PI staining measured at 1 hr intervals over 24 hr. N=3 for each concentration.

5.2.6.4 Isoprenaline toxicity testing

ISO was prepared in H_2O and the highest concentration used was 100 µM corresponding to a vehicle concentration of 1 % with subsequent concentrations of 10 µM, 1 µM and 0.1 µM tested. ISO treated cells did not show any statistically significant toxicity at any of the concentrations tested (figure 5.23 A). While ISO did not show any toxicity even at 100 µM, recent evidence has shown that at higher concentrations, potential ISO cardioprotection is impaired (Shin et al., 2014). 10 µM and 1 µM were taken forward as these concentrations had been previously tested

to model ISO-mediated cardioprotection from chemical insult (Shin et al., 2014, Henaff et al., 2000) corresponding to final vehicle concentrations of 0.1 % and 0.01 % H_2O.

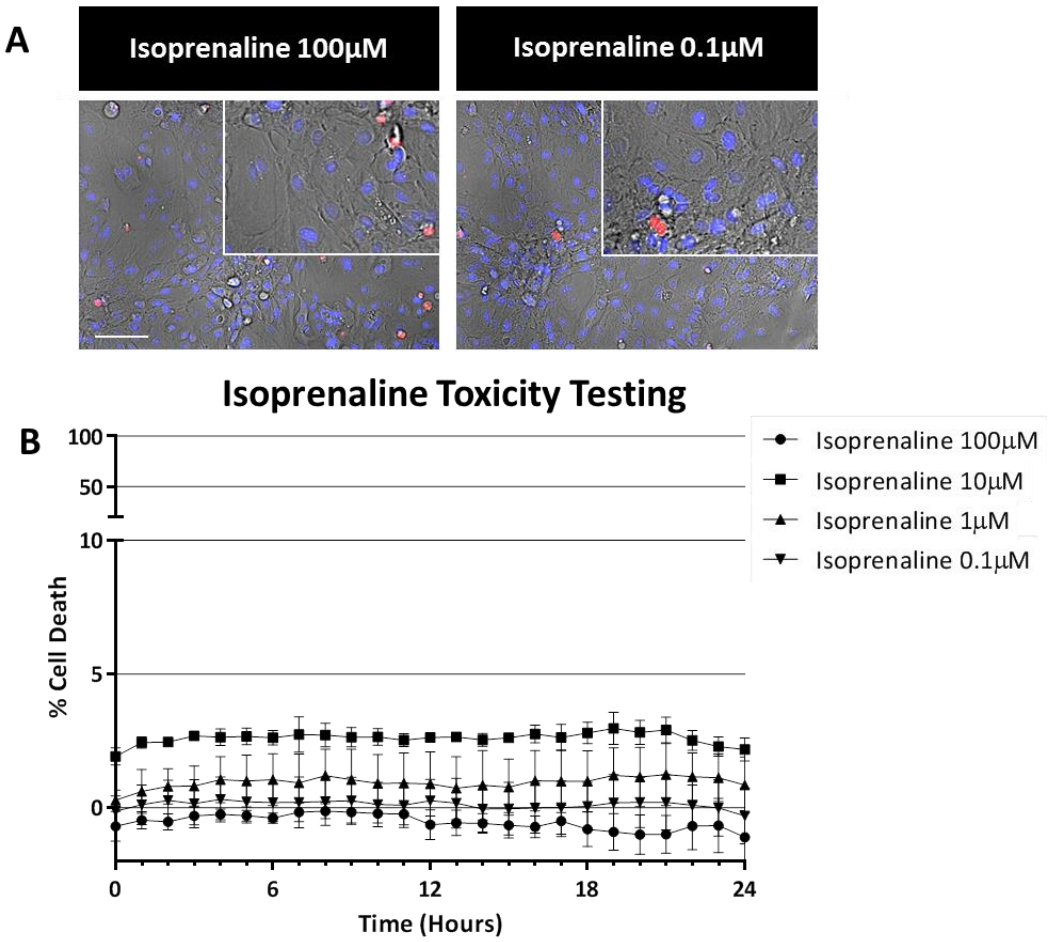


Figure 5.23 – Assessing toxicity of ISO over 24 hr.
Cardiomyocytes were treated with ISO at 100 µM (1% vehicle), 10 µM, 1 µM or 0.1µM for 24 hr. Images were taken at 1 hr intervals. **(A)** Representative images of fluorescent signal and brightfield taken at 24 hr following ISO treatment of cardiomyocytes at 100 µM and 0.1 µM. N=3 for each concentration.

5.2.7 Endpoint analysis of "rescue" drugs

In order to support the results seen in the time course experiments shown in sections 5.2.6 (and figures 5.20-5.23) an endpoint screen was carried out to

quantify cell death at 24 hr with the addition of Hoechst (figure 5.24). This screen (figure 5.24 graph) reinforced what was found at the end of the real time tests: DEX was toxic at 745.5 µM CAR at 49.2 µM and SIL at 299.9 µM. Increased toxicity was also detected for SIL at 2.99 µM. This result was partly due to one of three wells having an unusually high amount of cell death (6.9 %) compared to the other two wells (mean 2.1+/-0.14 %). The results from this test did not alter the decisions for drug concentrations to be carried through to the toxicity rescue experiments.

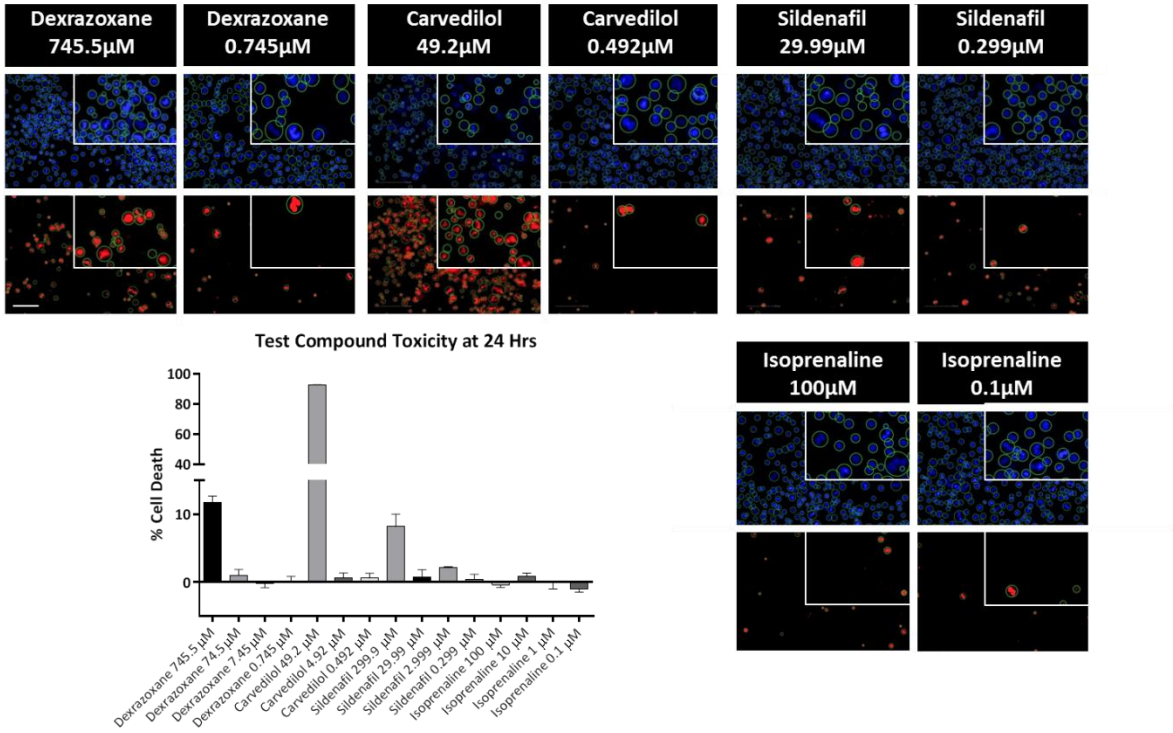


Figure 5.24 – Quantification of DEX, CAR, SIL and ISO toxicity at 24 hr with Hoechst and PI staining.
At the end of the 24 hr time course experiments (figures 5.20-5.23), wells were stained with Hoechst and percent cell death determined as proportion of Hoechst positive cells co-staining for PI. Representative images of Hoechst and PI staining at different drug concentrations are shown. A graph comparing the toxic response to these drugs at 24 hr is displayed bottom left. N=3 for each condition.

5.2.8 Time course quantification of DOX toxicity with or without co-incubation of rescue drugs

Earlier, the TD_{50} for DOX was calculated as between 37 µM and 16 µM based on time course and end point assays. With this in mind, in order to test whether the rescue drugs might be able to reduce DOX toxicity, a concentration range was chosen containing the predicted TD_{50} but also ensuring that a change in TD_{50} could be detected without falling outside the chosen concentration range. Additionally, in the endpoint assay, the difference between DOX toxicity at 10 µM and 50 µM was 65 %, placing the TD_{50} between these concentrations (figure 5.19). A range of concentrations that would give better resolution of this "gap" was sought. To this end, DOX was used at 50 µM, 40 µM, 30 µM, 20 µM, 10 µM and 1 µM each with two concentrations of the rescue drugs as well as DOX on its own. In order to facilitate such a large number of variables (64 variables, which in quadruplicate gave 216 wells excluding controls), 384-well plates were used. To carry out drug screening on this scale, the robotic platform (chapter 4) was used to enable rapid medium exchanges in these plates. Due to the increased number of wells, the time required for imaging each plate was higher; therefore sequential scans were carried out at 2 hr intervals.

At concentrations of 40 µM and 50 µM, the toxicity of DOX was enough to cause complete cell death with dead cells and apoptotic bodies forming aggregates that made dead-cell recognition unreliable, rendering the data inaccurate. For this

reason and because of high DOX background, this data was not plotted in real time graphs. At 30 µM DOX (figure 5.25), a significant ($p<0.0001$ – all two way ANOVA, DMCT) decrease of 13 % in toxicity was achieved with DOX-CAR at 4.92 µM (11.2+/-5.1 % at 8 hr) compared to DOX-only at 24.3+/-7.6 %. The difference remained significant until 20 hr (48.9+/-3.9 % for DOX-CAR and 56.9+/-5.8 % for DOX-only, $p<0.05$) and at 22 hr was no longer significant. With DOX on its own, time taken to reach TD_{50} was 13 hr. With DOX-CAR 4.92 µM this was extended to 20.8 hr. No other rescue drugs at this concentration of DOX caused a significant decrease in toxicity. At 16 hr, there was as significant increase ($p<0.05$) in toxicity from 55.3+/-5.8 % to 63.1+/-5.8 % with DOX-ISO at 10 µM which remained significant up to 22 hr (56.1+/-5.9 % and 65.6+/-13.2 %, $p<0.01$). With 1 µM DOX-ISO there was also a significant increase in toxicity between 8 hr (24.3+/-7.6 % and 32.7+/-3.7 % $p<0.05$) and 16 hr (55.3+/-5.8 % and 63.9+/-5.9 %, $p<0.05$).

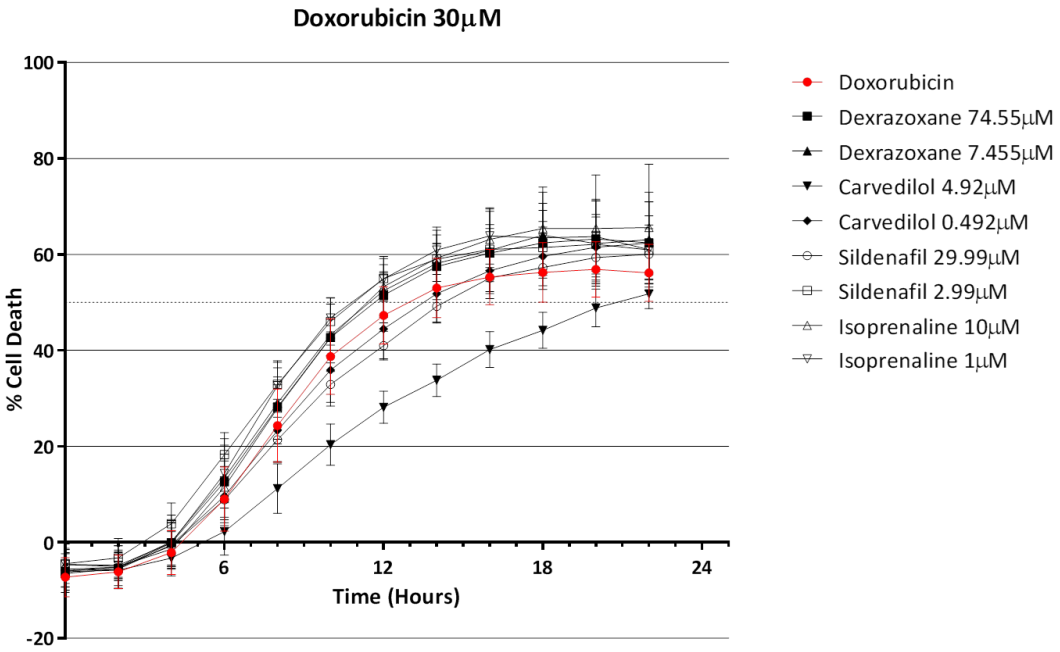


Figure 5.25 – Quantification of 30 µM DOX-induced toxicity over 24 hr with or without co-treatment with rescue drugs.
Cardiomyocytes were treated with 30 µM DOX-only or in combination with DEX, CAR, SIL or ISO at the concentrations shown (top right). Cardiomyocytes were co-incubated with PI and images were taken at 2 hr intervals up to 22 hr. Experiment was carried out in two rounds using 384-well plates incubated in an enclosed non-humidified chamber at 5 % CO_2 and 37°C for the duration of the test. N=8 wells tested for each condition. Error bars = SD.

At 20 µM DOX (figure 5.26) another significant decrease in toxicity occurred with co-incubation using CAR at 4.92 µM with this effect starting to occur at 4 hr, becoming significant at 8 hr (26+/-5.9 % for DOX, 15.3+/-4.4 % for DOX-CAR, $p<0.001$, $p<0.0001$ at 10 hr onwards) and remaining significant until the end of the assay at 22 hr (72.4+/-7.5 % for DOX and 55.5+/-3.9 % for DOX-CAR, $p<0.0001$). The time taken to reach TD_{50} was 11.6 hr for DOX and this was extended by CAR 4.92 µM co-treatment to 17.7 hr. Between 12 hr and 16 hr there was also a significant effect observed with SIL at 29.99 µM (at 12 hr this was 52.1+/-8 % for DOX and 45.3+/-2.9 % for DOX-SIL and at 16 hr, 66.3+/- 8.9 % and 59+/-4 % respectively, $p<0.05$). At 18 hr and at 22 hr there was also a significant decrease in toxicity with SIL at 2.99 µM (68.8+/-7.7 % for DOX and 62+/-7.6 % for DOX-SIL at 18 hr and 72.4+/-7.5 % and 64.8+/-5.9 % respectively at 22 hr, $p<0.05$). Between 10 and 22 hr, a significant increase in toxicity was observed between DOX and DOX-DEX at 7.455 µM (at 10 hr, 40.4+/-7.2 % for DOX and 47.2+/-4.1 % for DOX-DEX and at 22 hr, 72.4+/-7.5 % and 79.5+/-7.1 % respectively, $p<0.05$).

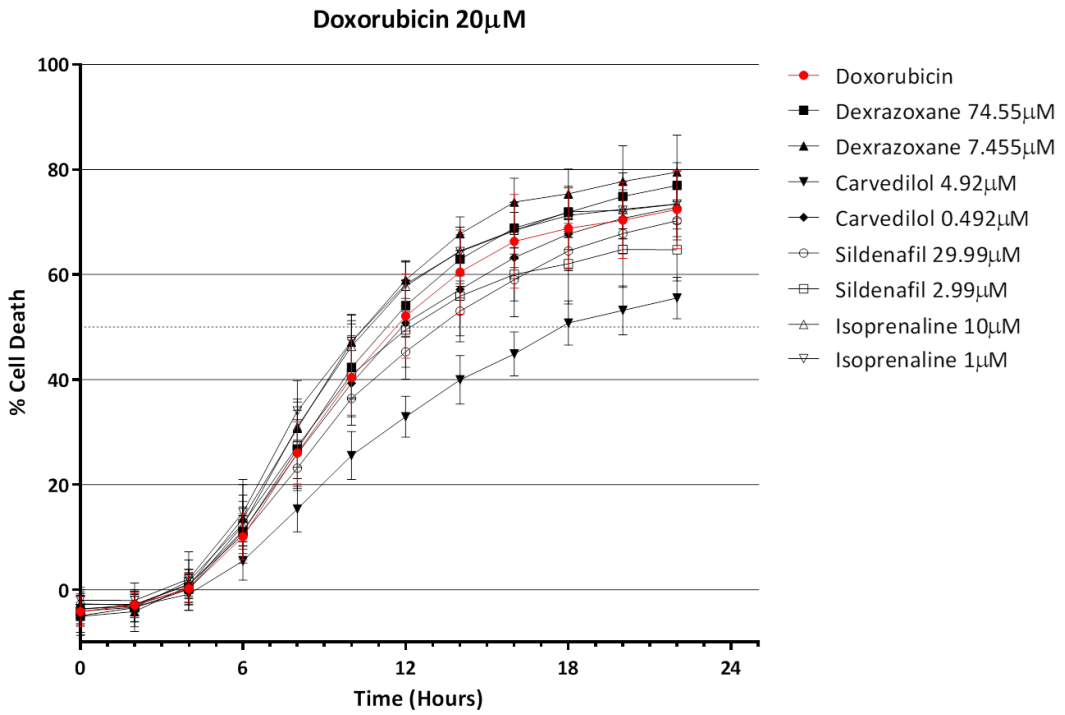


Figure 5.26 – Quantification of 20 µM DOX-induced toxicity over 24 hr with or without co-treatment with rescue drugs.
Cardiomyocytes were treated with 20 µM DOX-only or in combination with DEX, CAR, SIL or ISO at the concentrations shown (top right). Cardiomyocytes were co-incubated with PI and images were taken at 2 hr intervals up to 22 hr. Experiment was carried out in two rounds using 384-well plates incubated in an enclosed non-humidified chamber at 5 % CO_2 and 37°C for the duration of the test. N=8 wells tested. Error bars = SD.

At 10 µM DOX (figure 5.27), the only significant effect observed was a decrease in toxicity with DOX-CAR at 4.92 µM from 16 hr to 22 hr (35.4+/-5.2 % for DOX and 26.6+/-4.5 % for DOX-CAR at 16 hr and at 22 hr, 47+/-5.6 % and 35.5+/-4 % respectively)($p<0.05$ at 16 hr and 18 hr and $p<0.01$ 20 hr and 22 hr). There was no change in the TD_{50} as it was not reached by DOX at this concentration. At 1 µM DOX (figure 5.28) there were no significant reductions in toxicity achieved. However, between 14 hr and 22 hr there were statistically significant increases observed with both of the ISO co-treatments. For ISO at 10 µM, the increase was up to 27.9+/-3.7

% from 20.9+/-3.6 % for DOX-only ($p<0.05$, at 14 hr) ($p<0.01$ between 16 hr to 20 hr) and at 22 hr, 43.9+/-5.2 % for DOX-ISO and 33.9+/-3.7 % for DOX-only ($p<0.001$). For 1 µM ISO at 14 hr, toxicity was 28.1+/-5.6 % while DOX-only was 20.9+/-3.6 % ($p<0.05$ to 20 hr) and at 22 hr, ISO was 42.2+/-7.3 % compared to DOX at 33.9+/-3.7 % ($p<0.01$).

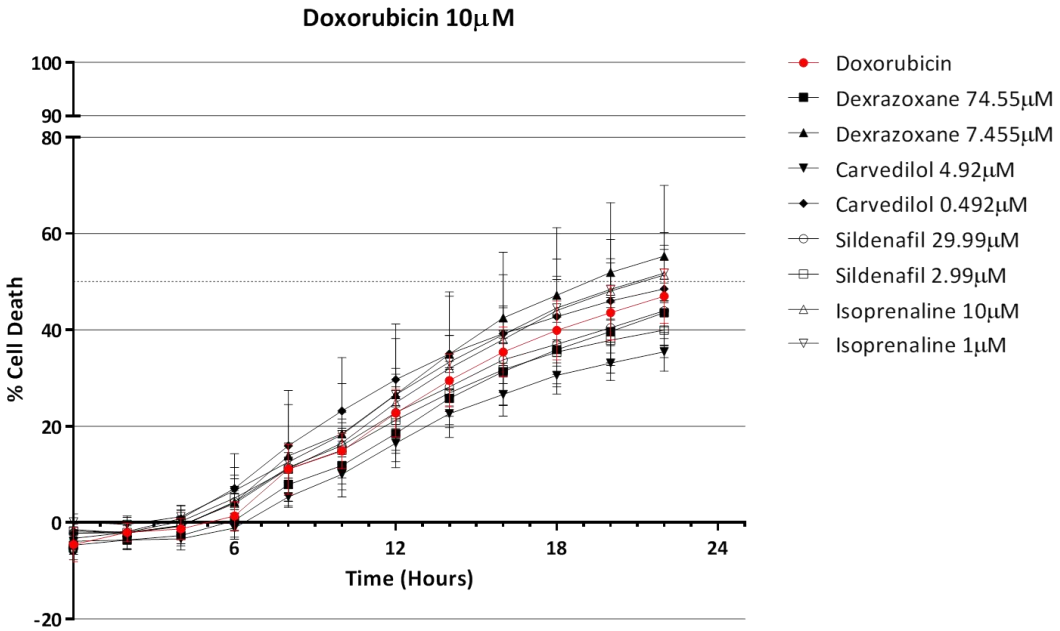


Figure 5.27 – Quantification of 10 µM DOX-induced toxicity over 24 hr with or without co-treatment with rescue drugs.
Cardiomyocytes were treated with 10 µM DOX-only or in combination with DEX, CAR, SIL or ISO at the concentrations shown (top right). Cardiomyocytes were co-incubated with PI and images were taken at 2 hr intervals up to 22 hr. Experiment was carried out in two rounds using 384-well plates incubated in an enclosed non-humidified chamber at 5 % CO_2 and 37°C for the duration of the test. N=8 wells tested. Error bars = SD.

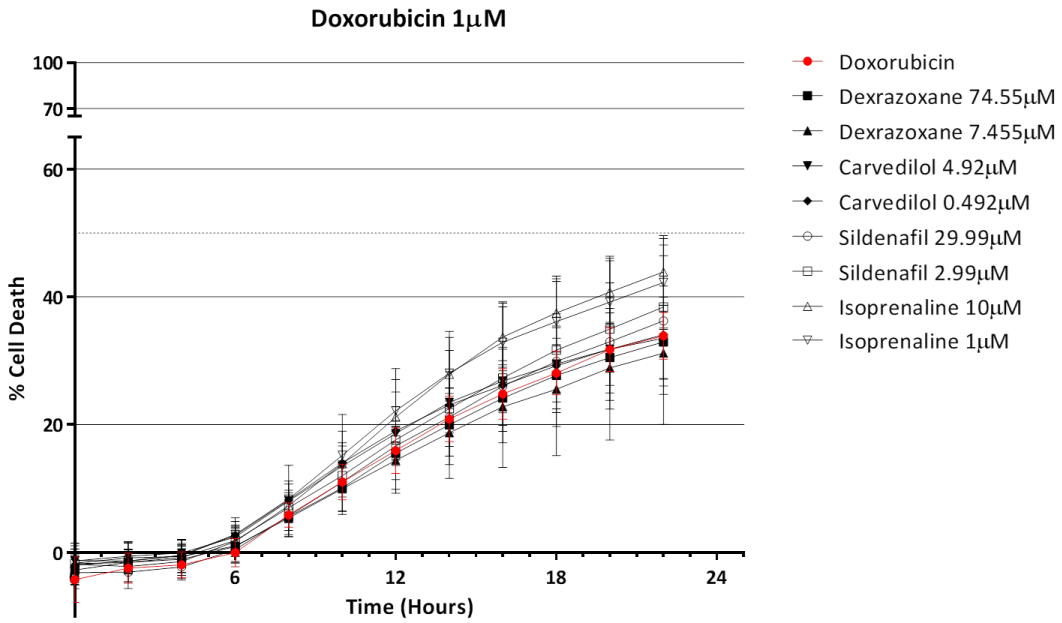


Figure 5.28 – Quantification of 1 µM DOX-induced toxicity over 24 hr with or without co-treatment with rescue drugs.
Cardiomyocytes were treated with 1 µM DOX-only or in combination with DEX, CAR, SIL or ISO at the concentrations shown (top right). Cardiomyocytes were co-incubated with PI and images were taken at 2 hr intervals up to 22 hr. Experiment was carried out in two rounds using 384-well plates incubated in an enclosed non-humidified chamber at 5% CO_2 and 37°C for the duration of the test. N=8 wells tested. Error bars = SD.

In summary, DOX concentrations of 40 µM and 50 µM, were sufficiently toxic to prevent accurate object identification and quantification and no beneficial or negative effect was observed with any of the rescue drugs. At 30 µM DOX, CAR at 4.92 µM significantly reduced toxicity between 8 hr and 20 hr while ISO at 10 µM increased toxicity between 16-22 hr and ISO at 1 µM increased toxicity between 8-16 hr. In cardiomyocytes treated with 20 µM DOX, CAR at 4.92 µM decreased toxicity between 8- 22 hr. SIL at 29.9 µM decreased toxicity between 12-16 hr and SIL at 2.99 µM decreased it between 18-22 hr while between 10-22 hr DEX at 7.455 µM increased toxicity. With 10 µM DOX, a decrease in toxicity occurred in CAR-

treated wells at 4.92 µM between 16-22 hr. Finally, at 1 µM DOX no reductions in toxicity were seen but increases were observed with ISO at 10 µM and 1 µM between 14 to 22 hr.

5.2.9 Endpoint quantification of doxorubicin toxicity and rescue drug effects

In order to support the data generated in figures 5.22-5.25, endpoint screens of the plates used in those figures were carried out by adding Hoechst at the 24 hr time point and quantifying cell death. A comparison of drug responses measured by endpoint scans revealed that at 30 µM, 40 µM and 50 µM DOX killed >90 % of cells by 24 hr with no sign of reduced toxicity from CAR at 4.92 µM (figure 5.29a B). Images of object recognition illustrate the clumping effect observed with dead cells (figure 5.29a A, 40 µM and 50 µM images) and a heterogeneous mixture of apoptotic cells (green arrows), apoptotic bodies (yellow arrows) and programmed necrosis cells (red arrows).

At 10 µM and 20 µM DOX, significantly lower toxicities were observed with CAR at 4.92 µM. For 20 µM the toxicity was 78.8+/-6 % for DOX and 63.5+/-14.4 % for DOX-CAR at 4.92 µM (all one-way ANOVA, $p<0.05$, DMCT) (figure 5.29b B- bottom right graph). For 10 µM DOX, the difference was from 57.1+/-8.4 % for DOX to 37.4+/-11.2 % (bottom centre graph, $p<0.0001$). At 1 µM DOX toxicity was 47.5+/-6.5 % and a significant decrease observed in DOX-CAR at 4.92 µM (27.6+/-6.8 % $p<0.001$) despite not appearing to be the case in the time course scan. There were also

significant decreases observed with DOX-DEX at 74.55 µM (29.4+/-12.7 % p<0.01,) and SIL at 29.99 µM (33.7+/-7.1 % p<0.05). A significant increase in DOX toxicity was observed with ISO at 10 µM up to 61.8+/-4.5 % (p<0.05).

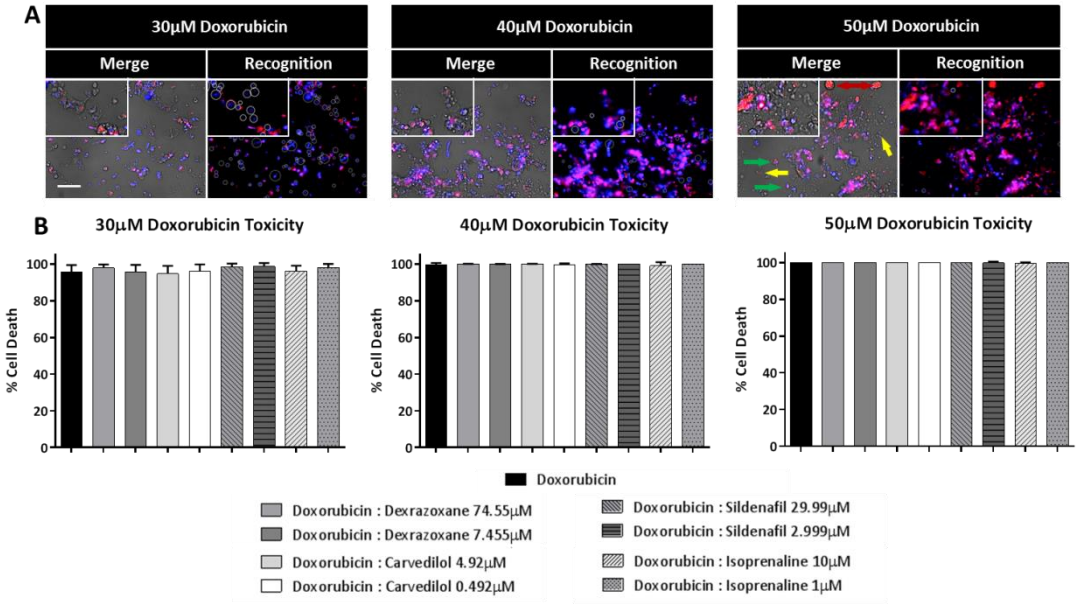


Figure 5.29a – Quantification of DOX toxicity at 24 hr with Hoechst and PI staining.

Cardiomyocytes were treated with 30 µM, 40 µM or 50 µM DOX-only or in combination with DEX, CAR, SIL or ISO at the concentrations shown (bottom key) for up to 24 hr. Cardiomyocytes were stained with Hoechst and images taken. Quantification of Hoechst and PI staining was carried out. Three 384-well plates were used to generate the data shown. As the duration of scanning took approximately 2 hr, 384-well plates were incubated in an enclosed non-humidified chamber at 5 % CO_2 and 37°C while scanning took place. **(A)** Representative images of fluorescent/brightfield merged images and fluorescent images showing object identification. **(B)** Graphs for toxicity observed in cardiomyocytes treated with the conditions shown (bottom key). No significant effect detected at any concentrations shown. N=12 for each condition tested. Error bars = SD, significance test = one-way ANOVA.

5.2.10 Determining and comparing TD_{50} value for doxorubicin with and without rescue drug co-treatment

Using the data from the end point assays in 5.2.9, dose response curves were plotted for all drug conditions (figure 5.30) tested with DOX and TD_{50} values calculated. This was not possible for both ISO concentrations as they never went below 50 % toxicity. The estimated TD_{50} for DOX based on these results was 2 µM, 8-fold lower than the predicted TD_{50} in figure 5.19 A, but was still within the range of concentrations used for this experiment. A comparison of the fold-change in TD_{50} values from rescue drug co-treatments compared to DOX-only showed that both DEX at 74.55 µM and SIL at 29.99 µM increased the TD_{50} by 3.5- and 3.75-fold, to 7 µM and 7.5 µM respectively. At 4.92 µM and 0.492 µM CAR a 7.5-fold and 2-fold increase to 15 µM and 4 µM was observed, respectively. DEX and SIL at 7.45 µM and 2.99 µM respectively, also achieved 1.5-fold increases in the TD_{50} to 3 µM in both cases. These results confirmed that DEX, CAR and SIL were capable of reducing DOX toxicity in cardiomyocytes but the extent to which this was possible was dose-dependent for DOX and for DEX, CAR and SIL, with high concentrations (≥30 µM) of DOX not showing any decreases in toxicity and lower concentrations of DEX, CAR and SIL showing reduced toxicity reduction. Additionally, co-treatment with ISO (10 µM) did not reduce DOX toxicity, but increased it even though, on its own, ISO proved non-toxic to cardiomyocytes at as high as 100 µM.

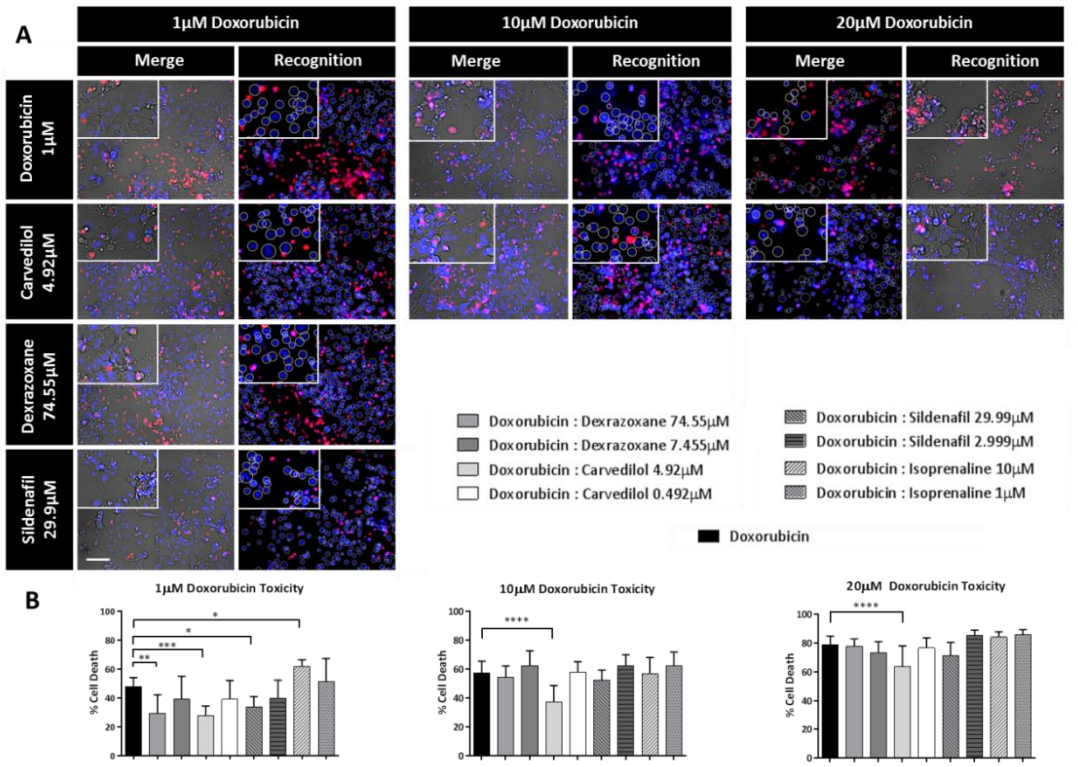


Figure 5.29b – Quantification of DOX toxicity at 24hr with Hoechst and PI staining.

Cardiomyocytes were treated with 1 µM, 10 µM or 20 µM DOX-only or in combination with DEX, CAR, SIL or ISO at the concentrations shown (key, right) for up to 24 hr. Cardiomyocytes were stained with Hoechst and images taken. Quantification of Hoechst and PI staining was carried out. Three 384-well plates were used to generate the data shown. As the duration of scanning took approximately 2 hr, 384-well plates were incubated in an enclosed non-humidified chamber at 5 % CO_2 and 37°C while scanning took place. **(A)** Representative images of fluorescent/brightfield merged images and fluorescent images showing object identification. **(B)** Graphs for toxicity observed in cardiomyocytes treated with the conditions shown (key, right). Significant decreases in cell death were observed with CAR (4.92 µM), at DOX concentrations of 20 µM ($p<0.0001$), 10 µM ($p<0.0001$) and 1 µM ($p<0.001$). At 1 µM DOX, significant decreases were also observed for SIL at 29.99 µM ($p<0.05$) and DEX at 74.55 µM ($p<0.01$) while a significant increase was detected with ISO at 10 µM ($p<0.01$). N=12 for each condition tested. Error bars = SD, significance test = one-way ANOVA.

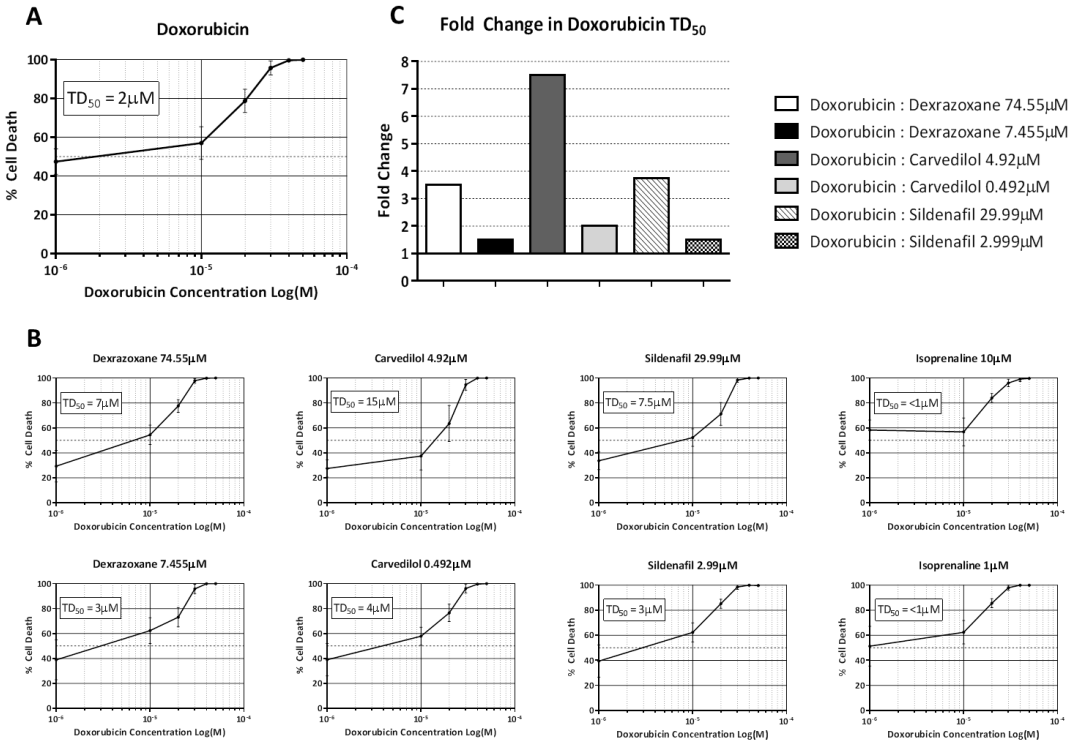


Figure 5.30 – The effect of rescue drug co-treatment on DOX TD_{50} in hiPSC cardiomyocytes.

TD_{50} values were calculated by plotting toxicity curves for DOX-only or after co-incubation with DEX, CAR, SIL or ISO at the concentrations shown (key, top right) for 24 hr as quantified with Hoechst and PI staining. **(A)** DOX toxicity at 24 hr without co-treatment. **(B)** DOX toxicity when co-treated with DEX, CAR, SIL or ISO for 24 hr (n=12, error bars = SD). **(C)** Fold change in the TD_{50} of DOX in cardiomyocytes when co-incubated with DEX, CAR or SIL for 24 hr. ISO could not be calculated as TD_{50} could not be determined (toxicity too high).

5.3 Discussion

5.3.1 Time course drug screening validation

For this chapter, a novel process was developed adapting the work of Wlodkowic et al. (Wlodkowic et al., 2009), to allow time course monitoring of toxicity *in vitro* using cardiomyocytes. As this method had not been used in our group before, several experiments were carried out to validate it. Stability of reagent signal was demonstrated over 24 hr with no photo-bleaching detected following repeated photo-excitation. Additionally neither of the reagents induced cell death when incubated with cells over 24 hr. To show that they could be used to accurately quantify cell death in time course experiments, STA, a known inducer of apoptosis was used as a positive control and data was compared to results generated by Cellular Dynamics in two published technical notes where STA was used to induce toxicity in hiPSC derived cardiomyocytes (Cellular Dynamics International, 2015a, Cellular Dynamics International, 2015b). This highlighted very similar results with PI staining, (490 +/- 28.3 nM, 123 nM less than the EC_{50} result from CDI at 613 nM – figure 5.14 A) but discrepancies with CEC staining were observed 650 nM (CEC only) or 700 nM (CEC-PI) compared to 1.49 µM for CDI (figure 5.15). Additionally, CEC was not compatible PI in co-staining experiments although PI was compatible with CEC as demonstrated by different levels of staining obtained in the same wells (figure 5.12 C). For these reasons, CEC was not used in subsequent experiments.

5.3.2 Time course and end-point screening of DOX cardiotoxicity with or without rescue drugs

After initial validation, time course monitoring of drug toxicity *in vitro* was achieved using PI to screen each rescue drug for cardiotoxicity and later, to model DOX cardiotoxicity and to test the potential cardioprotective effect of rescue drugs. This method identified unique toxicity profiles in some drugs such as varying initial toxicity "lag" phases of 0-11 hr for DEX (745.5 µM figure 5.20) and 0-5 hr for CAR (49.2 µM figure 5.21) for example. Additionally, when 30 µM DOX and 30 µM DOX-CAR (4.92 µM) toxicity were quantified, (figure 5.25) a significantly decreased level of toxicity was observed from 8 hr to 20 hr in DOX-CAR (13.1 % lower at 8 hr, 19.2 % at 14 hr and 8 % at 20 hr) which was no longer significantly different at 22 hr. As a result, this effect was not detected in the corresponding end-point screen however; 30 µM DOX is 30-fold higher than peak plasma levels (approximately 1 µM) following therapeutic DOX administration ((Barpe et al., 2010) figure 5.31) demonstrating that CAR had a partial cardioprotectant effect on DOX toxicity at high concentrations. CAR was also more effective at reducing DOX cardiotoxicity than the other rescue drugs which showed no beneficial effect in endpoint screens at 30, 20 or 10 µM. At 1 µM DOX however, DEX (74.55 µM), CAR (4.92 µM) and SIL (29.99 µM) all showed significantly lower ($p<0.01$, $p<0.001$ and $p<0.05$ respectively) levels of cardiotoxicity than in DOX-only wells. In patients, peak plasma levels following administration reach 36.5 µg/ml (from 500mg/m^2 infusion, FDA Label, 2012), equivalent to 136 µM for DEX, 75ng/ml (following 25 mg oral dose) for CAR (equivalent to 0.184 µM) ((Zarghi et al., 2007), figure 5.32) and following 200 mg dose, achieved a peak plasma concentration of 1000ng/ml (equivalent to 2.1 µM)

for SIL (Nichols et al., 2002). In 10 µM ISO treated wells with 1 µM DOX, toxicity significantly increased in the endpoint screen ($p<0.05$) while for the time course, at both 10 µM and 1 µM significant increases were observed from 14 hr to 22 hr (for 10 µM ISO, $p<0.05$ at 14 hr, $p<0.01$ between 16 hr to 20 hr and $p<0.001$ at 22 hr). For 1 µM ISO at 14 hr, $p<0.05$ up to 20 hr and at 22 hr, $p<0.01$. It is worth noting however, that when comparing patient plasma levels to concentrations used in these assays, albumin was present in the RPMI-B27 medium used and has been shown to bind drugs (Kerns, 2003). The concentration of free drug in these wells was not assessed but this would allow more accurate comparison with clinical data.

5.3.3 Limitations of the time course assay

As a cautionary note, although the time course experiments did provide useful information on toxicity kinetics over time, there were some limitations to these assays. Firstly, incubating cardiomyocytes with Hoechst for 24 hr induced apoptosis in these cells (figure 5.3) therefore, cell number could not be quantified in wells from the start and so, cell numbers from control wells had to be used to derive percentage cell death values. This implied equal numbers of cells seeded in all the wells across a 96- or 384-well plate but as demonstrated in chapter 4 section 4.2.19, cell seeding across 384- well plates was not perfectly uniform (4634+/-471.6 and 3904+/-550.8 cells across two plates seeded back-to-back). Additionally while quantification of dead cells lifting off the culture surface did not present a challenge for Operetta software at lower drug concentrations such as <5 µM for STA (figure 5.10 and 5.11) and <30 µM for DOX (figure 5.19). At higher (highly toxic concentrations; >30 µM DOX, >5 µM STA) dead cells or apoptotic bodies aggregated

in the wells preventing resolution between cells (i.e. figure 5.17 bottom row), reducing accuracy of quantification hence, some conditions which achieved maximal cell death did not reach 100 % in time course assays (see DOX 30 µM figure 5.29a with >90 % cell death at 24 hr and figure 5.25 DOX 30 µM 24 hr time course levelled off at 56.14+/-5.9 % achieved at 22 hr). Endpoint screens had improved accuracy as Hoechst staining could be carried out allowing total cell number and PI-Hoechst co-stained cell numbers to be quantified. Combined therefore, both methods proved beneficial in assessing cardiotoxicity but there remains scope to improve accuracy of the time course assays.

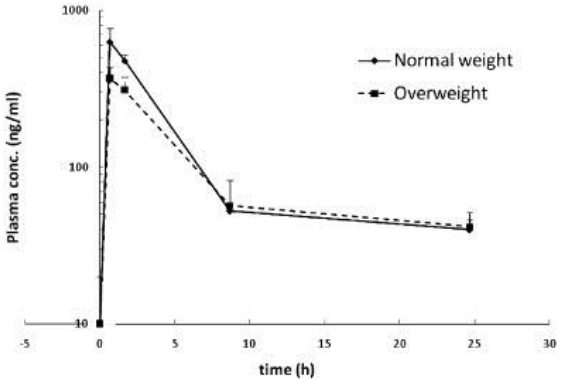


Figure 5.30 – Change in DOX plasma concentration in females over 24 hr.
DOX plasma concentrations in females (n=3) with normal weight (mean 62.2+/-6.9 kg) following administration at 60 mg/m^2 of body surface area. Mean age 55.7+/-4.4 years, mean body mass index 24 +/-1.4, mean body surface area 1.77 +/-0.13 m^2 (y-axis is shown as log scale). DOX plasma concentration at 40 min; 630.4+/-22.1 ng/ml, 1 hr 40 min; 478+/-7.9 ng/ml, 8 hr 40 min; 52.5+/-13.3 ng/ml, 24 hr 40 min; 39.8+/-15.3 ng/ml. For comparison, 580 ng/ml = 1 µM in drug screening experiments. Taken from (Barpe et al., 2010). See also (Mou et al., 1997).

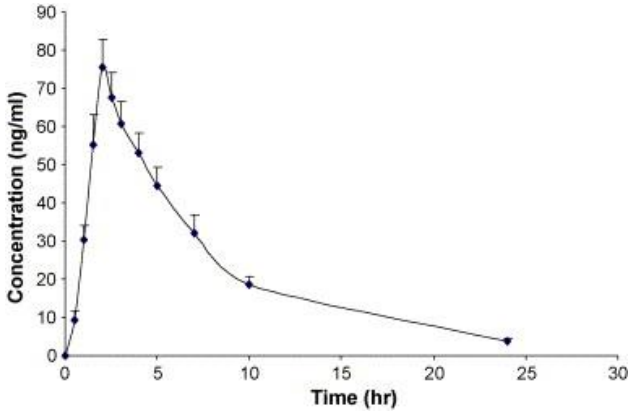


Figure 5.31 – Change in CAR plasma concentration over 24 hr.
CAR plasma concentration following administration of single 25 mg oral dose to healthy volunteers (n=12) (taken from (Zarghi et al., 2007)). CAR concentration of 75 ng/ml is equivalent to 0.184 µM.

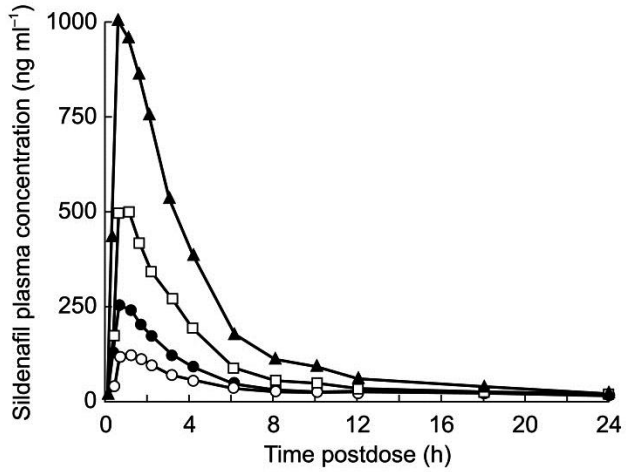


Figure 5.32 – Change in plasma concentration of SIL over 24 hr.
SIL plasma concentrations following oral administration at 25 mg (○), 50 mg (•), 100 mg (□), or 200 mg (▲)(n=32 per group) (taken from (Nichols et al., 2002)). Sildenafil concentration of 1000 ng/ml is equivalent to 2.1 µM.

6 Discussion

In this thesis three different protocols for differentiating hPSCs to cardiomyocytes were adopted and carried out manually. Attempts were then made to translate these to automated processes on the robotic platform. Although EB setup was unsuccessful at generating beating EBs, maintenance of EBs using the robotic platform from day 2 of differentiation onwards was considered successful, generating 95.8 % spontaneously beating EBs. Attempts to automate two monolayer methods, one using cells cultured in mTeSR and the other using cells cultured in E8 also both successfully automated generating $4.5x10^6$ cells and $39x10^6$ respectively both with cardiomyocyte purities >90 %.

Cryopreserved cardiomyocytes generated by the robot were then used in drug screening experiments set up in 384-well plates to quantify the toxicity of the anti-cancer drug DOX in real time and to test the potential cardioprotective effects of four other drugs, DEX, CAR, SIL and ISO. Drug toxicity kinetics were quantified over 24 or 22 hr periods and revealed that DEX, CAR and SIL were capable of significantly reducing cardiotoxicity of DOX and furthermore all led to >3-fold increases in the TD_{50} of DOX.

6.1 hPSC culture and differentiation

Feeder free culture of HUES7 hESCs using MEF-CM was a low cost (estimated at £0.11/ml) and scalable process that enabled the production of cardiomyocytes

using the EB differentiation method (Matsa et al., 2014, Pascut et al., 2013). Dissociating EBs from 96-well plates yielded 0.6+/-0.3x10^6 cells per plate but when carried out manually was time consuming to carry out and low throughput. While not explored in this work, improved EB-differentiation yields could be achieved by developing bioreactor-based differentiation systems to replace 96-well plates (Liu et al., 2014). Indeed, up to 2x10^8 hiPSCs have been generated in bioreactor systems containing 100 ml of medium (mTeSR) (Olmer et al., 2012), by comparison, 100 ml of medium was sufficient to sustain 5 x RoboFlasks with a maximum yield of approximately 1x10^8 hiPSCs. In chapter 3, EB differentiations were manually set up with 0.4x10^6 cells per plate and gave yields of 0.6x10^6 cells, an increase of 50 %. Therefore, in bioreactor systems generating 2x10^8 pluripotent cells, up to 3x10^8 cells could potentially be generated if the method could be translated into a bioreactor format, indicating that EB differentiation methods have the potential to generate large numbers of cardiomyocytes. However, before this can be achieved, issues such as batch variation from MEF-CM and subsequent variability in differentiation outcomes would require addressing. The proportion of beating EBs generated from manual differentiations ranged from as high as 94+/-0.3 % (MEF93) and 82+/-22.8 % (MEF89) to as low as 39+/-15.6 % (MEF70) and 25.6+/-39.7 % (MEF88) with considerable variability observed even within the same batches, ranging between 99 % and 33 % beating EBs (MEF89) and 79.8 and 0 % (MEF88). Undefined and batch variable reagents limit the usefulness of differentiation processes and as a result, there is a need to adopt more defined methods to avoid these limitations (Zanella and Sheikh, 2014). An EB differentiation method compatible with defined medium culture conditions has been achieved, generating

up to $8x10^7$ cells of which 80 % were positive for cardiac troponin T following culture in mTeSR in a 100 ml bioreactor (Matsuura et al., 2012) but it remains to be seen whether these systems can be used to scale up cardiomyocyte production even further in a consistent and cost-effective manner.

Adopting both the mTeSR culture system and monolayer differentiation method increased the quantity of cells that could be generated per-differentiation (4.9+/-$1.4x10^6$ total cells per T75 and 7.3+/-$1.2x10^6$ total cells per RoboFlask) as well as yielding high cardiomyocyte purities (98.7 % for α-actinin and 97.4 % for cardiac troponin T). Others have also demonstrated improved yields and purities >90 % from adopting monolayer methods over existing conditioned-medium based EB methods (Lian et al., 2012, Zhang et al., 2012a). The mTeSR monolayer method also simplified the differentiation process technically, removing lower throughput and time consuming procedures such as changing medium in 96-well plates using 8-channel pipettes or transferring EBs to U-bottom plates from V-bottom plates and replacing them with a simple medium change per flask. Dissociations of differentiations were also made simpler as the process was almost identical to routine cell passaging but the duration of enzyme exposure was increased. Differentiation of hiPSCs was attempted using this method but proved difficult and unreliable to achieve with the exception of the AT1 hiPSC line where purities of 99.5 % (α-actinin) and 90.9 % (cardiac troponin T) were achieved. Furthermore, mTeSR and StemPro-34 (used during the differentiation process) were both expensive media (£0.34/ml and £0.30/ml respectively) and to a lesser extent, still batch

variable because they both contained albumin (Chen et al., 2011). Additionally, cell lines cultured in mTeSR proved difficult to scale up due to the need for high seeding densities ($2x10^6$ cells per T25 or 80,000 cells/cm^2), while high population doubling times (69.9+/-7.7 hr for mTeSR and 43.2+/-0.4 hr for MEF-CM) meant that cultures took longer to achieve appropriate confluence for passaging.

A newer monolayer differentiation method for cells cultured in E8 (Burridge et al., 2014) was adopted using 2 hiPSC lines derived in E6/E8 conditions (LQT2 and CPVT). This had the effect of bringing down the cost of culture as E8 was less expensive (£0.20/ml) than mTeSR (£0.34/ml) while the population doubling time was also more than 2-fold lower (30.1 hr, n=1). Differentiations carried out using this method gave improved yields of up to 39 million cells from one RoboFlask ($4.2x10^5$ cells per cm^2) equivalent to 13 cells for each input cell. Cardiomyocyte purity was also high with α-actinin at 91.4+/-2.1 % and cardiac troponin T at 96.85+/-0.9 %. This cell yield was sufficient to seed 9 x 384 well plates for drug screening ($3.8x10^6$ required per plate), which was in theory was sufficient to test up to 864 different variables in quadruplicate. However, this represented the result of one flask. When the mean was calculated for the 22 other differentiations that were carried out using CPVT hiPSCs, (in RoboFlask format) mean cardiomyocyte yields per flask were lower, at $12.6+/-7.5x10^6$ cells with differentiation outcomes ranging from $22.5x10^6$ down to $1.75x10^6$ per harvested flask, indicating that some degree of optimisation was still required and that differentiation outcomes using this method were variable. Despite this however, this mean value still represented an improvement compared

to the yields achieved with the mTeSR monolayer method, in line with findings by others which suggest that using small molecules instead of growth factors in monolayer differentiation methods improved both overall differentiation yields and cardiomyocyte purities (Lian et al., 2013).

6.2 Automating differentiation and drug screening

In order to carry out high throughput drug screening or cell therapy, large numbers of cardiomyocytes would be needed, necessitating both high scale and reproducible cardiomyocyte production methods. When $1x10^9$ cardiomyocytes were injected into the damaged myocardium of non-human primates, re-muscularisation and improved LVEF were achieved but less than 10 % of the delivered cells successfully engrafted indicating that up to $10x10^9$ cells could be required in order to properly repair the damaged myocardium (Chong et al., 2014). A more recent study offered significant promise when it demonstrated after 3-month follow up that LVEF function could be improved when a patient was administered with as little as $4x10^6$ cardiomyocyte progenitor cells contained within a fibrin scaffold (Menasche et al., 2015b) although another study by the same group found in rats that the scaffold itself was capable of improving LVEF, and that although greater improvements were achieved with scaffolds loaded with cells, after 4 months, no engrafted cells were present (Bellamy et al., 2015). Therefore, it is likely that in order to re-muscularise the myocardium, large numbers of cells between $1\text{-}10x10^9$, would need to be delivered. Automation of cardiomyocyte differentiation could be used to generate such quantities of cardiomyocytes, while also reducing user variability. In order to automate cardiomyocyte production, existing manual processes were adapted to be

compatible with the robot. EB differentiations were not successfully set up by the robot as formation was achieved, but EBs were of significantly smaller size (ranging from 222.7+/-32.2x10^3 µm^2 to 262.8+/-61.3x10^3 µm^2) compared to manually set up EBs (ranging from 468.5+/-55.3x10^3 µm^2 to 550.4+/-54.2x10^3 µm^2) and didn't yield any spontaneously beating EBs at the end of differentiation compared to manual differentiations that achieved >85 % beating EBs. Others have also found that size of EBs can effect differentiation outcome and that smaller EBs tend to have poorer differentiation outcomes (Mohr et al., 2010) indicating that variables effecting EB size warrant investigating further. Automated quantification of EB size and transfer were achieved using the Cellavista, and others have also developed imaging systems for monitoring the size and spontaneous contraction of EBS (Ting et al., 2014) highlighting the relevance of these methods for quality control of scaled EB productions. On a similar note, monitoring cell culture confluence prior to differentiation proved useful in monolayer differentiation work by helping to define correct time points for initiating differentiations and in turn, both manually and on the robot, both monolayer methods proved to be more successful than the EB method by generating considerably higher cell yields on a plate vs flask basis.

6.3 DOX toxicity modelling and drug screening with hiPSC derived cardiomyocytes

Time course tracking of PI staining activity in cardiomyocytes treated with drugs allowed the measurement of cell death kinetics over 24 hr with automated cell seeding and maintenance, addition of drug solutions and image acquisition in 384-well plates. As such, this method was shown to be amenable to larger scale

automated and high throughput drug toxicity studies. The *in vitro* model of DOX toxicity that was generated enabled detection of reduced toxicity in wells treated with DEX, CAR and SIL demonstrating that this platform was sensitive enough to detect changes in cell toxicity in co-treated wells and interestingly, identified CAR to be capable of significantly reducing DOX toxicity at concentrations as high as 20 µM (20-fold higher than the peak plasma concentration in patients). The number of markers investigated in this chapter was limited to Hoechst, PI and CEC, there was potential to expand this repertoire to other markers to provide additional data outputs for high content screening. Although attempts to multiplex CEC with PI staining were not successful, other non-toxic markers of cell toxicity such as SYTOX probes (Wlodkowic et al 2009b) and the anthracycline derivative DRAQ7® (Akagi et al., 2013) were also commercially available working in a similar fashion to PI by binding to DNA when cell membrane integrity is lost and may have been capable of multiplexing with CEC. Reagents were also available to measure the redox environment in cells, a common marker of drug induced toxicity (Deavall et al., 2012) however, cross-reactivity between different oxidants, as well as anti-oxidants could negatively impact the accuracy of these assays (Winterbourn, 2014). Furthermore, while the cardiomyocyte banks used for drug screening had high cardiomyocyte purities (ranging from 91.4% to 97.1%) these were not pure populations. Multiplexing these assays with cardiac specific markers would have helped to determine the effects of drugs specifically on cardiomyocytes in these assays and allow the effects on non-cardiomyocytes to be excluded from calculations. This could be achieved by immunostaining for cardiac markers such as α-actinin or cardiac troponin T at the end of assays. This data could be further

analysed to determine the maturation state of the cells based on the level of sarcomere alignment (Veerman et al., 2015, Patel et al., 2015) and could also be used as a marker to identify sarcomere degradation resulting from DOX treatment (Patel et al., 2015). As the cells used in these experiments were in a confluent monolayer format, cell-cell borders could have been delineated by immunostaining for markers such as pan-cadherin (Matsa et al., 2014) which would aid analysis software in determining the outline of cells, allowing determination of their shape and size. This data could then be used to calculate cell aspect ratios or to quantify the number of nuclei in each cell both of which could be used as markers of maturation state in cardiomyocytes (Yang et al., 2014, Veerman et al., 2015). Multiplexing the real time or end point assays with voltage-sensitive dyes such as di-8-ANEPPS and imaging on platforms such as CELLOPTIQ could also be used to measure the action potentials of spontaneously beating cardiomyocytes and detect responses to drug treatments relative to untreated controls (Jouni et al., 2015).

Additionally, while cardio-protective effects were observed using the existing range of drug concentrations, further experiments to investigate DOX cardiotoxicity and potential rescue were needed with DOX and rescue drugs used at more therapeutically relevant concentrations to see whether any protective effect would still be observed at these doses. Investigating this process across a range of different patient-derived hiPSC derived cardiomyocytes would also be of interest to identify to what extent if any, patients show varying responses to DOX cardiotoxicity or rescue drug treatment.

6.4 Study limitations

The process of generating patient-specific cardiomyocytes can be achieved using protocols developed manually and on an automated cell culture platform to achieve yields of up to 39 million per RoboFlask with >90 % purity for cardiomyocytes without using selection to increase purity. While this represents a considerable improvement over the original EB-differentiation based method in terms of cell yields and success with automation, it remains to be demonstrated that such methods are reproducible and reliable and can be carried out across a range of hiPSC lines. In one set of differentiations, 29 RoboFlasks were set up by the robot of which 22 gave beating sheets (a success rate of 76 %) indicating that the process had good reproducibility but there was still scope to improve this. The precise mechanisms that determined differentiation success remain to be determined. Although growth factors (Burridge et al., 2011) and small molecules (Burridge et al., 2014) are key components of the directed cardiomyocyte differentiation process, in monolayer differentiations, cell confluence when initiating differentiation, seeding density prior to differentiation and the degree of cell-cell compaction also appeared to influence the differentiation outcome. While attempts were made to try and control these variables by monitoring confluence with the Cellavista, carrying out cell counts prior to seeding differentiation and visually monitoring the degree of cell compaction, variability in differentiation outcomes were observed. More detailed experiments to test these and any other possible variables affecting differentiation outcome were warranted and would have been attempted but for lack of time.

In addition to this, the methods used to differentiate hPSCs to cardiomyocytes have been shown to generate mixed populations of atrial, ventricular and pacemaker subtypes in both EB (Matsa et al., 2014) and monolayer methods (Burridge et al., 2014) each playing a different role in the fully developed heart. No experiments were carried out to determine which subtypes or how many of each were present in the cultures used for drug screening. Additionally, the maturity of these cardiomyocytes was not investigated. Ideally, to better model the effects of drugs on the fully developed heart, functionally mature cardiomyocytes would have been preferable in toxicity testing experiments however, protocols for generating mature cardiomyocytes had not yet been optimised or developed in our labs at the time. Recently, others have highlighted that adding T3 hormone, Insulin-like growth factor 1 and Dexamethasone to cardiomyocyte maintenance medium can aid in maturation of cardiomyocytes (Ribeiro et al., 2015, Birket et al., 2015). In these studies, maturity of cardiomyocytes was determined by immunostaining with α-actinin to quantify sarcomere alignment and organisation, contraction force measurements by microscopy and measurements of electrophysiology (Ribeiro et al., 2015, Birket et al., 2015). The latter method required the use of patch clamp electrophysiology and would not be amenable to assays in 384-well plates. However, the former two methods, relying on the use of microscopy were amenable to 384-well plate assays although due to time limits these strategies could not be developed in the timescale of this work. Additionally, it remains to be seen how well 2-dimensional monolayer cultures of cardiomyocytes recreate the drug responses that occur in the cardiac tissue; a 3-dimensional structure. Other groups have developed engineered heart tissues for the purpose of drug screening

(Eder et al., 2015) and it would be interesting to compare the outcomes of testing both systems side-by-side.

Methods were developed to dissociate, cryopreserve and culture cardiomyocytes generated by the differentiation methods highlighted previously. Results were presented providing evidence that cardiomyocytes could be dissociated (figure 3.13), cryopreserved, thawed and cultured (figure 3.16) under conditions optimised during this work and that they did not lose viability or detach from culture surfaces. However, the approach that was used lacked robust quantitative outputs, lacked biological replicates and relied on qualitative assessments of outputs (figure 3.13). A more robust approach would have been pursued had time allowed. This would have involved increasing biological replication, quantifying plating efficiency after dissociation and quantifying plating efficiency after dissociation. Data in figure 3.16 could have been made more robust by quantifying cell number rather than assessing confluence as cardiomyocytes spread out when cultured *in vitro* (Yang et al., 2014) potentially distorting confluency data. Quantified data such as plating efficiency post thaw would have allowed for comparison of results in relation to existing literature or commercial cardiomyocyte supplier data sheets.

6.5 Final remarks and future work

Automation and scale up of hiPSC culture and differentiation has been achieved with <700 million hiPSCs produced in one batch production and <250 million cardiomyocytes generated from one batch production. Cardiomyocytes generated by this method of differentiation were cryopreserved to generate cell banks and

cells taken from these cell banks were used in 96- and 384-well drug screening experiments to develop a model of DOX-induced cardiotoxicity. High-content image analysis of cells in these model systems enabled time course experiments to be carried out to observe and quantify the kinetics of drug toxicity over 24 hr and in so doing, identified cardioprotective effects from several already commercially-available therapeutic compounds. The pharmaceutical industry faces mounting pressure to overcome the impending “patent-cliff” whereby high value blockbuster drugs are approaching patent expiry and insufficient replacement with new blockbuster drugs to make up the shortfall (Kakkar, 2015). Additionally, there is a need for reliable toxicity prediction of existing drug candidates to avoid high profile and costly drug withdrawals. Presented here is a potential pipeline of processes developed which enable both academics and industry to harness the advantages of automation to improve drug development and toxicity screening *in vitro*.

7 Bibliography

AKAGI, J., KORDON, M., ZHAO, H., MATUSZEK, A., DOBRUCKI, J., ERRINGTON, R., SMITH, P. J., TAKEDA, K., DARZYNKIEWICZ, Z. & WLODKOWIC, D. 2013. Real-time cell viability assays using a new anthracycline derivative DRAQ7(R). *Cytometry A,* 83**,** 227-34.

ANDERSSON, H., STEEL, D., ASP, J., DAHLENBORG, K., JONSSON, M., JEPPSSON, A., LINDAHL, A., KAGEDAL, B., SARTIPY, P. & MANDENIUS, C. F. 2010. Assaying cardiac biomarkers for toxicity testing using biosensing and cardiomyocytes derived from human embryonic stem cells. *J Biotechnol,* 150**,** 175-81.

ARAKI, R., UDA, M., HOKI, Y., SUNAYAMA, M., NAKAMURA, M., ANDO, S., SUGIURA, M., IDENO, H., SHIMADA, A., NIFUJI, A. & ABE, M. 2013. Negligible immunogenicity of terminally differentiated cells derived from induced pluripotent or embryonic stem cells. *Nature,* 494**,** 100-4.

BARBARIC, I., BIGA, V., GOKHALE, P. J., JONES, M., STAVISH, D., GLEN, A., COCA, D. & ANDREWS, P. W. 2014. Time-lapse analysis of human embryonic stem cells reveals multiple bottlenecks restricting colony formation and their relief upon culture adaptation. *Stem Cell Reports,* 3**,** 142-55.

BARPE, D. R., ROSA, D. D. & FROEHLICH, P. E. 2010. Pharmacokinetic evaluation of doxorubicin plasma levels in normal and overweight patients with breast cancer and simulation of dose adjustment by different indexes of body mass. *Eur J Pharm Sci,* 41**,** 458-63.

BARTEL, D. P. 2009. MicroRNAs: target recognition and regulatory functions. *Cell,* 136**,** 215-33.

BELLAMY, V., VANNEAUX, V., BEL, A., NEMETALLA, H., EMMANUELLE BOITARD, S., FAROUZ, Y., JOANNE, P., PERIER, M. C., ROBIDEL, E., MANDET, C., HAGEGE, A., BRUNEVAL, P., LARGHERO, J., AGBULUT, O. & MENASCHE, P. 2015. Long-term functional benefits of human embryonic stem cell-derived cardiac progenitors embedded into a fibrin scaffold. *J Heart Lung Transplant,* 34**,** 1198-207.

BEN-DAVID, U. & BENVENISTY, N. 2011. The tumorigenicity of human embryonic and induced pluripotent stem cells. *Nat Rev Cancer,* 11**,** 268-77.

BERSELL, K., ARAB, S., HARING, B. & KUHN, B. 2009. Neuregulin1/ErbB4 signaling induces cardiomyocyte proliferation and repair of heart injury. *Cell,* 138**,** 257-70.

BIRKET, M. J., RIBEIRO, M. C., KOSMIDIS, G., WARD, D., LEITOGUINHO, A. R., VAN DE POL, V., DAMBROT, C., DEVALLA, H. D., DAVIS, R. P., MASTROBERARDINO, P. G., ATSMA, D. E., PASSIER, R. & MUMMERY, C. L. 2015. Contractile Defect Caused by Mutation in MYBPC3 Revealed under Conditions Optimized for Human PSC-Cardiomyocyte Function. *Cell Rep,* 13**,** 733-45.

BONDUE, A. & BLANPAIN, C. 2010. Mesp1: a key regulator of cardiovascular lineage commitment. *Circ Res,* 107**,** 1414-27.

BRAAM, S. R., TERTOOLEN, L., VAN DE STOLPE, A., MEYER, T., PASSIER, R. & MUMMERY, C. L. 2010. Prediction of drug-induced cardiotoxicity using

human embryonic stem cell-derived cardiomyocytes. *Stem Cell Res,* 4**,** 107-16.

BRAUCHLE, E., THUDE, S., BRUCKER, S. Y. & SCHENKE-LAYLAND, K. 2014. Cell death stages in single apoptotic and necrotic cells monitored by Raman microspectroscopy. *Sci Rep,* 4**,** 4698.

BRIGGS, R. & KING, T. 1952. Transplantation Of Living Nuclei From Blastula Cells Into Enucleated Frogs' Eggs. *Proc Natl Acad Sci U S A,* 38**,** 455-463.

BROWER, V. 2013. BioTime acquires Geron's stem cell program. *Nat Biotechnol,* 31**,** 94.

BURRIDGE, P. W., ANDERSON, D., PRIDDLE, H., BARBADILLO MUNOZ, M. D., CHAMBERLAIN, S., ALLEGRUCCI, C., YOUNG, L. E. & DENNING, C. 2007. Improved human embryonic stem cell embryoid body homogeneity and cardiomyocyte differentiation from a novel V-96 plate aggregation system highlights interline variability. *Stem Cells,* 25**,** 929-38.

BURRIDGE, P. W., KELLER, G., GOLD, J. D. & WU, J. C. 2012. Production of de novo cardiomyocytes: human pluripotent stem cell differentiation and direct reprogramming. *Cell Stem Cell,* 10**,** 16-28.

BURRIDGE, P. W., MATSA, E., SHUKLA, P., LIN, Z. C., CHURKO, J. M., EBERT, A. D., LAN, F., DIECKE, S., HUBER, B., MORDWINKIN, N. M., PLEWS, J. R., ABILEZ, O. J., CUI, B., GOLD, J. D. & WU, J. C. 2014. Chemically defined generation of human cardiomyocytes. *Nat Methods,* 11**,** 855-60.

BURRIDGE, P. W., THOMPSON, S., MILLROD, M. A., WEINBERG, S., YUAN, X., PETERS, A., MAHAIRAKI, V., KOLIATSOS, V. E., TUNG, L. & ZAMBIDIS, E. T. 2011. A universal system for highly efficient cardiac differentiation of human induced pluripotent stem cells that eliminates interline variability. *PLoS One,* 6**,** e18293.

BUSTAMANTE, J., WATANABE, T., MURPHY, D. & MCDONALD, T. 1982. Isolation of single atrial and ventricular cells from the human heart. *CMA Journal,* 126.

CAPRANICO, G., TINELLI, S., AUSTIN, C., FISHER, M. & ZUNINO, F. 1992. Different patterns of gene expression of topoisomerase II isoforms in differentiated tissues during murine development. *Biochimica et Biophysica Acta,* 1132**,** 43-48.

CARDINALE, D., COLOMBO, A., BACCHIANI, G., TEDESCHI, I., MERONI, C. A., VEGLIA, F., CIVELLI, M., LAMANTIA, G., COLOMBO, N., CURIGLIANO, G., FIORENTINI, C. & CIPOLLA, C. M. 2015. Early detection of anthracycline cardiotoxicity and improvement with heart failure therapy. *Circulation,* 131**,** 1981-8.

CASPI, O., HUBER, I., GEPSTEIN, A., ARBEL, G., MAIZELS, L., BOULOS, M. & GEPSTEIN, L. 2013. Modeling of Arrhythogenic Right Ventricular Cardiomyopathy With Human Induced Pluripotent Stem Cells. *Ciculation Cardiovascular Genetics,* 6**,** 557-568.

CELIZ, A. D., SMITH, J. G., PATEL, A. K., HOOK, A. L., RAJAMOHAN, D., GEORGE, V. T., FLATT, L., PATEL, M. J., EPA, V. C., SINGH, T., LANGER, R., ANDERSON, D. G., ALLEN, N. D., HAY, D. C., WINKLER, D. A., BARRETT, D. A., DAVIES, M. C., YOUNG, L. E., DENNING, C. & ALEXANDER, M. R. 2015. Discovery of a Novel Polymer for Human Pluripotent Stem Cell Expansion and Multilineage Differentiation. *Adv Mater,* 27**,** 4006-12.

CELLULAR DYNAMICS INTERNATIONAL 2015a. Assaying Caspase Activity and Apoptosis Application Note.

CELLULAR DYNAMICS INTERNATIONAL 2015b. Assaying Cytotoxicity Application Note.

CHEN, G., GULBRANSON, D. R., HOU, Z., BOLIN, J. M., RUOTTI, V., PROBASCO, M. D., SMUGA-OTTO, K., HOWDEN, S. E., DIOL, N. R., PROPSON, N. E., WAGNER, R., LEE, G. O., ANTOSIEWICZ-BOURGET, J., TENG, J. M. & THOMSON, J. A. 2011. Chemically defined conditions for human iPSC derivation and culture. *Nat Methods,* 8**,** 424-9.

CHEN, N.-T., WU, C.-Y., CHUNG, C.-Y., HWU, Y., CHENG, S.-H., MOU, C.-Y. & LO, L.-W. 2012. Probing the dynamics of doxorubicin-DNA intercalation during the initial activation of apoptosis by fluorescence lifetime imaging microscopy (FLIM).

CHETTY, S., PAGLIUCA, F. W., HONORE, C., KWEUDJEU, A., REZANIA, A. & MELTON, D. A. 2013. A simple tool to improve pluripotent stem cell differentiation. *Nat Methods,* 10**,** 553-6.

CHONG, J. J., YANG, X., DON, C. W., MINAMI, E., LIU, Y. W., WEYERS, J. J., MAHONEY, W. M., VAN BIBER, B., COOK, S. M., PALPANT, N. J., GANTZ, J. A., FUGATE, J. A., MUSKHELI, V., GOUGH, G. M., VOGEL, K. W., ASTLEY, C. A., HOTCHKISS, C. E., BALDESSARI, A., PABON, L., REINECKE, H., GILL, E. A., NELSON, V., KIEM, H. P., LAFLAMME, M. A. & MURRY, C. E. 2014. Human embryonic-stem-cell-derived cardiomyocytes regenerate non-human primate hearts. *Nature,* 510**,** 273-7.

CHOO, A., PADMANABHAN, J., CHIN, A., FONG, W. J. & OH, S. K. 2006. Immortalized feeders for the scale-up of human embryonic stem cells in feeder and feeder-free conditions. *J Biotechnol,* 122**,** 130-41.

CHUNG, Y. G., EUM, J. H., LEE, J. E., SHIM, S. H., SEPILIAN, V., HONG, S. W., LEE, Y., TREFF, N. R., CHOI, Y. H., KIMBREL, E. A., DITTMAN, R. E., LANZA, R. & LEE, D. R. 2014. Human somatic cell nuclear transfer using adult cells. *Cell Stem Cell,* 14**,** 777-80.

COLOMBO, A., MERONI, C. A., CIPOLLA, C. M. & CARDINALE, D. 2013. Managing cardiotoxicity of chemotherapy. *Curr Treat Options Cardiovasc Med,* 15**,** 410-24.

CONSORTIUM, H. D. I. 2012. Induced pluripotent stem cells from patients with Huntington's disease show CAG-repeat-expansion-associated phenotypes. *Cell Stem Cell,* 11**,** 264-78.

CONWAY, M., GERGER, M., BALAY, E., O'CONNELL, R., HANSON, S., DAILY, N. & WAKATSUKI, T. 2015. Scalable 96-well Plate Based iPSC Culture and Production Using a Robotic Liquid Handling System. *J Vis Exp*.

COWAN, C., KLIMANSKAYA, I., MCMAHON, J., ATIENZA, J., WITMYER, J., ZUCKER, J., WANG, S., MORTON, C., MCMAHON, A., POWERS, D. & MELTON, D. 2004. Derivation of Embryonic Stem-Cell Lines from Human Blastocysts. *New England Journal of Medicine,* 350.

CZABOTAR, P. E., LESSENE, G., STRASSER, A. & ADAMS, J. M. 2014. Control of apoptosis by the BCL-2 protein family: implications for physiology and therapy. *Nat Rev Mol Cell Biol,* 15**,** 49-63.

DE ALMEIDA, P. E., MEYER, E. H., KOOREMAN, N. G., DIECKE, S., DEY, D., SANCHEZ-FREIRE, V., HU, S., EBERT, A., ODEGAARD, J., MORDWINKIN, N. M., BROUWER, T. P., LO, D., MONTORO, D. T., LONGAKER, M. T., NEGRIN, R. S. & WU, J. C. 2014. Transplanted terminally differentiated induced pluripotent stem cells are accepted by immune mechanisms similar to self-tolerance. *Nat Commun,* 5**,** 3903.

DE ALMEIDA, P. E., RANSOHOFF, J. D., NAHID, A. & WU, J. C. 2013. Immunogenicity of pluripotent stem cells and their derivatives. *Circ Res,* 112**,** 549-61.

DEAVALL, D. G., MARTIN, E. A., HORNER, J. M. & ROBERTS, R. 2012. Drug-induced oxidative stress and toxicity. *J Toxicol,* 2012**,** 645460.

DENNING, C., ALLEGRUCCI, C., PRIDDLE, H., BARBADILLO-MUNOZ, M. D., ANDERSON, D., SELF, T., SMITH, N. M., PARKIN, C. T. & YOUNG, L. E. 2006. Common culture conditions for maintenance and cardiomyocyte differentiation of the human embryonic stem cell lines, BG01 and HUES-7. *Int J Dev Biol,* 50**,** 27-37.

DI, X., GENNINGS, C., BEAR, H. D., GRAHAM, L. J., SHETH, C. M., WHITE, K. L., JR. & GEWIRTZ, D. A. 2010. Influence of the phosphodiesterase-5 inhibitor, sildenafil, on sensitivity to chemotherapy in breast tumor cells. *Breast Cancer Res Treat,* 124**,** 349-60.

DRUKKER, M., KATCHMAN, H., KATZ, G., EVEN-TOV FRIEDMAN, S., SHEZEN, E., HORNSTEIN, E., MANDELBOIM, O., REISNER, Y. & BENVENISTY, N. 2006. Human embryonic stem cells and their differentiated derivatives are less susceptible to immune rejection than adult cells. *Stem Cells,* 24**,** 221-9.

DULIN, B. & ABRAHAM, W. T. 2004. Pharmacology of carvedilol. *Am J Cardiol,* 93**,** 3B-6B.

DUNAI, Z., IMRE, G., BARNA, G., KORCSMAROS, T., PETAK, I., BAUER, P. & MIHALIK, R. 2012. Staurosporine induces necroptotic cell death under caspase-compromised conditions in U937 cells. *PLoS One,* 7.

EDER, A., VOLLERT, I., HANSEN, A. & ESCHENHAGEN, T. 2015. Human engineered heart tissue as a model system for drug testing. *Adv Drug Deliv Rev*.

ERTRACHT, O., MALKA, A., ATAR, S. & BINAH, O. 2014. The mitochondria as a target for cardioprotection in acute myocardial ischemia. *Pharmacol Ther,* 142**,** 33-40.

EULALIO, A., MANO, M., DAL FERRO, M., ZENTILIN, L., SINAGRA, G., ZACCHIGNA, S. & GIACCA, M. 2012. Functional screening identifies miRNAs inducing cardiac regeneration. *Nature,* 492**,** 376-81.

FERNANDES, S., NAUMOVA, A. V., ZHU, W. Z., LAFLAMME, M. A., GOLD, J. & MURRY, C. E. 2010. Human embryonic stem cell-derived cardiomyocytes engraft but do not alter cardiac remodeling after chronic infarction in rats. *J Mol Cell Cardiol,* 49**,** 941-9.

FISHER, P. W., SALLOUM, F., DAS, A., HYDER, H. & KUKREJA, R. C. 2005. Phosphodiesterase-5 inhibition with sildenafil attenuates cardiomyocyte apoptosis and left ventricular dysfunction in a chronic model of doxorubicin cardiotoxicity. *Circulation,* 111**,** 1601-10.

FRANTZ, S. 2012. Embryonic stem cell pioneer Geron exits field, cuts losses. *Nat Biotechnol,* 30**,** 12-3.

FU, X. 2014. The immunogenicity of cells derived from induced pluripotent stem cells. *Cell Mol Immunol,* 11**,** 14-6.

FUSAKI, N., BAN, H., NISHIYAMA, A., SAEKI, K. & HASEGAWA, M. 2009. Efficient induction of transgene-free human pluripotent stem cells using a vector based on Sendai virus, an RNA virus that does not integrate into the host genome. *Proceedings of the Japan Academy, Series B,* 85**,** 348-362.

GALINDO, C. L., RYZHOV, S. & SAWYER, D. B. 2014. Neuregulin as a heart failure therapy and mediator of reverse remodeling. *Curr Heart Fail Rep,* 11**,** 40-9.

GAO, R., ZHANG, J., CHENG, L., WU, X., DONG, W., YANG, X., LI, T., LIU, X., XU, Y., LI, X. & ZHOU, M. 2010. A Phase II, randomized, double-blind, multicenter, based on standard therapy, placebo-controlled study of the efficacy and safety of recombinant human neuregulin-1 in patients with chronic heart failure. *J Am Coll Cardiol,* 55**,** 1907-14.

GARBERN, J. C. & LEE, R. T. 2013. Cardiac stem cell therapy and the promise of heart regeneration. *Cell Stem Cell,* 12**,** 689-98.

GARDNER, D., SCHOOLCRAFT, W., WAGLEY, L., SCHLENKER, T., STEVENS, J. & J, H. 1998. A prospective randomized trial of blastocyst culture and transfer in in-vitro fertilization. *Human Reproduction,* 13**,** 3434-3440.

GESCHER, A. 2000. Staurosporine analogues - pharmacological toys or useful antitumour agents? *Critical Reviews in Oncology / Hematology,* 34**,** 127-135.

GREGO-BESSA, J., LUNA-ZURITA, L., DEL MONTE, G., BOLOS, V., MELGAR, P., ARANDILLA, A., GARRATT, A. N., ZANG, H., MUKOUYAMA, Y. S., CHEN, H., SHOU, W., BALLESTAR, E., ESTELLER, M., ROJAS, A., PEREZ-POMARES, J. M. & DE LA POMPA, J. L. 2007. Notch signaling is essential for ventricular chamber development. *Dev Cell,* 12**,** 415-29.

GUHA, P., MORGAN, J. W., MOSTOSLAVSKY, G., RODRIGUES, N. P. & BOYD, A. S. 2013. Lack of immune response to differentiated cells derived from syngeneic induced pluripotent stem cells. *Cell Stem Cell,* 12**,** 407-12.

GURDON, J., ELSDALE, T. & FISCHBERG, M. 1958. Sexually Mature Individuals of Xenopus laevis from the Transplantation of Single Somatic Nuclei. *Nature,* 182**,** 64,65.

GURDON, J. B. 2016. Nuclear reprogramming and cell replacement therapies. *Nature Reviews Molecular Cell Biology,* 17**,** 137-138.

HALLEY-STOTT, R. P., PASQUE, V. & GURDON, J. B. 2013. Nuclear reprogramming. *Development,* 140**,** 2468-71.

HEALLEN, T., MORIKAWA, Y., LEACH, J., TAO, G., WILLERSON, J. T., JOHNSON, R. L. & MARTIN, J. F. 2013. Hippo signaling impedes adult heart regeneration. *Development,* 140**,** 4683-90.

HEKKALA, A. M., VIITASALO, M., VAANANEN, H., SWAN, H. & TOIVONEN, L. 2010. Abnormal repolarization dynamics revealed in exercise test in long QT syndrome mutation carriers with normal resting QT interval. *Europace,* 12**,** 1296-301.

HENAFF, M., HATEM, S. & MERCADIER, J.-J. 2000. Low Catecholamine Concentrations Protect Adult Rat Ventricular Myocytes against Apoptosis through cAMP-Dependent Extracellular Signal-Regulated Kinase Activation. *Molecular Pharmacology,* 58**,** 1546-1553.

HERPER, M. 2012. The Truly Staggering Cost Of Inventing New Drugs. *Forbes*.

HOCHEDLINGER, K. & JAENISCH, R. 2006. Nuclear reprogramming and pluripotency. *Nature,* 441**,** 1061-7.

HOLMGREN, G., SYNNERGREN, J., BOGESTAL, Y., AMEEN, C., AKESSON, K., HOLMGREN, S., LINDAHL, A. & SARTIPY, P. 2015. Identification of novel biomarkers for doxorubicin-induced toxicity in human cardiomyocytes derived from pluripotent stem cells. *Toxicology,* 328**,** 102-11.

HUSSAIN, W., MOENS, N., VERAITCH, F. S., HERNANDEZ, D., MASON, C. & LYE, G. J. 2013. Reproducible culture and differentiation of mouse embryonic stem cells using an automated microwell platform. *Biochem Eng J,* 77**,** 246-257.

ITSKOVITZ-ELDOR, J., SCHULDINER, M., KARSENTI, D., EDEN, A., YANUKA, O., AMIT, M., SOREQ, H. & BENVENISTY, N. 2000. Differentiation of Human Embryonic Stem Cells into Embryoid Bodies Comprising the Three Embryonic Germ Layers. *Molecular Medicine,* 6**,** 88-95.

ITZHAKI, I., MAIZELS, L., HUBER, I., ZWI-DANTSIS, L., CASPI, O., WINTERSTERN, A., FELDMAN, O., GEPSTEIN, A., ARBEL, G., HAMMERMAN, H., BOULOS, M. & GEPSTEIN, L. 2011. Modelling the long QT syndrome with induced pluripotent stem cells. *Nature,* 471**,** 225-9.

JABBOUR, A., HAYWARD, C. S., KEOGH, A. M., KOTLYAR, E., MCCROHON, J. A., ENGLAND, J. F., AMOR, R., LIU, X., LI, X. Y., ZHOU, M. D., GRAHAM, R. M. & MACDONALD, P. S. 2011. Parenteral administration of recombinant human neuregulin-1 to patients with stable chronic heart failure produces favourable acute and chronic haemodynamic responses. *Eur J Heart Fail,* 13**,** 83-92.

JIA, F., WILSON, K. D., SUN, N., GUPTA, D. M., HUANG, M., LI, Z., PANETTA, N. J., CHEN, Z. Y., ROBBINS, R. C., KAY, M. A., LONGAKER, M. T. & WU, J. C. 2010. A nonviral minicircle vector for deriving human iPS cells. *Nat Methods,* 7**,** 197-9.

JIN, Z. B., OKAMOTO, S., XIANG, P. & TAKAHASHI, M. 2012. Integration-free induced pluripotent stem cells derived from retinitis pigmentosa patient for disease modeling. *Stem Cells Transl Med,* 1**,** 503-9.

JOPLING, C., SLEEP, E., RAYA, M., MARTI, M., RAYA, A. & IZPISUA BELMONTE, J. C. 2010. Zebrafish heart regeneration occurs by cardiomyocyte dedifferentiation and proliferation. *Nature,* 464**,** 606-9.

JOUNI, M., SI-TAYEB, K., ES-SALAH-LAMOUREUX, Z., LATYPOVA, X., CHAMPON, B., CAILLAUD, A., RUNGOAT, A., CHARPENTIER, F., LOUSSOUARN, G., BARO, I., ZIBARA, K., LEMARCHAND, P. & GABORIT, N. 2015. Toward Personalized Medicine: Using Cardiomyocytes Differentiated From Urine-Derived Pluripotent Stem Cells to Recapitulate Electrophysiological Characteristics of Type 2 Long QT Syndrome. *J Am Heart Assoc,* 4**,** e002159.

JOZEFCZUK, J., DREWS, K. & ADJAYE, J. 2012. Preparation of mouse embryonic fibroblast cells suitable for culturing human embryonic and induced pluripotent stem cells. *J Vis Exp*.

KAKKAR, A. K. 2015. Patent cliff mitigation strategies: giving new life to blockbusters. *Expert Opin Ther Pat***,** 1-4.

KALAY, N., BASAR, E., OZDOGRU, I., ER, O., CETINKAYA, Y., DOGAN, A., INANC, T., OGUZHAN, A., ERYOL, N. K., TOPSAKAL, R. & ERGIN, A. 2006. Protective

effects of carvedilol against anthracycline-induced cardiomyopathy. *J Am Coll Cardiol,* 48**,** 2258-62.

KEMPF, H., OLMER, R., KROPP, C., RUCKERT, M., JARA-AVACA, M., ROBLES-DIAZ, D., FRANKE, A., ELLIOTT, D. A., WOJCIECHOWSKI, D., FISCHER, M., ROA LARA, A., KENSAH, G., GRUH, I., HAVERICH, A., MARTIN, U. & ZWEIGERDT, R. 2014. Controlling expansion and cardiomyogenic differentiation of human pluripotent stem cells in scalable suspension culture. *Stem Cell Reports,* 3**,** 1132-46.

KER, D. F., WEISS, L. E., JUNKERS, S. N., CHEN, M., YIN, Z., SANDBOTHE, M. F., HUH, S. I., EOM, S., BISE, R., OSUNA-HIGHLEY, E., KANADE, T. & CAMPBELL, P. G. 2011. An engineered approach to stem cell culture: automating the decision process for real-time adaptive subculture of stem cells. *PLoS One,* 6**,** e27672.

KERNS, E. 2003. Pharmaceutical profiling in drug discovery. *Drug Discovery Today,* 8**,** 316-323.

KERR, J., WYLLIE, A. & CURRIE, A. 1972. Apoptosis: A Basic Biological Phenomenon With Wide-Ranging Implications in Tissue Kinetics. *British Journal of Cancer,* 26**,** 239-257.

KHAN, M., MOHSIN, S., AVITABILE, D., SIDDIQI, S., NGUYEN, J., WALLACH, K., QUIJADA, P., MCGREGOR, M., GUDE, N., ALVAREZ, R., TILLEY, D. G., KOCH, W. J. & SUSSMAN, M. A. 2013. beta-Adrenergic regulation of cardiac progenitor cell death versus survival and proliferation. *Circ Res,* 112**,** 476-86.

KIKUCHI, K., HOLDWAY, J. E., WERDICH, A. A., ANDERSON, R. M., FANG, Y., EGNACZYK, G. F., EVANS, T., MACRAE, C. A., STAINIER, D. Y. & POSS, K. D. 2010. Primary contribution to zebrafish heart regeneration by gata4(+) cardiomyocytes. *Nature,* 464**,** 601-5.

KIM, D., KIM, C. H., MOON, J. I., CHUNG, Y. G., CHANG, M. Y., HAN, B. S., KO, S., YANG, E., CHA, K. Y., LANZA, R. & KIM, K. S. 2009. Generation of human induced pluripotent stem cells by direct delivery of reprogramming proteins. *Cell Stem Cell,* 4**,** 472-6.

KOWALSKI, M. P., YODER, A., LIU, L. & PAJAK, L. 2012. Controlling embryonic stem cell growth and differentiation by automation: enhanced and more reliable differentiation for drug discovery. *J Biomol Screen,* 17**,** 1171-9.

KRAMMER, P. H., ARNOLD, R. & LAVRIK, I. N. 2007. Life and death in peripheral T cells. *Nat Rev Immunol,* 7**,** 532-42.

KWON, C., QIAN, L., CHENG, P., NIGAM, V., ARNOLD, J. & SRIVASTAVA, D. 2009. A regulatory pathway involving Notch1/beta-catenin/Isl1 determines cardiac progenitor cell fate. *Nat Cell Biol,* 11**,** 951-7.

LAFLAMME, M. A., CHEN, K. Y., NAUMOVA, A. V., MUSKHELI, V., FUGATE, J. A., DUPRAS, S. K., REINECKE, H., XU, C., HASSANIPOUR, M., POLICE, S., O'SULLIVAN, C., COLLINS, L., CHEN, Y., MINAMI, E., GILL, E. A., UENO, S., YUAN, C., GOLD, J. & MURRY, C. E. 2007. Cardiomyocytes derived from human embryonic stem cells in pro-survival factors enhance function of infarcted rat hearts. *Nat Biotechnol,* 25**,** 1015-24.

LAFLAMME, M. A. & MURRY, C. E. 2011. Heart regeneration. *Nature,* 473**,** 326-35.

LECINA, M., TING, S., CHOO, A., REUVENY, S. & OH, S. 2010. Scalable platform for human embryonic stem cell differentiation to cardiomyocytes in suspended microcarrier cultures. *Tissue Eng Part C Methods,* 16**,** 1609-19.

LEFRAK, E., PITHA, J., ROSENHEIM, S. & GOTTLIEB, J. 1973. A clinicopathologic analysis of adriamycin cardiotoxicity. *Cancer,* 32**,** 302-314.

LI L, BAROJA ML, MAJUMDAR A, CHADWICK K, ROULEAU A, GALLACHER L, FERBER I, LEBKOWSKI J, MARTIN T, MADRENAS J & M., B. 2004. Human embryonic stem cells possess immune-privileged properties. *Science,* 22**,** 448-456.

LIAN, X., HSIAO, C., WILSON, G., ZHU, K., HAZELTINE, L., AZARIN, S., RAVAL, K., ZHANG, J., KAMP, T. & PALECEK, S. 2012. Robust cardiomyocyte differentiation from human pluripotent stem cells via temporal modulation of canonical Wnt signaling. *PNAS,* 109**,** 1848-1857.

LIAN, X., ZHANG, J., AZARIN, S. M., ZHU, K., HAZELTINE, L. B., BAO, X., HSIAO, C., KAMP, T. J. & PALECEK, S. P. 2013. Directed cardiomyocyte differentiation from human pluripotent stem cells by modulating Wnt/beta-catenin signaling under fully defined conditions. *Nat Protoc,* 8**,** 162-75.

LIFE-TECHNOLOGIES 2011. CellEvent™ Caspase 3/7 Green Detection Reagent Catalogue number C10423.

LIN, B., LI, Y., HAN, L., KAPLAN, A. D., AO, Y., KALRA, S., BETT, G. C., RASMUSSON, R. L., DENNING, C. & YANG, L. 2015. Modeling and study of the mechanism of dilated cardiomyopathy using induced pluripotent stem cells derived from individuals with Duchenne muscular dystrophy. *Dis Model Mech,* 8**,** 457-66.

LIPSHULTZ, S. E., RIFAI, N., DALTON, V. M., LEVY, D. E., SILVERMAN, L. B., LIPSITZ, S. R., COLAN, S. D., ASSELIN, B. L., BARR, R. D. & CLAVELL, L. A. 2004. The effect of dexrazoxane on myocardial injury in doxorubicin-treated children with acute lymphoblastic leukemia. *New England Journal of Medicine,* 351**,** 145-153.

LIPSHULTZ, S. E., SAMBATAKOS, P., MAGUIRE, M., KARNIK, R., ROSS, S. W., FRANCO, V. I. & MILLER, T. L. 2014. Cardiotoxicity and cardioprotection in childhood cancer. *Acta Haematol,* 132**,** 391-9.

LIU, N., ZANG, R., YANG, S.-T. & LI, Y. 2014. Stem cell engineering in bioreactors for large-scale bioprocessing. *Engineering in Life Sciences,* 14**,** 4-15.

LOHSE, M. J., ENGELHARDT, S. & ESCHENHAGEN, T. 2003. What is the role of beta-adrenergic signaling in heart failure? *Circ Res,* 93**,** 896-906.

LU, H., WHITTAKER, R., PRICE, J., VEGA, R., PFEIFFER, E., CERIGNOLI, F., R, T. & GALLACHER, D. 2015. High throughput measurement of Ca++ dynamics in human stem cell-derived cardiomyocytes by kinetic image cytometery: a cardiac risk assessment characterization using a large panel of cardioactive and inactive compounds. *Toxicological Sciences,* EPub ahead of print.

LUDWIG, T. E., BERGENDAHL, V., LEVENSTEIN, M. E., YU, J., PROBASCO, M. D. & THOMSON, J. A. 2006a. Feeder-independent culture of human embryonic stem cells. *Nat Methods,* 3**,** 637-46.

LUDWIG, T. E., LEVENSTEIN, M. E., JONES, J. M., BERGGREN, W. T., MITCHEN, E. R., FRANE, J. L., CRANDALL, L. J., DAIGH, C. A., CONARD, K. R., PIEKARCZYK, M. S., LLANAS, R. A. & THOMSON, J. A. 2006b. Derivation of human embryonic stem cells in defined conditions. *Nat Biotechnol,* 24**,** 185-7.

LYU, Y. L., KERRIGAN, J. E., LIN, C. P., AZAROVA, A. M., TSAI, Y. C., BAN, Y. & LIU, L. F. 2007. Topoisomerase IIbeta mediated DNA double-strand breaks: implications in doxorubicin cardiotoxicity and prevention by dexrazoxane. *Cancer Res,* 67**,** 8839-46.

MA, D., WEI, H., ZHAO, Y., LU, J., LI, G., SAHIB, N. B., TAN, T. H., WONG, K. Y., SHIM, W., WONG, P., COOK, S. A. & LIEW, R. 2013. Modeling type 3 long QT syndrome with cardiomyocytes derived from patient-specific induced pluripotent stem cells. *Int J Cardiol,* 168**,** 5277-86.

MALAN, D., ZHANG, M., STALLMEYER, B., MULLER, J., FLEISCHMANN, B. K., SCHULZE-BAHR, E., SASSE, P. & GREBER, B. 2016. Human iPS cell model of type 3 long QT syndrome recapitulates drug-based phenotype correction. *Basic Res Cardiol,* 111**,** 14.

MASON-PIVET, M., JONGSMA, H. & BRUIJNE, J. 1976. Collagenase and Trypsin Dissociated heart cells: A comparative Ultrstructural Study. *Journal of molecular and cellular cardiology,* 8**,** 747-757.

MATSA, E., DIXON, J. E., MEDWAY, C., GEORGIOU, O., PATEL, M. J., MORGAN, K., KEMP, P. J., STANIFORTH, A., MELLOR, I. & DENNING, C. 2014. Allele-specific RNA interference rescues the long-QT syndrome phenotype in human-induced pluripotency stem cell cardiomyocytes. *Eur Heart J,* 35**,** 1078-87.

MATSA, E., RAJAMOHAN, D., DICK, E., YOUNG, L., MELLOR, I., STANIFORTH, A. & DENNING, C. 2011. Drug evaluation in cardiomyocytes derived from human induced pluripotent stem cells carrying a long QT syndrome type 2 mutation. *Eur Heart J,* 32**,** 952-62.

MATSUURA, K., WADA, M., SHIMIZU, T., HARAGUCHI, Y., SATO, F., SUGIYAMA, K., KONISHI, K., SHIBA, Y., ICHIKAWA, H., TACHIBANA, A., IKEDA, U., YAMATO, M., HAGIWARA, N. & OKANO, T. 2012. Creation of human cardiac cell sheets using pluripotent stem cells. *Biochem Biophys Res Commun,* 425**,** 321-7.

MCSTAY, G. P. & GREEN, D. R. 2014. Measuring apoptosis: caspase inhibitors and activity assays. *Cold Spring Harb Protoc,* 2014**,** 799-806.

MEDEIROS-DOMINGO, A., ITURRALDE-TORRES, P. & ACKERMAN, M. J. 2007. Clinical and Genetic Characteristics of Long QT Syndrome. *Revista Espanola De Cardiologia,* 60**,** 739-752.

MEI, Y., SAHA, K., BOGATYREV, S., YANG, J., HOOK, A., KALCIOGLU, Z., CHO, S.-W., MITALIPOVA, M., PYZOCHA, N., ROJAS, F., VAN VLIET, K., DAVIES, M., ALEXANDER, M., LANGER, R. & ANDERSON, D. 2010. Combinatorial development of biomaterials for clonal growth of human pluripotent stem cells. *Nature Materials,* 9.

MENASCHE, P., VANNEAUX, V., FABREGUETTES, J. R., BEL, A., TOSCA, L., GARCIA, S., BELLAMY, V., FAROUZ, Y., POULY, J., DAMOUR, O., PERIER, M. C., DESNOS, M., HAGEGE, A., AGBULUT, O., BRUNEVAL, P., TACHDJIAN, G., TROUVIN, J. H. & LARGHERO, J. 2015a. Towards a clinical use of human embryonic stem cell-derived cardiac progenitors: a translational experience. *Eur Heart J,* 36**,** 743-50.

MENASCHE, P., VANNEAUX, V., HAGEGE, A., BEL, A., CHOLLEY, B., CACCIAPUOTI, I., PAROUCHEV, A., BENHAMOUDA, N., TACHDJIAN, G., TOSCA, L., TROUVIN, J. H., FABREGUETTES, J. R., BELLAMY, V., GUILLEMAIN, R., SUBERBIELLE BOISSEL, C., TARTOUR, E., DESNOS, M. & LARGHERO, J. 2015b. Human embryonic stem cell-derived cardiac progenitors for severe heart failure treatment: first clinical case report. *Eur Heart J,* 36**,** 2011-7.

MINOTTI, G., SALVATORELLI, E. & MENNA, P. 2010. Pharmacological foundations of cardio-oncology. *J Pharmacol Exp Ther,* 334**,** 2-8.

MIYOSHI, N., ISHII, H., NAGANO, H., HARAGUCHI, N., DEWI, D. L., KANO, Y., NISHIKAWA, S., TANEMURA, M., MIMORI, K., TANAKA, F., SAITO, T., NISHIMURA, J., TAKEMASA, I., MIZUSHIMA, T., IKEDA, M., YAMAMOTO, H., SEKIMOTO, M., DOKI, Y. & MORI, M. 2011. Reprogramming of mouse and human cells to pluripotency using mature microRNAs. *Cell Stem Cell,* 8**,** 633-8.

MOHR, J. C., ZHANG, J., AZARIN, S. M., SOERENS, A. G., DE PABLO, J. J., THOMSON, J. A., LYONS, G. E., PALECEK, S. P. & KAMP, T. J. 2010. The microwell control of embryoid body size in order to regulate cardiac differentiation of human embryonic stem cells. *Biomaterials,* 31**,** 1885-93.

MOLLOVA, M., BERSELL, K., WALSH, S., SAVLA, J., DAS, L., PARK, S., SILBERSTEIN, L., DOS REMEDIOS, C., GRAHAM, D., COLAN, S. & KÜHN, B. 2013. Cardiomyocyte proliferation contributes to heart growth in young humans. *PNAS,* 110**,** 1446-1451.

MORETTI, A., BELLIN, M., WELLING, A., JUNG, C. B., LAM, J. T., BOTT-FLUGEL, L., DORN, T., GOEDEL, A., HOHNKE, C., HOFMANN, F., SEYFARTH, M., SINNECKER, D., SCHOMIG, A. & LAUGWITZ, K.-L. 2010. Patient-Specific Induced Pluripotent Stem-Cell Models for Long-QT Syndrome. *The New England Journal of Medicine,* 363**,** 1397-1409.

MOU, C., GANJU, N., SRIDHAR, K. S. & KRISHAN, A. 1997. Simultaneous quantitation of plasma doxorubicin and prochlorperazine content by high-performance liquid chromatography. *Journal of Chromatography B: Biomedical Sciences and Applications,* 703**,** 217-224.

MURATORE, C. R., RICE, H. C., SRIKANTH, P., CALLAHAN, D. G., SHIN, T., BENJAMIN, L. N., WALSH, D. M., SELKOE, D. J. & YOUNG-PEARSE, T. L. 2014. The familial Alzheimer's disease APPV717I mutation alters APP processing and Tau expression in iPSC-derived neurons. *Hum Mol Genet,* 23**,** 3523-36.

MURRY, C. E., CHONG, J. J. & LAFLAMME, M. A. 2014. Letter by Murry et al regarding article, "Embryonic stem cell-derived cardiac myocytes are not ready for human trials". *Circ Res,* 115**,** e28-9.

MURRY, C. E., REINECKE, H. & PABON, L. M. 2006. Regeneration gaps: observations on stem cells and cardiac repair. *J Am Coll Cardiol,* 47**,** 1777-85.

NAKAGAWA, M., TANIGUCHI, Y., SENDA, S., TAKIZAWA, N., ICHISAKA, T., ASANO, K., MORIZANE, A., DOI, D., TAKAHASHI, J., NISHIZAWA, M., YOSHIDA, Y., TOYODA, T., OSAFUNE, K., SEKIGUCHI, K. & YAMANAKA, S. 2014. A novel efficient feeder-free culture system for the derivation of human induced pluripotent stem cells. *Sci Rep,* 4**,** 3594.

NAPOLITANO, C., BLOISE, R., MONTEFORTE, N. & PRIORI, S. G. 2012. Sudden cardiac death and genetic ion channelopathies: long QT, Brugada, short QT, catecholaminergic polymorphic ventricular tachycardia, and idiopathic ventricular fibrillation. *Circulation,* 125**,** 2027-34.

NICHOLS, D. J., MUIRHEAD, G. J. & HARNESS, J. A. 2002. Pharmacokinetics of sildenafil after single oral doses in healthy male subjects: absolute bioavailability, food effects and dose proportionality. *British journal of clinical pharmacology,* 53**,** 5S-12S.

NICOLETTI, I., MIGLIORATI, G., PAGLIACCI, M., GRIGNANI, F. & RICCARDI, C. 1991. A rapid and simple method for measuring thymocyte apoptosis by propidium

iodide staining and flow cytometry. *Journal of Immunological Methods,* 139**,** 271-279.

NUSSBAUM, J., MINAMI, E., LAFLAMME, M. A., VIRAG, J. A., WARE, C. B., MASINO, A., MUSKHELI, V., PABON, L., REINECKE, H. & MURRY, C. E. 2007. Transplantation of undifferentiated murine embryonic stem cells in the heart: teratoma formation and immune response. *FASEB J,* 21**,** 1345-57.

OKITA, K., NAKAGAWA, M., HYENJONG, H., ICHISAKA, T. & YAMANAKA, S. 2008. Generation of Mouse Induced Pluripotent Stem Cells Without Viral Vectors. *Science,* 322**,** 949-952.

OLMER, R., LANGE, A., SELZER, S., KASPER, C., HAVERICH, A., MARTIN, U. & ZWEIGERDT, R. 2012. Suspension culture of human pluripotent stem cells in controlled, stirred bioreactors. *Tissue Eng Part C Methods,* 18**,** 772-84.

OMURA, S., IWAI, Y., HIRANO, A., NAKAGAWA, A., AWAYA, J., TSUCHIYA, H., TAKAHASHI, Y. & MASUMA, R. 1977. A new alkaloid AM-2282 of *Steptomyces* origin taxonomy, fermentation, isolation and preliminary characterization. *The Journal of Antibiotics,* 30**,** 275-282.

PASCUT, F. C., KALRA, S., GEORGE, V., WELCH, N., DENNING, C. & NOTINGHER, I. 2013. Non-invasive label-free monitoring the cardiac differentiation of human embryonic stem cells in-vitro by Raman spectroscopy. *Biochim Biophys Acta,* 1830**,** 3517-24.

PATEL, A. K., CELIZ, A. D., RAJAMOHAN, D., ANDERSON, D. G., LANGER, R., DAVIES, M. C., ALEXANDER, M. R. & DENNING, C. 2015. A defined synthetic substrate for serum-free culture of human stem cell derived cardiomyocytes with improved functional maturity identified using combinatorial materials microarrays. *Biomaterials,* 61**,** 257-65.

PAULL, D., SEVILLA, A., ZHOU, H., HAHN, A. K., KIM, H., NAPOLITANO, C., TSANKOV, A., SHANG, L., KRUMHOLZ, K., JAGADEESAN, P., WOODARD, C. M., SUN, B., VILBOUX, T., ZIMMER, M., FORERO, E., MOROZIEWICZ, D. N., MARTINEZ, H., MALICDAN, M. C., WEISS, K. A., VENSAND, L. B., DUSENBERRY, C. R., POLUS, H., SY, K. T., KAHLER, D. J., GAHL, W. A., SOLOMON, S. L., CHANG, S., MEISSNER, A., EGGAN, K. & NOGGLE, S. A. 2015. Automated, high-throughput derivation, characterization and differentiation of induced pluripotent stem cells. *Nat Methods,* 12**,** 885-92.

PIETKIEWICZ, S., SCHMIDT, J. H. & LAVRIK, I. N. 2015. Quantification of apoptosis and necroptosis at the single cell level by a combination of Imaging Flow Cytometry with classical Annexin V/propidium iodide staining. *J Immunol Methods,* 423**,** 99-103.

POSS, K., WILSON, L. & KEATING, M. 2002. Heart Regeneration in Zebrafis. *Science,* 298**,** 2188-2190.

POWELL, T., STURRIDGE, M., SUVARNA, S., TERRAR, D. & TWIST, V. 1981. Intact individual heart cells isolated from human ventricular tissue. *British Medical Journal,* 283**,** 1013-1014.

RAJAMOHAN, D., MATSA, E., KALRA, S., CRUTCHLEY, J., PATEL, A., GEORGE, V. & DENNING, C. 2013. Current status of drug screening and disease modelling in human pluripotent stem cells. *Bioessays,* 35**,** 281-98.

RIBEIRO, M. C., TERTOOLEN, L. G., GUADIX, J. A., BELLIN, M., KOSMIDIS, G., D'ANIELLO, C., MONSHOUWER-KLOOTS, J., GOUMANS, M. J., WANG, Y. L.,

FEINBERG, A. W., MUMMERY, C. L. & PASSIER, R. 2015. Functional maturation of human pluripotent stem cell derived cardiomyocytes in vitro--correlation between contraction force and electrophysiology. *Biomaterials,* 51**,** 138-50.

RICHTER, A., VALDIMARSDOTTIR, L., HRAFNKELSDOTTIR, H. E., RUNARSSON, J. F., OMARSDOTTIR, A. R., WARD-VAN OOSTWAARD, D., MUMMERY, C. & VALDIMARSDOTTIR, G. 2014. BMP4 promotes EMT and mesodermal commitment in human embryonic stem cells via SLUG and MSX2. *Stem Cells,* 32**,** 636-48.

ROBINTON, D. A. & DALEY, G. Q. 2012. The promise of induced pluripotent stem cells in research and therapy. *Nature,* 481**,** 295-305.

ROCA-ALONSO, L., CASTELLANO, L., MILLS, A., DABROWSKA, A. F., SIKKEL, M. B., PELLEGRINO, L., JACOB, J., FRAMPTON, A. E., KRELL, J., COOMBES, R. C., HARDING, S. E., LYON, A. R. & STEBBING, J. 2015. Myocardial MiR-30 downregulation triggered by doxorubicin drives alterations in beta-adrenergic signaling and enhances apoptosis. *Cell Death Dis,* 6**,** e1754.

RODIN, S., DOMOGATSKAYA, A., STROM, S., HANSSON, E. M., CHIEN, K. R., INZUNZA, J., HOVATTA, O. & TRYGGVASON, K. 2010. Long-term self-renewal of human pluripotent stem cells on human recombinant laminin-511. *Nat Biotechnol,* 28**,** 611-5.

ROSS, A. M., NANDIVADA, H., RYAN, A. L. & LAHANN, J. 2012. Synthetic substrates for long-term stem cell culture. *Polymer,* 53**,** 2533-2539.

ROWLEY, S. D. & ANDERSON, G. L. 1993. Effect of DMSO exposure without cryopreservation on hematopoietic progenitor cells. *Bone Marrow Transplant,* 11**,** 389-393.

RYAN, S. D., DOLATABADI, N., CHAN, S. F., ZHANG, X., AKHTAR, M. W., PARKER, J., SOLDNER, F., SUNICO, C. R., NAGAR, S., TALANTOVA, M., LEE, B., LOPEZ, K., NUTTER, A., SHAN, B., MOLOKANOVA, E., ZHANG, Y., HAN, X., NAKAMURA, T., MASLIAH, E., YATES, J. R., 3RD, NAKANISHI, N., ANDREYEV, A. Y., OKAMOTO, S., JAENISCH, R., AMBASUDHAN, R. & LIPTON, S. A. 2013. Isogenic human iPSC Parkinson's model shows nitrosative stress-induced dysfunction in MEF2-PGC1alpha transcription. *Cell,* 155**,** 1351-64.

SAGER, P. T., GINTANT, G., TURNER, J. R., PETTIT, S. & STOCKBRIDGE, N. 2014. Rechanneling the cardiac proarrhythmia safety paradigm: a meeting report from the Cardiac Safety Research Consortium. *Am Heart J,* 167**,** 292-300.

SAHARA, M., SANTORO, F. & CHIEN, K. R. 2015. Programming and reprogramming a human heart cell. *EMBO J,* 34**,** 710-38.

SALVATORELLI, E., MENNA, P. & MINOTTI, G. 2015. Managing anthracycline-induced cardiotoxicity: beginning with the end in mind. *Future Cardiology,* 11**,** 363-366.

SCHWARTZ, S. D., REGILLO, C. D., LAM, B. L., ELIOTT, D., ROSENFELD, P. J., GREGORI, N. Z., HUBSCHMAN, J.-P., DAVIS, J. L., HEILWELL, G., SPIRN, M., MAGUIRE, J., GAY, R., BATEMAN, J., OSTRICK, R. M., MORRIS, D., VINCENT, M., ANGLADE, E., DEL PRIORE, L. V. & LANZA, R. 2015. Human embryonic stem cell-derived retinal pigment epithelium in patients with age-related macular degeneration and Stargardt's macular dystrophy: follow-up of two open-label phase 1/2 studies. *The Lancet,* 385**,** 509-516.

SENYO, S. E., LEE, R. T. & KUHN, B. 2014. Cardiac regeneration based on mechanisms of cardiomyocyte proliferation and differentiation. *Stem Cell Res,* 13**,** 532-41.

SERIO, A., NARULA, N., KODAMA, T., FAVALLI, V. & ARBUSTINI, E. 2012. Familial dilated cardiomyopathy. Clinical and genetic characteristics. *Herz,* 37**,** 822-9.

SHIBA, Y., FERNANDES, S., ZHU, W. Z., FILICE, D., MUSKHELI, V., KIM, J., PALPANT, N. J., GANTZ, J., MOYES, K. W., REINECKE, H., VAN BIBER, B., DARDAS, T., MIGNONE, J. L., IZAWA, A., HANNA, R., VISWANATHAN, M., GOLD, J. D., KOTLIKOFF, M. I., SARVAZYAN, N., KAY, M. W., MURRY, C. E. & LAFLAMME, M. A. 2012. Human ES-cell-derived cardiomyocytes electrically couple and suppress arrhythmias in injured hearts. *Nature,* 489**,** 322-5.

SHIGEMIZU, D., AIBA, T., NAKAGAWA, H., OZAKI, K., MIYA, F., SATAKE, W., TODA, T., MIYAMOTO, Y., FUJIMOTO, A., SUZUKI, Y., KUBO, M., TSUNODA, T., SHIMIZU, W. & TANAKA, T. 2015. Exome Analyses of Long QT Syndrome Reveal Candidate Pathogenic Mutations in Calmodulin-Interacting Genes. *PLoS One,* 10**,** e0130329.

SHIMIZU, W., NODA, T., TAKAKI, H., KURITA, T., NAGAYA, N., SATOMI, K., SUYAMA, K., AIHARA, N., KAMAKURA, S., SUNAGAWA, K., ECHIGO, S., NAKAMURA, K., OHE, T., TOWBIN, J. A., NAPOLITANO, C. & PRIORI, S. G. 2003. Epinephrine unmasks latent mutation carriers with LQT1 form of congenital long-QT syndrome. *Journal of the American College of Cardiology,* 41**,** 633-642.

SHIN, S. Y., KIM, T., LEE, H. S., KANG, J. H., LEE, J. Y., CHO, K. H. & KIM DO, H. 2014. The switching role of beta-adrenergic receptor signalling in cell survival or death decision of cardiomyocytes. *Nat Commun,* 5**,** 5777.

SMITH, J. L., ANDERSON, C. L., BRUGESS, D. E., ELAYI, C. S., JANUARY, C. T. & DELISLE, B. P. 2016. Molecular pathogenesis of long QT syndrome type 2. *Journal of Arrhythmia*.

SOARES, F. A., CHANDRA, A., THOMAS, R. J., PEDERSEN, R. A., VALLIER, L. & WILLIAMS, D. J. 2014. Investigating the feasibility of scale up and automation of human induced pluripotent stem cells cultured in aggregates in feeder free conditions. *J Biotechnol,* 173**,** 53-8.

SOMERS, A., JEAN, J. C., SOMMER, C. A., OMARI, A., FORD, C. C., MILLS, J. A., YING, L., SOMMER, A. G., JEAN, J. M., SMITH, B. W., LAFYATIS, R., DEMIERRE, M. F., WEISS, D. J., FRENCH, D. L., GADUE, P., MURPHY, G. J., MOSTOSLAVSKY, G. & KOTTON, D. N. 2010. Generation of transgene-free lung disease-specific human induced pluripotent stem cells using a single excisable lentiviral stem cell cassette. *Stem Cells,* 28**,** 1728-40.

STRAUSS, S. 2010. Geron trial resumes, but standards for stem cell trials remain elusive. *Nat Biotechnol,* 28**,** 989-90.

SUN, N., YAZAWA, M., LIU, J., HAN, L., SANCHEZ-FREIRE, V., ABILEZ, O. J., NAVARRETE, E. G., HU, S., WANG, L., LEE, A., PAVLOVIC, A., LIN, S., CHEN, R., HAJJAR, R. J., SNYDER, M. P., DOLMETSCH, R. E., BUTTE, M. J., ASHLEY, E. A., LONGAKER, M. T., ROBBINS, R. C. & WU, J. C. 2012. Patient-specific induced pluripotent stem cells as a model for familial dilated cardiomyopathy. *Sci Transl Med,* 4**,** 130ra47.

SWAIN, S. M., WHALEY, F. S. & EWER, M. S. 2003. Congestive heart failure in patients treated with doxorubicin: a retrospective analysis of three trials. *Cancer,* 97**,** 2869-79.

SWIJNENBURG, R. J., SCHREPFER, S., GOVAERT, J. A., CAO, F., RANSOHOFF, K., SHEIKH, A. Y., HADDAD, M., CONNOLLY, A. J., DAVIS, M. M., ROBBINS, R. C. & WU, J. C. 2008. Immunosuppressive therapy mitigates immunological rejection of human embryonic stem cell xenografts. *Proc Natl Acad Sci U S A,* 105**,** 12991-6.

SYLVA, M., VAN DEN HOFF, M. J. & MOORMAN, A. F. 2014. Development of the human heart. *Am J Med Genet A,* 164A**,** 1347-71.

TACHIBANA, M., AMATO, P., SPARMAN, M., GUTIERREZ, N. M., TIPPNER-HEDGES, R., MA, H., KANG, E., FULATI, A., LEE, H. S., SRITANAUDOMCHAI, H., MASTERSON, K., LARSON, J., EATON, D., SADLER-FREDD, K., BATTAGLIA, D., LEE, D., WU, D., JENSEN, J., PATTON, P., GOKHALE, S., STOUFFER, R. L., WOLF, D. & MITALIPOV, S. 2013. Human embryonic stem cells derived by somatic cell nuclear transfer. *Cell,* 153**,** 1228-38.

TAKAHASHI, K., TANABE, K., OHNUKI, M., NARITA, M., ICHISAKA, T., TOMODA, K. & YAMANAKA, S. 2007. Induction of pluripotent stem cells from adult human fibroblasts by defined factors. *Cell,* 131**,** 861-72.

TAKAHASHI, K. & YAMANAKA, S. 2006. Induction of pluripotent stem cells from mouse embryonic and adult fibroblast cultures by defined factors. *Cell,* 126**,** 663-76.

THOMAS, R. J., ANDERSON, D., CHANDRA, A., SMITH, N. M., YOUNG, L. E., WILLIAMS, D. & DENNING, C. 2009. Automated, scalable culture of human embryonic stem cells in feeder-free conditions. *Biotechnol Bioeng,* 102**,** 1636-44.

THOMSON, J., ITSKOVITZ-ELDOR, J., SHAPIRO, S., WAKNITZ, M., SWIERGIEL, J., MARSHALL, V. & JONES, J. 1998. Embryonic Stem Cell Lines Derived from Human Blastocysts. *Science,* 282**,** 1145-1147.

TING, S., LIEW, S. J., JAPSON, F., SHANG, F., CHONG, W. K., REUVENY, S., THAM, J. Y., LI, X. & OH, S. 2014. Time-resolved video analysis and management system for monitoring cardiomyocyte differentiation processes and toxicology assays. *Biotechnol J,* 9**,** 675-83.

TOHYAMA, S., HATTORI, F., SANO, M., HISHIKI, T., NAGAHATA, Y., MATSUURA, T., HASHIMOTO, H., SUZUKI, T., YAMASHITA, H., SATOH, Y., EGASHIRA, T., SEKI, T., MURAOKA, N., YAMAKAWA, H., OHGINO, Y., TANAKA, T., YOICHI, M., YUASA, S., MURATA, M., SUEMATSU, M. & FUKUDA, K. 2013. Distinct metabolic flow enables large-scale purification of mouse and human pluripotent stem cell-derived cardiomyocytes. *Cell Stem Cell,* 12**,** 127-37.

VALAMEHR, B., TSUTSUI, H., HO, C. M. & WU, H. 2011. Developing defined culture systems for human pluripotent stem cells. *Regen Med,* 6**,** 623-34.

VALLIER, L., ALEXANDER , M. & PEDERSEN, R. 2005. Activin/Nodal and FGF pathways cooperate to maintain pluripotency of human embryonic stem cells. *Journal of Cell Science,* 118**,** 4495-4509.

VANDEN BERGHE, T., LINKERMANN, A., JOUAN-LANHOUET, S., WALCZAK, H. & VANDENABEELE, P. 2014. Regulated necrosis: the expanding network of non-apoptotic cell death pathways. *Nat Rev Mol Cell Biol,* 15**,** 135-47.

VANDENABEELE, P., GALLUZZI, L., VANDEN BERGHE, T. & KROEMER, G. 2010. Molecular mechanisms of necroptosis: an ordered cellular explosion. *Nat Rev Mol Cell Biol,* 11**,** 700-14.

VEERMAN, C. C., KOSMIDIS, G., MUMMERY, C. L., CASINI, S., VERKERK, A. O. & BELLIN, M. 2015. Immaturity of human stem-cell-derived cardiomyocytes in culture: fatal flaw or soluble problem? *Stem Cells Dev,* 24**,** 1035-52.

VEJPONGSA, P. & YEH, E. T. 2014. Prevention of anthracycline-induced cardiotoxicity: challenges and opportunities. *J Am Coll Cardiol,* 64**,** 938-45.

VILLA-DIAZ, L. G., ROSS, A. M., LAHANN, J. & KREBSBACH, P. H. 2013. Concise review: The evolution of human pluripotent stem cell culture: from feeder cells to synthetic coatings. *Stem Cells,* 31**,** 1-7.

WAKEFIELD, I., POLLARD, C., REDFERN, W., HAMMOND, T. & VALENTIN, J.-P. 2002. The application of in vitro methods to safety pharmacology. *Fundamental & Clinical Pharmacology,* 16**,** 209-218.

WALSH, J. G., CULLEN, S. P., SHERIDAN, C., LUTHI, A. U., GERNER, C. & MARTIN, S. J. 2008. Executioner caspase-3 and caspase-7 are functionally distinct proteases. *Proc Natl Acad Sci U S A,* 105**,** 12815-9.

WANG, Y., CHENG, L. & GERECHT, S. 2014. Efficient and scalable expansion of human pluripotent stem cells under clinically compliant settings: a view in 2013. *Ann Biomed Eng,* 42**,** 1357-72.

WARREN, L., MANOS, P. D., AHFELDT, T., LOH, Y. H., LI, H., LAU, F., EBINA, W., MANDAL, P. K., SMITH, Z. D., MEISSNER, A., DALEY, G. Q., BRACK, A. S., COLLINS, J. J., COWAN, C., SCHLAEGER, T. M. & ROSSI, D. J. 2010. Highly efficient reprogramming to pluripotency and directed differentiation of human cells with synthetic modified mRNA. *Cell Stem Cell,* 7**,** 618-30.

WATANABE, K., UENO, M., KAMIYA, D., NISHIYAMA, A., MATSUMURA, M., WATAYA, T., TAKAHASHI, J. B., NISHIKAWA, S., NISHIKAWA, S., MUGURUMA, K. & SASAI, Y. 2007. A ROCK inhibitor permits survival of dissociated human embryonic stem cells. *Nat Biotechnol,* 25**,** 681-6.

WEISS, D., BRISCHWEIN, M., GROTHE, H., WOLF, B. & WIEST, J. 2013. Label-free monitoring of whole cell vitality. *35th Annual International Conference of the IEEE EMBS***,** 1607-1610.

WILMUT, I., SCHNIEKE, A., MCWHIR, J., AJ., K. & KHS., C. 1997. Viable offspring derived from fetal and adult mammalian cells. *Nature,* 385**,** 810-813.

WINTERBOURN, C. C. 2014. The challenges of using fluorescent probes to detect and quantify specific reactive oxygen species in living cells. *Biochim Biophys Acta,* 1840**,** 730-8.

WLODKOWIC, D., SKOMMER, J., MCGUINNESS, D., FALEY, S., KOLCH, W., DARZYNKIEWICZ, Z. & COOPER, J. M. 2009. Chip-based dynamic real-time quantification of drug-induced cytotoxicity in human tumor cells. *Anal Chem,* 81**,** 6952-9.

WOLTJEN, K., MICHAEL, I. P., MOHSENI, P., DESAI, R., MILEIKOVSKY, M., HAMALAINEN, R., COWLING, R., WANG, W., LIU, P., GERTSENSTEIN, M., KAJI, K., SUNG, H. K. & NAGY, A. 2009. piggyBac transposition reprograms fibroblasts to induced pluripotent stem cells. *Nature,* 458**,** 766-70.

WU, J., DING, W.-G. & HORIE, M. H. 2016. Molecular pathogenesis of long QT syndrome type 1. *Journal of Arrhythmia*.

XIN, M., KIM, Y., SUTHERLAND, L. B., MURAKAMI, M., QI, X., MCANALLY, J., PORRELLO, E. R., MAHMOUD, A. I., TAN, W., SHELTON, J. M., RICHARDSON, J. A., SADEK, H. A., BASSEL-DUBY, R. & OLSON, E. N. 2013. Hippo pathway effector Yap promotes cardiac regeneration. *Proc Natl Acad Sci U S A,* 110**,** 13839-44.

XU, C., INOKUMA, S., DENHAM, J., GOLDS, K., KUNDU, P., GOLD, J. & CARPENTER, M. 2001. Feeder-free growth of undifferentiated human embryonic stem cells. *Nature Biotechnology,* 19.

XU, C., POLICE, S., HASSANIPOUR, M., LI, Y., CHEN, Y., PRIEST, C., O'SULLIVAN, C., LAFLAMME, M. A., ZHU, W. Z., VAN BIBER, B., HEGEROVA, L., YANG, J., DELAVAN-BOORSMA, K., DAVIES, A., LEBKOWSKI, J. & GOLD, J. D. 2011. Efficient generation and cryopreservation of cardiomyocytes derived from human embryonic stem cells. *Regen Med,* 6**,** 53-66.

YANG, X., PABON, L. & MURRY, C. E. 2014. Engineering adolescence: maturation of human pluripotent stem cell-derived cardiomyocytes. *Circ Res,* 114**,** 511-23.

YU, J., CHAU, K. F., VODYANIK, M. A., JIANG, J. & JIANG, Y. 2011. Efficient feeder-free episomal reprogramming with small molecules. *PLoS One,* 6**,** e17557.

YU, J., VODYANIK, M., SMUGA-OTTO, K., ANTOSIEWICZ-BOURGET, J., FRANE, J., TIAN, S., NIE, J., JONSODDIR, G., RUOTTI, V., STEWART, R., SLUKVIN, I. & THOMSON, J. 2007. Induced Pluripotent Stem Cell Lines Derived from Human Somatic Cells. *Science,* 318**,** 1917-1920.

YUE, T.-L., WANG, C., ROMANIC, A. M., KIKLY, K., KELLER, P., DEWOLF JR, W. E., HART, T. K., THOMAS, H. C., STORER, B. & GU, J.-L. 1998. Staurosporine-induced apoptosis in cardiomyocytes: a potential role of caspase-3. *Journal of molecular and cellular cardiology,* 30**,** 495-507.

ZANELLA, F. & SHEIKH, F. 2014. Patient-Specific Induced Pluripotent Stem Cell Models: Generation and Characterization of Cardiac Cells. *Methods Mol Biol*.

ZARGHI, A., FOROUTAN, S. M., SHAFAATI, A. & KHODDAM, A. 2007. Quantification of carvedilol in human plasma by liquid chromatography using fluorescence detection: application in pharmacokinetic studies. *J Pharm Biomed Anal,* 44**,** 250-3.

ZHANG, J., KLOS, M., WILSON, G. F., HERMAN, A. M., LIAN, X., RAVAL, K. K., BARRON, M. R., HOU, L., SOERENS, A. G., YU, J., PALECEK, S. P., LYONS, G. E., THOMSON, J. A., HERRON, T. J., JALIFE, J. & KAMP, T. J. 2012a. Extracellular matrix promotes highly efficient cardiac differentiation of human pluripotent stem cells: the matrix sandwich method. *Circ Res,* 111**,** 1125-36.

ZHANG, S., LIU, X., BAWA-KHALFE, T., LU, L. S., LYU, Y. L., LIU, L. F. & YEH, E. T. 2012b. Identification of the molecular basis of doxorubicin-induced cardiotoxicity. *Nat Med,* 18**,** 1639-42.

ZHAO, B., TUMANENG, K. & GUAN, K. L. 2011a. The Hippo pathway in organ size control, tissue regeneration and stem cell self-renewal. *Nat Cell Biol,* 13**,** 877-83.

ZHAO, T., ZHANG, Z. N., RONG, Z. & XU, Y. 2011b. Immunogenicity of induced pluripotent stem cells. *Nature,* 474**,** 212-5.

ZHAO, Z., CUI, W., ZHANG, H., GAO, H., LI, X., WANG, Y., HU, H. & LI, B. 2015. Pre-treatment of a single high-dose of atorvastatin provided cardioprotection in

different ischaemia/reperfusion models via activating mitochondrial KATP channel. *Eur J Pharmacol,* 751**,** 89-98.

8 Appendix

Supplementary video 1 – LQT2 hiPSCs differentiated with 2 µM Chir99021 to initiate differentiation and 1 µM Wnt-C59 48 hours later (see section 3.2.12 and figure 3.12).

Supplementary video 2 – LQT2 hiPSCs differentiated with 2 µM Chir99021 to initiate differentiation and 2 µM Wnt-C59 48 hours later (see section 3.2.12 and figure 3.12).

Supplementary video 3 – LQT2 hiPSCs differentiated with 2 µM Chir99021 to initiate differentiation and 4 µM Wnt-C59 48 hours later (see section 3.2.12 and figure 3.12).

Supplementary video 4 – LQT2 hiPSCs differentiated with 2 µM Chir99021 to initiate differentiation and 6 µM Wnt-C59 48 hours later (see section 3.2.12 and figure 3.12).

Supplementary video 5 – LQT2 hiPSCs differentiated with 4 µM Chir99021 to initiate differentiation and 1 µM Wnt-C59 48 hours later (see section 3.2.12 and figure 3.12).

Supplementary video 6 – LQT2 hiPSCs differentiated with 4 µM Chir99021 to initiate differentiation and 2 µM Wnt-C59 48 hours later (see section 3.2.12 and figure 3.12).

Supplementary video 7 – LQT2 hiPSCs differentiated with 2 µM Chir99021 to initiate differentiation and 4 µM Wnt-C59 48 hours later (see section 3.2.12 and figure 3.12).

Supplementary video 8 – LQT2 hiPSCs differentiated with 2 µM Chir99021 to initiate differentiation and 6 µM Wnt-C59 48 hours later (see section 3.2.12 and figure 3.12).

Supplementary video 9 – LQT2 hiPSCs differentiated with 6 µM Chir99021 to initiate differentiation and 1 µM Wnt-C59 48 hours later (see section 3.2.12 and figure 3.12).

Supplementary video 10 – LQT2 hiPSCs differentiated with 6 µM Chir99021 to initiate differentiation and 2 µM Wnt-C59 48 hours later (see section 3.2.12 and figure 3.12).

Supplementary video 11 – LQT2 hiPSCs differentiated with 6 µM Chir99021 to initiate differentiation and 4 µM Wnt-C59 48 hours later (see section 3.2.12 and figure 3.12).

Supplementary video 12 – LQT2 hiPSCs differentiated with 6 µM Chir99021 to initiate differentiation and 6 µM Wnt-C59 48 hours later (see section 3.2.12 and figure 3.12).

Supplementary video 13 – LQT2 hiPSCs differentiated with 8 µM Chir99021 to initiate differentiation and 1 µM Wnt-C59 48 hours later (see section 3.2.12 and figure 3.12).

Supplementary video 14 – LQT2 hiPSCs differentiated with 8 µM Chir99021 to initiate differentiation and 2 µM Wnt-C59 48 hours later (see section 3.2.12 and figure 3.12).

Supplementary video 15 – LQT2 hiPSCs differentiated with 8 µM Chir99021 to initiate differentiation and 4 µM Wnt-C59 48 hours later (see section 3.2.12 and figure 3.12).

Supplementary video 16 – LQT2 hiPSCs differentiated with 8 µM Chir99021 to initiate differentiation and 6 µM Wnt-C59 48 hours later (see section 3.2.12 and figure 3.12).

Supplementary video 17 – CPVT hiPSC derived cardiomyocytes contracting as a spontaneously beating sheet. Cardiomyocytes generated by automated differentiation protocols (see section 4.2.18 and figure 4.26).